UNIVERSITAT DE BARCELONA

Fish and mammalian glut4 traffic characteristics: an evolutionary perspective on the importance of glut4 protein motifs for trafficking

Francisco Manuel de Carvalho Simões

FRANCISCO SIMÕES

FISH AND MAMMALIAN GLUT4 TRAFFIC CHARACTERISTICS: AN EVOLUTIONARY PERSPECTIVE ON THE IMPORTANCE OF GLUT4 PROTEIN MOTIFS FOR TRAFFICKING

2018

FISH AND MAMMALIAN GLUT4 TRAFFIC CHARACTERISTICS: AN EVOLUTIONARY PERSPECTIVE ON THE IMPORTANCE OF GLUT4 PROTEIN MOTIFS FOR TRAFFICKING

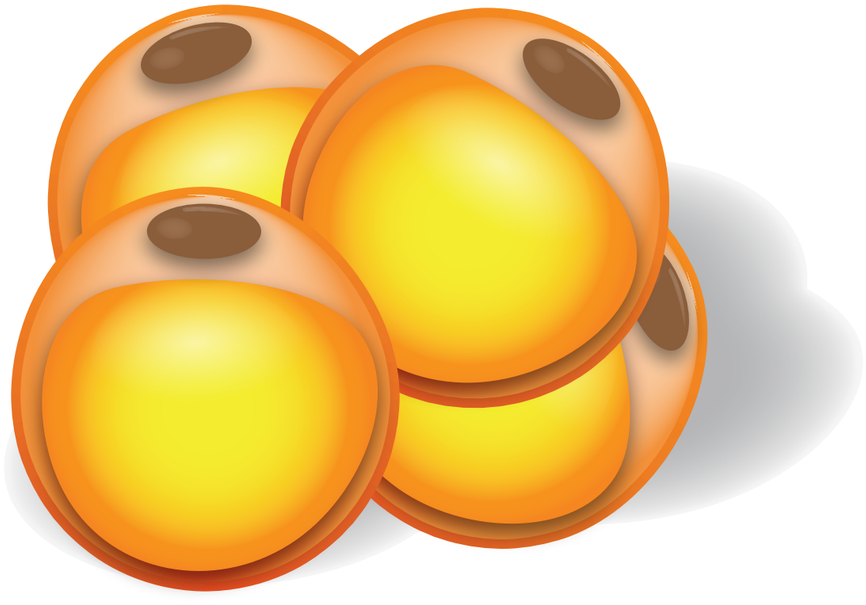

Francisco Manuel de Carvalho Simões

Barcelona, July 2018

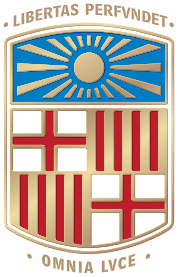

UNIVERSITAT DE BARCELONA

DOCTORAL PROGRAMME IN BIOMEDICINE
FACULTY OF BIOLOGY
UNIVERSITAT DE BARCELONA

FISH AND MAMMALIAN GLUT4 TRAFFIC CHARACTERISTICS: AN EVOLUTIONARY PERSPECTIVE ON THE IMPORTANCE OF GLUT4 PROTEIN MOTIFS FOR TRAFFICKING

A THESIS TO BE SUBMITTED BY:
Francisco Manuel de Carvalho Simões

FOR THE AWARD OF THE DEGREE OF:
Doctor by the Universitat de Barcelona

Supervisor: Marta Camps Camprubí

Co-supervisor: Josep Planas Vilarnau

Tutor: Anna Maria Gumà Garcia

Barcelona, July 2018

Very much like the research process, the melody of a 12-bar blues is composed of questions, answers, and finally, a conclusion. Underwater jam is a melody about my experience as a phd student; my way of thanking everybody that, in a way or another, helped me during this time; my jazz blues.

Underwater Jam

Francisco Simões

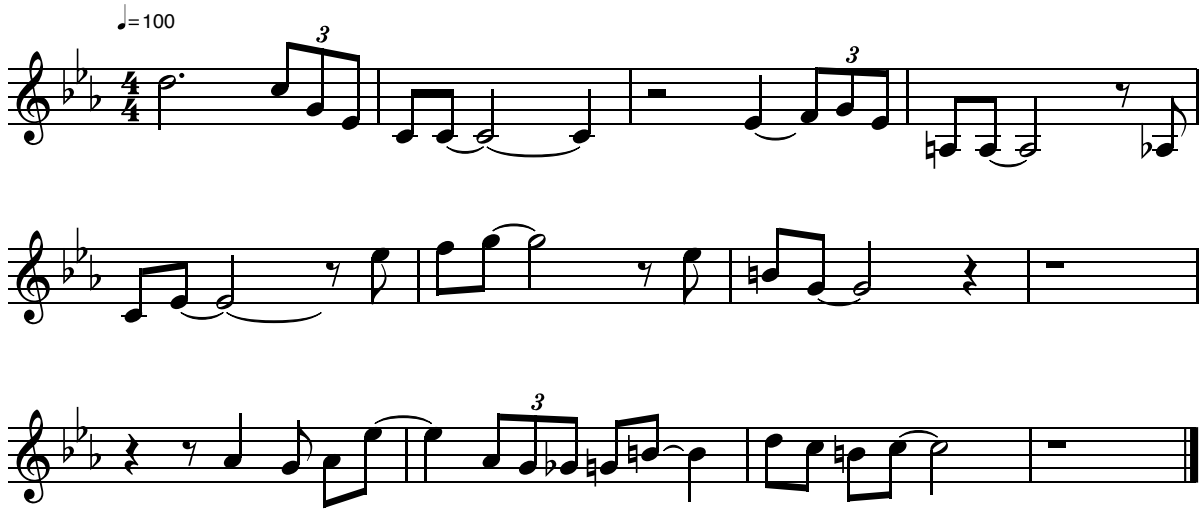

To the family I chose, and
to the one I was blessed with.

INDEX

ABBREVIATIONS

Akt (PKB)	Protein kinase B
AMPK	AMP-activated protein kinase
AP	Adaptor protein complex
APS	Adaptor protein substrate
ARF	ADP-ribosylation factor
ARHGAP10	Rho GTPase activating protein 10
ARP	Acidic ribosomal phosphoprotein
AS160	Akt substrate of 160 kDa
BSA	Bovine serum albumin
BtGLUT4	Brown trout GLUT4
C3G	Guanine nucleotide-releasing factor 2, specific for Crk
CAP	c-Cbl-associated protein
Cav	Caveolin
Cbl	c-Cbl proto-oncogene
CCP	Clathrin-coated pits
CCV	Clathrin-coated vesicles
CD44	Cluster of differentiation 44
Cdc42	Cell division cycle 42
CDP138	138 kDa C2 domain-containing phosphoprotein
CIP4	Cdc42-interacting protein 4
CLIC	Clathrin-independent carrier
CME	Clathrin-mediated endocytosis
CrkII	CRK proto-oncogene, adaptor protein
CTB	Cholera toxin B subunit
DMEM	Dulbecco's modified eagle's medium
DMSO	Dimethyl sulfoxide
DNP	2,4-Dinitrophenol
DTT	Ditriotheitol
EAAC1	Excitatory amino-acid carrier 1
ECL	Enhanced chemiluminescence
EDTA	Ethylenediaminetetraacetic acid
EE	Early endosome
EEA-1	Early endosome antigen-1
EHD2	Eps15 homology domain-containing 2
EPS15	EGFR pathway substrate 15
ERC	Endocytic recycling compartment
EXO70	Exocyst complex component 7
FBS	Fetal bovine serum
FCHO	FCH domain only
GAP	GTPase activating protein
Gapex-5	GTPase activating protein and VPS9 domains 1
GEEC	GPI-AP-enriched early endosomal compartment
GEF	Guanine nucleotide exchange factor
GFP	Green fluorescent protein

GGA	Golgi-localized, γ-ear-containing ARF binding proteins
GLUT	Glucose transporter
GPI-APs	Glycosylphosphatidylinositol-anchored proteins
GRAF1	GTPase regulator associated with focal adhesion kinase1
GRASP	Grp1-associated scaffold protein
Grp1	General receptor for phophoinositides 1
GSV	GLUT4 storage vesicles
HEPES	4-(2-hydroxyethyl)-1-piperazineethanesulfonic acid
HMIT	Proton myo-inositol cotransporter
HRP	Horseradish peroxidase
hsc70	Heat shock cognate 71 kDa protein
IBMX	3-isobutyl-1-methylxanthine
IgE	Immunoglobulin E
IL-2	Interleukin 2
IR	Insulin receptor
IRAP	Insulin-regulated aminopeptidase
IRS	Insulin-receptor substrate
KD	Knockdown
LB	Luria-Bertani
LOX-1	Lectin-like oxidized low-density lipoprotein receptor-1
mAb	Monoclonal antibody
MHC I	Major histocompatibility complex class I
mLST8	Mammalian lethal with SEC13 protein 8
MOI	Multiplicity of infection
mSIN1	Mammalian stress-activated protein kinase interacting protein 1
mTOR	Mammalian target of rapamycin
MUNC18C	Protein unc-18 homolog C
N-WASP	Neuronal Wiskott-Aldrich syndrome protein
OkGLUT4	Coho salmon GLUT4
OPD	o-Phenylenediamine
PBS	Phosphate buffered saline
PDK	Phosphoinositide-dependent protein kinase
PEI	Polyethylenimine
PH	Pleckstrin homology
PI(3)P	Phosphatidylinositol 3-phosphate
PI3K	Phosphatidylinositol-3-kinase
PIP_2	Phosphatidylinositol-4,5-bisphosphate
PIP_3	Phosphatidylinositol-3,4,5-triphosphate
PIST	PDZ protein interacting specifically with TC10
PKC λ/ζ	Protein kinase C lambda/zeta
PM	Plasma membrane
PTB	Phosphotyrosine binding domain
PVDF	Polyvinylidene difluoride
Rac1	Ras-related C3 botulinum toxin substrate 1

RALA	RAS like proto-oncogene A
RatGLUT4	Rat GLUT4
Rictor	Rapamycin-insensitive companion of mTOR
RT	Room temperature
SDS	Sodium dodecyl sulfate
SEC5	Exocyst complex component SEC5
SH	Src homology
SNAP23	Synaptosomalassociated protein 23
SNARE	N-ethylmaleimide-sensitive factor attachment protein receptor
SoHo	Sorbin homology
STX	Syntaxin
SUMO	Small ubiquitin-related modifier
SV40	Simian virus
SYNIP	STX4-interacting protein
TBC1D4	TBC1 domain family member 4
TF	Transferrin
TGN	Trans-Golgi network
TR	Transferrin receptor
TU	Transducing units
TUG	Tether containing UBX domain for GLUT4
qPCR	Quantitative real-time polymerase chain reaction
Ubc9	Ubiquitin carrier protein 9
VacA	Vacuolating cytotoxic A
VAMP2	Vesicle-associated membrane protein 2
wtGLUT4	Wild type GLUT4
γ-c	Gamma chain

I. INTRODUCTION

1. GLUCOSE TRANSPORTERS

Glucose is one of the most abundant molecules on the planet and consequently, organisms have evolved to utilize glucose as a source of energy. Because the eukaryotic plasma membrane is impermeable to hydrophilic molecules, glucose is transported across it by membrane carrier proteins, named glucose transporters (GLUTs) (Walmsley et al. 1998).

GLUTs, encoded by the SLC2 genes, belong to the major facilitator superfamily of membrane transporters. GLUTs catalyze the transport of monosaccharides across eukaryotic membranes through an energy-independent mechanism (Mueckler and Thorens 2013).

Although still not fully described, several studies suggest that the transport of substrates across the membrane occurs through an alternating conformation mechanism: substrate binding sites are sequentially exposed to either the cell exterior or cytoplasm (Carruthers et al. 2009, Yan 2017).

GLUTs are proteins of approximately 500 amino acids that share between 25-68 % amino acid sequence identity with one another and possess 12 transmembrane domains (alpha helixes), a single glycosylation site, a large central cytoplasmic loop and intracellular amino (N-) and carboxy (C-) terminal ends (Joost and Thorens 2001, Scheepers et al. 2004, Thorens and Mueckler 2010, Cura et al. 2012).

Based on gene sequence similarity, members of the GLUT family are grouped into 3 classes: Class I includes GLUT1 through 4 and GLUT14; Class II comprises GLUT5, 7, 9 and 11; and finally, class III includes GLUT6, 8, 10, 12 and 13 (Figure I-1) (Joost and Thorens 2001, Scheepers et al. 2004).

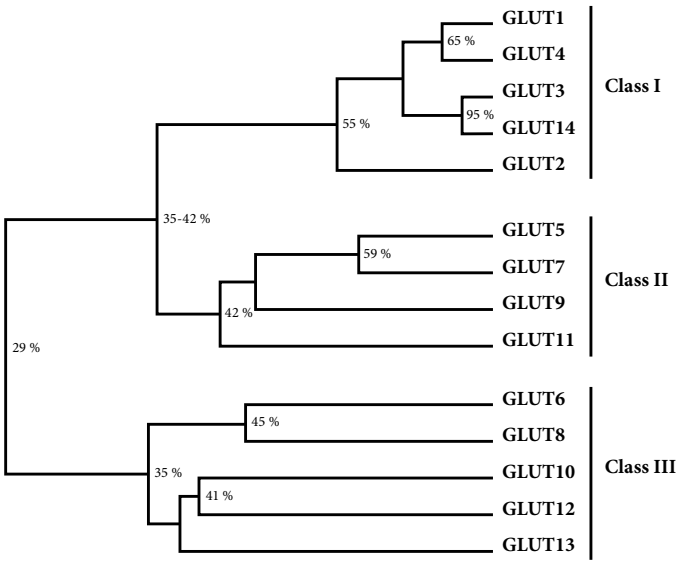

Figure I-1. Dendrogram of human GLUT genes. Numbers at the branches of the tree indicate percentage of identity. Adapted from (Scheepers et al. 2004).

Members of the first two classes possess one large exofacial loop between transmembrane domains I and II which harbors one glycosylation site. Class III GLUTs also contain one

glycosylation site in the large exofacial loop but in members of this class the loop is located between transmembrane domains IX and X, instead (Figure I-2) (Mueckler and Thorens 2013).

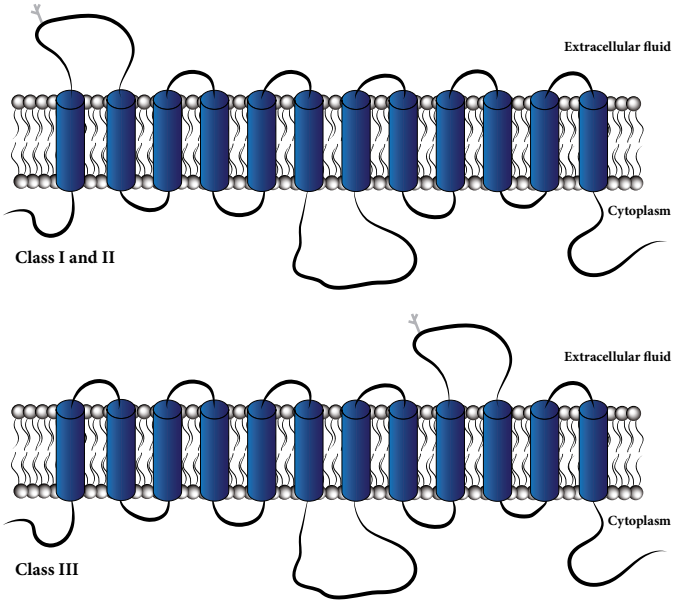

Figure I-2. Schematic representation of the bidimensional structure of class I, II and III GLUT family members.

GLUT expression occurs virtually in every cell type of the human body and often more than one GLUT is expressed in the same cell type (Figure I-3). Different cell type-based patterns of expression and differences in kinetics among GLUTs allows for a fine tuning of glucose uptake and metabolism in order to preserve metabolic homeostasis (Scheepers et al. 2004, Mueckler and Thorens 2013).

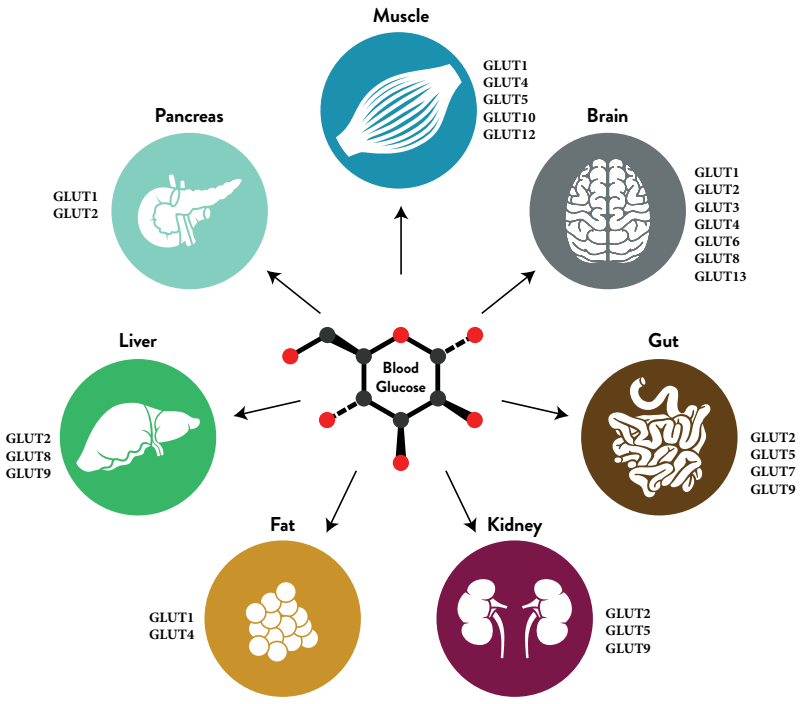

Figure I-3. Glucose transporter expression in different organs.

1.1 GLUT1

GLUT1 was first cloned in 1985 by Mueckler and colleagues and is one of the most extensively studied GLUTs. GLUT1 belongs to class I of the GLUTs family and is comprised of 492 amino acids residues. Its main substrate is glucose (Km≈5-7 mM) but it can also transport mannose, galactose and glucosamine (Mueckler et al. 1985, Burant and Bell 1992, Augustin 2010, Mueckler and Thorens 2013).

GLUT1, often expressed in conjunction with other GLUTs, is expressed in various tissues but it is expressed at high levels in erythrocytes where it mediates equilibration of glucose concentration between serum and the erythrocyte's cytoplasm (Mueckler and Thorens 2013). This transporter is also abundantly found in brain endothelial cells and it plays a critical role in fueling cerebral cells through glucose uptake (Simpson et al. 2007, Yeh et al. 2008). Also noteworthy is its role in transporting glucose across the placenta supplying the fetus with energy (Illsley 2000). Finally, GLUT1 expression is also upregulated during oncogenesis which probably contributes to tumor growth by helping cancer cells overcome a size limit imposed by their glycolytic capacity (Ganapathy et al. 2009, Thorens and Mueckler 2010, Barron et al. 2016).

1.2. GLUT2

GLUT2, in contrast to the other members of this family of transporters, has a surprisingly low affinity for glucose (Km≈17 mM), despite being its principal substrate. GLUT2 is also able to transport galactose, mannose, fructose and glucosamine (Uldry et al. 2002, Mueckler and Thorens 2013).

GLUT2 is the major glucose transporter in hepatocytes and it is involved in glucose uptake and release in the fed and fasted states, respectively (Mueckler and Thorens 2013). GLUT2 is also expressed in intestinal absorptive cells, kidney, brain and pancreatic b-cells where it is responsible for the glucose uptake needed for glucose-stimulated insulin secretion (Fukumoto et al. 1988, Scheepers et al. 2004, Thorens 2014).

1.3. GLUT3

This transporter has the highest affinity for glucose within the GLUT family, with a Km≈2 mM and, as such, glucose is clearly its principal physiological substrate. Nonetheless, GLUT3 can also transport mannose and galactose (Colville et al. 1993, Simpson et al. 2008, Augustin 2010). GLUT3 is the major neuronal glucose transporter and its high affinity for glucose makes it the perfect transporter because the concentration of cerebral glucose is considerably lower than that in circulating blood (Mueckler and Thorens 2013). GLUT3 is also important in mediating transfer of glucose across the placenta along with GLUT1 and it is also present in sperm where it controls glucose uptake necessary for motility and maturation (Shin et al. 1997, Urner and Sakkas 1999, Illsley 2000, Thorens and Mueckler 2010). Finally, GLUT3 is also abundantly expressed in human white blood cells, where it translocates from intracellular compartments to

the membrane in response to proliferative stimuli (Simpson et al. 2008).

1.4. GLUT4

GLUT4 was first identified in 1988 in rat adipocytes (James et al. 1988) and cloned one year later by various research groups (Birnbaum 1989, Charron et al. 1989, James et al. 1989). The GLUT4 gene (SLC2A4) shares 65 % sequence identity with GLUT1 and codes for a protein of 509 amino acids found primarily in adipose and muscle tissue and with a Km value for glucose around 5 mM (Burant and Bell 1992, Augustin 2010, Mueckler and Thorens 2013). GLUT4 has a very unique feature, as it is an insulin-responsive transporter: GLUT4 resides primarily in intracellular membrane compartments but upon insulin signaling it translocates to the plasma membrane to uptake glucose preventing chronic elevations in blood glucose levels (Cushmans and Wardzala 1980, Suzuki and Kono 1980, Bryant et al. 2002, Huang and Czech 2007). Because the bulk of blood glucose is cleared up by skeletal muscle in response to insulin and GLUT4 is in charge of this process, GLUT4 plays a critical role in the regulation of whole body glucose homeostasis (Mueckler 1995). In fact, defects in GLUT4 insulin-mediated translocation in conjunction with defects in pancreatic b-cells insulin secretion, result in type 2 diabetes (Watson et al. 2004a, Mueckler and Thorens 2013).

1.5. GLUT5

GLUT5 was the first class II member to be identified, and surprisingly it has a high specificity and affinity for fructose (Km6 mM) (Burant and Bell 1992, Rand et al. 1993, Douard and Ferraris 2008, Thorens and Mueckler 2010). The main function of GLUT5 is to mediated the uptake of dietary fructose across the apical membrane of the small intestine (Douard and Ferraris 2008, Augustin 2010). GLUT5 is also expressed in kidney, fat, skeletal muscle and brain but, since circulating fructose levels are generally low, its role in these tissues is uncertain (Mueckler and Thorens 2013).

1.6. GLUT6

GLUT6, originally named GLUT9, displays an intracellular localization in spleen, brain, and leukocytes (Doege et al. 2000). It has been suggested that its localization may be due to the presence of a dileucine motif in its N-terminal end (Lisinski et al. 2001). Because of its cellular location, the function of GLUT6 may be to transport hexose molecules across the membrane of intracellular organelles (Mueckler and Thorens 2013).

1.7. GLUT7

GLUT7 is the most recently characterized GLUT. It shows high sequence similarity with GLUT5 and it is also expressed in the apical membrane of the small intestine and colon, but it exhibits low transport levels of fructose and glucose (Cheeseman 2008, Thorens and Mueckler 2010).

1.8. GLUT8

GLUT8 is expressed solely intracellularly due to a dileucine motif in its N-terminal end. Mutations in this motif induce GLUT8 surface expression (Ibberson et al. 2000). GLUT8 shows high affinity for glucose (Km≈2 mM) and fructose and galactose compete with glucose transport activity. It is primarily expressed in testis and at lower levels in cerebellum adrenal gland, liver, spleen, brown adipose tissue and lung (Ibberson et al. 2002, Mueckler and Thorens 2013).

1.9. GLUT9

Alternative splicing of the SLC2A9 gene results in two GLUT9 variants (Phay et al. 2000, Augustin et al. 2004). GLUT9a is a 540 amino acids protein whereas GLUT9b is comprised of 512 amino acids. The two variants differ in their N-terminal cytoplasmic ends. GLUT9 is a urate transporter and while GLUT9a is present in liver, kidney, intestine, leukocytes and chondrocytes, GLUT9b is solely expressed in liver and kidney (Augustin et al. 2004, Keembiyehetty et al. 2006, Bibert et al. 2009). The differences in the N-terminus of these variants target GLUT9 to opposite poles of epithelial cells: GLUT9a is targeted to the basolateral pole whereas GLUT9b is expressed in the apical pole (Augustin et al. 2004).

1.10. GLUT10

GLUT10, a 541-amino acid protein, transports glucose and galactose and exhibits a very wide tissue distribution: pancreas, placenta, heart, lung, liver, brain, fat, muscle, and kidney (Dawson et al. 2001, McVie-Wylie et al. 2001). GLUT10 shows high affinity for glucose when expressed in Xenopus oocytes (Dawson et al. 2001). Studies also found that homozygous mutations in GLUT10 gene cause arterial tortuosity syndrome, a rare genetic disorder that causes morphological abnormalities in arteries including elongation, aneurysms, and tortuosity (Coucke et al. 2006).

1.11. GLUT11

GLUT11 exhibits a high degree of sequence similarity with the fructose transporter GLUT5 (approximately 42%) and it also transports fructose and glucose (Scheepers et al. 2005). Like GLUT9, GLUT11 possesses multiple variants that differ in their N-terminal end which target them to different tissues (Sasaki et al. 2001, Scheepers et al. 2005): GLUT11a is expressed heart, skeletal muscle, and kidney; GLUT11b is expressed in kidney, adipose tissue, and placenta; and GLUT11c is expressed in adipose tissue, heart, skeletal muscle, and pancreas. Surprisingly, rodents lack the SLC2A11 gene (Mueckler and Thorens 2013).

1.12. GLUT12

GLUT12 consists of a 617 amino acid protein whose expression distribution spans the heart, skeletal muscle, prostate and small intestine (Rogers et al. 2002). Similarly to GLUT4, GLUT12 has been proposed to translocate from intracellular compartments to the plasma

membrane in an insulin-responsive manner in skeletal muscle (Stuart et al. 2009). In heart, on the other hand, GLUT12 has been suggested to be insulin-independent and to function as a basal GLUT located primarily at cell surface (Waller et al. 2013). Recently, studies in zebrafish showed that GLUT12 is also essential for heart development (Jimenez-Amilburu et al. 2015). However, the role of GLUT12 in glucose homeostasis is still unclear.

1.13. GLUT13 (HMIT)

GLUT13 or Proton myo-inositol cotransporter (HMIT) is encoded by the SLC2A13 gene (Uldry et al. 2001). It is expressed predominantly in the brain, especially in the hippocampus, hypothalamus, cerebellum and brainstem. In neurons, HMIT is present in intracellular vesicles and can be induced to translocate to the plasma membrane to increase myo-inositol uptake (Uldry et al. 2004). HMIT is also expressed in white and brown adipose tissues and in kidney, albeit at lower levels (Uldry et al. 2001, Mueckler and Thorens 2013).

1.14. GLUT14

GLUT14 is included in class I GLUTs and its gene, SLC2A14, shares 95 % sequence identity with the SLC2A3 gene (GLUT3). Hence, it appears to be the result of gene duplication (Wu and Freeze 2002). GLUT14 can be expressed (as a result of alternative slicing) as a shorter version (497 amino acids) or longer version (520 amino acids); both isoforms differ in the N-terminus end. GLUT14 expression was initially thought to be confined to the testis; however, more recent studies indicate that GLUT14 is expressed in ovarian cancer cells, leukemia cell lines and in peripheral blood of patients with Parkinson's disease (Taylor et al. 2007, Januchowski et al. 2013, Infante et al. 2015, Amir Shaghaghi et al. 2016).

2. GLUT4 TRAFFICKING

Glucose is the main source of energy in mammals. After a meal or through the breakdown of glycogen stores in the liver, glucose is distributed among the different tissues of the body. The uptake of glucose at the delivery sites requires the presence of glucose transporters of the GLUT family. Tissues that need constant supply of glucose, like the brain, are endowed with GLUT isoforms that are constitutively targeted to the plasma membrane (PM) (e.g. GLUT1-3) (Hudson et al. 1992, Vannucci et al. 1997, Bryant et al. 2002, Watson et al. 2004a). On the other hand, tissues like muscle and adipose tissue have developed more sophisticated glucose transport systems that can be up- or down-regulated in response to stimuli, like insulin and exercise and, by doing so, control glucose uptake (Reviewed in (Bryant et al. 2002)).

Muscle and adipose tissues are key regulators of normal blood glucose levels (4-7 mM), are essential to prevent hyperglycemia and its toxic effects, and serve as the major storage sites for glucose (Watson et al. 2004a, Huang and Czech 2007, Foley et al. 2011). Among the GLUT family, GLUT4 was identified as the main glucose transporter in these tissues (Huang and Czech 2007, Mueckler and Thorens 2013). GLUT4 displays a unique feature: in the unstimulated state, GLUT4 is retained intracellularly, excluding it from the PM and restricting glucose uptake (only 5 % of the total pool of GLUT4 remains at cell surface); in response to insulin or other stimuli, GLUT4 is redistributed to the PM (about 50 % of total pool of GLUT4) to increase glucose transport up to 20-fold (Watson et al. 2004a, Dugani and Klip 2005, Hou and Pessin 2007, Blot and McGraw 2008, Rubin and Bogan 2009, Leto and Saltiel 2012). This process is reversible and upon stimuli withdrawal, GLUT4 returns to its intracellular localization (unstimulated state).

The retention of GLUT4 within the cell is a dynamic process, it continuously recycles between the PM and several intracellular compartments. In unstimulated cells, GLUT4 is sequestered intracellularly through rapid internalization and slow recycling back to PM. In the presence of insulin, GLUT4 exocytosis is accelerated and its endocytosis is slowed, creating an increase of GLUT4 steady-state PM levels (Bryant et al. 2002, Karylowski et al. 2004, Martin et al. 2006, Blot and McGraw 2006, Leto and Saltiel 2012). Ultimately, the balance of endocytosis to exocytosis determines the steady-state distribution of GLUT4 at the cell surface.

GLUT4 trafficking is a complex and dynamic process that is yet to be fully understood; however, GLUT4 intracellular trafficking can be divided in two cycles (Figure I-4) (Bryant et al. 2002, Foley et al. 2011, Leto and Saltiel 2012). After internalization to early endosome s (EE), GLUT4 can recycle quickly to the PM or can be sorted through the endocytic recycling compartment (ERC) before returning to the PM (cycle 1). Accumulation of GLUT4 in the EE can direct the transporter to late endosomes for further lysosomal degradation. GLUT4 cycle 1 corresponds to the transferrin receptor (TR) recycling pathway; in fact, during this stage, GLUT4 vesicles are enriched in TR. In unstimulated cells, only 30 % of total GLUT4 is present in this cycle, the majority of it is kept in an apparent idle cycle (cycle 2) between the ERC, a subdomain of the trans-Golgi network (TGN), and GLUT4 storage vesicles (GSV). This subdomain of the

TGN is characterized by the presence of mannose-6-phosphate receptors, Syntaxin 6 and 16 but not furin and TGN38, which are common markers of TGN (Shewan et al. 2003, Karylowski et al. 2004). GSVs on the other hand are 50-80 nM vesicles, devoid of endosomal proteins such as TR and rich in insulin-regulated aminopeptidase (IRAP), tether containing UBX domain for GLUT4 (TUG), Akt substrate of 160 kDa (AS160), sortilin and vesicle-associated membrane protein 2 (VAMP2) (Volchuk et al. 1995, Ross et al. 1996, Lin et al. 1997, Xu and Kandror 2002, Bogan et al. 2003, Larance et al. 2005). After sorting into the ERC, GLUT4 can return to the PM (small fraction) as indicated above (cycle 1) or can be transported into the subdomain of TGN or into the GSVs (Blot and McGraw 2008, Foley et al. 2011, Leto and Saltiel 2012). On the other hand, newly synthetized GLUT4 travels to the GSVs directly from TGN in a process that requires Golgi-localized, γ-ear-containing ARF binding proteins (GGA) (Watson et al. 2004b). Cycling between the ERC, TGN and GSVs leads to an efficient removal of the transporter from the PM in the absence of insulin or other stimuli (Bryant et al. 2002, Zeigerer et al. 2002, Karylowski et al. 2004, Blot and McGraw 2008). Insulin signals the translocation and fusion of GSVs with the PM (Livingstone et al. 1996, Ploug et al. 1998, Govers et al. 2004, Gonzalez and McGraw 2006, Bai et al. 2007, Xiong et al. 2010, Foley et al. 2011). Therefore, correct sorting of GLUT4 into GSVs is critical for an efficient and potent translocation to the PM in response to insulin. In addition to the effect on GSV translocation, insulin stimulates exocytosis of the general endosomal recycling pathway (cycle 1) and slows GLUT4 endocytosis from the PM. Together, these changes cause and overall redistribution of GLUT4 at the PM and the respective increase in glucose uptake (Zeigerer et al. 2004, Huang and Czech 2007, Hou and Pessin 2007). Interestingly, Stenkula and colleagues (2010) observed that in 3T3-L1 adipocytes, GLUT4 exists in the PM as freely diffusing molecules and as relatively stationary clusters. Upon fusion, GLUT4 is either dispersed (fusion with release) or retained at the site of fusion (fusion with retention). Insulin accelerates the fusion with release event by more than 60-fold while increasing only 2-fold the fusion with retention (Stenkula et al. 2010, Lizunov et al. 2013). There is still some debate on whether GSVs mobilize or not to the PM in unstimulated cells; however, it is widely accepted that a slow rate of cycling between the GSVs and the surface exists, however GSVs do not efficiently engage with the PM in the absence of insulin (Dugani and Klip 2005, Lizunov et al. 2005, Hou and Pessin 2007, Xiong et al. 2010, Stöckli et al. 2011, Foley et al. 2011, Tan et al. 2012). Alternatively, Kioumourtzoglou and colleagues suggest the existence of a GLUT4 population (distinct from GSVs) in cellugyrin-containing vesicles that traffics to the PM in unstimulated cells. Insulin would re-route GLUT4 in these vesicles to GSVs, functioning as a reservoir of GLUT4 (Kioumourtzoglou et al. 2015).

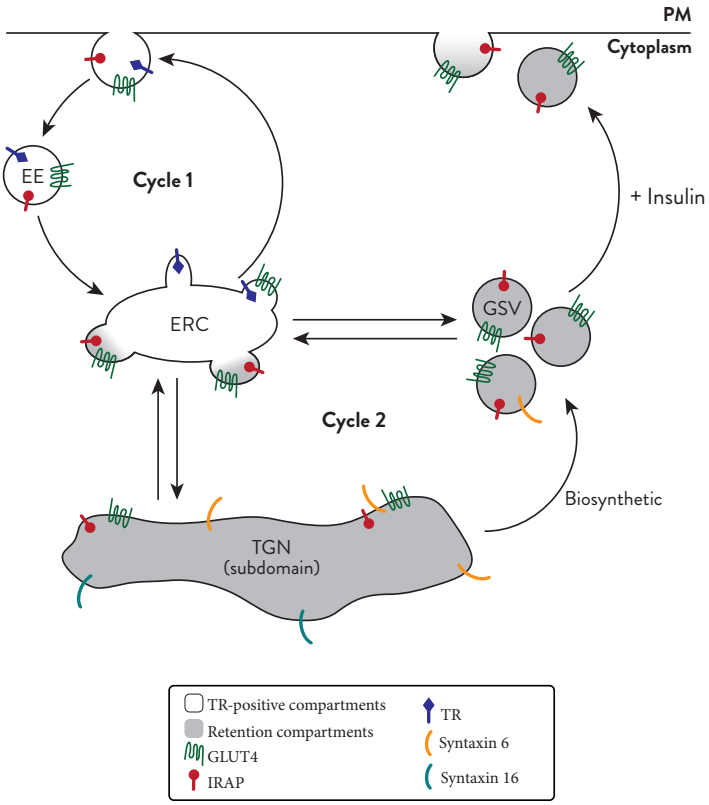

Figure I-4. Model of GLUT4 trafficking. EE: early endosome; ERC: endocytic recycling compartment; GSV: GLUT4 storage vesicles; IRAP: insulin-regulated aminopeptidase; PM: plasma membrane; TGN: trans-Golgi network; TR: transferrin receptor.

2.1. GLUT4 ACCESSORY PROTEINS

The complex trafficking of GLUT4 and sorting through the various compartments is governed by its interaction or colocalization with coat complexes throughout the cell (Bryant et al. 2002, Watson et al. 2004a, Foley et al. 2011). Although the mechanisms that direct GLUT4 trafficking are still poorly understood, several proteins have been identified to participate in the process.

2.1.1. Insulin-regulated aminopeptidase (IRAP)

Insulin-Regulated Aminopeptidase (IRAP), described as a receptor for angiotensin IV, is highly responsive to insulin and is the only protein known to co-traffic with GLUT4 throughout its entire itinerary (Figure I-4) (Albiston et al. 2001, Huang and Czech 2007, Rubin and Bogan 2009); however, no direct interaction between GLUT4 and IRAP has been described.

IRAP has been described to play an essential role in sorting GLUT4 from endosomes to the GSVs and, therefore, in an efficient insulin-driven GLUT4 translocation. But while IRAP knockdown affected GLUT4 sorting into GSVs, GLUT4 knockdown had no such effect on IRAP (Yeh et al. 2007, Jordens et al. 2010). However, this observation challenged previous studies that concluded that GLUT4 overexpression or deficiency increased by 45 % or decrease by 35 %, respectively, the amount of IRAP (Carvalho et al. 2004). As such, whether GLUT4 and IRAP

are interdependent is not clear.

2.1.2. Sortilin

Sortilin has also been extensively implicated in GLUT4 trafficking. Sortilin is abundant in GSVs and has been defined as a cargo adaptor that guides GLUT4 in two critical steps: retrieval from endosomes to the TGN and sorting of newly synthesized GLUT4 from the TGN to GSVs (Lin et al. 1997, Shi and Kandror 2005, Hou and Pessin 2007, Bogan and Kandror 2010, Jedrychowski et al. 2010, Pan et al. 2017, Kandror 2017) (Figure I-5).

Retrieval from endosomes is a very important step in GLUT4 trafficking because in addition to bridge GLUT4 internalization to intracellular retention, it rescues GLUT4 from sorting into late endosome and protein degradation in lysosomes (Shewan et al. 2003, Rubin and Bogan 2009, Kandror 2017). Sortilin's role in the endosomes-TGN retrograde traffic is to function as a transmembrane scaffold protein that binds GLUT4 and IRAP in their luminal domains and recruits retromer (retrograde trafficking machinery) to the cytoplasmic side of the endosome. Retromer then delivers the sortilin-GLUT4 complex to the TGN (Pan et al. 2017, Kandror 2017). Transport from the TGN to GSVs may occur via the same general mechanism but, in this case, sortilin interacts with Golgi- localized, γ-ear-containing ARF binding proteins (GGA) that, in turn, recruit ARF (ADP ribosylation factors) GTPases and clathrin, to initiate the budding of coated vesicles (Watson et al. 2004b, Li and Kandror 2005, Shi and Kandror 2005, Capilla et al. 2007, Canuel et al. 2008, Rubin and Bogan 2009, Kandror 2017). It has also been suggested by Lamb and colleagues that ubiquitination of GLUT4 is also necessary for this process by acting as a signal for GGA-dependent sorting (Lamb et al. 2010).

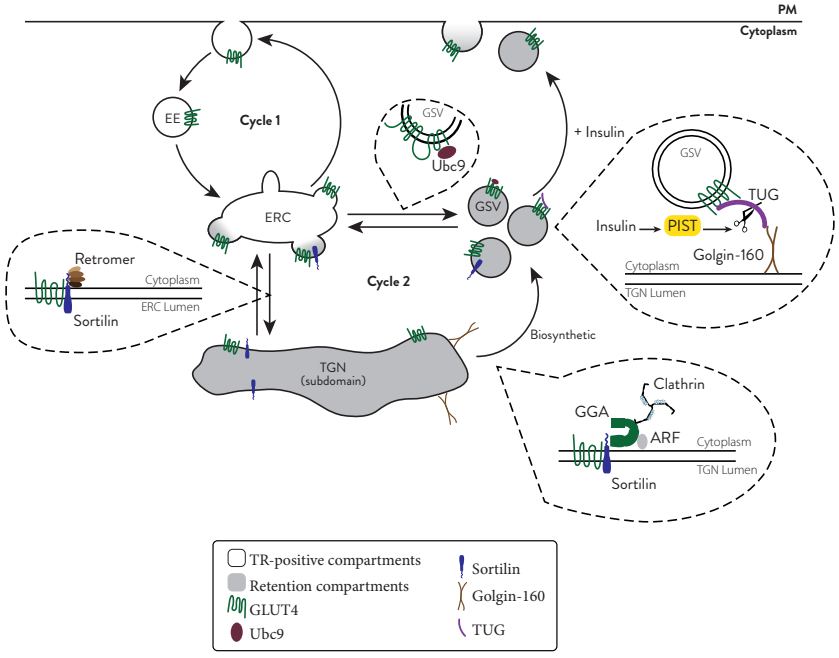

Figure I-5. GLUT4 trafficking and accessory proteins. ARF: ADP ribosylation factors; EE: early endosome; ERC: endocytic recycling compartment; GGA: golgi-localized, γ-ear-containing ARF binding; GSV: GLUT4 storage vesicles; PIST: PDZ protein interacting specifically with TC10; PM: plasma membrane; TGN: trans-Golgi network; TUG: tether containing UBX domain for GLUT4; Ubc9: ubiquitin Carrier Protein 9.

2.1.3. Tether containing UBX domain for GLUT4 (TUG)

In recent years the role of TUG in GLUT4 trafficking has been investigated. TUG is abundantly present in GSVs but not in TR-positive structures and has been associated with sequestration of GSVs in unstimulated cells (Bogan et al. 2003, Yu et al. 2007, Rubin and Bogan 2009) (Figure I-5). In fact, it has been shown that TUG ablation causes an increase of GLUT4 surface levels and dispersion throughout the endosomal system in the absence of insulin, similar to insulin action (Yu et al. 2007). Conversely, TUG overexpression increases the rapidly mobilizable pool of GLUT4 in unstimulated 3T3-L1 cells (Bogan et al. 2003). TUG has been proposed to mediate GSV intracellular sequestration by linking GLUT4 to golgin-160 located in the TGN (Williams et al. 2006, Bogan et al. 2012, Belman et al. 2014). By doing so, TUG "tethers" GSVs to a TGN subdomain in the absence of insulin. Moreover, the presence of insulin induces cleavage of TUG which separates its N-terminal region binding the large cytoplasmic loop of GLUT4 from its C-terminal end binding golgin-160, releasing GSVs (Yu et al. 2007, Bogan et al. 2012, Belman et al. 2014). In addition, insulin is thought to induce TUG cleavage by activation of the Rho-family GTPase, TC10, whose effector was believed to be the PDZ protein interacting specifically with TC10 (PIST) (additional information in insulin signaling section) (Bogan et al. 2012, Belman et al. 2014).

Because GLUT4 in GSVs still traffics through the TGN and endosomal compartments and GSVs still reach the PM in unstimulated cells, it is more likely that TUG constrains GSV traffic rather than statically hold GSVs to the TGN subdomain (Rubin and Bogan 2009).

2.1.4. Syntaxin 6 (STX6)

Syntaxin 6 is part of the family of target SNAREs (N-ethylmaleimide-sensitive factor attachment protein receptor) and is expressed in a subdomain of the TGN that contains Syntaxin 16 but that excludes the typical TGN markers TGN38 and furin (Martin et al. 1994, Karylowski et al. 2004, Huang and Czech 2007). It has been shown that STX6 expression increases during adipocyte differentiation (Shewan et al. 2003). STX6 and Syntaxin 16 have also been implicated in ERC to TGN GLUT4 traffic (Mallard et al. 2002, Shewan et al. 2003, Proctor et al. 2006). Furthermore, STX6 has been observed in GSVs (Perera et al. 2003, Shewan et al. 2003) and it has been proposed that it is necessary for the sorting of GLUT4 and IRAP into this compartment (Perera et al. 2003, Watson et al. 2008).

2.1.5. Ubiquitin Carrier Protein 9 (Ubc9)

The small ubiquitin-related modifier (SUMO)-conjugating enzyme, Ubc9, has been associated with GLUT4 turnover. GLUT4 has a long half-life of approximately 48 hours (Sargeant and Pâquet 1993); nonetheless, it is believed that GLUT4 is sorted away from the continuously recycling pathway (cycle 1) to avoid lysosomal degradation (Rubin and Bogan 2009, Foley et al. 2011). Overexpression of Ubc9 reduces GLUT4 degradation and promotes GLUT4 sorting into GSVs; conversely, Ubc9 knockdown accelerates GLUT4 degradation and reduces GLUT4

presence in GSVs (Giorgino et al. 2000, Liu et al. 2007). In addition to its effects on GLUT4 levels, Ubc9 knockdown reduces the abundance of IRAP, sortilin and Syntaxin-6 (Rubin and Bogan 2009). The exact Ubc9 modus operandi is not yet defined but evidence suggests that Ubc9 binds GLUT4 and shepherds it to GSVs, thereby sparing GLUT4 from degradation (Giorgino et al. 2000, Foley et al. 2011) (Figure I-5). Moreover, data suggests that Ubc9's role in GLUT4 turnover and targeting to GSV is independent of its catalytic activity since overexpression of the catalytically inactive mutant of Ubc9 produced the same effects as overexpression of wild-type Ubc9 (Liu et al. 2007).

2.1.6. Akt substrate of 160 kDa (AS160)

Akt substrate of 160 kDa, originally named TBC1 domain family member 4 (TBC1D4), contains two phosphotyrosine binding domains (PTB) at the N-terminus and a Rab GTPase activating protein (GAP) domain at the C-terminus (Nagase et al. 1998, Mîinea et al. 2005). AS160 is present in GSVs, where it binds to the cytosolic C-terminus of IRAP, and plays a pivotal role in insulin-stimulated GLUT4 translocation (Kane et al. 2002, Sano et al. 2003, Larance et al. 2005, Peck et al. 2006). Using non-phosphorylatable and GAP domain AS160 mutants it was possible to unveil that in the basal state, activated GSV-bound AS160 maintains its targets, GTPase Rab proteins, in an inactive, GDP-bound state. Upon insulin action (additional information in the Insulin Signaling section), Akt phosphorylates AS160, which renders its GAP domain inactive, thereby relieving the inhibitory effect of AS160 on its target Rab proteins (Kane et al. 2002, Sano et al. 2003, Zeigerer et al. 2004, Eguez et al. 2005, Larance et al. 2005). Active GTP-bound Rab proteins regulate movement, speed, and docking of GSVs with the PM; hence, preparing vesicles for fusion (Gonzalez and McGraw 2006, Xiong et al. 2010). Furthermore, Ramm and colleagues proposed that interaction of 14-3-3 proteins with phosphorylated AS160 is also necessary for GLUT4 translocation to the PM in response to insulin and suggested that 14-3-3 proteins may help to regulate AS160 GAP activity (Ramm et al. 2006). Later, the same research group proposed that the PTB domain of AS160 interacts with the PM to facilitate GLUT4 trafficking. They suggested a model in which in the absence of insulin, GSVs bind to the PM through AS160's PTB domain but that without further interaction the vesicle dissociates from the membrane. Furthermore, in the presence of insulin, activated Akt phosphorylates AS160 upon PTB binding to the PM causing 14-3-3 proteins bind to AS160 and that leads to inhibition of AS160 GAP activity and therefore GTP loading of Rab proteins (Tan et al. 2012) (Figure I-6).

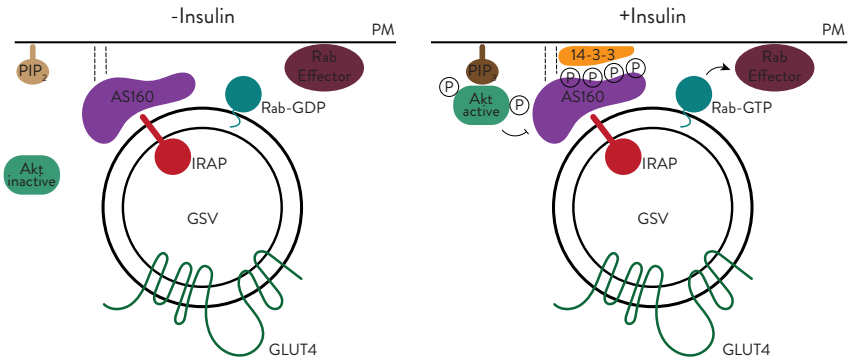

Figure I-6. Model for the role of AS160 in GLUT4 trafficking. Akt: protein kinase B or PKB; AS160: Akt substrate of 160 kDa; GSV: GLUT4 storage vesicles; IRAP: insulin-regulated aminopeptidase; PIP_2: phosphatidylinositol-4,5-bisphosphate; PIP_3: phosphatidylinositol-3,4,5-triphosphate; PM: plasma membrane.

2.1.7. Rab proteins

Rab proteins are critical organizers of intracellular membrane trafficking and GLUT4 vesicle sorting relies heavily on these small GTPases. Rabs are considered molecular switches that oscillate between a GDP-bound (off) and a GTP-bound (on) state and that link signal transduction cascades to molecular effectors. When activated, Rab proteins interact with their effector proteins in order to regulate intracellular trafficking (Zerial and McBride 2001). Although Rab involvement in GLUT4 trafficking is yet to be completely defined, several Rab proteins have been suggested to participate in the process. In adipocytes and muscle cells, Rab4, Rab5, Rab8, Rab10, Rab11, Rab14 and RAB31 have been implicated in regulating different steps of GLUT4 sorting (Zaid et al. 2008, Foley et al. 2011, Leto and Saltiel 2012) (Figure I-7).

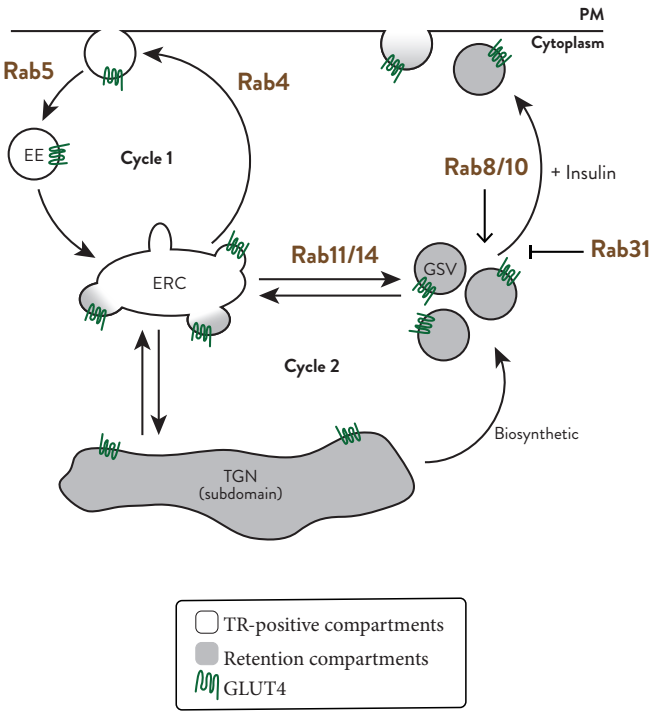

Figure I-7. Rab proteins involved in GLUT4 trafficking. EE: early endosome; ERC: endocytic recycling compartment; GSV: GLUT4 storage vesicles; PM: plasma membrane; TGN: trans-Golgi network.

2.1.7.1. Rab4

Rab4 has been proposed to promote fast recycling of GLUT4 from EE (Figure I-7). This function has been suggested due to Rab4's role in protein sorting in other systems and due to the observation that changing Rab4 expression in adipocytes affects GLUT4 levels at the plasma membrane in the absence and presence of insulin (Zerial and McBride 2001, Leto and Saltiel 2012).

2.1.7.2. Rab5

Rab5 has been suggested to regulate mobility and sorting of GLUT4-containing vesicles after endocytosis by regulating the attachment of EE to microtubules (Figure I-7) (Zerial and McBride 2001, Huang et al. 2001, Leto and Saltiel 2012). Furthermore, it has been suggested that insulin reduces Rab5 activity to reduce endocytosis and, therefore, favoring the localization of GLUT4 at the cell surface (Huang et al. 2001). Rab5 was also reported to be necessary for insulin-stimulated phosphatidylinositol 3-phosphate (PI(3)P) production which is an essential step in the insulin signaling cascade (Lodhi et al. 2008).

2.1.7.3. Rab8

Rab8 involvement in GLUT4 trafficking is specific to muscle cells. Rab8 has been identified as a target of AS160 and as such plays a major role in GLUT4 translocation to the PM (Figure I-7). It has been observed that overexpression of Rab8 rescued the inhibition of GLUT4 translocation induced by expression of a non-phosphorylatable AS160 mutant; additionally, Rab8 knockdown reduced insulin-dependent GLUT4 translocation (Ishikura et al. 2007, Ishikura and Klip 2008, Randhawa et al. 2008, Klip 2009, Sun et al. 2010).

2.1.7.4. Rab10

Rab10 is the Rab8 corresponding Rab in adipocytes; as such, Rab10 is one of the AS160 target proteins responsible for recruiting and docking GSVs near the PM during GLUT4 translocation (Figure I -9). Similarly to studies on Rab8, Rab10 knockdown reduced insulin-induced GLUT4 translocation and its re-expression rescued this effect. Additionally, the increase in basal GLUT4 PM levels caused by AS160 knockdown was partially reduced by Rab10 silencing (Bai et al. 2007, Sano et al. 2007, 2008, Sadacca et al. 2013).

2.1.7.5. Rab11

The Rab11 protein is necessary for GLUT4 exit from ERC to GSVs (Figure I-7). Rab11 inhibition traps GLUT4 in the ERC and depletes it from GSVs and, consequently, blunts insulin-stimulated translocation in adipocytes and cardiomyocytes (Zeigerer et al. 2002, Uhlig et al. 2005).

2.1.7.6. Rab14

Rab14 regulates GLUT4 sorting into GSVs (Figure I-7). It has been suggested that Rab14 and Rab10 act sequentially to regulate glucose uptake in adipocytes by mediating GLUT4 sorting and GSV activity, respectively (Sadacca et al. 2013).

2.1.7.7. Rab31

Rab31 has been implicated in GLUT4 translocation to the PM (Figure I-7). It has been suggested that Rab31 negatively regulates GLUT4 translocation in adipocytes since its overexpression blocks insulin-stimulated GLUT4 translocation, whereas its knockdown has the inverse effect (Lodhi et al. 2007, Leto and Saltiel 2012). Rab31 activation depends on the GTPase activating protein and VPS9 domains 1 (also known as Gapex-5), its guanine nucleotide exchange factor (GEF). In the absence of insulin, Gapex-5 activates Rab31 but, in the presence of insulin, activated TC10 (Rho-family GTPase) relocates Gapex-5 and its binding partner CIP4 (Cdc42-interacting protein 4) to the plasma membrane; thus, reducing Rab31 activity (Lodhi et al. 2007).

2.1.8. Exocyst

Exocyst is crucial for GLUT4 insertion in the plasma membrane (Figure I-8). This octameric protein complex tethers GLUT4 vesicles to the PM. In the presence of insulin, exocyst assembles at the plasma membrane through an insulin-driven interaction of TC10 and the exocyst scaffolding subunit EXO70 (exocyst complex component 7). Once at the PM, the exocyst SEC5 (exocyst complex component SEC5) subunit recognizes and interacts with the GSV small-GTPase, RALA (Ras like proto-oncogene A), which is activated (GTP-bound) in the presence of insulin. Briefly, in the presence of insulin, Akt phosphorylates and inactivates RAL-GAP which keeps RALA in its GDP-bound form (inactive). Inactivation of RAL-GAP allows GTP loading and subsequent activation of RALA. After tethering, the exocyst disengages to allow the fusion of GSVs with the PM (Inoue et al. 2003, Munson and Novick 2006, Leto and Saltiel 2012).

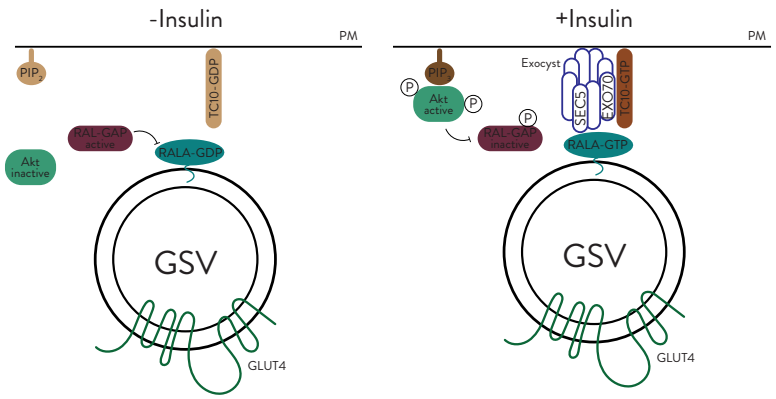

Figure I-8. Model for exocyst assembly and GSV plasma membrane tethering. Akt: protein kinase B or PKB; EXO70: exocyst complex component 7; GSV: GLUT4 storage vesicles; PIP_2: phosphatidylinositol-4,5-bisphosphate; PIP_3: phosphatidylinositol-3,4,5-triphosphate; PM: plasma membrane; RALA: Ras like proto-oncogene A; SEC5: exocyst complex component SEC5.

2.1.9. SNARE (N-ethylmaleimide–sensitive factor attachment protein receptor) ternary complex

GSV fusion with the PM is the last step in GLUT4 translocation (Figure I-9). GSV fusion with the PM is driven by the SNARE ternary complex: VAMP2 (v-SNARE at GSV), Syntaxin 4 (tSNARE at PM) and SNAP23 (synaptosomalassociated protein 23) (accessory protein at PM) (Bryant and Gould 2011, Leto and Saltiel 2012, Sadler et al. 2015). The mechanism of fusion is not completely defined but it has been proposed that in the absence of insulin, the regulatory proteins MUNC18C (protein unc-18 homolog C) and SYNIP (STX4-interacting protein) block the interaction of VAMP2 with its target Syntaxin 4 and therefore preventing GSV fusion. Upon insulin stimulation, SYNIP is phosphorylated by Akt and released from Syntaxin 4, exposing Syntaxin 4 binding site, and MUNC18C undergoes conformational changes that in turn facilitate the interaction between Syntaxin 4 and VAMP2. CDP138 (138 kDa C2 domain-containing phosphoprotein) also acts as a positive regulator of GSV fusion after phosphorylation by Akt. However, its exact role in the process is unclear. Assembly of VAMP2-Syntaxin 4-SNAP23 complex induces GSV fusion with the PM (Min et al. 1999, Watson et al. 2004a, Yamada et al. 2005, Foley et al. 2011, Xie et al. 2011, Leto and Saltiel 2012).

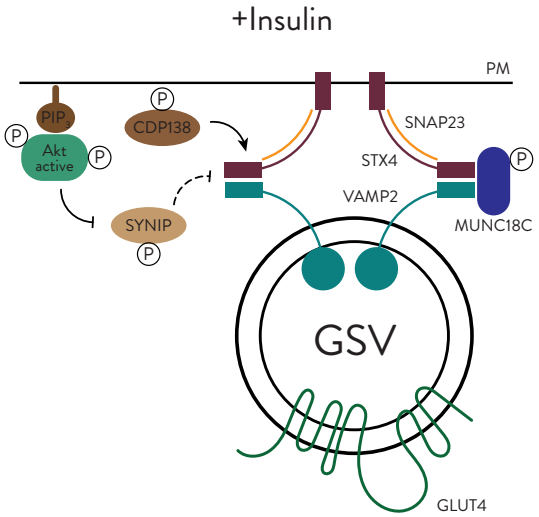

Figure I-9. Model for SNARE complex formation and GSV fusion with the plasma membrane. Akt: protein kinase B or PKB; CDP138: 138 kDa C2 domain-containing phosphoprotein; GSV: GLUT4 storage vesicles; MUNC18C: protein unc-18 homolog C; PIP_3: phosphatidylinositol-3,4,5-triphosphate; PM: plasma membrane; STX4: Syntaxin 4; SYNIP: STX4-interacting protein; VAMP2: vesicle-associated membrane protein 2; SNAP23: synaptosomalassociated protein 23.

2.2. GLUT4 TRAFFICKING MOTIFS

Regulation of GLUT4 trafficking by the cellular machinery requires the reading and recognition of a variety of motifs embodied in GLUT4. Several studies have attempted to identify these domains and although there is general agreement on the motifs, their roles still generate controversy.

GLUT4 contains four major motifs that together with the cellular machinery orchestrate

its trafficking: FQQI[8] (N-terminus), large cytoplasmic loop between transmembrane domain VI and VII, dileucine motif (LL[490]) and TELEY[502] (C-terminus) (Figure I-10).

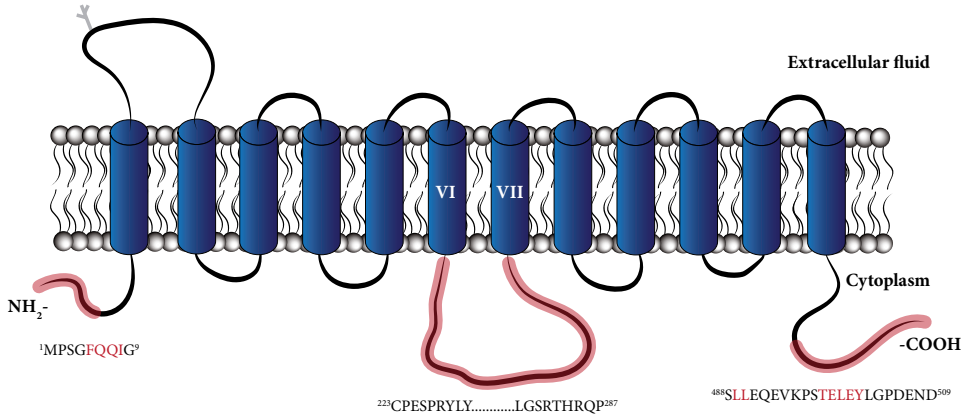

Figure I-10. GLUT4 trafficking motifs. Red letters represent FQQI[8], LL[490] and TELEY[502] motifs. Red areas represent N-terminus, large cytoplasmic loop and C-terminus.

FQQI[8] and TELEY[502] are the most intensively studied motifs and while some studies suggest that the N-terminus FQQI[8] motif is the major determinant for intracellular trafficking and endocytosis (Piper et al. 1993, Marsh et al. 1995, Palacios et al. 2001, Al-Hasani et al. 2002, Blot and McGraw 2006), others emphasize the role of the TELEY[502] motif (Shewan et al. 2000, 2003, Govers et al. 2004). Comparison of the various studies is often challenging due to the variety of methodology and cell systems employed. Notwithstanding, more recent studies have further analyzed the roles of these GLUT4 motifs which helped conciliate the different data and reach some agreement on the matter (Figure I-11). By mutating FQQI[8], TELEY[502] or both motifs in adipocytes, Blot and McGraw (Blot and McGraw 2008) suggested that both N-terminus FQQI[8] and C-terminus TELEY[502] motifs are required for full basal intracellular retention of GLUT4 in adipocytes. These motifs however, regulate different steps of GLUT4 traffic. The FQQI[8] motif, a member of the aromatic-based internalization motif family, mediates GLUT4 trafficking between the ERC and the TGN subdomain. TELEY[502], on the other hand, mediates sorting from ERC to GSVs. It is important to note that the TELEY[502] motif probably requires additional amino acid residues for correct functioning. Based on sequence similarity between IRAP and GLUT4, Song and colleagues identified the following TELEY cluster: TELEYLXPDEXD (Xiao et al. 2008).

Additionally, the FQQI[8] motif serves as the recognition domain for adaptor protein 2 (AP-2) binding which is required for clathrin-mediated endocytosis, and mutating the phenylalanine to alanine results in loss of GLUT4 from clathrin-coated pits (Al-Hasani et al. 2002, Owen et al. 2004, Blot and McGraw 2006). However, recent data suggests that GLUT4 internalization through clathrin-mediated endocytosis occurs mainly in the presence of insulin (Blot and McGraw 2006, 2008, Antonescu et al. 2009) (additional information in Endocytosis section).

The dileucine motif is a member of the LL-based family of trafficking motifs and its function in GLUT4 trafficking is not well defined. However, it has been proposed that upon insulin

withdrawal, the LL^{490} motif in cooperation with adaptor protein complex 1 (AP-1) sorts GLUT4 from EE to ERC, away from the rapidly recycling membrane compartment, which is necessary for further intracellular retention by $FQQI^{8}$ and $TELEY^{502}$ motifs (Rapoport et al. 1998, Blot and McGraw 2006, 2008) (Figure I-11). The dileucine domain has also been suggested to participate in the GGA-dependent sorting of newly synthetized IRAP into GSVs (Hou et al. 2006, Watson et al. 2008). Moreover, mutations of the LL^{490} motif ultimately result in poor GLUT4 sorting into GSVs; whether the LL^{490} motif directly participates in the GSV sorting step or in any other upstream process in GLUT4 trafficking is not clear (Song et al. 2013). Additionally, the LL^{490} sequence bears similarities to motifs generally required for clathrin-mediated endocytosis and as such this motif has been implicated in GLUT4 endocytosis. However, the exact role of this motif in endocytosis is still unclear; some suggest that this motif acts during the initial rate of endocytosis while others suggest that it is only important for GLUT4 endocytosis during insulin retrieval (Corvera et al. 1994, Blot and McGraw 2006, 2008, Capilla et al. 2007, Antonescu et al. 2009).

Despite being less studied, the large cytoplasmic loop has also been suggested to regulate GLUT4 trafficking. As stated above, the large cytoplasmic loop has been suggested to be the binding site for TUG, a protein involved in GLUT4 sequestration in the basal state (Yu et al. 2007). Additionally, Capilla and colleagues (Capilla et al. 2007) generated several GLUT1/GLUT4 chimeras and determined that the N-terminal region in conjunction with the large cytoplasmic loop are sufficient to recapitulate the complete GLUT4 trafficking when placed in a GLUT1 backbone, in contrast with the inefficient intracellular retention of native GLUT1 in the basal state (Hudson et al. 1992, Yeh et al. 1995, Watson et al. 2004a). It is important to stress that substitution of both regions was necessary since none of the single-domain chimeras accomplished the full recapitulation of GLUT4 trafficking. In a previous work, the N-terminus and large cytoplasmic loop had already been suggested to be crucial for trafficking of newly synthesized GLUT4 (GGA-dependent) into GSVs (Khan et al. 2004). In the work by Capilla et al. (2007) it was also suggested that the integrity and three-dimensional structure of the large cytoplasmic loop is critical for the correct interaction with the N-terminal domain. Protein structure is often overlooked when mutating these motifs, but it is certainly important for motif-intracellular machinery interactions.

Every study on GLUT4 motifs gives away clues about the individual roles of each motif. Nonetheless, all motifs work as a whole and are required for the correct trafficking and functioning of GLUT4.

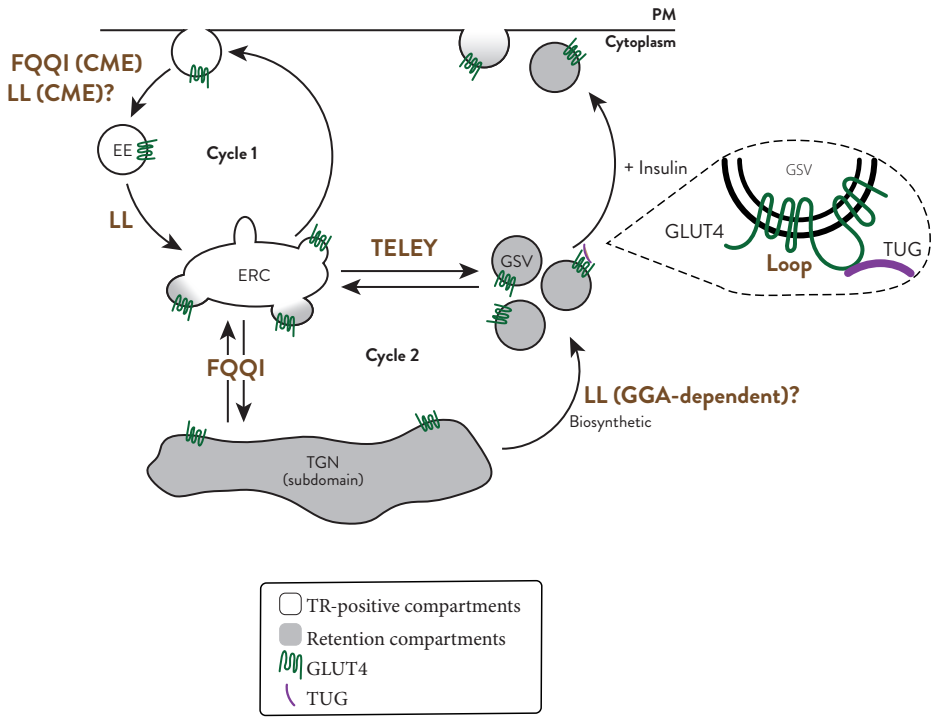

Figure I-11. Roles of GLUT4 motifs in GLUT4 cellular trafficking. EE: early endosome; ERC: endocytic recycling compartment; GGA: golgi-localized, γ-ear-containing ARF binding; GSV: GLUT4 storage vesicles; PM: plasma membrane; TGN: trans-Golgi network; TUG: tether containing UBX domain for GLUT4.

3. INSULIN SIGNALLING

Insulin plays a fundamental role in maintaining glucose homeostasis. After a meal, insulin is secreted from pancreatic β-cells and inhibits glucose output from the liver via suppression of glycogenolysis and gluconeogenesis (Gastaldelli et al. 2001, Saltiel and Kahn 2001). Nonetheless, the most significant effect of insulin is the stimulation of GLUT4 translocation to the PM and consequently the increase of glucose uptake in muscle and adipose tissue which is widely believed to be the limiting step for most glucose metabolism processes (e.g. glycolysis, glycogen synthesis, lipogenesis) (Yki-Järvinen et al. 1990, Choi and Kim 2010, Rowland et al. 2011, Leto and Saltiel 2012). Impairment in glucose transport in muscle and adipose tissues represent early defects in the onset of insulin resistance (Rothman et al. 1995).

3.1. The PI3K/Akt signaling pathway

The canonical insulin signaling pathway is initiated by hormone binding to the insulin receptor (IR) (Figure I-12). The mature cell surface IR contains two extracellular - and two transmembrane b-subunits linked by disulfide bonds forming a a2b2-heterotetrameric structure (Lee and Pilch 1994, Watson et al. 2004a). Insulin binding to the IR a-subunit induces autophosphorylation of the β-subunit and activation of intrinsic tyrosine kinase activity (Gammeltoft and Van Obberghen 1986, Rowland et al. 2011). Mutations in the human IR are very rare and represent less than 5% of all cases of type 2 diabetes (Watson et al. 2004a).

Activated tyrosine kinase phosphorylates insulin-receptor substrate (IRS) protein which generates docking sites for the src homology 2 (SH2) domain in the p85 subunit of the phosphatidylinositol-3-kinase (PI3K). Binding of IRS to the p85 regulatory subunit of PI3K induces activation of the p110 catalytic subunit of PI3K (Alessi and Downes 1998, Watson et al. 2004a, Zaid et al. 2008). Once activated PI3K, catalyzes the conversion of phosphatidylinositol-4,5-bisphosphate (PIP_2) to phosphatidylinositol-3,4,5-triphosphate (PIP_3) on the cytosolic leaflet of the PM (Corvera and Czech 1998, Choi and Kim 2010, Rowland et al. 2011). Activation of PI3K and synthesis of PIP_3 are essential for GLUT4 translocation as it has been shown that inhibition of PI3K prevents insulin-dependent GLUT4 translocation (Clarke et al. 1994, Okada et al. 1994). Furthermore, expression of constitutively active p110 subunit or addition of a PIP_3 analog to cells induces GLUT4 translocation (Martin et al. 1996, Jiang et al. 1998, Zaid et al. 2008).

PIP_3 production in the PM provides docking sites for pleckstrin homology (PH) domains of protein kinase B (PKB or Akt) and phosphoinositide-dependent protein kinase (PDK-1). At the PM, PDK-1 phosphorylates Akt on Thr308; however, Akt requires a second phosphorylation on Ser473 for full activation (Rowland et al. 2011). Because PDK-1 is not capable of further phosphorylating Akt, efforts have been made to identify the kinase responsible for this step. The mammalian target of rapamycin (mTOR) in complex with rapamycin-insensitive companion of mTOR (Rictor), mammalian lethal with SEC13 protein 8 (mLST8) and mammalian stress-activated protein kinase interacting protein 1 (mSIN1), known as the mTORC2 complex, has emerged as a strong candidate for the kinase that phosphorylates Akt at Ser473. The mTORC2 complex has been shown to directly phosphorylate Akt at Ser473 in Drosophila melanogaster and mammalian cells, including adipocytes (Sarbassov et al. 2005, Hresko and Mueckler 2005). Although it is clear that Akt activation requires three steps, namely Akt recruitment and binding to PIP_3 at the PM, phosphorylation on Thr308 and phosphorylation on Ser473, the exact order of these events is not completely established. Interestingly, there are three Akt isoforms in mammals encoded by different genes sharing more than 85 % homology; nonetheless, only deletion of the Akt2 gene results in defects in glucose metabolism (Bae et al. 2003). Moreover, Akt2 is the main isoform recruited to the PM in response to an insulin stimulus (Gonzalez and McGraw 2009).

In addition to phosphorylation of Akt on Thr308 (as referred above), PDK-1 also phosphorylates protein kinase C zeta (PKCz) on Thr410 which leads to its activation (Le Good et al. 1998, Taniguchi et al. 2006). Although PKC l/z targets are still unknown, several studies have suggested the involvement of atypical protein kinases C, such as PKC l/z, in GLUT4 translocation in response to insulin possibly by facilitating tethering of GSVs to the PM (Standaert et al. 1999, Bandyopadhyay et al. 2002, Ishiki and Klip 2005, Farese et al. 2005, 2007, Hou and Pessin 2007).

Activated Akt functions as a hub for signal transmission and is relevant for GLUT4 trafficking since Kane and colleagues identified AS160 as the main Akt substrate by using an antibody specific for the phosphorylated form of the Akt target motif (RXRXXS/T) (Kane et al.

2002). As explained in the section on GLUT4 accessory proteins (see above), AS160 is one of the major proteins involved in promoting GLUT4 translocation to the plasma membrane and the subsequent increase of glucose uptake. Active Akt phosphorylates AS160 rendering it inactive which releases its repression over its target Rabs (Rab8, Rab10) inducing GLUT4 translocation (Sano et al. 2003, Zeigerer et al. 2004, Eguez et al. 2005, Larance et al. 2005). In addition, SNARE regulatory proteins involved in GLUT4 vesicle fusion with the PM, such as SYNIP and CD138, are also direct substrates of Akt (Min et al. 1999, Yamada et al. 2005, Xie et al. 2011).

3.2. The CAP–Cbl signaling pathway

In early 2000, the Pessin and Saltiel groups proposed that insulin also initiates a PI3K-independent signaling pathway in adipocytes: the CAP–Cbl signaling pathway (Figure I-12). Activation of both PI3K-dependent and -independent pathways seems to be required for full insulin-stimulated glucose uptake in adipocytes (Baumann et al. 2000, Chiang et al. 2001).

Insulin signaling through the CAP–Cbl signaling pathway initiates with the binding of insulin to its receptor, IR. Insulin receptor undergoes activation by autophosphorylation, recruits and binds the SH2 domain of the adaptor protein APS (adapter protein substrate) and phosphorylates it on Tyr618 (Liu et al. 2002, Hu et al. 2003). In turn, activated APS recruits the c-Cbl proto-oncogene (Cbl) which forms a complex with the c-Cbl-associated protein (CAP) (Ribon et al. 1998b, Liu et al. 2002). The complex is formed by the binding of the CAP C-terminus SH3 domain to proline residues in the Cbl sequence (Ribon et al. 1998a). Once recruited to the PM, Cbl is tyrosine-phosphorylated by the IR which induces APS-Cbl-CAP complex dissociation from the insulin receptor and movement to lipid rafts, which are plasma membrane subdomains rich in cholesterol and glycosphingolipids. The association of APS-Cbl-CAP complex with lipid rafts occurs through the binding of the sorbin homology (SoHo) domain of CAP with flotillin, a lipid raft-abundant protein (Baumann et al. 2000, Kimura et al. 2001, Saltiel and Kahn 2001). After movement to lipid rafts, phosphorylated Cbl recruits the adaptor protein CrkII (Crk proto-oncogene, adaptor protein) which forms a complex with the C3G protein (guanine nucleotide-releasing factor 2, specific for Crk) (Ribon et al. 1996). C3G in turn activates the lipid raft-localized GTPase, TC10, which, once activated TC10, enhances GLUT4 translocation to the plasma membrane (additional information in the GLUT4 accessory proteins section) (Chiang et al. 2001, Watson et al. 2001). Briefly, activated TC10 recruits Gapex-5 to the PM which inactivates Rab31 (Lodhi et al. 2007). TC10 also recruits the Exocyst complex to the PM through binding of the exocyst EXO70 subunit (Inoue et al. 2003, Leto and Saltiel 2012). Recently TC10 has also been proposed to activate PIST which induces cleavage of TUG, thereby reducing GSVs intracellular retention (Bogan et al. 2012). Interestingly, it has been described that the CAP–Cbl insulin pathway is adipocyte-specific, therefore non-existent in muscle cells (Bickel 2002, JeBailey et al. 2004, Satoh 2014).

INTRODUCTION

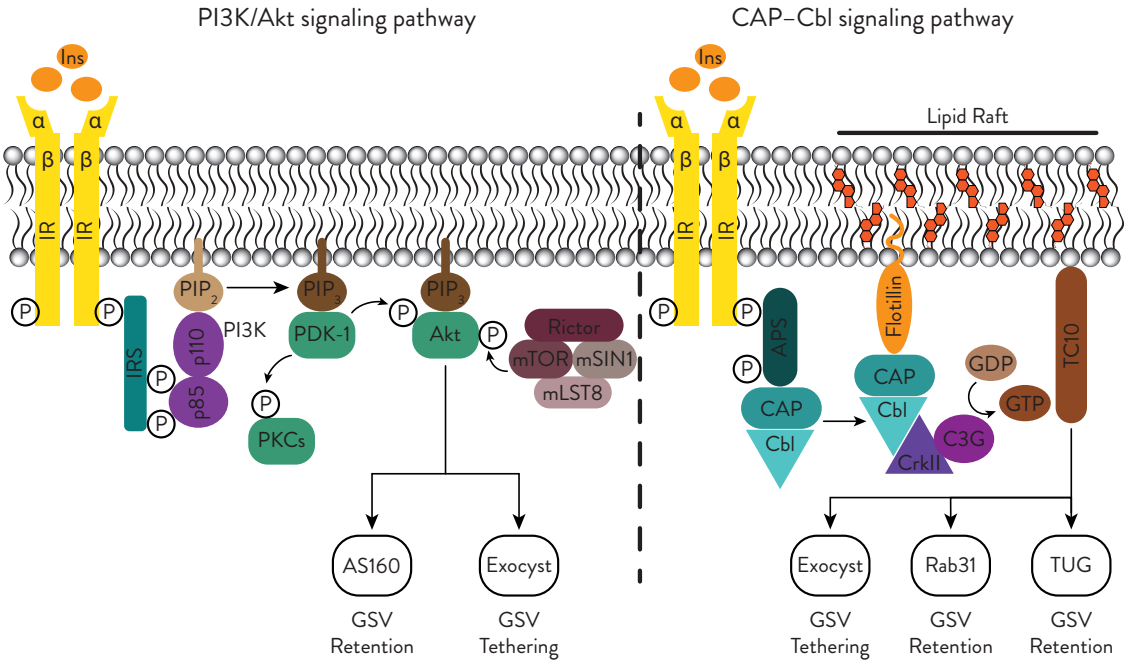

Figure I-12. Insulin signaling pathways. The canonical insulin signaling pathway (PI3K/Akt signaling pathway) is represented on the left side of the figure; the CAP–Cbl signaling pathway is represented on the right side. Schematic representation of cholesterol (orange molecules) indicates lipid rafts. Akt: protein kinase B or PKB; APS: adapter protein substrate; AS160: Akt substrate of 160 kDa; C3G: guanine nucleotide-releasing factor 2, specific for Crk; CAP: c-Cbl-associated protein; Cbl: c-Cbl proto-oncogene; CrkII: Crk proto-oncogene, adaptor protein; GSV: GLUT4 storage vesicles; Ins: insulin; IR: insulin receptor; IRS: insulin-receptor substrate; mLST8: mammalian lethal with SEC13 protein 8; mSIN1: mammalian stress-activated protein kinase interacting protein 1; mTOR: mammalian target of rapamycin; PDK-1: phosphoinositide-dependent protein kinase; PI3K: phosphatidylinositol-3-kinase; PIP_2: phosphatidylinositol-4,5-bisphosphate; PIP_3: phosphatidylinositol-3,4,5-triphosphate; PKC: protein kinase C; Rictor: rapamycin-insensitive companion of mTOR; TUG: tether containing UBX domain for GLUT4.

4. ENDOCYTOSIS

Endocytosis is a fundamental cellular process that allows cells to internalize various molecules. This mechanism intimately regulates nutrient uptake, signaling, pathogen entry, synaptic transmission, receptor downregulation, antigen presentation, and several other essential cellular processes. It is the coordination of endocytic and exocytic events at the plasma membrane that control the interaction of the cell with its environment.

Mammalian cells display a variety of endocytic pathways (Kirkham and Parton 2005, Mayor and Pagano 2007, Doherty and McMahon 2009, Mayor et al. 2014). The scientific community has been active in trying to understand the functioning of these pathways but although some of the cargos of the various endocytic pathways are known, the mechanisms and molecules that direct and regulate them are still poorly understood.

In this introduction we will cover solely five routes of internalization and based on the requirement for clathrin, cholesterol and dynamin, the internalization pathways can be organized as shown in Figure I-13.

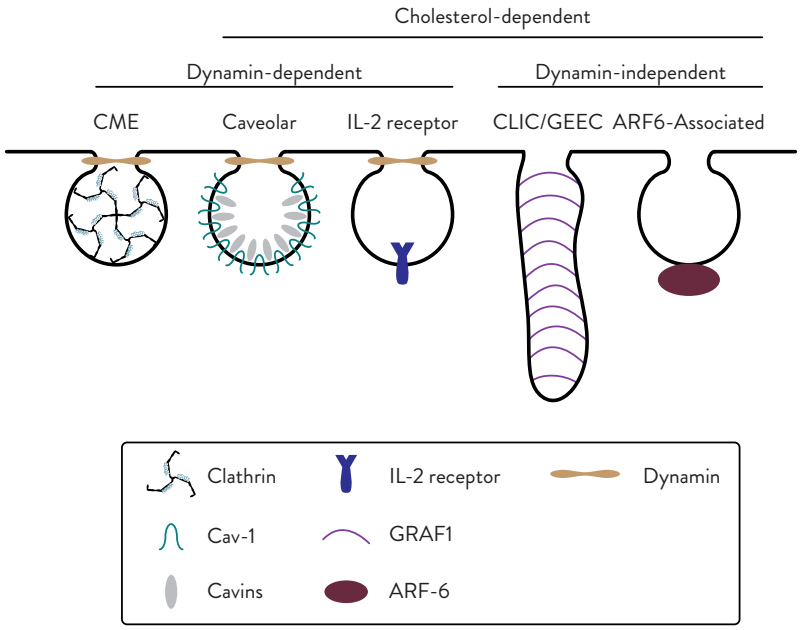

Figure I-13. Schematic representation of endocytic pathways. ARF6: ADP-ribosylation factor 6; Cav-1: caveolin-1; CME: clathrin-mediated endocytosis; CLIC/GEEC: clathrin-independent carrier/GPI-AP-enriched early endosomal compartment; GRAF1: GTPase regulator associated with focal adhesion kinase 1; IL-2: interleukin 2.

4.1. Clathrin-mediated endocytosis (CME)

CME is the best studied endocytic mechanism. It is characterized by the involvement of clathrin, a triskelion-shaped scaffold protein composed of three 190 kDa heavy chains, each with an associated 23-26 kDa light chain (Takei and Haucke 2001, Kirchhausen 2009). The endocytic event through CME starts with the binding of FCHO (FCH domain only) proteins to PIP_2-rich areas of the PM and recruitment of EPS15 (EGFR pathway substrate 15) and intersectins (Jost et al. 1998, Henne et al. 2010). Assembly of these proteins at the PM is thought to recruit AP-2 which in turn leads to binding of clathrin that polymerizes into pentagons and hexagons to form the clathrin-coated pit (CCP) (Mousavi et al. 2004, McMahon and Boucrot 2011). AP-2 serves as an adaptor protein that binds simultaneously the PM, cargo molecules, and clathrin. Dynamin (GTPase) is recruited at the neck of the forming vesicle, self-polymerizes and, upon GTP hydrolysis, mediates the fission of the vesicle from the PM leading to the formation of a 100-150 nm-diameter clathrin-coated vesicle (CCV). The clathrin coat is subsequently released from the vesicle by auxilin and hsc70 (heat shock cognate 71 kDa protein) and becomes available for another round of clathrin coat formation (Schlossman et al. 1984, Ungewickell et al. 1995, Mousavi et al. 2004, McMahon and Boucrot 2011). Since the roles of clathrin and AP-2 in this pathway are extremely important, knockdown or interference with their function results in CME inhibition (Hinrichsen et al. 2003, Blot and McGraw 2006, Antonescu et al. 2008). In addition, hypertonic sucrose disrupts CME by altering the morphology of assembled clathrin (Heuser and Anderson 1989, Antonescu et al. 2008). Transferrin receptor and G protein-coupled receptors are typical cargos of CME (Doherty and McMahon 2009).

4.2. Cholesterol-dependent endocytosis (Clathrin-independent endocytosis)

Although CME is a major endocytic mechanism, accounting for a large portion of internalization events, there is a variety of endocytic pathways independent of clathrin but dependent of cholesterol. Cholesterol-dependent pathways can be divided based on dynamin requirement for vesicle scission. In this introduction we will take only four of them into consideration: Two dynamin-dependent and two dynamin-independent pathways as shown in Figure I-13. Interestingly, despite the pathway of entry, eventually all routes merge at the Rab5-positive EE, indicating some degree of communication between the various pathways (Mayor and Pagano 2007, Doherty and McMahon 2009).

4.2.1. Caveolar pathway

Caveolar endocytosis represents the best studied clathrin-independent and cholesterol-dependent endocytic pathway. Caveolae (or little caves) are a subtype of lipid rafts and consist of 50-100 nm flask-shaped PM invaginations rich in sphingolipids and cholesterol (Rothberg et al. 1992, Kurzchalia et al. 1992, Simons and Ikonen 1997, Kurzchalia and Parton 1999, Mayor and Pagano 2007). Caveolae function as endocytic structures but they are also important platforms for cellular signaling (Parton and Simons 2007, Parton and Del Pozo 2013). In adipocytes, caveolae represent 30 % of the PM surface and are characterized by the presence of a palmitoylated integral membrane protein that binds to cholesterol, named caveolin-1 (Cav-1) (Fan et al. 1983, Kurzchalia and Parton 1999). Caveolin-1 possesses a hairpin domain embedded within the PM while its N-and C-terminus face the cytoplasm (Williams and Lisanti 2004). Caveolae are stabilized by approximately 140 molecules of oligomeric caveolin-1 per caveolae as well as by 30-70 molecules of caveolin-2 (Cav-2). Additionaly, caveolae stability has been shown to also require proteins of the cavins family, more specifically cavin-1, -2 and -3 (Liu and Pilch 2008, Hansen and Nichols 2010, Parton and Del Pozo 2013, Mayor et al. 2014, Kovtun et al. 2015). In muscle cells however, Cav-1 and Cav-2 are replaced by Cav-3 and, in addition to cavin-1, -2 and -3, these cells express cavin-4 as well (Bastiani et al. 2009, Briand et al. 2011, Parton and Del Pozo 2013). Moreover, the Eps15 homology domain-containing 2 (EHD2) protein negatively constrains caveolar dynamics through interaction with Cav-1 and cavin-1 (Moren et al. 2012). As stated above, caveolae endocytosis requires cholesterol since its depletion collapses caveolae and increases Cav-1 mobility (Rothberg et al. 1992, Doherty and McMahon 2009, Breen et al. 2012) and, similarly to CCV, budding of caveolae also requires the GTPase dynamin (Henley et al. 1998, Oh et al. 1998, Mayor et al. 2014). After scission, some vesicles refuse directly with the PM, whereas others reach the EE in a Rab5-dependent manner before being recycled back to the PM (Hayer et al. 2010, Mayor et al. 2014). Several molecules internalize through this pathway, including the cholera toxin B subunit (CTB), simian virus (SV40), glycosylphosphatidylinositol-anchored proteins (GPI-APs), glycosphingolipid analogs, β1 integrins and excitatory amino-acid carrier 1 (EAAC1) glutamate transporter (Mayor and Pagano 2007, Antonescu et al. 2009).

4.2.2. IL-2 receptor endocytic pathway

The internalization of the interleukin 2 (IL-2) receptor occurs through a cholesterol- and dynamin- dependent but caveolae-independent pathway (Lamaze et al. 2001, Mayor and Pagano 2007, Doherty and McMahon 2009, Antonescu et al. 2009). Electron microscopy studies reveal that IL-2 receptors concentrate and bud in small (50-100 nm) uncoated vesicles (Lamaze et al. 2001, Mayor et al. 2014). This pathway is dependent on the small GTPase RhoA and is regulated by PI3K (Lamaze et al. 2001, Gesbert et al. 2004, Basquin et al. 2013). Briefly, IL-2 receptor interacts with the p85 subunit of PI3K, which leads to the production of PIP_3 at the PM. In turn, PIP_3 induces GEF-mediated activation of Rac1 (Ras-related C3 botulinum toxin substrate 1) which also binds p85. Activation of Rac1 ultimately leads to actin polymerization via neuronal Wiskott-Aldrich syndrome protein (N-WASP) that together with dynamin mediate vesicle budding (Grassart et al. 2008, 2010, Basquin and Sauvonnet 2013). The role of RhoA role in this pathway is unclear; it is known that overexpression of an inactive form of RhoA abolishes IL-2 internalization (Lamaze et al. 2001) but whether RhoA is required for the correct sorting of the IL-2 receptor into the endocytic pathway or during the endocytic process itself is currently unknown. Along with the IL-2 receptor, other molecules use this route, including the gamma chain (γ-c) receptor, Immunoglobulin E (IgE) and lectin-like oxidized low-density lipoprotein receptor-1 (LOX-1) (Antonescu et al. 2009).

4.2.3. CLIC/GEEC pathway

Among the cholesterol-dependent pathways, some are dynamin-independent. One of such pathways is the clathrin-independent carrier/GPI-AP-enriched early endosomal compartment (CLIC/GEEC) pathway (Kirkham and Parton 2005, Kalia et al. 2006). The CLIC/GEEC endocytic pathway is mediated by uncoated tubulovesicular primary carriers, the CLICs, that bud rapidly from the PM and acquire Rab5 and early endosome antigen-1 (EEA-1), maturing into the GEEC before fusing with EE (Kirkham et al. 2005, Kalia et al. 2006). Internalization through this pathway requires cycling of the Rho family GTPase cell division cycle 42 (cdc42) between its active (GTP-bound) and inactive (GDP-bound) states.

Dynamic Cdc42 cycling is critical for recruitment of the actin polymerization machinery (Chadda et al. 2007, Schultz et al. 2014, Mayor et al. 2014). Internalization through this pathway is initiated by activation of ARF1 (ADP-ribosylation factor 1) which recruits the Rho GTPase activating protein 10 (ARHGAP10), that in turn inactivates cdc42 (cdc42 GDP-bound state) (Kumari and Mayor 2008, Kumari et al. 2010). Another regulator of cdc42 and CLIC/GEEC pathway is the GTPase regulator associated with focal adhesion kinase 1 (GRAF1), that, like ARHGAP10, can inactivate cdc42 and that has been suggested to act as a vesicular "coat" in this pathway (Lundmark et al. 2008, Kumari et al. 2010, Kim et al. 2017). Cdc42 GTP reloading is facilitated by GEF proteins (Schultz et al. 2014).

This pathway mediates internalization of GPI-APs, CD44 (cluster of differentiation 44),

dysferlin, CTB, vacuolating cytotoxic A (VacA) and large bulks of fluid phase (Sabharanjak et al. 2002, Gauthier et al. 2005, Kirkham and Parton 2005, Kumari et al. 2010, Howes et al. 2010).

4.2.4. ARF6-Associated Pathway

Another cholesterol-dependent and dynamin-independent pathway is the ARF6-associated route. Several proteins such as class I major histocompatibility complex molecules (MHC I), GLUT1, E-cadherin, b1 integrin, carboxypeptidase E and GPI-APs internalized through this route (Naslavsky et al. 2004, Eyster et al. 2009, Grant and Donaldson 2009, Mayor et al. 2014). In this pathway, active GTP-bound ARF6 facilitates cargo internalization using energy from GTP hydrolysis; ARF6-GDP is also internalized and fuses with ERC. In the ERC, GEF such as Grp1-associated scaffold protein (GRASP) in cooperation with Grap-1 activate ARF6 (ARF6-GTP). ARF6-GTP relocates to the PM and can initiate a fresh round of ARF6-dependent internalization (Grant and Donaldson 2009, Venkataraman et al. 2012). Interestingly, in this model ARF6 inactivation is important for internalization whereas ARF6 activation is required for recycling to the PM.

5. GLUT4 ENDOCYTOSIS

Study of GLUT4 traffic revealed that this transporter is continuously cycling between intracellular compartments and the PM and that regulation of such recycling is essential for GLUT4 functioning since it can only transport glucose when localized at the PM. The distribution of GLUT4 at the plasma membrane is determined by the balance between its exocytosis and endocytosis; therefore, it is crucial to understand both mechanisms. GLUT4 exocytosis has been studied extensively, whereas GLUT4 endocytosis and its regulation have not been studied as much.

Despite some controversy, insulin is believed to reduce the rate of GLUT4 endocytosis in 3T3-L1 adipocytes and by doing so extends GLUT4 presence at the PM (Blot and McGraw 2006, Hou and Pessin 2007, Leto and Saltiel 2012). Additionally, Blot and McGraw (2006) suggested that insulin induces a change of GLUT4 internalization pathways in 3T3-L1 adipocytes. GLUT4 has been shown to use at least two internalization pathways: a clathrin-mediated and a cholesterol-dependent pathway (Robinson et al. 1992, Ros-Baro et al. 2001, Shigematsu et al. 2003, Blot and McGraw 2006, Antonescu et al. 2009) (Figure I-14a). In the absence of insulin, most GLUT4 endocytosis (80 %) occurs through a cholesterol-dependent pathway, as shown by the reduction of GLUT4 internalization upon nystatin treatment (cholesterol-aggregating drug); the remaining GLUT4 enters the cell by a nystatin-resistant and AP-2-dependent pathway: the CME. The presence of insulin inhibits the nystatin-sensitive route and GLUT4 internalizes solely through the CME pathway (Figure I-14a) (Blot and McGraw 2006). Consistent with this, insulin causes an increase in GLUT4 presence within clathrin puncta at the PM in adipocytes (Huang et al. 2007). Blot and McGraw (2006) also demonstrated that internalization through CME, but not cholesterol-dependent endocytosis, required the GLUT4 N-terminus motif FQQI[8]

while being independent of the LL^{490} motif. The $FQQI^{8}$ sequence is similar to the tyrosine-sorting signal sequence, YXXØ (Y, tyrosine; X, any amino acid; Ø, bulky hydrophobic residue), that is recognized by the AP-1 and AP-2 proteins (Bonifacino and Dell'Angelica 1999). $FQQI^{8}$ possesses a phenylalanine instead of a tyrosine in the first position, which results in a weaker interaction with AP-2 (Al-Hasani et al. 2002, Bonifacino and Traub 2003). Because $FQQI^{8}$ interaction with AP-2 is suboptimal, GLUT4 internalization through CME is slower as shown by comparing the $FQQI^{8}$-GLUT4 and $YQQI^{8}$-GLUT4 internalization rates (Blot and McGraw 2006). It is then reasonable to suggest that in adipocytes, both the shift of the predominant internalization pathway and the use of a suboptimal internalization motif contribute to slow down GLUT4 endocytosis in the presence of insulin.

In the work of Blot and McGraw (2006) it was not disclosed what was the specific cholesterol-dependent endocytic pathway involved in GLUT4 internalization. However, the bulk of studies suggest that caveolar endocytosis is the predominant GLUT4 cholesterol-dependent and clathrin-independent internalization pathway in adipocytes due to the abundance of caveolae in adipocytes (30 % of the PM surface) and to GLUT4 presence in these structures (Scherer et al. 1994, Ros-Baro et al. 2001, Shigematsu et al. 2003, Antonescu et al. 2009). Interestingly, the ARF6-associated pathway has also been associated with GLUT4 endocytosis since the transporter was observed in vesicle formation induced by ARF6 in 3T3-L1 adipocytes (Li et al. 2012). Further studies are required to assess the importance of this pathway in GLUT4 endocytosis.

In muscle cells, GLUT4 is also able to internalize through a clathrin-mediated and a cholesterol-dependent pathway as shown by Dr. Klip's group (Figure I-14b). Studies done by this group showed that GLUT4 internalization in L6 muscle cells was inhibited in part by hypertonicity or clathrin heavy-chain knockdown and in part by cholesterol depletion using methyl-β-cyclodextrin (cholesterol-depleting agent); thus, underscoring the participation of a clathrin-mediated and a cholesterol-dependent pathways in GLUT4 internalization (Li et al. 2001, Antonescu et al. 2008). In contrast to adipocytes, caveolae are not abundant in the PM of muscle cells and GLUT4 internalization is not perturbed by caveolae disruption; therefore, it has been suggested that, in muscle cells, cholesterol-dependent internalization of GLUT4 does not occur through the caveolar route. Alternatively, the IL-2 receptor pathway has been proposed to be the default cholesterol-dependent internalization route in muscle cells (Antonescu et al. 2008, 2009). In support of this notion, IL-2 receptor colocalizes with GLUT4 at the cell surface in L6 myoblasts; furthermore, electron microscopy shows that GLUT4 is present in CCP and in uncoated pits at the PM, which suggests that apart from CME, GLUT4 internalizes through a route that involves uncoated vesicles (Antonescu et al. 2008, 2009). Moreover, the study by Antonescu and colleagues (2008) showed that the clathrin- and caveolae- independent internalization of GLUT4 was dynamin-dependent, like the IL-2 receptor pathway. In addition, the authors suggested that in L6 cells, half of GLUT4 internalization occurs through CME and the other half through the IL-2 receptor pathway.

It has also been shown that insulin does not affect GLUT4 internalization in L6 cells and cardiomyocytes (Li et al. 2001, Yang and Holman 2005, Antonescu et al. 2008). However, several studies using 2,4-Dinitrophenol (DNP) (energy stress-inducing drug) suggest that muscle contraction might lead to reduction of GLUT4 endocytosis through increase of Ca2+ and activation of AMP-activated protein kinase (AMPK) and PKCs (Khayat et al. 1998, Wijesekara et al. 2006, Li et al. 2014). Interestingly, activation of AMPK and PKCs reduced GLUT4 and IL-2 receptor endocytosis without affecting the internalization through CME as measured by TR internalization (Antonescu et al. 2008). These data suggest that muscle contraction halts the endocytosis of GLUT4 through the IL-2 receptor pathway (Figure I-14b).

Although endocytosis plays an important role in GLUT4 trafficking in both adipocytes and muscle cells, the operating mechanisms are different. In adipocytes and muscle cells, GLUT4 internalization occurs through a CME and a cholesterol-dependent pathway. However, in adipocytes the caveolar pathway seems to be the cholesterol-dependent route involved whereas in muscle cells the IL-2 receptor pathway operates instead. Moreover, insulin reduces GLUT4 endocytosis exclusively in adipocytes (inhibiting cholesterol-dependent route) while signals generated from muscle contraction delay GLUT4 internalization (throught the IL-2 receptor route) in muscle cells.

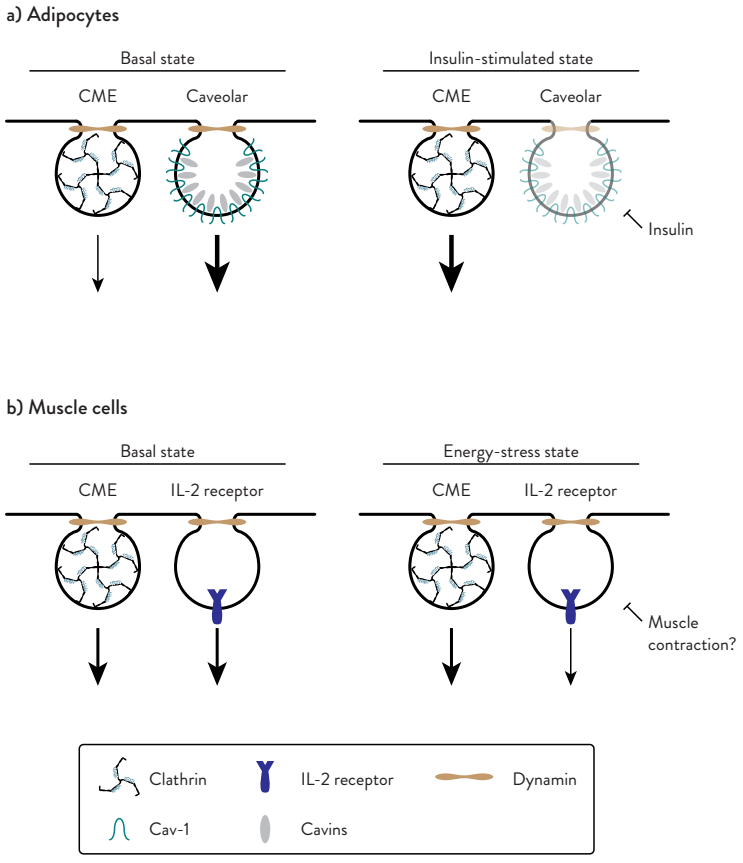

Figure I-14. Schematic representation of GLUT4 endocytic pathways in adipocytes (a) and muscle cells (b). Arrows indicate GLUT4 internalization; arrow thickness represents amount of GLUT4 internalization. Cav-1: caveolin-1; CME: clathrin-mediated endocytosis; IL-2: interleukin 2.

6. GLUCOSE TRANSPORTERS IN FISH

In fish, metabolism and energy supply rely strongly in an amino acid-rich diet. Nonetheless, fish also use glucose although to a lower extent than mammals. Since the year 2000, several fish GLUTs isoforms have been cloned and they show remarkably high function similarities and sequence conservation to mammalian GLUTs.

6.1. GLUT1

The first GLUT1 fish isoform was cloned in 2000 in juvenile rainbow trout (Teerijoki et al. 2000, 2001b). It is comprised of 492 amino acid residues and shares 77-79 % protein identity with chicken and mammalian GLUT1 isoforms. It is predominantly expressed in heart; however, it is also found at lower levels in skeletal muscle, liver and brain. GLUT1 was also cloned from a carp epithelial cell line, corresponding to a protein of 478 amino acids, slightly smaller than trout GLUT1 but that also shares 78 % protein identity with chicken and mammalian GLUT1 isoforms (Teerijoki et al. 2001a). In 2004, Hall and colleagues (Hall et al. 2004) also cloned a GLUT1 isoform in cod, corresponding to a 489-amino acid protein that is 80-85 % identical to carp and rainbow trout GLUT1. Cod GLUT1 also shares 78 % protein identity with mammalian GLUT1 and is highly expressed in brain, gill, heart and kidney. Fish GLUT1 affinity for glucose (Km≈8-15 mM) has been suggested to be slightly higher than that of its human counterpart (Km≈7 mM) (Burant and Bell 1992, Teerijoki et al. 2001b, 2001a).

6.2. GLUT2

Similarly to GLUT1, fish GLUT2 was initially found in rainbow trout (Krasnov et al. 2001). GLUT2 gene encodes a 483 amino acid protein which shares 58 % and 52 % protein identity with chicken and mammalian GLUT2, respectively. Trout GLUT2 is expressed in liver, kidney and intestine. Later in 2006, Hall and colleagues cloned GLUT2 in Atlantic cod (Hall et al. 2006). This GLUT2 isoform contains 503 amino acids and shares 75 % protein identity with the previously referred trout GLUT2 and 62 % identity with chicken GLUT2. It shows a similar pattern of expression to its trout homolog: Atlantic cod GLUT2 is highly expressed in liver and at lower levels in intestine and kidney. GLUT2 was also cloned in zebrafish and encodes a 504 amino acid protein with high expression levels in testis, brain, skin, kidney, and intestine (Castillo et al. 2009). The affinity for glucose of zebrafish GLUT2 is similar to that of mammalian GLUT2 (Km≈11 mM) (Castillo et al. 2009).

6.3. GLUT3

Fish GLUT3 was identified in 2003 in grass carp (Zhang et al. 2003). It is predicted to possess 533 amino acids and it shares 60 % identity with other vertebrate GLUT3 isoforms. It is expressed mainly in kidney but was also found in eye, gill, brain, heart, liver and skeletal muscle. In 2005, GLUT3 was cloned in Atlantic cod and was predicted to comprise 519 amino acids and was substantially expressed in kidney but also in spleen, gill, brain and heart at lower

levels (Hall et al. 2005). Atlantic cod GLUT3 shares 66 % protein identity with grass carp GLUT3 and about 61 % with avian and mammalian isoforms.

6.4. GLUT4

Fish, after mammals, is the vertebrate group with the largest number of species for which there is genomic information corresponding to the GLUT4 gene (e.g. Brown trout, coho salmon, stickleback, medaka, Atlantic cod). However, zebrafish seems to be the only fish species with a sequenced genome for which the GLUT4 gene appears to be absent.

Known fish GLUT4 variants range in length between 503 and 511 amino acids and, like mammalian GLUT4 it has a predicted molecular mass of 55 kDa. GLUT4 is extremely well conserved among fish species: they show more than 90 % of protein identity and comparison of human and fish GLUT4 also shows a relatively high degree of conservation at the primary structure level, with fish variants sharing an 80 % homology to human GLUT4 (Figure I-15) (Reviewed in (Marín-Juez et al. 2014)). Moreover, phylogenetic analyses reveal that all fish GLUT4 proteins are evolutionarily related to human GLUT4 (Figure I-16).

In comparison to mammalian GLUT4, fish variants show a wider pattern of tissue distribution (Planas et al. 2000, Hall et al. 2006). They coincide with skeletal muscle being the main site of expression tissue, but fish variants are also found in gill and kidney, gut, adipose tissue, brain, liver and heart.

The functionality of GLUT4 in fish has been researched by Capilla and colleagues and they showed that coho salmon GLUT4 had an affinity for glucose with a Km≈7,6 mM, slightly lower than that of mammalian GLUT4 (Km≈5 mM), which could at some degree explain the lower ability of fish to a clear glucose load (Burant and Bell 1992, Capilla et al. 2004). More importantly, these studies showed that, like mammalian GLUT4, coho salmon GLUT4 was able to translocate to the plasma membrane in response to insulin when expressed in 3T3-L1 adipocytes. Subsequently, Diaz et al. (2007) also showed that insulin induces an increase of trout GLUT4 levels at plasma membrane when expressed in the L6 muscle cell line (Díaz et al. 2007a).

It is known that in mammals insulin induces expression of the GLUT4 gene. Similarly, in fish, GLUT4 mRNA and protein levels also appear to be regulated by insulin levels in the blood in a muscle type specific manner (Capilla et al. 2002). Supporting these data, brown trout GLUT4 protein content in red muscle decreases after fasting and increases after insulin administration (Díaz et al. 2007b). Furthermore, in mammals exercise also promotes GLUT4 expression and glucose utilization in skeletal muscle (Dohm 2002). In trout, swimming-induced exercise was also shown to induce glucose uptake and utilization in skeletal muscle (Felip et al. 2012).

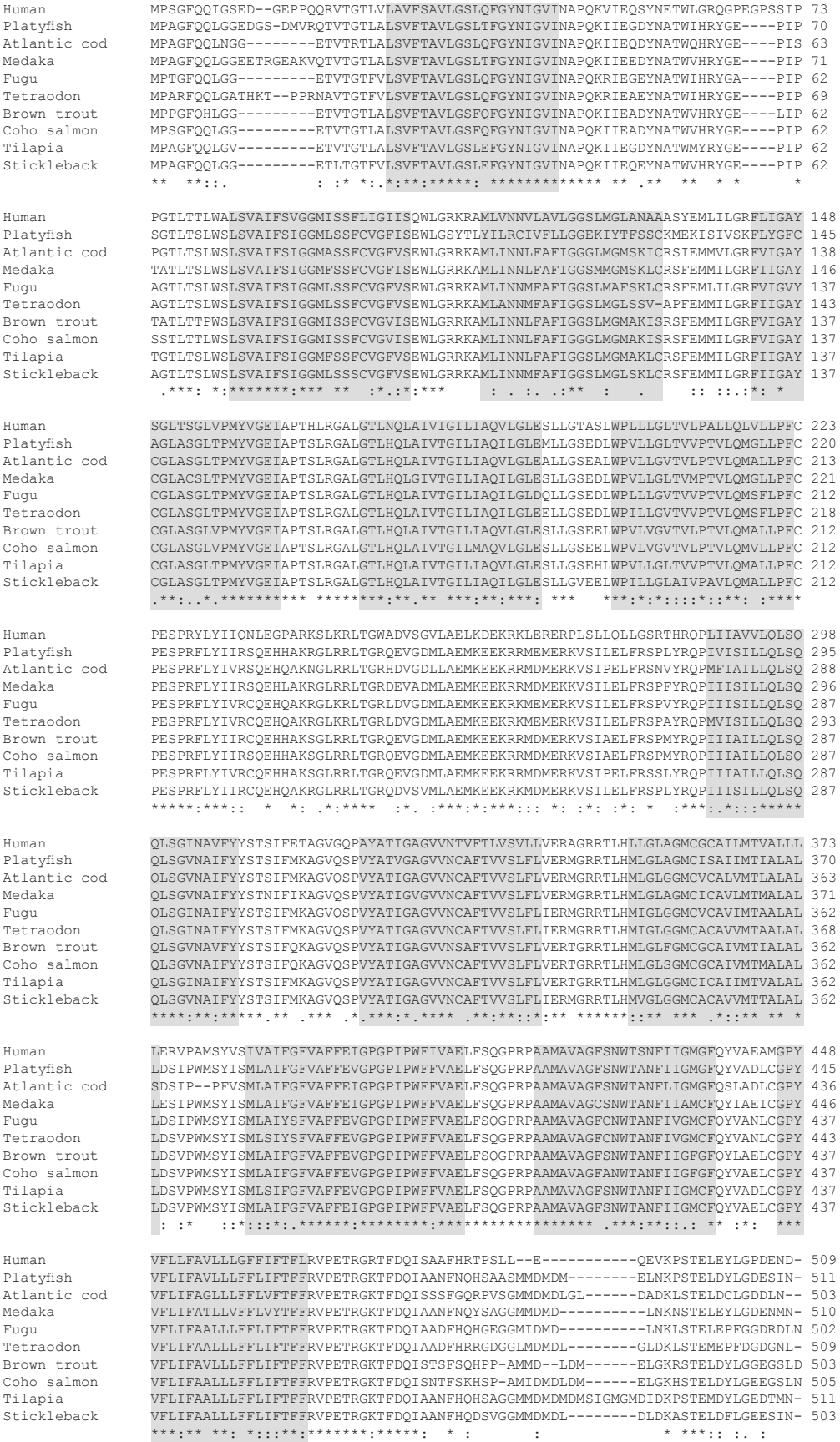

Figure I-15. Multiple alignment of protein GLUT4 sequences from human and different fish species. Alignment performed using ClustalW. (*) indicates positions which have a single, fully conserved residue; (:) indicates conservation between groups of strongly similar properties; (.) indicates conservation between groups of weakly similar properties; (blank) indicates no conservation. Grey indicates transmembrane domains. Sequence

references: Human: ENSG00000181856; Platyfish: ENSX-MAG00000015723; Atlantic cod: AAZ15731.1; Medaka: ENSORLG00000006341; Fugu: ENSTRUG00000011935; Tetraodon: ENSTNIG00000010138; Brown trout: AAG12191.1; Coho salmon: AAM22227.1; Tilapia: ENSO-NIG00000018958; Stickleback: ENSGACG00000019384.

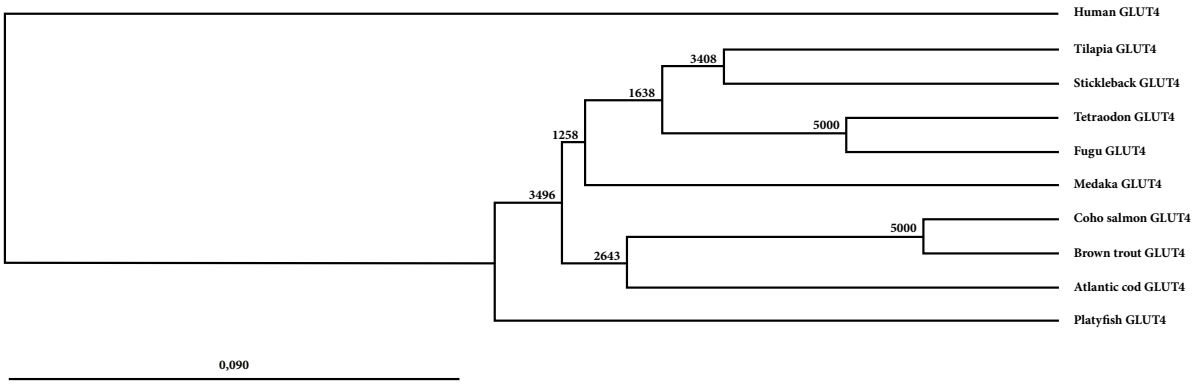

Figure I-16. Unrooted phylogenetic tree of human and fish GLUT4 amino acid sequences. The tree was created by the UPGMA method using ClustalW multiple alignment and bootstrapped 5000 times. Scale, 0,09 amino acid substitutions per site. Sequence references: Human: ENSG00000181856; Tilapia: ENSO-NIG00000018958; Stickleback: ENSGACG00000019384; Tetraodon: ENSTNIG00000010138; Fugu: ENSTRUG00000011935; Medaka: ENSORLG00000006341; Coho salmon: AAM22227.1; Brown trout: AAG12191.1; Atlantic cod: AAZ15731.1; Platyfish: ENSX-MAG00000015723. Adapted from (Marín-Juez et al. 2014).

7. FISH GLUT4 TRAFFICKING

Since the cloning of the brown trout (BtGLUT4) and coho salmon (OkGLUT4) variants of GLUT4 from muscle and adipose tissue, respectively, there has been increasing interest in using fish GLUT4 isoforms as tools for studying GLUT4 trafficking (Planas et al. 2000, Capilla et al. 2004). Hence, several studies have shed some light on fish GLUT4 trafficking features when expressed in heterologous systems: mammalian adipocytes and muscle cells. BtGLUT4 (503 amino acids) and OkGLUT4 (505 amino acids) share approximately 80 % sequence similarity to mammalian GLUT4 but possess differences in motifs and domains involved in GLUT4 trafficking such as the mammalian N-terminus FQQI[8], the large cytoplasmic loop (50 % identity between fish and mammalian GLUT4) and the C-termini motifs LL[490] and TELEY[502] (Figure I-17).

Transient expression of BtGLUT4 and OkGLUT4 in 3T3-L1 adipocytes revealed that ,in unstimulated conditions, BtGLUT4 exhibited higher protein levels at the PM (40 %) than RatGLUT4 (10 %), whereas OkGLUT4, on the other hand, showed an increase of surface levels but to a lesser extent (15-20 %) (Capilla et al. 2004, 2010). Supporting these data, stable expression of BtGLUT4 in L6 muscle cells showed that BtGLUT4 levels at the PM in unstimulated cells (25 %) were significantly higher than RatGLUT4 (10 %) (Díaz et al. 2007a). Moreover, the higher levels of BtGLUT4 at the PM are due to a faster exocytic rate rather than to a decrease in the rate of endocytosis, in both 3T3-L1 and L6 cells (Díaz et al. 2007a, Capilla et al. 2010). Therefore, the basal intracellular retention of fish GLUT4 appears to be less efficient when compared to mammalian GLUT4.

As described above, insulin induces GLUT4 translocation to the plasma membrane in

adipocytes and muscle cells. Insulin stimulation in 3T3-L1 adipocytes separately expressing BtGLUT4 or OkGLUT4 induced translocation of these transporters to the PM, although to a lesser extent than RatGLUT4 due to their higher basal surface levels (Capilla et al. 2004, 2010). Furthermore, Diaz et. al. also demonstrated that BtGLUT4 translocates to the PM in response to insulin when expressed in L6 muscle cells (Díaz et al. 2007a). Therefore, fish GLUT4 are capable of translocating to the membrane in response to insulin (insulin-responsive) despite their higher PM levels at the basal state. Interestingly, when transiently expressed in adipocytes, BtGLUT4 and OkGLUT4 acquire insulin-stimulated translocation earlier than RatGLUT4 (Capilla et al. 2010).

Several proteins assist GLUT4 in its trafficking. Two of the proteins that intervene in GLUT4 trafficking are sortillin and GGA. As detailed above, these proteins cooperate to sort newly synthesized GLUT4 from the TGN to the GSVs (Watson et al. 2004b, Li and Kandror 2005). Capilla and colleagues showed that in 3T3-L1 adipocytes, BtGLUT4 translocation to the PM in response to insulin was only partially affected by the expression of a dominant-interfering form of GGA. RatGLUT4 and OkGLUT4 translocation on the other hand was significantly blunted when co-expressed with the GGA mutant (Capilla et al. 2010). Moreover, Capilla et. al. also assessed the role of AS160 on BtGLUT4 and OkGLUT4 insulin-induced translocation. AS160 phosphorylation by Akt in response to insulin is pivotal for GLUT4 translocation to the PM. Through co-expression of BtGLUT4 or OkGLUT4 with a non-phosphorylatable mutant of AS160 (AS160-4P) in 3T3-L1 adipocytes, Capilla et. al. showed that OkGLUT4 translocation was halted in the presence of AS160-4P, similarly to RatGLUT4, whereas BtGLUT4 translocation was significantly less inhibited in the presence of AS160-4P (Capilla et al. 2010). Both GGA and AS160 data suggest that newly synthetized OkGLUT4, similarly to RatGLUT4, is sorted from TGN to GSVs through a pathway that is dependent on GGA and from GSVs to the surface in a AS160-dependent pathway. On the other hand, BtGLUT4 may be partially escaping the regular biosynthetic traffic route and failing efficient sorting into GSVs, probably due to lack of appropriate signaling motifs. One of such motifs could be the N-terminus $FQQI^{8}$ given that while RatGLUT4 possesses the $FQQI^{8}$ sequence, BtGLUT4 and OkGLUT4 possess the $FQHL^{8}$ and $FQQL^{8}$ variants, respectively (Figure I-17).

In 2008, a study approached a different aspect of fish GLUT4 traffic: its endocytic pathways. Antonescu and colleagues observed that BtGLUT4 and RatGLUT4, despite having similar internalization rates they followed different endocytic pathways (Díaz et al. 2007a, Antonescu et al. 2008). BtGLUT4 internalization was unaffected by hypertonic sucrose shock or clathrin depletion (CME ablation) but was halted by cholesterol depletion (cholesterol-dependent pathway ablation) whereas RatGLUT4 endocytosis was affected by all treatments. Therefore, these data indicate that BtGLUT4 internalizes solely through a cholesterol-dependent pathway, whereas RatGLUT4 utilizes both CME and cholesterol-dependent pathways. Moreover, Antonescu et.al. suggested that the cholesterol-dependent endocytosis involved in BtGLUT4 internalization is the IL-2 receptor pathway (Antonescu et al. 2008).

Despite the relative glucose intolerance observed in fish, the ability of GLUT4 to translocate to the PM in response to insulin has been conserved throughout evolution; however, the trafficking pathways involved seem to be somewhat different between fish and mammals. Moreover, fish GLUT4 intracellular sequestration in the absence of insulin seems to be less efficient. These differences appear to be associated with alterations in GLUT4 primary structure. Thus, understanding the trafficking roles of GLUT4 motifs is imperative and fish GLUT4 isoforms may prove to be powerful tools to that end.

```
RatGLUT4     MPSGFQQIGSEDGEPPQQRVTGTLVLAVFSAVLGSLQFGYNIGVINAPQKVIEQSYNATWLGRQGPGGPDSIPQG 75
BtGLUT4      MPPGFQHLGGE-------TVTGTLALSVFTAVLGSFQFGYNIGVINAPQKIIEADYNATWVHRYGE----LIPTA 64
OkGLUT4      MPSGFQQLGGE-------TVTGTLALSVFTAVLGSFQFGYNIGVINAPQKIIEADYNATWVHRYGE----PIPSS 64
             ** ***::*.*        *****.*:**:*****:**************:** .*****: * *      ** .

RatGLUT4     TLTTLWALSVAIFSVGGMISSFLIGIISQWLGRKRAMLANNVLAVLGGALMGLANAAASYEILILGRFLIGAYSG 150
BtGLUT4      TLTTPWSLSVAIFSIGGMISSFCVGVISEWLGRRKAMLINNLFAFIGGSLMGMAKISRSFEMMILGRFVIGAYCG 139
OkGLUT4      TLTTLWSLSVAIFSIGGMISSFCVGVISEWLGRRKAMLINNLFAFIGGGLMGMAKISRSFEMMILGRFVIGAYCG 139
             **** *:*******:******* :*:**:****::*** **::*.:**.***:*: : *:*::*****:****.*

RatGLUT4     LTSGLVPMYVGEIAPTHLRGALGTLNQLAIVIGILVAQVLGLESMLGTATLWPLLLAITVLPALLQLLLLPFCPE 225
BtGLUT4      LASGLVPMYVGEIAPTSLRGALGTLHQLAIVTGILIAQVLGLESLLGSEELWPVLVGVTVLPTVLQMALLPFCPE 214
OkGLUT4      LASGLVPMYVGEIAPTSLRGALGTLHQLAIVTGILMAQVLGLESLLGSEELWPVLVGVTVLPTVLQMVLLPFCPE 214
             *:************** ********:***** ***:********:**:  ***:*:.:****::**: *******

RatGLUT4     SPRYLYIIRNLEGPARKSLKRLTGWADVSDALAELKDEKRKLERERPLSLLQLLGSRTHRQPLIIAVVLQLSQQL 300
BtGLUT4      SPRFLYIIRCQEHHAKSGLRRLTGRQEVGDMLAEMKEEKRRMDMERKVSIAELFRSPMYRQPIIIAILLQLSQQL 289
OkGLUT4      SPRFLYIIRSQEHHAKSGLRRLTGRQEVGDMLAEMKEEKRRMDMERKVSIAELFRSPMYRQPIIIAILLQLSQQL 289
             ***:*****  *  *:..*:****  :*.* ***:*:***::: ** :*: :*: *  :***:***::*******

RatGLUT4     SGINAVFYYSTSIFELAGVEQPAYATIGAGVVNTVFTLVSVLLVERAGRRTLHLLGLAGMCGCAILMTVALLLLE 375
BtGLUT4      SGVNAVFYYSTSIFQKAGVQSPVYATIGAGVVNSAFTVVSLFLVERTGRRTLHMLGLFGMCGCAIVMTIALALLD 364
OkGLUT4      SGVNAIFYYSTSIFQKAGVQSPVYATIGAGVVNCAFTVVSLFLVERTGRRTLHMLGLSGMCGCAIVMTMALALLD 364
             **:**:********: ***:.*.********** .**:**::****:******:*** *******:**:** **:

RatGLUT4     RVPSMSYVSIVAIFGFVAFFEIGPGPIPWFIVAELFSQGPRPAAMAVAGFSNWTCNFIVGMGFQYVADAMGPYVF 450
BtGLUT4      SVPWMSYISMLAIFGFVAFFEVGPGPIPWFFVAELFSQGPRPAAMAVAGFSNWTANFIIGFGFQYLAELCGPYVF 439
OkGLUT4      SVPWMSYISMLAIFGFVAFFEVGPGPIPWFFVAELFSQGPRPAAMAVAGFANWTANFIIGFGFQYVAELCGPYVF 439
             ** ***:*::**********:********:******************:***.***:*:****:*:  *****

RatGLUT4     LLFAVLLLGFFIFTFLRVPETRGRTFDQISATFRRTPSLLE------QEVKPSTELEYLGPDEND- 509
BtGLUT4      LIFAVLLLFFLIFTFFRVPETRGKTFDQISTSFSQHPPAMMD--LDMELGKRSTELDYLGGEGSLD 503
OkGLUT4      LIFAALLLFFLIFTFFRVPETRGKTFDQISNTFSKHSPAMIDMDLDMELGKHSTELDYLGEEGSLN 505
             *:**.*** *:****:*******:****** :* :    :       :  * ****:*** : .
```

Figure I-17. Multiple alignment of Rat (RatGLUT4), Brown trout (BtGLUT4) and Coho salmon (OkGLUT4) GLUT4 protein sequences. Alignment performed using ClustalW. (*) indicates positions which have a single, fully conserved residue; (:) indicates conservation between groups of strongly similar properties; (.) indicates conservation between groups of weakly similar properties; (blank) indicates no conservation. Red residues indicate GLUT4 trafficking motifs. Grey boxes indicate transmembrane domains. Sequence references: Rat: NM_012751.1; Brown trout: AAG12191.1; Coho salmon: AAM22227.1.

II. OBJECTIVES

Glucose uptake by GLUT4 is extremely important for the maintenance of whole-body glucose homeostasis. GLUT4-mediated glucose uptake is dependent on the presence of the transporter at the cell surface that is controlled by a complex and not fully understood trafficking mechanism. Thus, fully grasping cellular trafficking of GLUT4 is of the utmost importance. In this regard, we propose that fish GLUT4 variants can be used as tools to study GLUT4 trafficking since they share a high degree of protein identity to mammalian GLUT4 variants while possessing differences in motifs thought to be involved in GLUT4 trafficking. In this work, we aim to study rat (RatGLUT4) and brown trout GLUT4 (BtGLUT4) trafficking in 3T3-L1 adipocytes. As such the objectives of this work are as follows:

1. Characterize RatGLUT4 and BtGLUT4 general trafficking events in 3T3-L1 adipocytes.

- To transiently express RatGLUT4 and BtGLUT4 constructs in 3T3-L1 adipocytes. RatGLUT4 and BtGLUT4 constructs possess myc epitopes in the first exofacial loop, between transmembrane domains I and II, and are also tagged with GFP in their C-terminal end.
- To determine RatGLUT4 and BtGLUT4 cell surface levels in the absence and in the presence of insulin but also after insulin removal.
- To determine RatGLUT4 and BtGLUT4 rates of exocytosis and endocytosis in the absence and presence of insulin in 3T3-L1 adipocytes.

2. Determine RatGLUT4 and BtGLUT4 routes of internalization in 3T3-L1 adipocytes.

- To stably express RatGLUT4 and BtGLUT4 constructs in 3T3-L1 adipocytes.
- To inhibit clathrin-mediated endocytosis, cholesterol-dependent endocytosis and caveolar endocytosis and analyze the contribution of these pathways for the internalization of RatGLUT4 and BtGLUT4 in 3T3-L1 adipocytes stably expressing these constructs.

3. Determine RatGLUT4 and BtGLUT4 presence in GSVs in 3T3-L1 adipocytes.

- To immunoadsorb the RatGLUT4 and BtGLUT4 constructs and blot for markers of GSVs to determine the presence of RatGLUT4 and BtGLUT4 in this compartment in 3T3-L1 adipocytes.

4. Analyze the roles of GLUT4 protein motifs in GLUT4 trafficking in 3T3-L1 adipocytes.

- To mutate BtGLUT4 in its N-terminus (FQHI^{8}) and C-terminus (TELDY^{495}) motifs to the corresponding RatGLUT4 (FQQI^{8}/TELEY^{502}) and OkGLUT4 (FQQL^{8}) sequences.
  - To determine mutant surface levels in the absence and presence of insulin in 3T3-L1 adipocytes.
  - To analyze the presence of the mutants in GSVs in 3T3-L1 adipocytes.

- To study the traffic of RatGLUT4/BtGLUT4 chimeras in 3T3-L1 adipocytes. These chimeras consist of a RatGLUT4 backbone with the N-terminus of BtGLUT4 (N-GLUT4) or the large cytoplasmic loop of BtGLUT4 (L-GLUT4).
  - To determine the cell surface levels of the chimeras in the absence and presence of insulin in 3T3-L1 adipocytes.
  - To analyze the endocytic rate constant of RatGLUT4/BtGLUT4 chimeras in 3T3-L1 adipocytes.

III. METHODS

1. CELL CULTURE

1.1. Cell Lines

1.1.1. 3T3-L1

The main cell line used during this thesis was the Mus musculus (mouse) embryo 3T3-L1 cell line acquired from ATCC (ATCC CL-173™). L1 is a continuous sub-strain of 3T3 (Swiss albino) developed through clonal isolation. The cells undergo a pre-adipose to adipose-like conversion as they progress from a rapidly dividing to a confluent and contact-inhibited state. Cells were manipulated as stipulated by ATCC. Media was changed every 2-3 days; confluency was avoided during growth phase; and cells were cultured at 37 ºC, 95 % humidity and 10 % CO_2.

1.1.2. Hek293T

This is the 293 clone of transformed human embrionary kidney cell lines, generated by infection with the adenovirus 5 (Ad 5) DNA. This cell line contains the "early expression region 1" (E1) from Ad 5, thus allowing the growth of adenoviruses lacking E1. 293 cells are efficiently infected by adenoviruses and are generally used for adenovirus amplification and their quantification. Hek 293T cells are a sub-line of Hek 293 cells that stably express SV40 large T antigen, allowing episomal replication of plasmids containing an origin of replication of SV40. Cells were cultured at 37 ºC, 95 % humidity and 5 % CO_2.

1.2. Cell Thawing

» Thaw vial in water bath at 37 ºC until ice starts to melt.
» Dilute cell suspension in 5 mL of warm growth media (table III-1).
» Centrifuge at 1200 rpm for 4 min.
» Decant supernatant and resuspend cells in fresh growth media (table III-1).
» Transfer to 10 cm culture dish or smaller if expecting low cell survival.
» After 24 hours, feed cells with fresh growth media (table III-1).

1.3. Cell Cryopreservation

» Grow cells to 80 % confluence.
» Rinse cells once with 1x PBS.
» Add 1:4 trypsin in 1x PBS and place dish into incubator to detach cells.
» Recover supernatant into centrifuge tube; Wash dish with 1x PBS to recover remaining cells.
» Centrifuge at 1200 rpm for 4 min and discard supernatant.
» Gently resuspend cells in cold freezing media (table III-1).
» Prepare 0,5-1 mL aliquots and place vials into a controlled-rate freeze chamber -80 ºC for

24 hours.

» Transfer vials into liquid nitrogen tank.

1.4. Cell Growth and Propagation

» Maintain cells at 30-70 % confluence.
» Rinse cells once with 1x PBS.
» Add 1:4 trypsin in 1x PBS and place dish into incubator to detach cells.
» Recover supernatant into centrifuge tube; Wash dish with 1x PBS to recover remaining cells.
» Centrifuge at 1200 rpm for 4 min and discard supernatant.
» Gently resuspend cells in warm growth media (table III-1).
» Transfer cells to new container at desired split ratio.
» Feed cells with fresh growth media every other day.

1.5. 3T3-L1 Differentiation

» Feed 3T3-L1 preadipocytes with warm growth media every other day until 100 % confluency (table III-1).
» Add fresh growth media to 3T3-L1 preadipocytes at 100 % confluency and leave for 3 days (Starvation stage).
» Remove growth media and add differentiation media (table III-1); Leave for 3 days (Differentiation stage).
» Remove differentiation media and add post-differentiation media (table III-1). Leave for 24 hours (Post Differentiation stage).
» Remove post-differentiation media and add DMEM-FBS media (table III-1). Change media every other day.

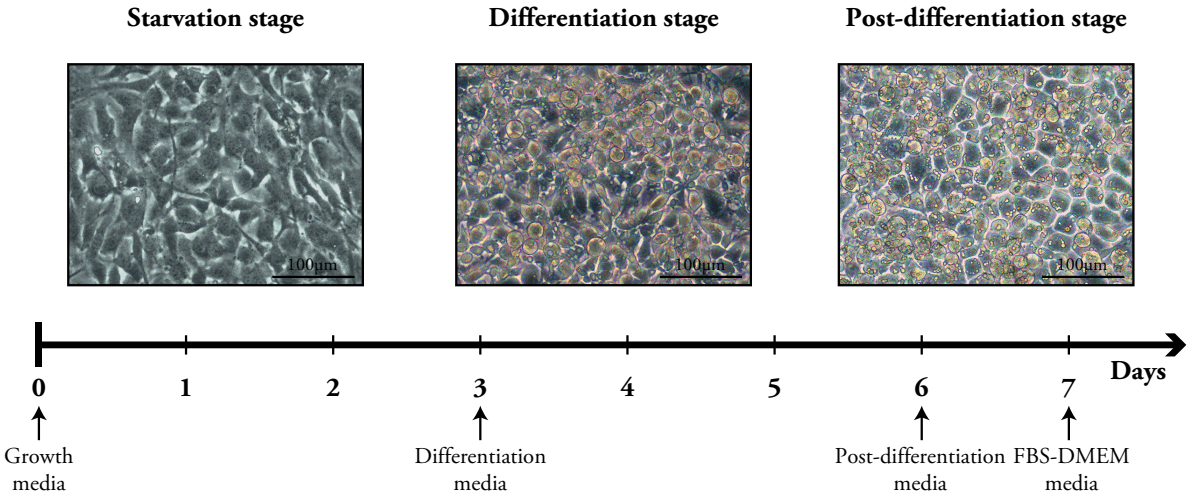

Figure III-1. 3T3-L1 cell line diferentiation protocol.

Table III-1. Cell culture media composition.

Hek293T Growth media	
Ingredient	**Final Concentration**
DMEM 4,5 g/l Glucose; w/ L-Gln; w/ sodium pyruvate	10 %
Fetal bovine serum (FBS)	10 % (v/v)
Penicillin – Streptomycin	100 U/mL - 100 µg/mL
HEPES	0,02 M
3T3-L1 Growth media	
Ingredient	**Final Concentration**
DMEM 4,5 g/l Glucose; w/ L-Gln; w/ sodium pyruvate	10 %
Newborn calf serum (CS)	10 % (v/v)
Penicillin – Streptomycin	100 U/mL - 100 µg/mL
3T3-L1 Differentiation media	
Ingredient	**Final Concentration**
DMEM 4,5 g/l Glucose; w/ L-Gln; w/ sodium pyruvate	10 %
Fetal bovine serum (FBS)	10 % (v/v)
Penicillin – Streptomycin	100 U/mL - 100 mg/mL
Insulin	1 mg/mL
Dexamethasone	0,25 mM
IBMX	0,11mg/mL
Rosiglitazone	1 mM
3T3-L1 Post-differentiation media	
Ingredient	**Final Concentration**
DMEM 4,5 g/l Glucose; w/ L-Gln; w/ sodium pyruvate	10 %
Fetal bovine serum (FBS)	10 % (v/v)
Penicillin – Streptomycin	100 U/mL - 100 µg/mL
Insulin	1 µg/mL
DMEM-FBS	
Ingredient	**Final Concentration**
DMEM 4,5 g/l Glucose; w/ L-Gln; w/ sodium pyruvate	10 %
Fetal bovine serum (FBS)	10 % (v/v)
Penicillin – Streptomycin	100 U/mL - 100 µg/mL
Freezing media	
Ingredient	**Final Concentration**
Fetal bovine serum (FBS)	90 %
DMSO	10 %
DMEM-BB	
Ingredient	**Final Concentration**
DMEM 4,5 g/l Glucose; w/ L-Gln; w/ sodium pyruvate	10 %
Penicillin – Streptomycin	100 U/mL - 100 µg/mL
HEPES	0,02 M

2. GENE EXPRESSION

2.1. Transient Gene Expression

2.1.1. Electroporation

In the following protocol, we electroporate 3T3-L1 adipocytes grown in 10 cm dishes and then transfer them into coverslip dishes. Coverslip dishes consist of a 35 mm dish with a Ø10 mm coverslip chamber.

Per 10 cm dish of differentiated adipocytes:

» Wash once with warm 1x PBS.
» Add 1:4 trypsin in 1x PBS and 1:100 collagenase D. Leave inside incubator until cells start to detach.
» Recover media and wash dish with 1x PBS to collect remaining cells.
» Spin down at 1200 rpm for 4 minutes.
» Remove supernatant and add fresh 1x PBS.
» Spin down at 1200 rpm for 4 minutes.
» Remove supernatant and add 3 mL of warm DMEM. Gently resuspend cells.
» To each cuvette, add 45 µg of desired DNA and 0,5 mL of cells suspension (one 10 cm dish = six cuvettes).
» Electroporate at 180 V and 950 mF. Scrape and discard thick white foam at the top of the cuvette. Gently pipette up and down to mix.
» To each coverslip add 110 mL of warm DMEM-FBS and 70 mL of electroporated cells (one cuvette = six coverslip dishes).
» Place into incubator for 30 minutes to 1 hour.
» Gently add 2 mL of warm DMEM-FBS to each coverslip dish.
» Place into incubator for 24 hours.

2.2. Stable Gene Expression

2.2.1. Lentiviral production, titration and infection

2.2.1.1. Viral production and purification

The following protocol describes the procedure per 10 cm dish of Hek293T cells, however multiples dishes can be used to increase amount of purified virus; Adapt volumes if using multiples 10 cm dishes. In this work, we used three 10 cm dishes for each lentiviral vector.

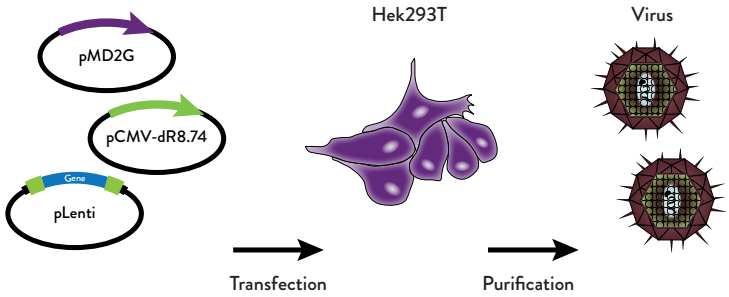

Figure III-2. Schematic representation of the viral production and purification protocol steps.

Per 10 cm dish of differentiated adipocytes:

» Grow Hek293T cells to 100 % confluency on 10 cm dish; Cells can be split and seeded to 80-90 % confluency on the previous day.
» Mix 10 µg of lentiviral vector, 7 µg of pCMV-dR8.74 and 3 µg of pMD2G. Plasmids pCMV-dR8.74 and pMD2G encode for viral packaging system and envelope proteins, respectively.
» Bring volume to 1560 mL with sterile 150 mM NaCl.
» Add 78 mL of PEI.
» Vortex for 20 seconds and leave to settle for 15 minutes.
» Gently add mix to dish and incubate for 7-8 hours.
» Remove media and add 5 mL of warm Hek 293T growth media.
» Incubate at 33 ºC, 95 % humidity and 5 % CO_2 for 24 hours.
» Recover media and centrifuge at 2500 rpm, 4 ºC for 10 minutes; Filter using 0,45 mm pore size filter and store at 4 ºC.
» Feed cells with 5 mL of fresh Hek 293T growth media.
» After 24 hours, recover media, centrifuged and filter as described above.
» Transfer recovered media (from both days) to an ultracentrifuge tube and using a syringe, carefully place 4 mL of sterile 20 % sucrose underneath it, to create a sucrose cushion at the bottom of the tube.
» Centrifuge at 26.000 rpm and 4 ºC for 90 minutes.
» Decant supernatant and air dry pellet (invisible) for 10 min.
» Resuspend pellet in 100 µL of DMEM-BB. Avoid bubbles when resuspending.
» At this point virus can be used or stored at -80 ºC.

2.2.1.2. Titration

Per 6-well dish:

» Seed 100.000 Hek293T cells per well.

» Prepare 1:100 dilution of virus stock in DMEM-BB.

» Add the indicated volumes to a 6-well dish. Incubate at 33 ºC, 95 % humidity and 5 % CO_2 for 24 hours.

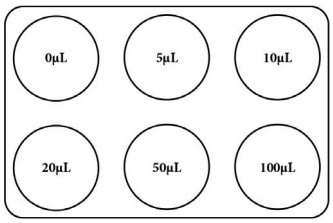

Figure III-3. Schematic representation of the volumes used in the viral titration protocol.

» Remove media, add fresh Hek 293T growth media and incubate at 37 ºC, 95 % humidity and 5 % CO_2 for 72 hours.

» Wash once with 1x PBS.

» Add 100 µL of trypsin and 200 µL of 1x PBS (per well) to detach cells.

» Collect supernatant and add 700 µL of DMEM-BB to each well to recover remaining cells.

» Determine the percentage of infected cells in each well (GFP-Positive cells) using FACS.

» Select dilutions yielding 5 - 20 % of GFP-positive cells: Below 5 % FACS determination of GFP-positive cells may not be accurate enough; Above 20 % risk of each cell getting infected twice increases significantly, resulting in underestimation of the number of transducing particles.

» Use selected dilutions and the mathematical equation below to calculate the titer obtained. Average titers.

$$\text{Titer (Hek293T TU/mL)} = \text{Number Hek293T} \cdot \frac{\frac{\text{GFP Positive cells (\%)}}{100}}{\text{Virus Volume (mL)}} \cdot 100 \text{ (dilution factor)}$$

2.2.1.3. Viral infection

Per well of 6-well dish:

» Seed 20.000 3T3-L1 preadipocytes, place into incubator and leave for 5-6 hours.
» Add virus at desired MOI and incubate at 33 ºC, 95 % humidity and 10 % CO_2 for 24 hours.
» Remove media, add fresh growth media and incubate at 37 ºC, 95 % humidity and 10 % CO_2 for 48 hours.
» Add fresh media containing selection antibiotic. In this work we used pLenti CMV/TO Puro DEST (coding for different GLUT4 variants) which has puromycin selection marker (3 μg/mL). We also used pLVTHM coding for Caveolin-1 siRNA.
» Grow cells and prepare aliquots for cryopreservation (Section: 1.3. Cells Cryopreservation).

3. MICROSCOPY

3.1. Translocation Assays

The following protocols are performed in coverslip dishes containing 3T3-L1 adipocytes electroporated with GLUT4 constructs.

3.1.1.GLUT4 surface levels

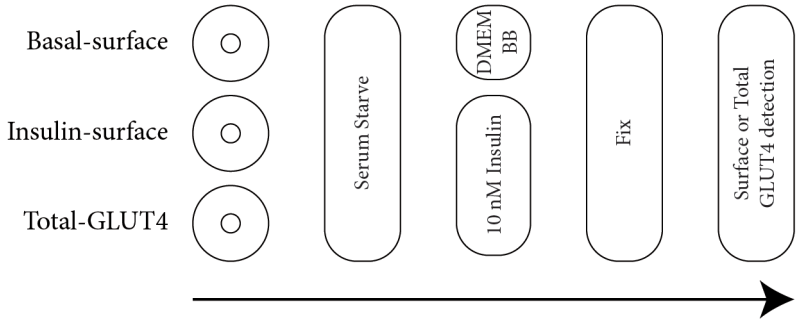

Figure III-4. Schematic representation of the GLUT4 surface levels protocol.

- » Prepare three coverslips dishes (Basal-surface; Insulin-surface; Total GLUT4) with 3T3-L1 adipocytes expressing GLUT4 constructs. Include replicates.
- » Wash cells twice with warm DMEM-BB.
- » Serum starve cells in DMEM-BB for 2 hours inside incubator.
- » **Basal-surface dishes:** Add fresh DMEM-BB and place into incubator for 30 minutes; **Insulin-surface and Total GLUT4 dishes:** Challenge cells with 10 nM insulin in DMEM-BB for 30 minutes inside incubator.
- » Proceed to: Cell fixation and antibody labeling (Translocation assays).

3.1.2. GLUT4 surface levels after insulin removal

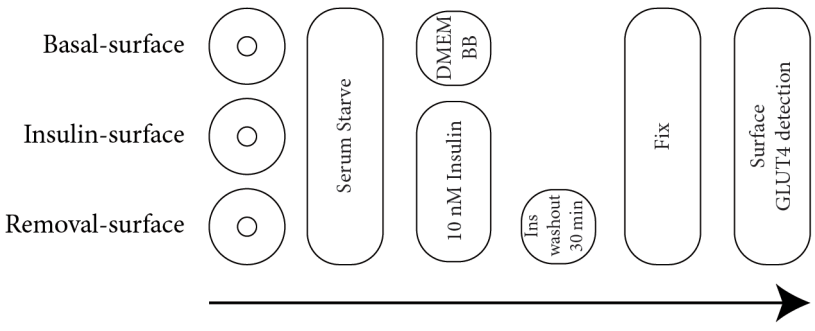

Figure III-5. Schematic representation of the GLUT4 surface levels after insulin removal protocol.

- » Prepare three coverslips dishes (Basal-surface; Insulin-surface; Removal-surface) with 3T3-L1 adipocytes expressing GLUT4 constructs. Include replicates.
- » Wash cells twice with warm DMEM-BB.
- » Serum starve in DMEM-BB for 2 hours inside incubator.

» **Basal-surface dishes:** Add fresh DMEM-BB and place into incubator for 30 minutes;
Insulin-surface and Removal-surface dishes: Challenge cells with 10 nM insulin in DMEM-BB for 30 minutes inside incubator.
» **Basal-surface and Insulin-surface dishes:** Proceed to: Cell fixation and antibody labeling (Translocation assays);
Removal-surface dishes: Wash twice with warm DMEM-BB and place into incubator for 30 minutes. Proceed to: Cell fixation and antibody labeling (Translocation assays).

Cell fixation and antibody labeling (Translocation assays).

» Wash twice with cold 1x Media II.
» Fix in 3,7 % paraformaldehyde at RT for 6 minutes.
» Wash thrice with 1x PBS.
» Incubate with primary antibody at 37 ºC for 45 minutes:
If labeling surface GLUT4: 1:300 dilution of α-myc in 5 % FBS-PBS.
If labeling total GLUT4: 1:300 dilution of α-myc in 5 % FBS-PBS with 0,25 mg/mL saponin.
» Wash thrice with 1x PBS.
» Incubate with secondary antibody at 37 ºC for 45 minutes:
If labeling surface GLUT4: 1:300 dilution of α-mouse Alexa Fluor 555 in 5 % FBS-PBS.
If labeling total GLUT4: 1:300 dilution of α-mouse Alexa Fluor 555 in 5 % FBS-PBS with 0,25 mg/mL saponin.
» Wash thrice with 1x PBS.
» Observe under fluorescence microscope or store in dark at 4 ºC.

3.2. GLUT4 Cell Cycling Assays

3.2.1. Exocytosis

In the Absence of Insulin

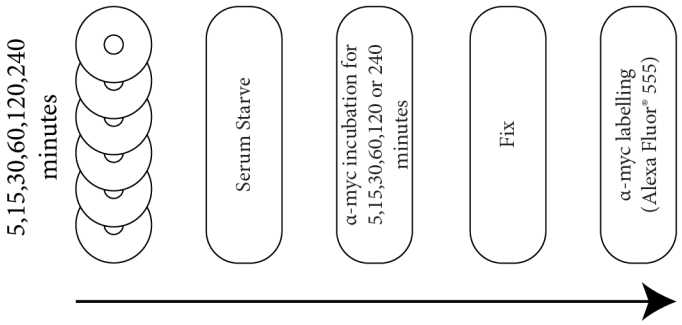

Figure III-6. Schematic representation of the exocytosis in the absence of insulin protocol.

» Prepare six coverslips dishes (5, 15, 30, 60, 120 and 240 minutes) with 3T3-L1 adipocytes expressing GLUT4. Include replicates.
» Wash twice with warm DMEM-BB.
» Serum starve in DMEM-BB for 2 hours inside incubator.
» Incubate with 1:250 dilution of α-myc in 10 nM insulin-DMEM-BB for 5, 15, 30, 60, 120 or 240 minutes.
» Proceed to: Cell fixation and antibody labeling (Exocytosis).

In the Presence of Insulin

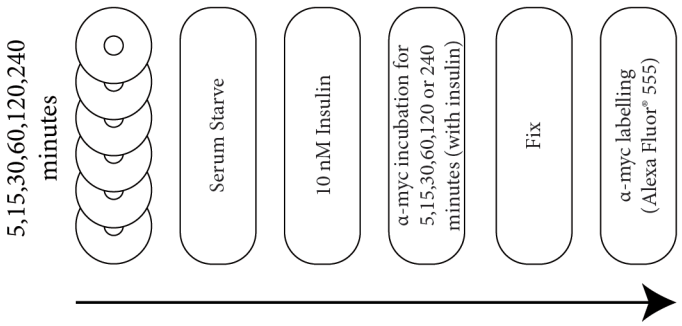

Figure III-7. Schematic representation of the exocytosis in the presence of insulin protocol.

» Prepare six coverslips dishes (5, 15, 30, 60, 120 and 240 minutes) with 3T3-L1 adipocytes expressing GLUT4. Include replicates.
» Wash twice with warm DMEM-BB.
» Challenge cells with 10 nM insulin in DMEM-BB for 30 minutes inside incubator.
» Incubate with 1:250 dilution of α-myc in 10 nM insulin-DMEM-BB for 5, 15, 30, 60, 120 or 240 minutes.
» Proceed to: Cell fixation and antibody labeling (Exocytosis).

Cell Fixation and Antibody Labeling (Exocytosis).

» Wash twice with cold 1x Media II.
» Fix in 3,7 % paraformaldehyde for 6 minutes at RT.
» Wash thrice with 1x PBS.
» Probe α-myc antibody with 1:300 dilution of α-mouse Alexa Fluor 555 in 5 % FBS-PBS with 0,25 mg/mL saponin for 45 minutes at 37 ºC.
» Wash thrice with 1x PBS
» Observe under fluorescence microscope or store in dark at 4 ºC.

3.2.2. Endocytosis

In the Absence of Insulin

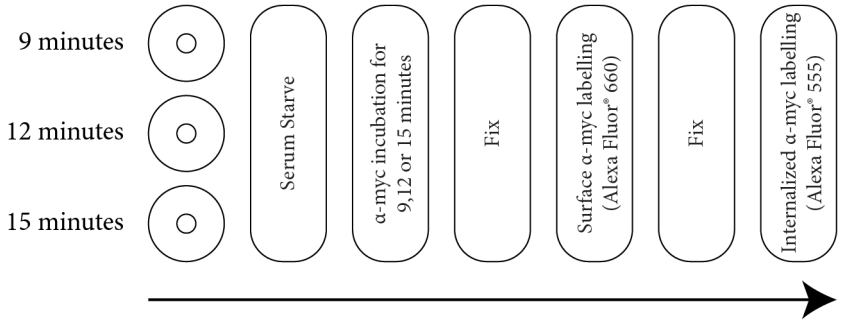

Figure III-8. Schematic representation of the endocytosis in the absence of insulin protocol.

» Prepare three coverslips dishes (9, 12 and 15 minutes) with 3T3-L1 adipocytes expressing GLUT4. Include replicates.
» Wash twice with warm DMEM-BB.
» Serum starve in DMEM-BB for 2 hours inside incubator.
» Add α-myc at 1:75 dilution in DMEM-BB to the coverslip chamber. Place into incubator for 9, 12 or 15 minutes.
» Proceed to: Cell fixation and antibody labeling (Endocytosis).

In the Presence of Insulin

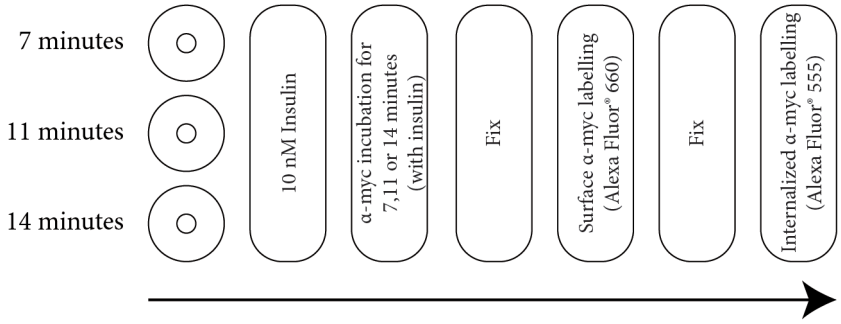

Figure III-9. Schematic representation of the endocytosis in the presence of insulin protocol.

» Prepare three coverslips dishes (7, 11 and 14 minutes) with 3T3-L1 adipocytes expressing GLUT4. Include replicates.
» Wash twice with warm DMEM-BB.
» Challenge cells with 10 nM insulin in DMEM-BB for 30 minutes inside incubator.
» Add α-myc at 1:75 dilution in 10 nM insulin-DMEM-BB to the coverslip chamber. Place into incubator for 7, 11 or 14 minutes.
» Proceed to: Cell fixation and antibody labeling (Endocytosis).

Cell Fixation and Antibody Labeling (Endocytosis)

» Wash twice with cold 1x Media II.
» Fix in 3,7 % paraformaldehyde at RT for 6 minutes.
» Wash thrice with 1x PBS.
» Probe surface α-myc antibody (surface GLUT4) with 1:50 dilution of α-mouse Alexa Fluor 660 in 5 % FBS-PBS at 37 °C for 45 minutes.
» Wash thrice with 1x PBS.
» Fix in 3,7 % paraformaldehyde at RT for 6 minutes.
» Wash thrice with 1x PBS.
» Probe internalized α-myc antibody (internal GLUT4) with 1:300 dilution of α-mouse Alexa Fluor 555 in 5 % FBS-PBS with 0,25 mg/mL saponin at 37 °C for 45 minutes.
» Wash thrice with 1x PBS.
» Observe under fluorescence microscope or store in dark at 4 °C.

3.3. Clathrin-mediated and Cholesterol-dependent Endocytosis

3.3.1. Transferrin clathrin-mediated endocytosis

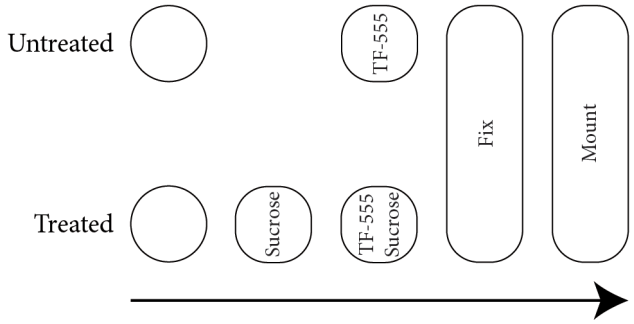

Figure III-10. Schematic representation of the transferrin clathrin-mediated endocytosis protocol.

- » Prepare two coverslips with 3T3-L1 adipocytes. Include replicates.
- » Wash twice with warm DMEM-BB.
- » Treat cells on one coverslip with 450 mM sucrose in DMEM-BB and place into incubator for 30 minutes; Leave other coverslip untreated.
- » Incubate cells with 25 µg/mL Transferrin-Alexa Fluor 555 (TF-555) in DMEM-BB, in the presence (previously treated coverslip) or absence of sucrose (untreated coverslip), for 20 minutes in incubator.
- » Wash twice with cold 1x Media II.
- » Fix in 3,7 % paraformaldehyde at RT for 6 minutes.
- » Wash thrice with 1x PBS.
- » Mount coverslips with ProLong® Gold Antifade.
- » Observe under fluorescence microscope or store in dark at 4 ºC.

3.3.2. Cholera toxin B subunit cholesterol-dependent endocytosis

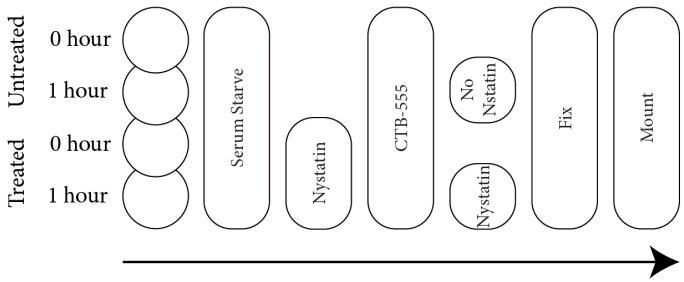

Figure III-11. Schematic representation of the cholera toxin B subunit cholesterol-dependent endocytosis protocol.

- » Prepare four coverslips with 3T3-L1 adipocytes. Include replicates
- » Wash twice with warm DMEM-BB.
- » Serum starve in DMEM-BB for 2 hours inside incubator.
- » Treat two coverslips with 50 µg/mL nystatin in DMEM-BB for 30 minutes inside incubator;

Leave other coverslips untreated.

» Incubate all coverslips with 4 µg/mL Cholera toxin B subunit-Alexa Fluor 555 (CTB-555) in DMEM-BB at 4 °C for 30 minutes.

» **For the 0 hour time point:**
Take one untreated and one treated coverslip and wash twice with cold 1x Media II.
Fix in 3,7 % paraformaldehyde at RT for 6 minutes.
Wash thrice with 1x PBS.

» **For the 1 hour time point:**
Take one untreated and one treated coverslip and add DMEM-BB alone or DMEM-BB with 50 µg/mL nystatin, respectively. Place into incubator for 1 hour.
Wash twice with cold 1x Media II.
Fix in 3,7 % paraformaldehyde at RT for 6 minutes.
Wash thrice with 1x PBS.

» Mount coverslips with ProLong® Gold Antifade.

» Observe under fluorescence microscope or store in dark at 4 °C.

3.4. GLUT4 and Syntaxin 6 colocalization

3.4.1.Airyscan

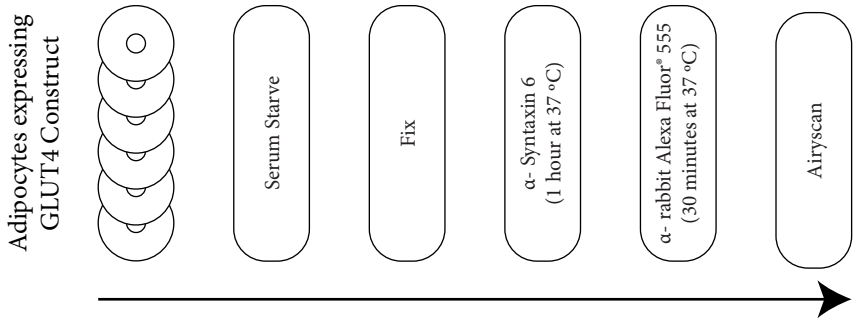

Figure III-12. Schematic representation of the GLUT4 and Syntaxin 6 colocalization protocol.

- Prepare coverslip dishes with 3T3-L1 adipocytes expressing GLUT4. Include replicates.
- Wash twice with warm DMEM-BB.
- Serum starve in DMEM-BB for 2 hours inside incubator.
- Wash twice with cold 1x Media II.
- Fix in 3,7 % paraformaldehyde for 6 minutes at RT.
- Wash thrice with 1x PBS.
- Incubate with 1:200 dilution of α-Syntaxin 6 antibody in 5 % FBS-PBS with 0,25 mg/mL saponin. Leave for 1 hour at 37 °C.
- Wash thrice with 1x PBS.
- Probe α-Syntaxin 6 antibody with 1:300 dilution of α-rabbit Alexa Fluor 555 in 5 % FBS-PBS with 0,25 mg/mL saponin. Leave for 45 minutes at 37 °C.
- Wash thrice with 1x PBS.
- Observe under laser scanning microscope with airyscan or store in dark at 4 °C.

3.5. Image Analysis

Image analysis was done using Fiji (Fiji Is Just ImageJ).

3.5.1. Translocation assays

- Image files obtained from these experiments contain GFP (protein tag) and Alexa Fluor 555 (antibody labeling) fluorescence.
- Circle individual cells and measure their GFP and Alexa Fluor 555 integrated densities (typically 30-60 cells were analyzed per experimental condition).
- Circle background cells and measure their GFP and Alexa Fluor 555 integrated densities (typically 30-60 cells were analyzed per experimental condition).
- Average background GFP and Alexa Fluor 555 measurements.
- Subtract background averages from GFP and Alexa Fluor 555 intensities of cells of interest.
- For each cell, divide its Alexa Fluor 555 by its GFP intensity to normalize labeling signal to

own expression level.

» Determine outliers in each experimental condition using the following equations:

Lower fence = Quartile 1 - 1,5 . (Quartile 3 - Quartile 1)

Upper fence = Quartile 3 + 1,5 . (Quartile 3 - Quartile 1)

» Discard values falling outside fences.

» Average Alexa Fluor 555:GFP ratios of individual cells within the same experimental condition.

3.5.2. GLUT4 cell cycling assays

Exocytosis

» Image files obtained from these experiments contain GFP (protein tag) and Alexa Fluor 555 (antibody labeling) fluorescence.

» Circle individual cells and measure their GFP and Alexa Fluor 555 integrated densities (typically 30-60 cells were analyzed per experimental condition).

» Circle background cells and measure their GFP and Alexa Fluor 555 integrated densities (typically 30-60 cells were analyzed per experimental condition).

» Average background GFP and Alexa Fluor 555 measurements.

» Subtract background averages from GFP and Alexa Fluor 555 intensities of cells of interest.

» For each cell, divide its Alexa Fluor 555 by its GFP intensities to normalize labeling signal to own expression level.

» Determine outliers in each experimental condition using the following equations:

Lower fence = Quartile 1 - 1,5 . (Quartile 3 - Quartile 1)

Upper fence = Quartile 3 + 1,5 . (Quartile 3 - Quartile 1)

» Discard values falling outside fences.

» Average Alexa Fluor 555:GFP ratios of individual cells within the same experimental condition.

» Normalize Alexa Fluor 555:GFP ratios of the various time points to 240 minutes ratio.

» Fit a one-phase association curve to data points. This curve describes the first order association kinetics of the interaction between a ligand and its receptor, or a substrate and an enzyme.

$$\mathbf{Y=Y_0 + (Plateau - Y_0) \,.\, (1 - e^{(-Kx)})}$$

K is the rate constant, expressed in reciprocal of the X axis time units (min^{-1}).

Endocytosis

- Image files obtained from these experiments contain Alexa Fluor 660 (surface GLUT4) and Alexa Fluor 555 (internalized GLUT4) fluorescence.
- Circle individual cells and measure their Alexa Fluor 660 and Alexa Fluor 555 integrated densities (typically 30-50 cells were analyzed per experimental condition).
- Circle background cells and measure their Alexa Fluor 660 and Alexa Fluor 555 integrated densities (typically 30-60 cells were analyzed per experimental condition).
- Average background Alexa Fluor 660 and Alexa Fluor 555 measurements.
- Subtract background averages from Alexa Fluor 660 and Alexa Fluor 555 intensities of cells of interest.
- For each cell, divide its Alexa Fluor 555 by its Alexa Fluor 660 intensity to normalize internalized GLUT4 to own surface levels.
- Determine outliers in each experimental condition using the following equations:

Lower fence = Quartile 1 - 1,5 . (Quartile 3 - Quartile 1)

Upper fence = Quartile 3 + 1,5 . (Quartile 3 - Quartile 1)

- Discard values falling outside fences.
- Average Alexa Fluor 555 (internalized):Alexa Fluor 660 (surface) ratios of individual cells within the same experimental condition.
- Normalize Alexa Fluor 555 and Alexa Fluor 660 ratios of the various time points to longer time point ratio.
- Fit a linear regression curve to data points.

$$y=mx+b$$

m (slope) is the rate constant, expressed in reciprocal of the X axis time units (min^{-1}).

4. MOLECULAR BIOLOGY

4.1. Transformation

» Thaw competent bacteria on ice until it has just completely thawed.
» Add 1 - 5 µL (usually 1 - 100 ng) of DNA to 50 µL of competent bacteria.
» Mix gently by flicking tube 4 - 5 times and leave on ice for 30 minutes.
» Heat shock in 42 ºC water bath for 40 seconds (do not flick tube).
» Put back on ice for 2 minutes.
» Add 950 µL of pre-warmed LB broth (without antibiotic) and place into shaker at 37 ºC, 225 rpm for 1 hour.
» Plate 50 - 100 µL onto agar plates (warmed to 37 ºC or room temperature) containing appropriate selection antibiotic.
» Incubate overnight at 37 ºC.

4.2. Mutagenesis

» Add the following components to PCR tube:

Table III-2. Mutagenesis PCR reaction.

Component	Volumes	Final concentration
ddH2O	Up to 20 µL	-
2x Phusion High-Fidelity DNA Polymerase Master Mix	10 µL	1x
2 µM Forward Primer	1 µL	0,1 µM
2 µM Reverse Primer	1 µL	0,1 µM
DNA template ($pcDNA_3$-GLUT4)	Varies	500 pg

» Use the following templates and primers to obtain the corresponding mutant:

Table III-3. Mutagenesis primers.

Mutant	Template	Primer	
BtG4-QL	BtGLUT4	F	5'-CCTGGGTTTCAGCAGCTTGGAGGGGAGAC-3'
		R	5'-GTCTCCCCTCCAAGCTGCTGAAACCCAGG-3'
BtG4-QI	BtGLUT4	F	5'-CCTGGGTTTCAGCAGATTGGAGGGGAGAC-3'
		R	5'-GTCTCCCCTCCAATCTGCTGAAACCCAGG-3'
BtG4-CT	BtGLUT4	F	5'-GCAAGCCGAGTACAGAGCTGGAGTACCTGGGGCCGGAGGGAAGCCTTGACTCG-3'
		R	5'-CCCTCCGGCCCCAGGTACTCCAGCTCTGTACTCGGCTTGCCCAGCTCCATGTCCAGG-3'
BtG4-QLCT	BtG4-QL	F	5'-GCAAGCCGAGTACAGAGCTGGAGTACCTGGGGCCGGAGGGAAGCCTTGACTCG-3'
		R	5'-CCCTCCGGCCCCAGGTACTCCAGCTCTGTACTCGGCTTGCCCAGCTCCATGTCCAGG-3'
BtG4-QICT	BtG4-QI	F	5'-GCAAGCCGAGTACAGAGCTGGAGTACCTGGGGCCGGAGGGAAGCCTTGACTCG-3'
		R	5'-CCCTCCGGCCCCAGGTACTCCAGCTCTGTACTCGGCTTGCCCAGCTCCATGTCCAGG-3'

» Run the following PCR protocol:

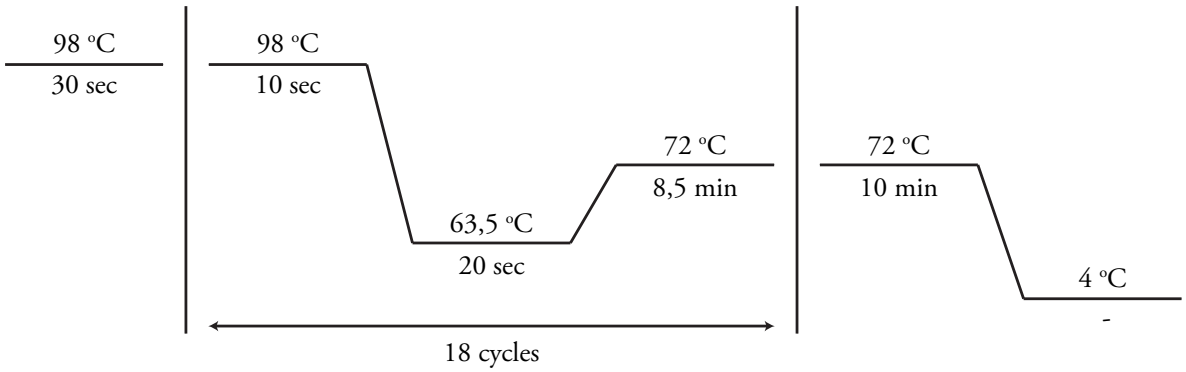

Figure III-13. Schematic representation of the mutagenesis PCR protocol.

» Add 1 µL of Dpn I to PCR tube and incubate for 150 minutes at 37 °C. Dpn I cleaves methylated DNA enabling us to destroy DNA template (not the mutated).
» Transform 15 µL of PCR reaction per 50 µL of competent bacteria, as described in section 4.1. Transformation. Use 100 µg/mL ampicillin as selection antibiotic.
» Extract DNA from different colonies (at least five) using PureLink® HiPure Plasmid Miniprep Kit, or equivalent, as described in section: 4.4. Plasmid Purification.
» Sequence DNA using the appropriate primers from table III-8.

4.3. Gateway Cloning

4.3.1. Incorporation of attB sites on target gene (step 1)

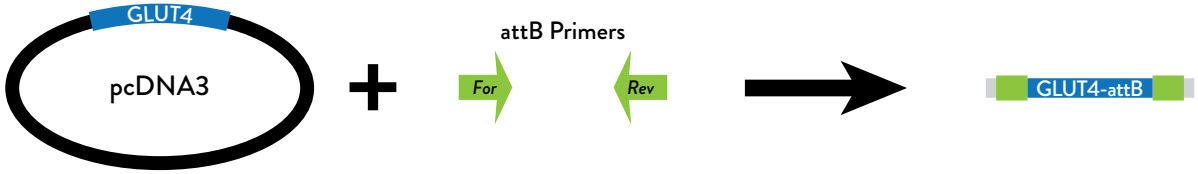

Figure III-14. Schematic representation of the gateway cloning step 1.

» Add the following components to PCR tube:

Table III-4. Gateway step 1 PCR reaction.

Component	Volumes	Final concentration
ddH2O	Up to 50 µL	-
10x Taq Buffer	5 µL	1x
10 mM dNTP mix	1 µL	0,2 mM
50 mM $MgSO_4$	2 µL	2 mM
10 µM Forward Primer	1 µL	0,2 mM
10 µM Reverse Primer	1 µL	0,2 mM
DNA template ($pcDNA_3$-GLUT4)	Varies	< 500 ng
Platinium® Taq High Fidelity Polymerase (5 U/µL)	0,2 µL	1 U

Table III-5. Forward and reverse primers containing attB incorporation sites.

Template		Primer
RatGLUT4	F	5'-GGGGACAAGTTTGTACAAAAAAGCAGGCTGCCACCATGCCGTCGGGTTTCCAGC-3'
	R	5'-GGGGACCACTTTGTACAAGAAAGCTGGGTTTACTTGTACAGCTCGTCCATGCC-3'
BtGLUT4	F	5'-GGGACAAGTTTGTACAAAAAAGCAGGCTGCCACCATGCCGCCTGGGTTTCAGC-3'
	R	5'-GGGGACCACTTTGTACAAGAAAGCTGGGTTTACTTGTACAGCTCGTCCATGCC-3'
N-GLUT4	F	5'-GGGACAAGTTTGTACAAAAAAGCAGGCTGCCACCATGCCGCCTGGGTTTCAGC-3'
	R	5'-GGGGACCACTTTGTACAAGAAAGCTGGGTTTACTTGTACAGCTCGTCCATGCC-3'
L-GLUT4	F	5'-GGGGACAAGTTTGTACAAAAAAGCAGGCTGCCACCATGCCGTCGGGTTTCCAGC-3'
	R	5'-GGGGACCACTTTGTACAAGAAAGCTGGGTTTACTTGTACAGCTCGTCCATGCC-3'
BtG4-QL	F	5'-GGGACAAGTTTGTACAAAAAAGCAGGCTGCCACCATGCCGCCTGGGTTTCAGC-3'
	R	5'-GGGGACCACTTTGTACAAGAAAGCTGGGTTTACTTGTACAGCTCGTCCATGCC-3'

» Run the following PCR protocol:

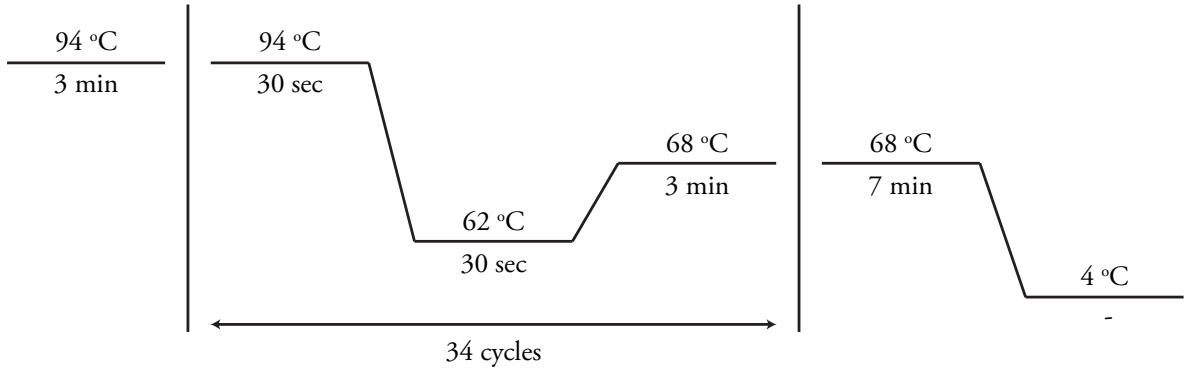

Figure III-15. Schematic representation of the gateway reaction 1 PCR protocol.

» Load reaction volume on a 1 % agarose gel.

» Extract desired band and purify PCR product using PureLink™ Quick Gel Extraction & PCR Purification COMBO kit or equivalent.

4.3.2. BP recombination reaction (step 2)

Figure III-16. Schematic representation of the gateway BP reaction.

» Add the following components to tube:

Table III-6. Gateway BP reaction.

Component	Volumes	Final concentration
ddH2O	Up to 10 µL	-
pDONR™221	Varies	150 ng
GLUT4-attB	Varies	150 ng
5x BP Clonase™ Reaction buffer	2 µL	1x

» Incubate at 25 ºC for 2 hours.
» Add 1 µL of proteinase K and incubate at 37 ºC for 10 minutes.
» Transform 2 µL of reaction per 50 µL of competent bacteria as described in section: 4.1. Transformation. Use 50 µg/mL kanamycin as selection antibiotic. (Do not use E. coli strains that contain the F' episome. These strains contain the ccdA gene and will prevent negative selection with the ccdB gene.)
» Extract DNA from different colonies (at least five) using PureLink Quick Plasmid Miniprep Kit, or equivalent, as described in section: 4.4. Plasmid Purification.
» Sequence DNA using the appropriate primers from primers from table III-8.

4.3.3. LR recombination reaction (step 3)

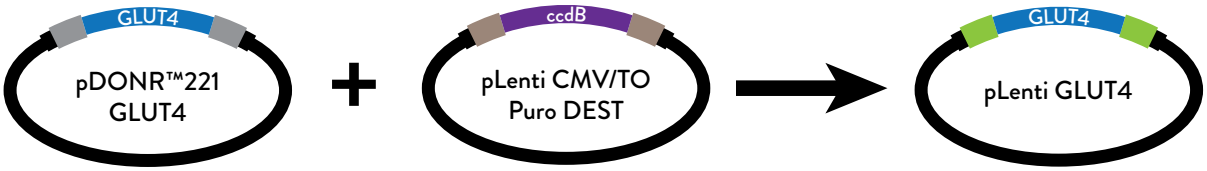

Figure III-17. Schematic representation of the gateway LR reaction.

» Add the following components to tube:

Table III-7. Gateway LR reaction.

Component	Volumes	Final concentration
ddH2O	Up to 10 µL	-
pLenti CMV/TO Puro DEST	Varies	150 ng
pDONR™ 221 - GLUT4	Varies	150 ng
5x LR Clonase™ Reaction buffer	2 µL	1x

» Incubate at 25 ºC for 2 hours.
» Add 1 µL of proteinase K and incubate at 37 ºC for 10 minutes.
» Transform 2 µL of reaction per 50 µL of competent bacteria as described in section: 4.1. Transformation. Use 100 µg/mL ampicillin as selection antibiotic.
» Extract DNA from different colonies (at least five) using PureLink® HiPure Plasmid Miniprep Kit, or equivalent, as described in section: 4.4. Plasmid Purification.
» Sequence DNA using the appropriate primers from primers from table III-8.

Table III-8. Sequencing primers.

Name	Target	Primer	
RatGLUT4 INT	RatGLUT4	F	5'-ATGGCTGTAGTTGGTTTCTCC-3'
		R	5'-CCTAAGAGTGCCTGAAACCA-3'
BtGLUT4 INT	BtGLUT4	F	5'-GAACACTGTCCAATAAGGCGAG-3'
		R	5'-CTCGCCTTATTGGACAGTGTTC-3'
M13	pDONR™	F	5'-GTTTTCCCAGTCACGAC-3'
		R	5'-CAGGAAACAGCTATGAC-3'
CMV MSCV	pLenti CMV/TO	F	5'-CGCAAATGGGCGGTAGGCGTG-3'
		R	5'-CAGCGGGGCTGCTAAAGCGCATGC-3'

4.4. Plasmid Purification

4.4.1.Bacterial growth

Minipreps

» Prepare a sterile tube containing 5 mL of LB broth and selection antibiotic.
» Pick a single colony or glycerol stock with sterile pipette tip or toothpick and drop it into the tube.
» Incubate bacterial culture at 37 ºC and under shaking (225 rpm) for 15-16 hours.

Midipreps

» Prepare a sterile tube with 3 mL of LB broth and selection antibiotic.
» Pick a single colony or glycerol stock with sterile pipette tip or toothpick and drop it into the tube.
» Incubate bacterial culture at 37 ºC and under shaking (225 rpm) for 7-8 hours (starter culture).
» Prepare a sterile Erlenmeyer flask with 50 mL of LB broth and selection antibiotic.
» Add 500 µL of starter culture to Erlenmeyer.
» Place Erlenmeyer into shaker at 37 ºC and under shaking (225 rpm) for 15-16 hours.

Maxipreps

» Prepare a sterile tube with 3 mL of LB broth and selection antibiotic.
» Pick a single colony or glycerol stock with sterile pipette tip or toothpick and drop it into the tube.
» Incubate bacterial culture at 37 ºC and under shaking (225 rpm) for 7-8 hours (starter culture).
» Prepare a sterile Erlenmeyer flask with 250 mL of LB broth and selection antibiotic.
» Add 500 -1000 µL of starter culture to Erlenmeyer.
» Place Erlenmeyer into shaker at 37 ºC and under shaking (225 rpm) for 15-16 hours.

4.4.2. Plasmid purification

Plasmid extraction is done according to the kit's specifications except the elution step. Elute in sterile DNase-free water instead of the kit's elution buffers.

For plasmid purification we use the following commercial kits:

» PureLink® HiPure Plasmid Miniprep Kit
» PureLink® HiPure Plasmid Midiprep Kit
» PureLink® HiPure Plasmid Maxiprep Kit

4.5. Gene expression analysis

4.5.1. RNA isolation

Per well of 6-well dishes containing differentiated 3T3-L1 adipocytes:

» Remove media and add 1 mL of TRI Reagent® Solution.
» Scrape cells into clean tube and leave at RT for 5 minutes.
» Add 200 µL of chloroform, vortex at medium speed for 10 seconds and leave at RT for 10 minutes.
» Centrifuge at 12000 rpm and 4 ºC for 15 minutes.
» Transfer ~500 µL of the colorless, upper aqueous phase containing the RNA to a new tube.
» Add 500 µL of isopropanol and mix by inversion. Leave at RT for 10 minutes.
» Centrifuge at 12.000 rpm and 4 ºC for 10 minutes.
» Remove isopropanol without disturbing the pellet.
» Gently add 1 mL of cold 75 % ethanol and centrifuge at 12.000 rpm and 4 ºC for 5 minutes.
» Remove ethanol without disturbing the pellet.
» Air dry the pellet at RT for 15 minutes.
» Resuspend the pellet in 20 µL RNase-free water.
» Quantify samples and determine A_{260}/A_{230} and A_{260}/A_{280} ratios; If $A_{260}/A_{230} < 1,6$ or
» $A_{260}/A_{280} < 1,8$, proceed to nucleic acid precipitation section to improve sample purity.

4.5.2. Nucleic acid precipitation

» Measure sample volume, approximately.
» Add 1/10 volume of 3 M Sodium Acetate and 2-3 volumes of 100 % ethanol.
» Mix and freeze overnight in -80 ºC freezer.
» Centrifuge at 12.000 rpm and 4 ºC for 15 minutes.
» Remove supernatant without disturbing the pellet.
» Add 2 volumes of cold 70 % ethanol (twice the volume of Sodium Acetate plus 100 % ethanol of previous step).
» Centrifuge at 12.000 rpm and 4 ºC for 10 minutes.
» Remove ethanol without disturbing the pellet.
» Air dry the pellet at RT for 15 minutes.
» Resuspend the pellet in 20 µL RNase-free water.

4.5.3. Reverse transcription

» Add the following components to clean tube:

Table III-9. Reverse transcription reaction 1.

Component	Volumes	Final concentration
ddH2O	Up to 20 µL	-
10x DNase I Buffer	2 µL	1x
DNase I (1 U/µL)	2 µL	0,1 U/µL
RNA template	Varies	2 µg

» Incubate at 37 ºC for 40 minutes.
» Add 1 µL of DNase I stop mix (sold with DNase I).
» Incubate at 65 ºC for 10 minutes.
» Add the following components to current tube:

Table III-10. Reverse transcription reaction 2.

Component	Volumes	Final concentration
ddH2O	2 µL	-
Random primers (500 µg/mL)	1 µL	18,5 ng/mL
Oligo(dT) 15 primer (500 µg/mL)	1 µL	18,5 ng/mL
10 mM dNTP mix	2 µL	0,74 mM

» Incubate at 65 ºC for 5 minutes.
» Add the following components to current tube:

Table III-11. Reverse transcription reaction 3.

Component	Volumes	Final concentration
5x SuperScript™ III buffer	8 µL	1x
100 mM DTT	2 µL	5,2 mM
SuperScript™ III (200 U/µL)	1,8 µL	9,3 U/µL

» Incubate at 55 ºC for 1 hour.
» Incubate at 70 ºC for 15 minutes.
» Use or store at -80 ºC.

4.5.4. qPCR (Quantitative real-time polymerase chain reaction)

In this work we analyzed the expression of GFP and ARP (housekeep) genes.

» Add the following components to well of 96-well PCR plate (load triplicates of each sample):

Table III-12. qPCR reaction.

Component	Volumes	Final concentration
ddH2O	Up to 20 µL	-
2x SYBR GreenER™ Super mix	10 µL	1x
10 µM Forward Primer	1 µL	0,5 µM
10 µM Reverse Primer	1 µL	0,5 µM
cDNA Template	Varies	1 µg

Table III-13. GFP and ARP primers.

Gene		Primer
GFP	F	5'- AAGCAGCACGACTTCTTCAAGTC -3'
	R	5'- TCGCCCTCGAACTTCACCTC -3'
ARP	F	5'- AAGCGCGTCCTGGCATTGTCT -3'
	R	5'- CCGCAGGGGCAGCAGTGGT -3'

» Follow the qPCR protocol below on a Bio-Rad iCycler®.

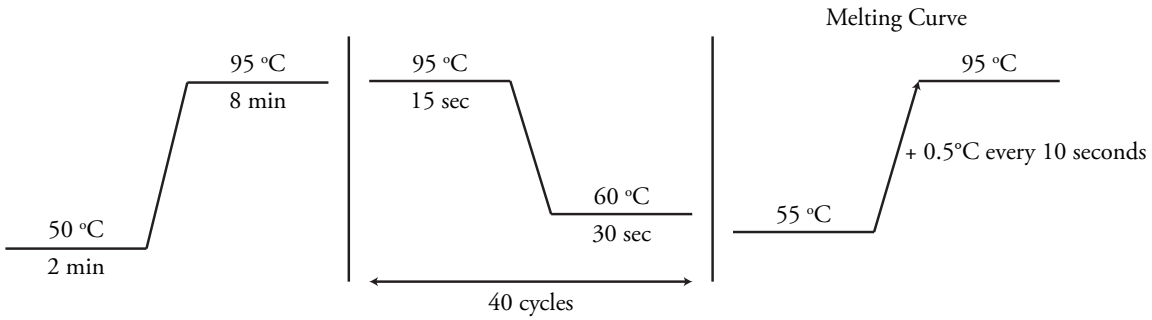

Figure III-18. Schematic representation of the qPCR reaction protocol.

5. BIOCHEMISTRY

5.1. Protein Quantification

In this thesis we used Pierce® BCA Protein Assay Reagent kit.

» Using albumin standard (BSA, Bovine serum albumin) (2 mg/mL) included in the kit, generate a 0-30 µg standard curve by loading the appropriate volumes on ELISA plate. Load replicates as well.
» Load samples and its replicates. Loading volumes depend on sample concentration. In this thesis we use volumes ranging from 2,5-10 µL.
» Prepare working reagent by mixing solution A with B at 50:1 ratio.
» Add 200 µL of working reagent to each well and incubate at 37 ºC for 30 minutes.
» Read absorbance at 562 nm.
» Plot each BSA measurements against its concentration and use standard curve equation (linear regression) to determine the concentration of each unknown sample.

5.2. SDS-PAGE and Western Blot

In this thesis we used BioRad Mini-PROTEAN® and Mini-Trans Blot® Cells.

5.2.1. Gel preparation

» Prepare resolving gel solution according to table III-14.
» Transfer solution into glass plates (7,5 mL per gel) and gently add a layer of isopropanol on top. Allow polymerization for 20 minutes.
» Remove isopropanol and prepare stacking gel solution according to table III-15.
» Add stacking gel solution on top of resolving gel and place comb. Allow gel polymerization for 20 minutes.

Table III-14. Polyacrylamide resolving gel solution.

Resolving gel solution				
	8 %	**10 %**	**12 %**	**Final Concentration**
30 % Acrylamide	2,67 mL	3,33 mL	4 mL	Varies
1,5 M Tris pH=8,8	2,5 mL	2,5 mL	2,5 mL	0,375 M
10 % SDS	100 µL	100 µL	100 µL	0,1 %
10 % APS	100 µL	100 µL	100 µL	0,1 %
100 % TEMED	10 µL	10 µL	10 µL	0,1 %
ddH2O	Up to 10 mL	Up to 10 mL	Up to 10 mL	

Table III-15. Polyacrylamide stacking gel solution.

Stacking gel solution		
	5 %	**Final Concentration**
30 % Acrylamide	0,83 mL	5 %
0,5 M Tris pH=6,8	1,26 mL	0,125 M
10 % SDS	50 µL	0,1 %
10 % APS	50 µL	0,1 %
100 % TEMED	5 µL	0,1 %
ddH2O	Up to 5 mL	

5.2.2. Electrophoresis

» Prepare samples by adding 1x Laemmli buffer and 100 mM DTT (optional) and boil at 95 ºC for 5 minutes.
» Assemble electrophoresis system and fill with 1x running buffer (table III-16).
» Load samples and ladder.
» Run electrophoresis at 80-90 V during stacking gel migration and 100-110 V during resolving gel migration.

5.2.3.Transfer

» Prepare a tray with cold 1x transfer buffer (table III-16).
» Assemble gel cassette sandwich inside the tray as follows (from bottom to top): fiber pad, two pieces of filter paper, resolving gel, PVDF membrane, two pieces of filter paper and fiber pad. Avoid air bubbles.
» Insert cassette in transfer module (top towards positive pole). Place module and frozen cooling unit in transfer tank and fill with cold 1x transfer buffer.
» Run transfer at 100 V and 4 ºC for 90 minutes.

Table III-16. Running and transfer buffers.

	Running buffer	Transfer buffer
	Final Concentration	
Glycine	192 mM	
Tris-Base	25 mM	
SDS	0,1 %	-
Ethanol	-	10 %

5.2.4.Blocking and blotting

» Place membrane in blocking solution (5 % nonfat dry milk in 1x PBS with 0,1 % TWEEN® 20) at RT for 1 hour on rocking platform.
» Incubate membrane in primary antibody solution at 4 ºC overnight.
» Wash membrane three times, for 5 minutes each, in washing buffer (1 % nonfat dry milk in 1x PBS with 0,02 % TWEEN® 20).

» Incubate membrane in secondary antibody solution at RT for 90 minutes.
» Wash membrane three times, for 5 minutes each, in washing buffer (1 % nonfat dry milk in 1x PBS with 0,02 % TWEEN® 20).

5.2.5. Develop

» Mix ECL 1 and ECL 2 solutions at 1:1 ratio (6. General Solutions Recipes).
» Incubate membrane in mixture for 1 minute.
» Expose x-ray film to membrane. Exposure times vary with signal intensity.
» Develop using a radiographic film developer.

5.3. Immunoadsorption

In this thesis we used µMACS Anti-GFP Starting Kit.

Per 6 cm dish:

» Wash twice with warm DMEM-BB.
» Serum starve cells in DMEM-BB for 2 hours inside incubator.
» Wash twice with cold 1x Media II.
» Add 700 µL of cold lysis buffer (20 mM HEPES; 1 mM EDTA; 250 mM Sucrose; 1x Protease Inhibitor Cocktail) and scrape cells.
» Pass through 27g ½ syringe about 7 times.
» Spin down at 2000 rpm and 4 °C for 7 minutes. Recover supernatant.
» Repeat centrifugation and supernatant recovery two more times.
» Incubate lysate with α-GFP magnetic beads on rotating shaker at 4 °C for 90 minutes.
» Place separating column on magnetic stand and prime with 500 µL of lysis buffer. Let buffer run through.
» Transfer lysate and beads mix onto column; Let mix run through.
» Wash thrice with 200 µL of lysis buffer.
» Apply 20 µL of 95 °C hot 1x Laemmli buffer with 100 mM DTT to column and incubate for 5 minutes. Collect eluate.
» Apply 50 µL of 95 °C hot 1x Laemmli buffer with 100 mM DTT to column and collect eluate.
» Repeat with another 50 µL of 1x Laemmli buffer with 100 mM DTT.

5.4. GLUT4 INTERNALIZATION PATHWAYS

In the following protocols we use 3T3-L1 adipocytes grown in coverslips. Prepare five sets of coverslips (Background; T=0 untreated; T=0 treated; T=10 untreated; T=10 treated) with 3T3-L1 adipocytes. Include replicates.

5.4.1. GLUT4 clathrin-mediated endocytosis

Clathrin-mediated endocytosis is inhibited by hyperosmotic shock with sucrose, in the absence and presence of insulin.

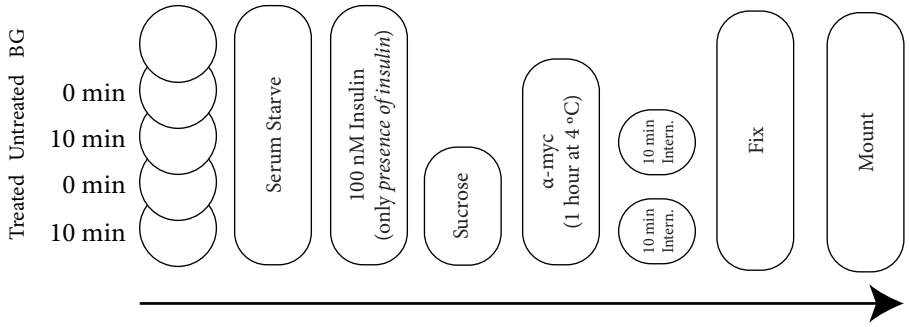

Figure III-19. Schematic representation of the GLUT4 clathrin-mediated endocytosis protocol.

Absence of insulin

» Serum starve cells in DMEM-BB for 2 hours inside incubator.
» Treat cells with or without 450 mM sucrose in DMEM-BB for 30 minutes inside incubator.
» Proceed to: Antibody binding and internalization.

Presence of insulin

» Serum starve cells in DMEM-BB for 2 hours inside incubator.
» Challenge cells with 100 nM insulin in DMEM-BB for 30 minutes inside incubator.
» Add fresh 100 nM insulin-DMEM-BB media with or without 450 mM sucrose and place into incubator for 30 minutes.
» Proceed to: Antibody binding and internalization.

Antibody binding and internalization

» Incubate with 1:100 dilution of α-myc in 5 % FBS-DMEM-BB with or without sucrose/nystatin, in the absence or presence of insulin, at 4 °C for 1 hour. Leave background in 5 % FBS-DMEM-BB without α-myc.
» **For T=0 untreated; T=0 treated; background:**
Wash twice with cold 1x Media II.
Fix in 3,7 % paraformaldehyde at RT for 6 minutes.
» **For T=10 untreated; T=10 treated:**
Wash twice with lukewarm 1x Media II.

Incubate with DMEM-BB with or without sucrose/nystatin, in the absence or presence of insulin, for 10 minutes inside incubator.
Wash twice with cold 1x Media II.
Fix in 3,7 % paraformaldehyde at RT for 6 minutes.

» Wash once with 100 mM glycine-PBS.
» Wash thrice with 1x PBS.
» Proceed to: Detection of GLUT4 remaining at the cell surface.

5.5.2. GLUT4 cholesterol-dependent endocytosis

Cholesterol-dependent endocytosis is inhibited by nystatin-induced cholesterol depletion. Inhibition is carried out in the absence and presence of insulin.

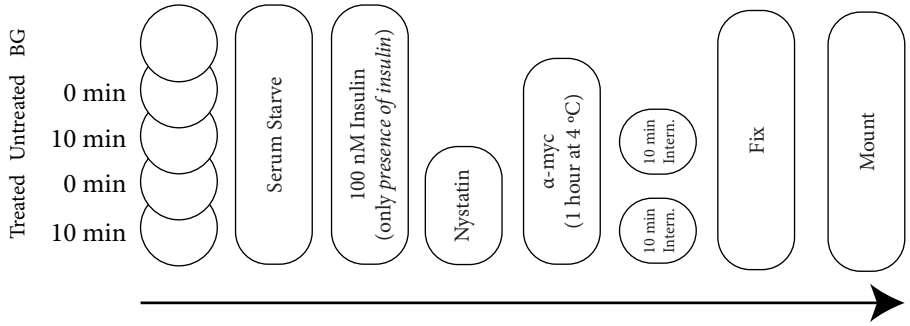

Figure III-20. Schematic representation of the GLUT4 cholesterol-dependent endocytosis protocol.

Absence of insulin

» Serum starve cells in DMEM-BB for 2 hours inside incubator.
» Treat cells with or without 50 µg/mL nystatin in DMEM-BB for 30 minutes inside incubator.
» Proceed to: Antibody binding and internalization.

Presence of insulin:

» Serum starve cells in DMEM-BB for 2 hours inside incubator.
» Challenge cells with 100 nM insulin in DMEM-BB for 30 minutes inside incubator.
» Add fresh 100 nM insulin-DMEM-BB media with or without 50 µg/mL nystatin and place into incubator for 30 minutes.
» Proceed to: Antibody binding and internalization.

Antibody binding and internalization

» Incubate with 1:100 dilution of α-myc in 5 % FBS-DMEM-BB with or without sucrose/nystatin, in the absence or presence of insulin, at 4 °C for 1 hour. Leave background in 5 % FBS-DMEM-BB without α-myc.
» **For T=0 untreated; T=0 treated; background:**
Wash twice with cold 1x Media II.

Fix in 3,7 % paraformaldehyde at RT for 6 minutes.

» **For T=10 untreated; T=10 treated:**
Wash twice with lukewarm 1x Media II.
Incubate with DMEM-BB with or without sucrose/nystatin, in the absence or presence of insulin, for 10 minutes inside incubator.
Wash twice with cold 1x Media II.
Fix in 3,7 % paraformaldehyde at RT for 6 minutes.

» Wash once with 100 mM glycine-PBS.

» Wash thrice with 1x PBS.

» Proceed to: Detection of GLUT4 remaining at the cell surface.

Detection of GLUT4 remaining at the cell surface

» Incubate with 1:500 dilution of α-mouse HRP in DMEM-BB at 37 ºC for 1 hour.

» Wash thrice with 1x PBS.

» Dilute one OPD tablet in 50 mL of OPD buffer (50 mM Na_2HPO_4; 37 mM $C_6H_8O_7$; pH=5.0). Just before using add 20 µL of 30 % H_2O_2.

» Add OPD solution and leave for 10 minutes.

» Stop reaction by adding 3 M HCl (250 µL per 1 mL of OPD solution).

» Read absorbance at 492 nm.

5.5. Glucose transport

The following protocol is performed using fibroblasts stably-expressing GLUT4 constructs.

Per well of 6-well dishes:

» Wash twice with DMEM-BB and challenged with 100 nM insulin in DMEM-BB for 30 minutes inside incubator.
» Wash thrice with 1x Media II.
» Add 0,9 mL of Krebs-Ringer-HEPES buffer (137 mM NaCl; 4,7 mM KCl; 1,18 mM $MgSO_4$.7H2O; 1,18 mM KH_2PO_4; 2,5 mM $CaCl_2.H_2O$; 20 mM HEPES; 0,2 % (w/v) BSA; 2 mM sodium pyruvate; pH=7,4) and place plates into incubator for 30 minutes.
» Add 0,1 mL of 2-deoxyglucose mix (10 µCi/ml [^{3}H] 2-deoxyglucose and 1 mM 2-deoxyglucose in Krebs-Ringer-HEPES buffer) and leave inside incubator for 5 minutes.
» Halt transport by adding cold STOP buffer (50 mM D-(+)-glucose in 1x PBS).
» Wash thrice with cold STOP buffer to remove non-incorporated radioactivity.
» Add 800 µL of lysis buffer (100 mM NaOH; 0,1 % (v/v) SDS) and scrape off cells.
» Mix 250 µL of lysate with 3 mL of scintillation liquid and measure incorporated radioactivity in a β-counter.
» Determine protein concentration on 20 µL of remaining lysate (5.1. Protein Quantification).
» Calculate [^{3}H]-2-deoxyglucose uptake (nmol/mg of protein) using the following mathematical equation:

$$\frac{\textbf{dpm (vial)}}{\textbf{dpm (total)}} \cdot \frac{\textbf{800 µL (lysis volume)}}{\textbf{250 µL (measured volume)}} \cdot \frac{\textbf{100 nmol (2DG)}}{\textbf{µg (protein in 800 µL)}} \cdot \frac{\textbf{1000 µg}}{\textbf{1 mg}}$$

6. GENERAL SOLUTIONS RECIPES

10x Phosphate buffered saline (PBS):

» 1,37 M NaCL;
» 27 mM KCl;
» 100 mM Na2HPO4.2H2O;
» 18 mM KH2PO4;
» pH=6,9;
» Sterilize in autoclave.

10x Media II:

» 1,5 M NaCL;
» 0,2 M HEPES;
» 50 mM KH2PO4;
» 10 mM CaCl2.2H2O;
» 10 mM MgCl2.6H2O;
» pH=7,55;
» Sterilize in autoclave.

Enhanced chemiluminescence (ECL) solutions:

ECL1

» 5 mL of 1 M Tris-HCl, pH=8,5;
» 250 µL of 0,5 M luminol;
» 250 µL of 79,2 mM p-Coumaric acid;
» Bring to 50 mL with dH2O.

ECL2

» 5 mL of 1 M Tris-HCl, pH=8,5;
» 32 µL of 8,8 M of 30 % hydrogen peroxide;
» Bring to 50 mL with dH2O.

Working solution

» Mix equal parts of ECL1 and ECL2 to prepare working solution.

4x Laemmli buffer

» 0,125 M Tris-HCl, pH=6,8;
» 8 % sodium dodecyl sulfate (SDS);
» 40 % glycerol;
» 0,04 % bromophenol blue.

Polyethylenimine (PEI)

- 1 mg/mL;
- dH2O;
- pH=7
- 0,2 µm filtered.

Insulin stock

- 1 mg/mL = 170 mM;
- 0,01N HCl;
- 0,2 µm filtered.

Dexamethasone stock

- 2,5 mM;
- dH2O;
- 0,2 µm filtered.

IBMX stock

- 55,6 mg/mL;
- 0,35 N KOH;
- 0,2 µm filtered.

Rosiglitazone stock

- 10 mM;
- DMSO;
- 0,2 µm filtered.

Collagenase D stock

- 50 mg/mL;
- 1x PBS;
- 0,2 µm filtered.

7. PRODUCT REFERENCES

Table III-17. Reagent information.

Product	Vendor	Catalog Number
2-deoxy[3H]-glucose	American Radiolabeled	ART-103A
2-deoxyglucose	Sigma	D8375
Acrylamide/Bis-Acrylamide 30%	Sigma	A3574
Ammonium persulfate (APS)	Sigma	A3678
Ampicillin	Sigma	A9518
Bromophenol Blue	Sigma	B0126
BSA – Fatty acid free	Sigma	A6003
Chloroform	Merck Millipore	102445
Cholera Toxin Subunit B-Alexa Fluor 555	Thermo Fisher	C34776
Collagenase D	Sigma	11088866001
D-(+)-glucose	Sigma	G8270
Dexamethazone	Sigma	D2915
DMEM 4,5 g/l Glucose; w/ L-Gln; w/ sodium pyruvate	LabClinics	L0104
DMSO	Sigma	D2650
DNase I	Thermo Fisher	18068015
dNTPs mix (10 mM each)	Biotools	20.031
Dpn I	NEB	R0176
DTT	Sigma	43819
Ethanol absolute pure	Panreac	141086.1212
Fetal Bovine Serum	Thermo Fisher	10067164
Filter Paper (Whatman)	Whatman	3030-917
Gateway® BP Clonase® II Enzyme mix	Thermo Fisher	11789100
Gateway® LR Clonase® II Enzyme mix	Thermo Fisher	11791020
Glycine	Roche	03117251001
Halt™ Protease Inhibitor Cocktail	Thermo Fisher	78430
HEPES	Sigma	H3375
IBMX	Sigma	I5879
Insulin	Sigma	I5500
Isopropanol	Panreac	131090.1611
Kanamycin	Sigma	K1377
LB broth	Sigma	L3022
LB broth with agar	Sigma	L2897
Luminol	Sigma	09253
MicroPulser™ Electroporation Cuvettes	BioRad	1652088
Newborn Calf Serum	Thermo Fisher	16010159
Nystatin	Sigma	N4014
o-Phenylenediamine	Sigma	P5412
Oligo(dT) 15 primer	Promega	C1101
OPD tablets	Sigma	P5412
p-Coumaric acid	Sigma	28200
Paraformaldehyde 16% aqueous solution	Anema	15700
PEI	Polysciences	23966
Penicillin-Streptomycin (10,000 U/mL)	Thermo Fisher	15140122
Phusion® High-Fidelity DNA Polymerase	NEB	M0531
Pierce® BCA Protein Assay Reagent	Thermo Fisher	23225

Platinum® Taq DNA Polymerase High Fidelity	Thermo Fisher	11304011
ProLong® Gold Antifade	Thermo Fisher	P36930
Protein Ladder	Bioline	BIO-33066
PureLink® HiPure Plasmid Maxiprep Kit	Thermo Fisher	K210006
PureLink® HiPure Plasmid Midiprep Kit	Thermo Fisher	K210004
PureLink® HiPure Plasmid Miniprep Kit	Thermo Fisher	K21002
PureLink™ Quick Gel Extraction and PCR Purification COMBO kit	Thermo Fisher	K220001
Puromycin	Sigma	P9620
PVDF Membrane	Merck Millipore	IPVH00010
Random primers	Promega	C1181
Rosiglitazone	Sigma	R2408
Saponin from quillaja bark	Sigma	S4521
Scintillation liquid	Ecolite	882475
Sodium acetate (3 M), pH 5.5	Thermo Fisher	AM9740
Sodium chloride	Panreac	A2942
Sodium dodecyl sulfate (SDS)	Panreac	142363
Sodium pyruvate	Sigma	P2256
Sucrose	Sigma	S0389
SuperScript™ III Reverse Transcriptase	Thermo Fisher	18080044
SYBR GreenER™ qPCR SuperMix for iCycler®	Thermo Fisher	11761500
TEMED	Sigma	T22500
Transferrin-Alexa Fluor 555	Thermo Fisher	T35352
TRI Reagent® Solution	Thermo Fisher	AM9738
TRIS-Base	Sigma	T1503
Trypsin-EDTA (0,05%)	Thermo Fisher	25300062
Tween®20	Sigma	P1379
Water (Sterile, DNase-free, RNase-free)	Sigma	W4502
X-Ray films	Fujifilm	4741008389
µMACS Anti-GFP Starting Kit	Miltenyi Biotec	130-091-288

Table III-18. Primary antibody information.

Antibody	Host	Vendor	Catalog Number	MW (kDa)	Dilution
Myc Tag	Mouse	Life Tech	13-2500	-	IF: 1:75-1:300; IC: 1:100
Syntaxin 6	Rabbit	Cell Signaling	2869T	32	WB: 1:1000; IF: 1:200
TUG	Rabbit	Cell Signaling	2049S	70	WB: 1:1000
GAPDH	Rabbit	Cell Signaling	5174T	37	WB: 1:3000
AS-160	Rabbit	Millipore	07-741	160	WB: 1:1000
IRAP	Rabbit	Cell Signaling	3808S	165	WB: 1:1000
TR	Rabbit	Abcam	Ab84036	98	WB: 1:10000
Caveolin-1	Rabbit	Transduction Lab.	610406	22	WB: 1:3000
GFP	Rabbit	GenScript	A01388	-	WB: 1:1000
β-Actin	Mouse	Sigma	AC-15	45	WB: 1:1000

Table III-19. Secondary antibody information.

Antibody	Host	Vendor	Catalog Number	Dilution
α-mouse Alexa Fluor 555	Goat	Thermo Fisher	A31570	1:300
α-mouse Alexa Fluor 660	Goat	Thermo Fisher	A21055	1:50
Donkey α-Rabbit IgG	Donkey	Jackson I. R.	711-165-152	1:10000
Donkey α-Mouse IgG	Donkey	Jackson I. R.	715-035-150	1:500; 1:10000

IV. RESULTS

1. CHARACTERIZATION OF THE GENERAL TRAFFICKING OF RatGLUT4 AND BtGLUT4.

1.1. Transient expression of RatGLUT4 and BtGLUT4 in 3T3-L1 adipocytes.

In this work, we characterized the cellular trafficking of rat (*Rattus norvegicus*, RatGLUT4) and brown trout GLUT4 (*Salmo trutta*, BtGLUT4) in 3T3-L1 adipocytes by transient expression. 3T3-L1 adipocytes were electroporated with RatGLUT4 or BtGLUT4 cloned in the pcDNA3 vector (kindly provided by Dr. Encarnacion Capilla) that allowed us to express these transporters fused with GFP at their C-terminal end. These constructs were also engineered for the insertion of the myc tag in the first extracellular loop (Figure IV-1a).

When expressing our GLUT4 constructs, first and foremost, we wanted to ensure that the constructs were expressed correctly and that we obtained similar expression levels. To do so, we electroporated 3T3-L1 adipocytes with the RatGLUT4 or BtGLUT4 constructs, fixed cells and measured their total GFP fluorescence.

In Figure IV-1b we observe that, despite presenting similar intracellular localization, BtGLUT4-expressing cells presented rims on their plasma membrane in the absence of insulin, in contrast to RatGLUT4-expressing adipocytes. In Figure IV-1c we observe that RatGLUT4 and BtGLUT4 presented similar levels and distribution of GFP signal, which indicates that the constructs were expressed similarly across the cell population. In summary, at similar expression levels and in the absence of insulin, BtGLUT4 showed increased targeting to the plasma membrane when compared to RatGLUT4. It is also noteworthy that when expressing our GLUT4 constructs we did not obtain any aberrant GFP bodies which would indicate overexpression and saturation of the cellular trafficking machinery.

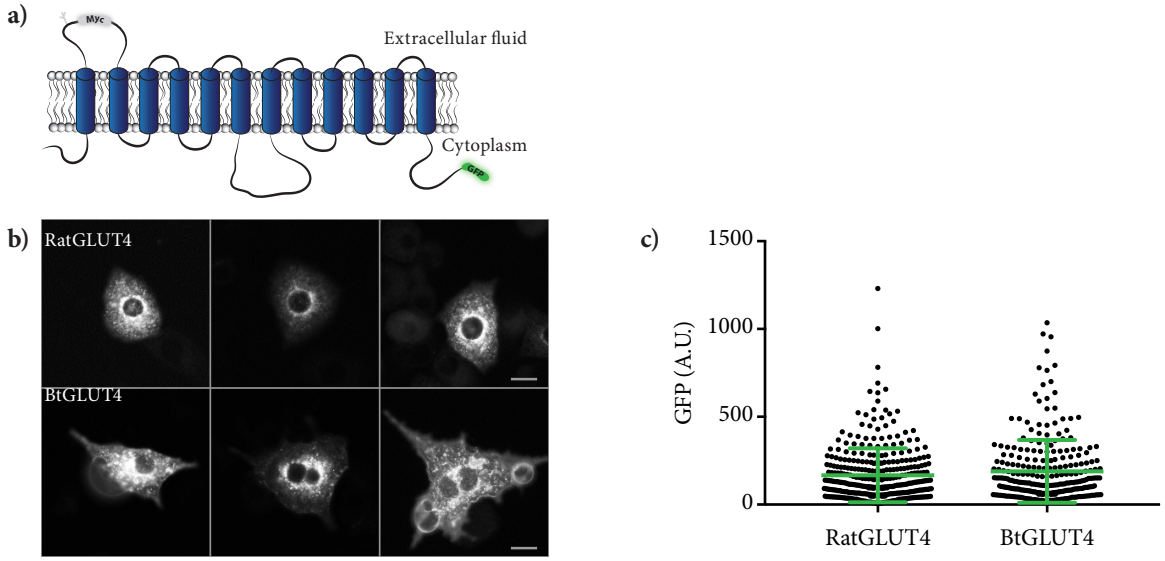

Figure IV-1. RatGLUT4 and BtGLUT4 expression in 3T3-L1 adipocytes. **a)** Schematic representation of RatGLUT4 and BtGLUT4 constructs. Both constructs possess a myc tag on the first extracellular loop and GFP on the C-terminal end. **b)** 3T3-L1 adipocytes electroporated with RatGLUT4 or BtGLUT4 were serum starved for 2 hours. Cells were then fixed with 3,7 % paraformaldehyde for 6 minutes at RT and imaged under a DMIRB inverted Leica microscope using a 20 x air objective. **c)** GFP signal of individual cells was measured using Fiji

processing software, background corrected and plotted using GraphPad Prism software. Scale bar, 20 μm. A.U.: Arbitrary units.

1.2. Characterization of RatGLUT4 and BtGLUT4 cell surface levels.

1.2.1. RatGLUT4 and BtGLUT4 translocation and plasma membrane levels.

GLUT4 is a very mobile transporter: it is constantly cycling between intracellular compartments and the plasma membrane. In the absence of insulin, most GLUT4 is kept inside the cell (about 95 %) but in the presence of insulin it is mobilized to the plasma membrane to uptake glucose (>50 % at the cell surface). This feature characterizes GLUT4 and it is essential for its correct functioning. Because this is such an important mechanism we wanted to quantify the percentage of rat and brown trout GLUT4 at the plasma membrane in the absence and presence of insulin when expressed in 3T3-L1 adipocytes.

To assess how much GLUT4 is distributed to the plasma membrane we electroporated 3T3-L1 cells with RatGLUT4 or BtGLUT4 and probed the exofacial myc epitope to label surface GLUT4, in serum-starved and insulin-stimulated adipocytes. We also used myc to label the entire pool of RatGLUT4 and BtGLUT4 in permeabilized cells (Figure IV-2a).

As observed in Figure IV-2b, only 8-9 % of RatGLUT4 is present at the plasma membrane in the absence of insulin while that value increases to about 40 % for BtGLUT4. In the presence of insulin RatGLUT4 increases its distribution to the plasma membrane by almost 10-fold whereas BtGLUT4 increases 1,5-fold (Figure IV-2c). This shy translocation of BtGLUT4 is mainly a consequence of its higher basal surface levels but also due to lower surface levels in the presence of insulin.

In summary, BtGLUT4 showed an impaired translocation to the plasma membrane especially due to poor intracellular retention in the absence the insulin.

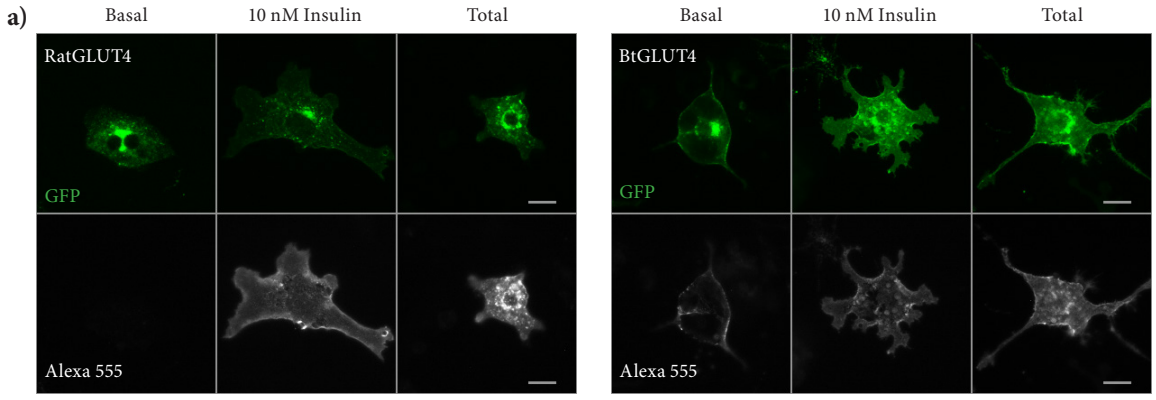

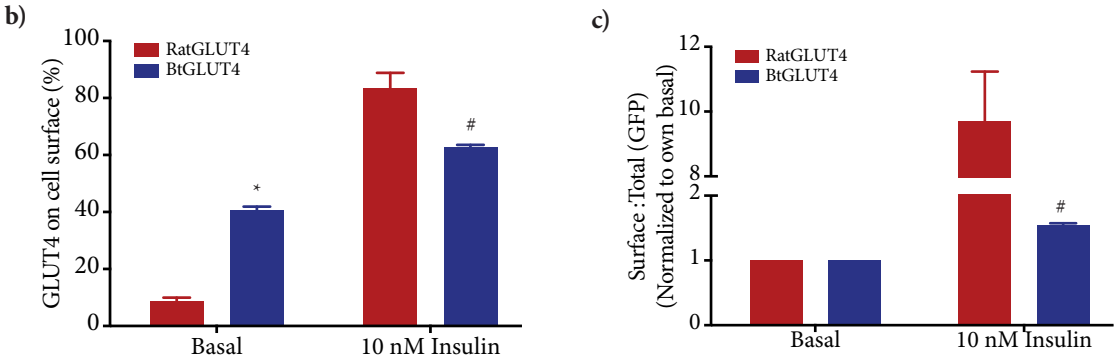

Figure IV-2. RatGLUT4 and BtGLUT4 plasma membrane levels in 3T3-L1 adipocytes. **a)** Images of RatGLUT4- and BtGLUT4-expressing 3T3-L1 adipocytes under a DMIRB inverted Leica microscope using a 20 x air objective showing GFP (total GLUT4 expression) and Alexa 555 (surface GLUT4) signals of individual cells. Graphs show cell surface levels of RatGLUT4 and BtGLUT4 in the absence and presence of 10 nM Insulin and data were expressed as **b)** cell surface levels normalized to total levels to determine GLUT4 percentage at cell surface and as **c)** cell surface levels in the presence of 10 nM Insulin normalized to the basal levels to determine GLUT4 translocation to the plasma membrane. Data were plotted and Student's t test was performed using GraphPad Prism software. Red bars represent RatGLUT4 and blue bars represent BtGLUT4. Figure represents the mean ± SEM of four independent experiments. *, $p<0,05$ vs RatGLUT4 Basal; #, $p<0,05$ vs RatGLUT4 10 nM Insulin. Scale bar, 20 μm.

1.2.2. RatGLUT4 and BtGLUT4 translocation at lower temperatures.

As an ectothermic vertebrate, the body temperature of brown trout varies with water temperature, ranging from 0 ºC to 26 ºC. On the other hand, body temperature in mammals is stable throughout the year at 37 ºC. Because BtGLUT4 naturally performs at lower temperatures than RatGLUT4 we decided to analyze its translocation at 25 ºC, which falls within the range of the body temperature of trout and is a temperature at which 3T3-L1 adipocytes can still cope. To do so, we electroporated 3T3-L1 cells with RatGLUT4 or BtGLUT4 and probed surface GLUT4 in serum-starved and insulin-stimulated adipocytes at 37 ºC and 25 ºC (Figure IV-3a).

In Figure IV-3b we observe that RatGLUT4 translocation at 25 ºC was 26 % lower than at 37 ºC, especially as a result of poor intracellular retention in the absence of insulin (Figure IV-3a). Conversely, BtGLUT4 translocation at 25 ºC was only 6 % lower than at 37 ºC (Figure IV-3B).

Even though the translocation of BtGLUT4 did not improve at 25 ºC, which is within the upper rage of body temperature of trout, it was less affected than that of RatGLUT4.

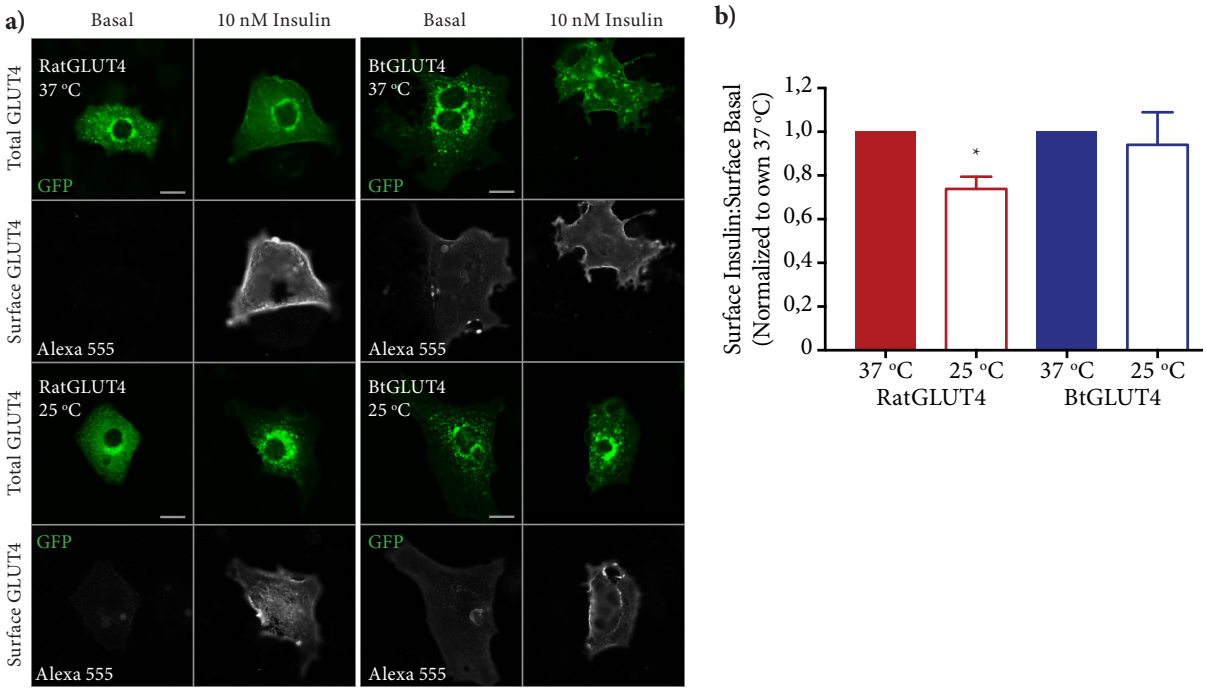

Figure IV-3. Effect of temperature on RatGLUT4 and BtGLUT4 translocation to the plasma membrane. **a)** Images of RatGLUT4- and BtGLUT4-expressing 3T3-L1 adipocytes under a DMIRB inverted Leica microscope using a 20 x air objective showing GFP (total GLUT4 expression) and Alexa 555 (surface GLUT4) signals of individual cells. **b)** Graph shows translocation of RatGLUT4 and BtGLUT4 cell surface levels in response to insulin at 25 °C and 37 °C. Data were expressed as surface levels in the presence of 10 nM Insulin normalized to the basal levels to determine GLUT4 translocation to the plasma membrane. Translocation of RatGLUT4 and BtGLUT4 were normalized to their own 37 °C treatment. Data were plotted and Student's t test was performed using GraphPad Prism software. Red represents RatGLUT4 data and blue represents BtGLUT4 data. Figure represents the mean ± SEM of four independent experiments. *, $p<0,05$ vs own 37 °C treatment. Scale bar, 20 µm.

1.2.3. RatGLUT4 and BtGLUT4 plasma membrane levels after insulin removal (Return-to-basal).

The efficient functioning of GLUT4 relies on the its ability of GLUT4 to traffic to and from the plasma membrane. Upon insulin action, GLUT4 is fast mobilized from intracellular compartments to the plasma membrane where it uptakes glucose. However, when glucose transport is not required anymore, GLUT4 must be removed from the cell surface into its intracellular compartments – return to basal state. To assess the ability of RatGLUT4 and BtGLUT4 to return to the basal state after insulin challenge, we electroporated 3T3-L1 adipocytes with one or the other construct and detected their surface levels in serum-starved, in insulin-stimulated and in insulin-stimulated plus insulin-removed (washout) adipocytes (Figure IV-4a).

In Figure IV-4b we observe that 30 minutes after insulin washout, RatGLUT4 returned to its basal levels (serum-starved). After insulin challenge RatGLUT4 increased its surface levels by 85 % and reduced them by 72 % after insulin removal. On the other hand, BtGLUT4 increased its surface levels by 45 % in the presence of insulin and reduced them by 26 %, 30 minutes after insulin washout.

In summary, we observed that RatGLUT4 was able to return to its basal state after 30 minutes of insulin removal whereas BtGLUT4 did not return to its basal cell surface levels.

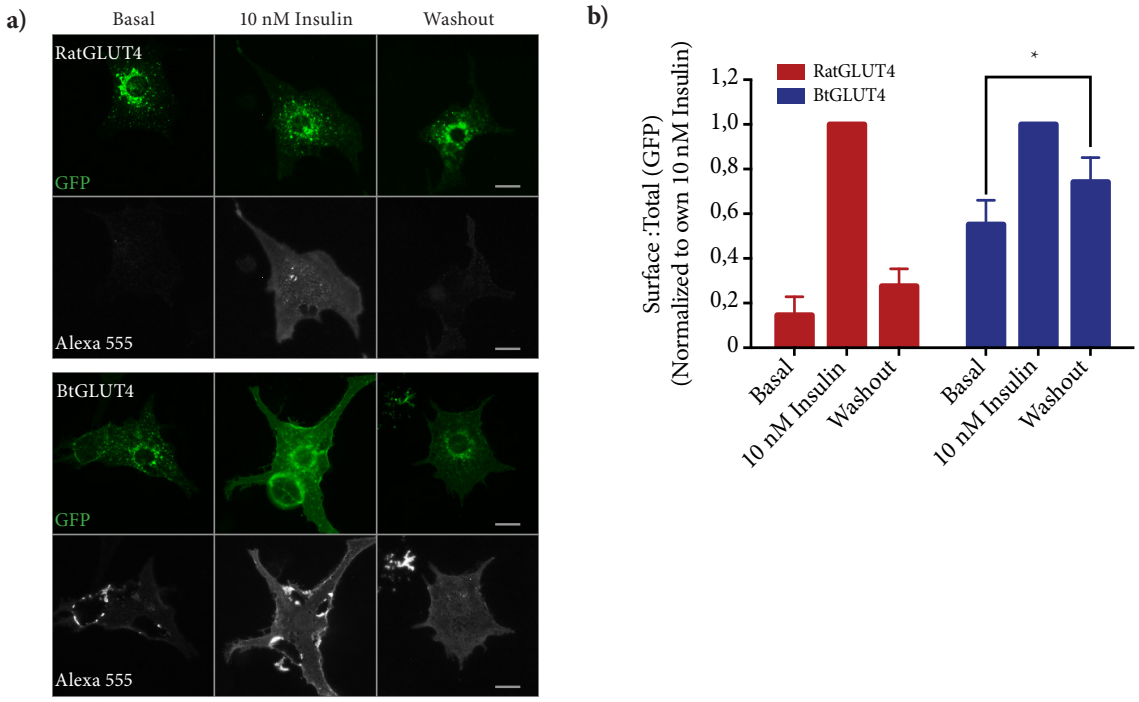

Figure IV-4. RatGLUT4 and BtGLUT4 plasma membrane removal after insulin washout: return-to-basal. **a)** Images of RatGLUT4- and BtGLUT4-expressing 3T3-L1 adipocytes under a DMIRB inverted Leica microscope using a 20 x air objective showing GFP (total GLUT4 expression) and Alexa 555 (surface GLUT4) signals of individual cells. **b)** Graph shows cell surface levels of RatGLUT4 and BtGLUT4 in the absence, presence of 10 nM Insulin and after insulin removal (washout). Data were expressed as cell surface levels normalized to total expression (GFP) to determine the fraction of GLUT4 at the cell surface. Fractions of RatGLUT4 and BtGLUT4 at the cell surface were normalized to their own 10 nM Insulin treatment. Data were plotted and Student's t test was performed using GraphPad Prism software. Red bars represent RatGLUT4 data and blue bars represent BtGLUT4 data. Figure represents the mean ± SEM of five independent experiments. *, $p<0,05$. Scale bar, 20 µm.

1.3. Characterization of RatGLUT4 and BtGLUT4 exocytosis and endocytosis.

1.3.1. Exocytosis of RatGLUT4 and BtGLUT4.

One of the most interesting features of GLUT4 is its ability to control its functioning by changing its cellular localization. GLUT4 is constantly cycling between intracellular compartments and the plasma membrane but in the absence of insulin the majority of GLUT4 localizes in intracellular compartments whereas in the presence of insulin the bulk of GLUT4 is recruited to the plasma membrane to uptake glucose. GLUT4 cellular distribution is highly determined by the balance between the rates of endocytosis and exocytosis. Exocytosis greatly outweighs endocytosis as a regulator of GLUT4 localization: in the absence of insulin the exocytosis of GLUT4 is slow but in the presence of insulin it increases up to 20-fold; on the other hand, GLUT4 endocytosis only slightly decreases in the presence of insulin (Karylowski et al. 2004, Blot and McGraw 2006).

Because exocytosis is such an important mechanism for GLUT4 functioning and because BtGLUT4 shows high surface levels in the absence of insulin and a poor translocation in response to the hormone, we wanted to analyze its exocytosis in the absence and presence of insulin. To do so, we electroporated 3T3-L1 adipocytes with RatGLUT4 or BtGLUT4, we serum starved the

cells and challenged them with or without insulin and then we incubated the adipocytes with a saturating concentration of α-myc antibody and monitored the labeling of GLUT4 as it cycled to the cell surface in the absence or presence of insulin (Figure IV-5a and IV-6a, respectively).

We determined the exocytic rate constants for both constructs (Figure IV-5b and IV-5c) and observed that in the absence of insulin, RatGLUT4 exocytosis was 1,6-fold faster than that of BtGLUT4 (0,005 min^{-1} and 0,003 min^{-1}, respectively). After challenging cells with insulin, the exocytic rate constant for RatGLUT4 (0,031 min^{-1}) increased 6-fold while the rate constant for BtGLUT4 (0,004 min^{-1}) increased only 1,3-fold (Figure IV-6b and IV-6c) and the difference was not statistically significant. In summary, we observed that RatGLUT4 was able to increase its exocytosis in response to insulin while BtGLUT4 was not.

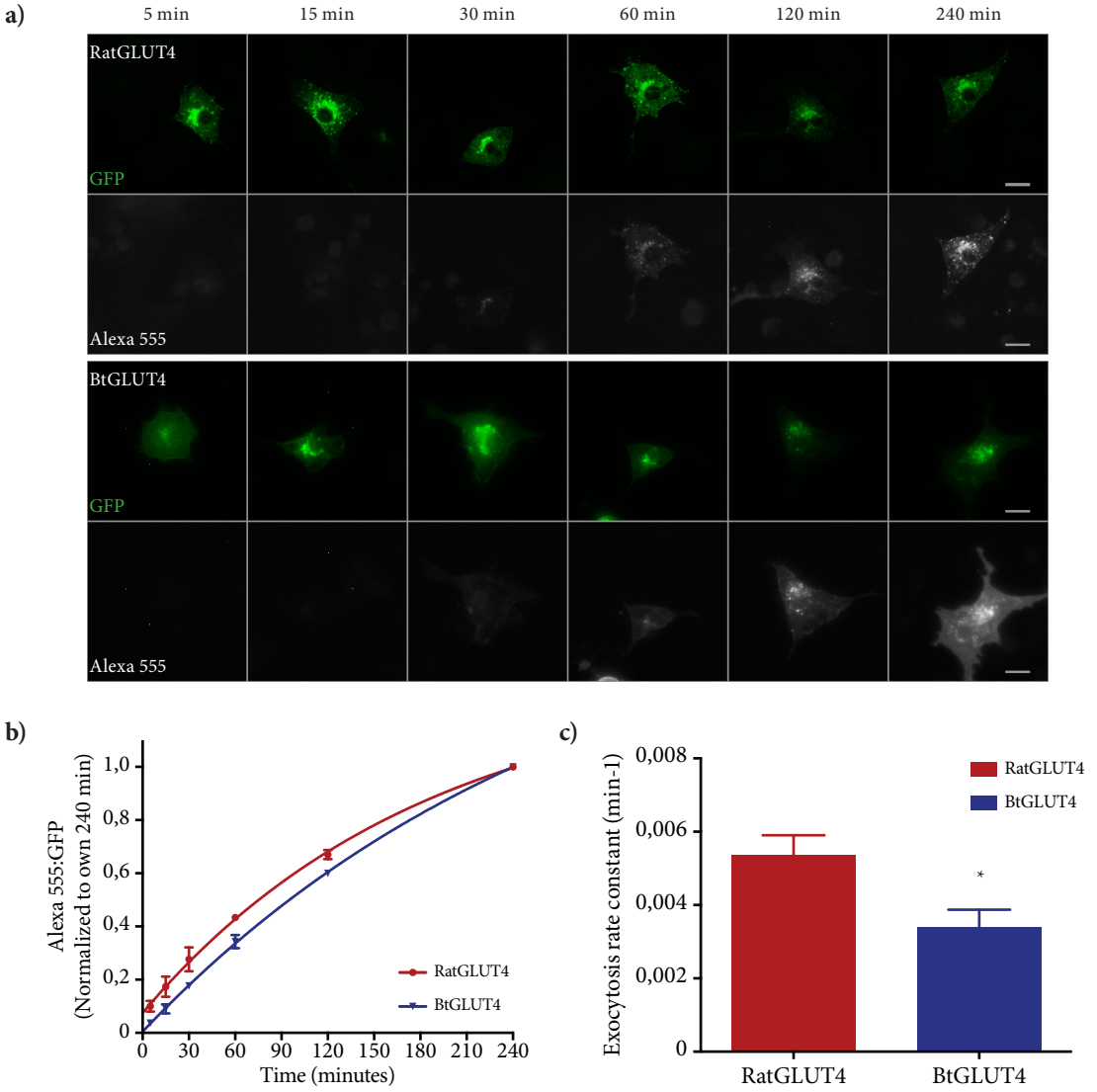

Figure IV-5. RatGLUT4 and BtGLUT4 exocytosis in the absence of insulin. **a)** Images of RatGLUT4- and BtGLUT4-expressing 3T3-L1 adipocytes under a DMIRB inverted Leica microscope using a 20 x air objective showing GFP (total GLUT4 expression) and Alexa 555 (recycled GLUT4) signals of individual cells. **b)** Graph shows recycling (exocytosis) of GLUT4 in the absence of insulin, represented as the increase of α-myc-bound GLUT4 over time, when incubated with saturating concentration of α-myc antibody. Levels of α-myc-bound RatGLUT4 and BtGLUT4 were corrected to total expression levels (GFP) and normalized to their own 240 minute time point. One-phase association curves were fit to data using GraphPad Prism software. Figure represents the mean ± SEM of four independent experiments. **c)** Graph shows exocytic rate constants of RatGLUT4 and BtGLUT4 and were

determined by measuring and averaging the individual slopes of the curves of four independent experiments (mean ± SEM). Red represents RatGLUT4 and blue represents BtGLUT4. Student's t test was performed using GraphPad Prism software; *, p<0,05 vs RatGLUT4. Scale bar, 20 µm.

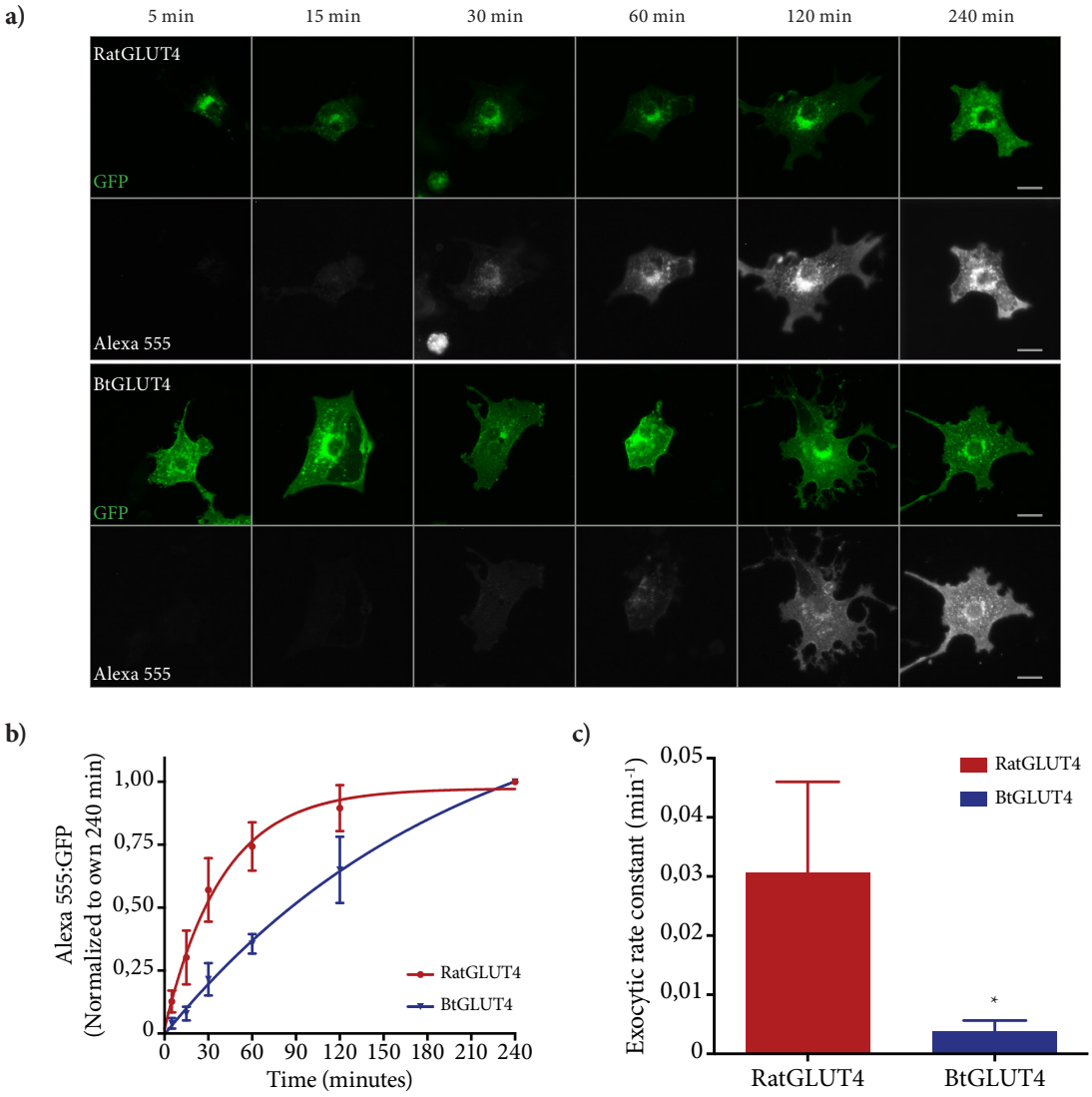

Figure IV-6. RatGLUT4 and BtGLUT4 exocytosis in the presence of insulin. **a)** Images of RatGLUT4- and BtGLUT4-expressing 3T3-L1 adipocytes under a DMIRB inverted Leica microscope using a 20 x air objective showing GFP (total GLUT4 expression) and Alexa 555 (recycled GLUT4) signals of individual cells. **b)** Graph shows recycling (exocytosis) of GLUT4 in the presence of insulin, represented as the increase of α-myc-bound GLUT4 over time, when incubated with saturating concentration of α-myc antibody. Levels of α-myc-bound RatGLUT4 and BtGLUT4 were corrected to total expression levels (GFP) and normalized to their own 240 minute time point. One-phase association curves were fit to data using GraphPad Prism software. Figure represents the mean ± SEM of four independent experiments. **c)** Graph shows exocytic rate constants of RatGLUT4 and BtGLUT4 and were determined by measuring and averaging the individual slopes of the curves of four independent experiments (mean ± SEM). Red represents RatGLUT4 and blue represents BtGLUT4. Student's t test was performed using GraphPad Prism software; *, p<0,05 vs RatGLUT4. Scale bar, 20 µm.

1.3.2. Endocytosis of RatGLUT4 and BtGLUT4.

As stated above, the cellular distribution of GLUT4 is determined by the balance between the rates of exocytosis and endocytosis; thus, after analyzing the exocytosis of ratGLUT4 and BtGLUT4 we studied their endocytosis in the absence and presence of insulin. To analyze the endocytosis of RatGLUT4 and BtGLUT4, we electroporated these constructs into 3T3-L1 adipocytes, we serum starved or insulin stimulated cells and incubated them with α-myc antibody for different times. We then detected surface GLUT4 and the fraction of it that was internalized (Figure IV-7a and IV-8a). It is important to use short incubation times to avoid recycling of α-myc-bound GLUT4 back to the surface.

As shown in Figures IV-7b, c and 8b, c, we observed that RatGLUT4 endocytosis was less than 2-fold faster than that of BtGLUT4 in the absence and presence of insulin, as shown by their endocytic rate constants (absence of insulin: 0,102 min^{-1} vs 0,058 min^{-1}; presence of insulin: 0,093 min^{-1} vs 0,054 min^{-1}). We also observed that although the difference was not statistically relevant, the endocytosis of both constructs slowed down in the presence of insulin (10 % and 7 % for RatGLUT4 and BtGLUT4, respectively).

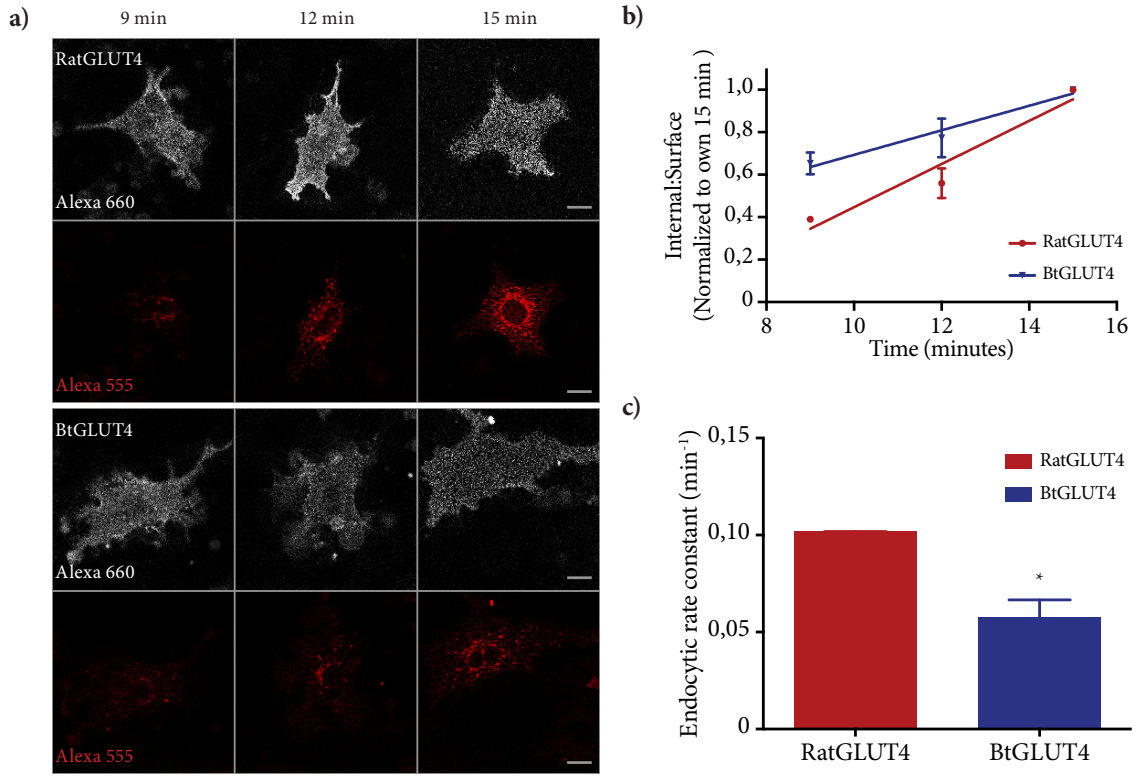

Figure IV-7. RatGLUT4 and BtGLUT4 endocytosis in the absence of insulin. **a)** Images of RatGLUT4- and BtGLUT4-expressing 3T3-L1 adipocytes under a Leica TCS SP2 microscope using a 20 x air objective showing Alexa 660 (surface GLUT4) and Alexa 555 (internalized GLUT4) signals of individual cells. **b)** Graph shows internalization of RatGLUT4 and BtGLUT4 over time in the absence of insulin, expressed as internalized GLUT4 normalized to cell surface GLUT4. Data were also normalized to their own 15 minute time point. Data were plotted and linear regression curves were fit to data using GraphPad Prism software. Figure represents the mean ± SEM of three independent experiments. **c)** Graph shows endocytic rate constants of RatGLUT4 and BtGLUT4 and were determined by measuring and averaging the individual slopes of the curves of three independent experiments (mean ± SEM). Red represents RatGLUT4 and blue represents BtGLUT4. Student's t test was performed using GraphPad Prism software; *, p<0,05 vs RatGLUT4. Scale bar, 20 µm.

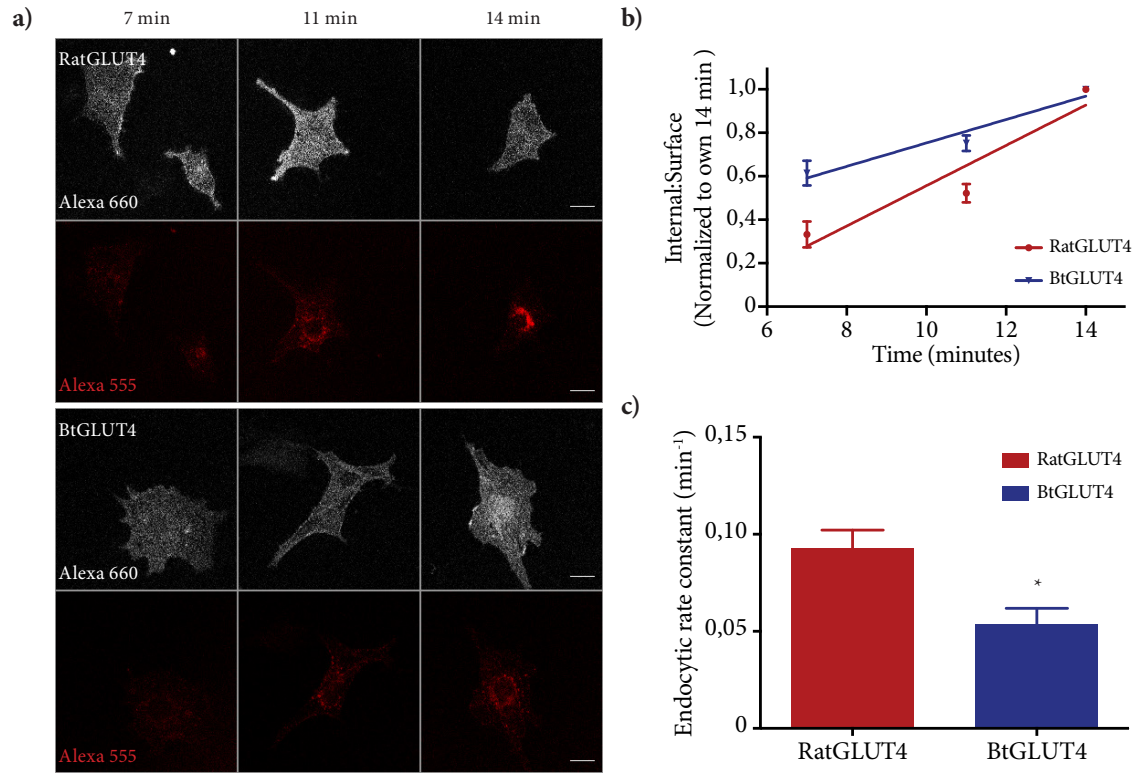

Figure IV-8. RatGLUT4 and BtGLUT4 endocytosis in the presence of insulin. **a)** Images of RatGLUT4- and BtGLUT4-expressing 3T3-L1 adipocytes under a Leica TCS SP2 microscope using a 20 x air objective showing Alexa 660 (surface GLUT4) and Alexa 555 (internalized GLUT4) signals of individual cells. **b)** Graph shows internalization of RatGLUT4 and BtGLUT4 over time in the presence of insulin, expressed as internalized GLUT4 normalized to cell surface GLUT4. Data were also normalized to their own 14 minute time point. Data were plotted and linear regression curves were fit to data using GraphPad Prism software. Figure represents the mean ± SEM of three independent experiments. **c)** Graph shows endocytic rate constants of RatGLUT4 and BtGLUT4 and were determined by measuring and averaging the individual slopes of the curves of four independent experiments (mean ± SEM). Red represents RatGLUT4 and blue represents BtGLUT4. Student's t test was performed using GraphPad Prism software; *, $p<0,05$ vs RatGLUT4. Scale bar, 20 µm.

2. DETERMINATION OF THE ROUTES OF INTERNALIZATION OF RATGLUT4 AND BTGLUT4.

2.1. STABLE EXPRESSION OF RATGLUT4 AND BTGLUT4 IN 3T3-L1 ADIPOCYTES.

For the next set of experiments, we switched from transient expression (electroporation) to stable expression by retroviral infection. The main reason for this change relies on the higher efficiency rate of the latter method. By using retroviral infection we are able to obtain a cell line where virtually every cell expresses our constructs, which translates in increased total expression levels.

To stably express RatGLUT4 and BtGLUT4 in 3T3-L1 adipocytes we produced lentivirus by transfecting Hek293T cells with RatGLUT4 or BtGLUT4 cloned in the lentiviral vectors, pCMV-dR8.74 and pMD2G which encode for viral packaging system and enveloped proteins, respectively. Transfected cells produced viruses which were collected, purified and used to infect preadipocytes. These infected cells were grown and differentiated in the presence of puromycin to select cells expressing RatGLUT4 or BtGLUT4 (Figure IV-9a).

We measured mRNA and protein expression levels using GFP tag (Figure IV-9b and IV-9c, respectively) and confirmed that we were able to obtain 3T3-L1 adipocytes, stably expressing similar levels of RatGLUT4 and BtGLUT4.

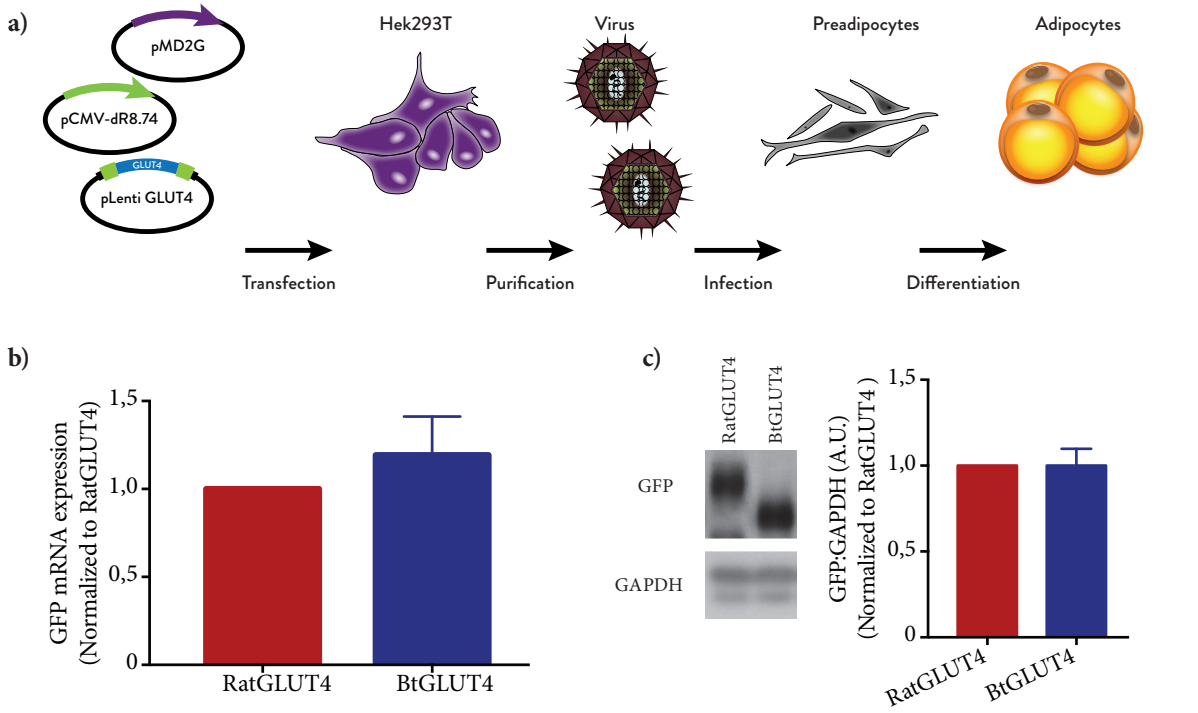

Figure IV-9. Generation of 3T3-L1 cell lines stably expressing RatGLUT4 and BtGLUT4. **a)** Schematic representation of the protocol used to stably express GLUT4 constructs in 3T3-L1 adipocytes. Lentivirus production and infection of 3T3-L1 cell workflow. Lentiviral vectors (pLenti CMV/TO Puro DEST) expressing RatGLUT4 or BtGLUT4 were transfected into Hek293T cells, using PEI transfection, along with plasmids encoding for viral packaging system and enveloped proteins (pCMV-dR8.74 and pMD2G, respectively). Hek293T growth media was collected twice, once a day, and media was centrifuged at 26000 rpm and purified using a sucrose cushion. After viral titration using flow cytometry, 3T3-L1 preadipocytes were infected at 75 MOI. Successfully infected cells were selected using puromycin (lentiviral vector selection antibiotic). Preadipocytes were induced to differentiate into adipocytes when needed. **b)** Graph shows GFP mRNA expression levels (RatGLUT4 and BtGLUT4) relative to the mRNA expression levels of the ARP housekeeping gene. BtGLUT4 mRNA expression levels were normalized to RatGLUT4 mRNA expression levels and data from three independent experiments were averaged and plotted (mean ± SEM) using GraphPad Prism software. **c)** Image on the left shows GFP (RatGLUT4 and BtGLUT4) and GAPDH protein levels in total lysates of 3T3-L1 adipocytes expressing RatGLUT4 and BtGLUT4.Graph shows protein expression levels of RatGLUT4 and BtGLUT4. Band intensities were quantified using Fiji processing software, and GFP level was normalized to GAPDH. BtGLUT4 data were normalized to RatGLUT4 and data from six independent experiments were plotted (mean ± SEM) using GraphPad Prism software. Red bars represent RatGLUT4 and blue bars represent BtGLUT4. A.U.: Arbitrary units.

2.1.2. RatGLUT4 and BtGLUT4 transporter activity.

The role of GLUT4 is to transport glucose. To verify if RatGLUT4 and BtGLUT4 were functional transporters, we measured the glucose uptake of cells expressing these constructs. To do so we used preadipocytes instead of fully differentiated adipocytes because non-differentiated cells do not express wild type GLUT4 (wtGLUT4), otherwise we would be measuring not only glucose uptake mediated by our constructs but by wtGLUT4 as well.

To determine glucose uptake in preadipocytes stably expressing RatGLUT4, BtGLUT4 or

no construct, we added [^{3}H]-2-deoxyglucose to cells (insulin-stimulated cells) for 5 minutes and measured the amount of incorporated radioactivity on a β-counter.

As shown in Figure IV-10, preadipocytes expressing RatGLUT4 or BtGLUT4 transported more glucose than control preadipocytes, almost 2-fold for RatGLUT4 (1,8-fold) and 1,5-fold for BtGLUT4. We also observed that BtGLUT4 transported 17 % less glucose than RatGLUT4.

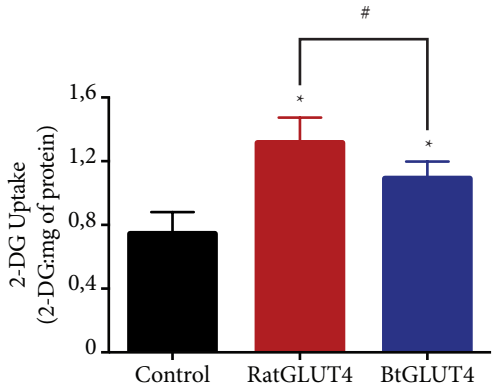

Figure IV-10. RatGLUT4 and BtGLUT4 glucose uptake in 3T3-L1 preadipocytes. Graph shows [3H] 2-deoxyglucose (2-DG) uptake performed by control 3T3-L1 preadipocytes and preadipocytes expressing RatGLUT4 and BtGLUT4. Incorporated radioactivity in total lysates was measured on a b-counter and values were normalized to total protein content (mg). Data from nine independent experiments were plotted (mean ± SEM) and Student's t test was performed using GraphPad Prism software. Red bar represents RatGLUT4, blue bar represents BtGLUT4, and black bar represents control preadipocytes. #, p<0,05; *, p<0,05 vs control.

2.2. Clathrin-mediated endocytosis.

2.2.1 Inhibition of clathrin-mediated endocytosis by hypertonic sucrose shock.

In this work, we were interested in studying the endocytosis of RatGLUT4 and BtGLUT4. As stated above, the internalization of GLUT4 plays a pivotal role in its functioning and it can occur through different internalization pathways. The more common routes of internalization are clathrin-mediated endocytosis and cholesterol-dependent endocytosis. In adipocytes, the most commonly reported cholesterol-dependent pathway is the caveolar endocytosis. In this work, we analyzed the extent of the contribution of these pathways to the internalization of RatGLUT4 and BtGLUT4.

To analyze the contribution of the clathrin-mediated pathway, we blocked this route by hypertonic sucrose shock and to confirm that the sucrose shock was inhibiting this pathway we treated 3T3-L1 adipocytes with or without 450 mM sucrose and then incubated cells with labelled transferrin. Transferrin and transferrin receptor are well-defined cargos of clathrin-mediated endocytosis. The amount of internalized transferrin was measured by fluorescence microscopy (Figure IV-11a). As shown in Figure IV-11b, hypertonic sucrose shock inhibited the endocytosis of transferrin by more than 2-fold.

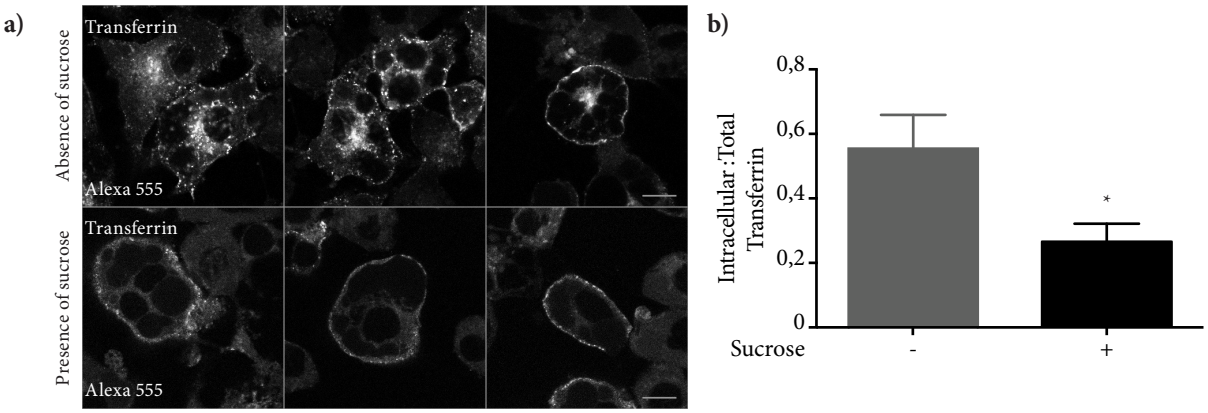

Figure IV-11. Inhibition of transferrin internalization by sucrose hypertonic shock. **a)** Images of 3T3-L1 adipocytes under a TCS SP5 confocal microscope using a 63x glycerol immersion objective showing transferrin-Alexa Fluor 555 signal of various cells. **b)** Graph shows transferrin-Alexa Fluor 555 levels in the absence and presence of sucrose and data were expressed as intracellular transferrin normalized to total transferrin to determine the fraction of internalized transferrin. Transferrin-Alexa Fluor 555 signal of individual cells was quantified using Fiji processing software. Data were plotted and Student's t test was performed using GraphPad Prism software. Figure represents the mean ± SEM of three independent experiments. Grey bar represents data in the absence of sucrose and black bar represents data in the presence of sucrose. *, $p<0,05$ vs absence of sucrose. Scale bar, 10 µm.

2.2.2. RatGLUT4 and BtGLUT4 clathrin-mediated endocytosis.

After confirming that hypertonic sucrose shock blocks clathrin-mediated endocytosis in our system, we analyzed the effect of sucrose treatment on RatGLUT4 and BtGLUT4 internalization.

These experiments were done in adipocytes stably expressing RatGLUT4 or BtGLUT4. We treated serum-starved cells with or without 450 mM sucrose in the absence and presence of insulin and, after cells were cooled down, the exofacial myc epitope was probed by a α-myc antibody (surface GLUT4 labelling). Cells were rewarmed and incubated for 0 minutes or 10 minutes (internalization stage). After internalization, we detected the remaining GLUT4-bound α-myc antibody at the cell surface.

We observed that after 10 minutes of incubation, the internalization of RatGLUT4 and BtGLUT4 was significantly inhibited by sucrose shock by approximately 65 % and 40 %, respectively, in the absence and presence of insulin (Figure IV-12a and IV-12b, respectively).

In summary, RatGLUT4 and BtGLUT4 internalized through clathrin-mediated endocytosis in the absence and presence of insulin (Figure IV-12c).

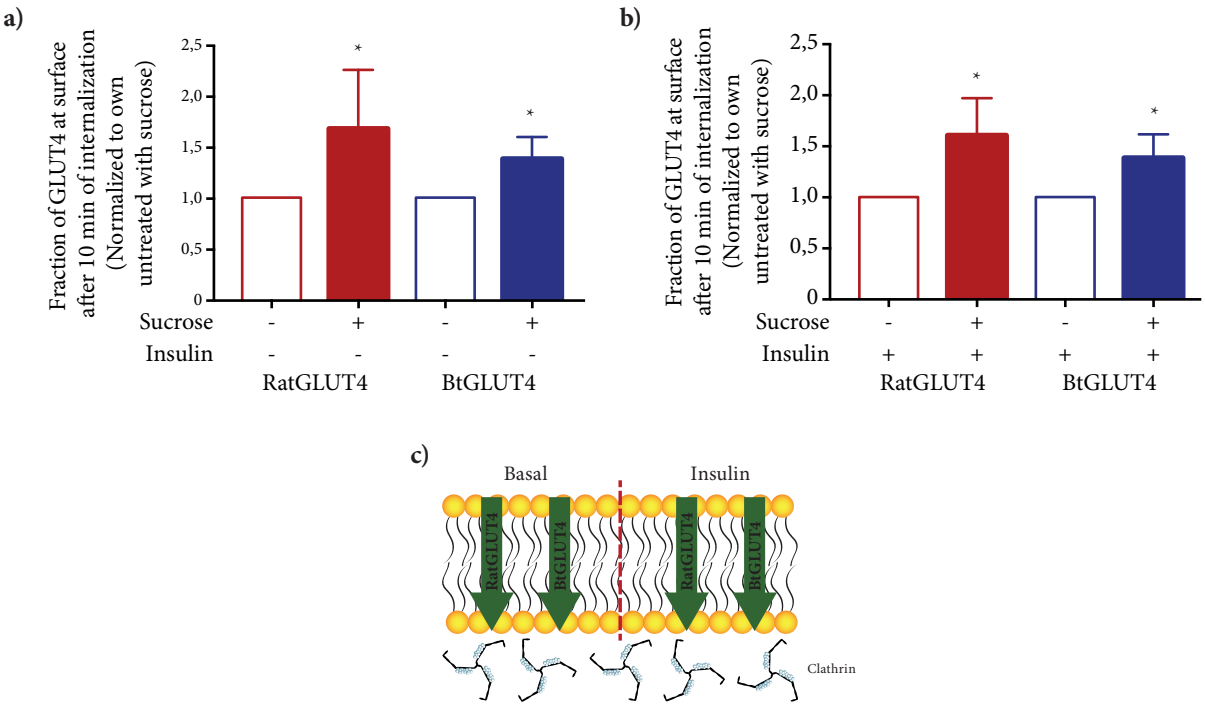

Figure IV-12. Inhibition of clathrin-mediated endocytosis. Graphs represent the cell surface levels of RatGLUT4 and BtGLUT4 in 3T3-L1 adipocytes treated with or without hypertonic sucrose, after 10 minutes of internalization, in the **a)** absence and **b)** presence of insulin. GLUT4 at the cell surface after 10 minutes of internalization was normalized to cell surface GLUT4 at the beginning of the internalization to determine the fraction of non-internalized GLUT4. The fraction of non-internalized GLUT4 was normalized to their own control (absence of sucrose) and data from **a)** six or **b)** nine independent experiments were plotted (mean ± SEM) and Student's t test was performed using GraphPad Prism software. Red represents RatGLUT4 and blue represents BtGLUT4. *, $p<0,05$ vs own control (absence of sucrose). **c)** Schematic representation of the obtained data. Green arrows represent internalization through clathrin-mediated route.

2.3. Cholesterol-dependent endocytosis.

2.3.1. Inhibition of cholesterol-dependent endocytosis by cholesterol depletion.

GLUT4 can be internalized through a cholesterol-dependent pathway. Similarly to what we did for clathrin-mediated endocytosis, we inhibited the cholesterol-dependent endocytosis and observed how it affected RatGLUT4 and BtGLUT4 internalization. To block this route we used nystatin, a cholesterol-aggregating drug. To test the effect of nystatin on cholesterol-dependent endocytosis we treated 3T3-L1 adipocytes with or without nystatin (50 μg/mL) and then incubated cells with cholera toxin B subunit-Alexa 555 conjugate (CTB), which is a marker for cholesterol-dependent endocytosis. Following incubation cells were either fixed (0 hours) or reincubated, in the absence or presence of nystatin, for 1 hour. Cells were then fixed and observed under the fluorescence microscope (Figure IV-13a).

As observed in Figure IV-13b, nystatin treatment reduced CTB internalization by 50 %, confirming that 50 μg/mL nystatin treatment inhibited the cholesterol-dependent pathway in 3T3-L1 adipocytes.

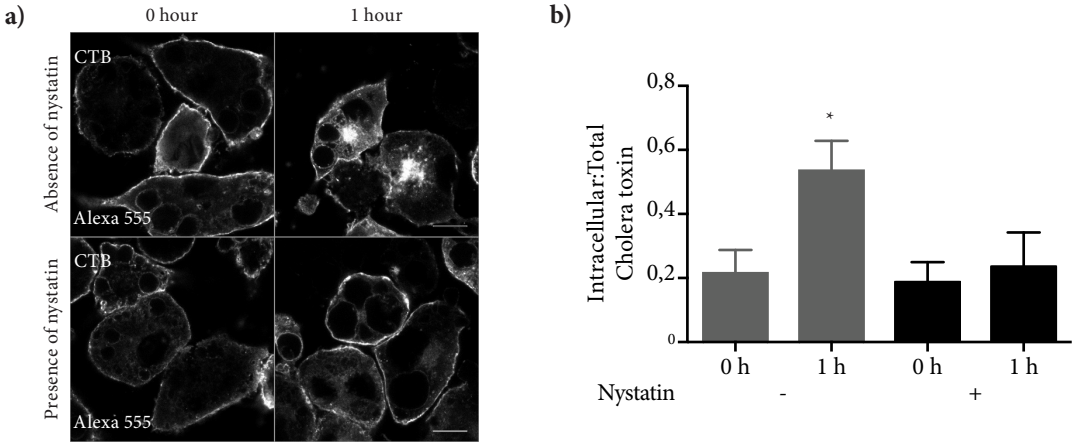

Figure IV-13. Inhibition of cholera toxin B subunit internalization by nystatin sequestration of cholesterol. **a)** Images of 3T3-L1 adipocytes under a TCS SP5 confocal microscope using a 63x glycerol immersion objective showing Cholera toxin B subunit-Alexa Fluor 555 signal of various cells. **b)** Graph shows Cholera toxin B subunit-Alexa Fluor 555 levels in the absence and presence of nystatin and data were expressed as intracellular cholera toxin normalized to total cholera toxin to determine the fraction of internalized cholera toxin. Cholera toxin B subunit-Alexa Fluor 555 signal of individual cells was quantified using Fiji processing software. Data were plotted and Student's t test was performed using GraphPad Prism software. Figure represents the mean ± SEM of three independent experiments. Grey bar represents data in the absence of nystatin and black bar represents data in the presence of nystatin. *, $p<0,05$ vs absence of sucrose. Scale bar, 10 µm.

2.3.2. RatGLUT4 and BtGLUT4 cholesterol-dependent endocytosis.

Having confirmed that nystatin halts cholesterol-dependent endocytosis, we analyzed how inhibition of cholesterol-dependent endocytosis affected RatGLUT4 and BtGLUT4 internalization. To do so we treated serum-starved adipocytes stably expressing our constructs with or without nystatin, in the absence and presence of insulin. We labelled cell surface GLUT4 by probing the myc epitope with a α-myc antibody at low temperature to arrest cellular trafficking. We then rewarmed cells and incubated them for 0 minutes or 10 minutes (internalization stage). After internalization, we measured the remaining GLUT4 at the plasma membrane.

As observed in Figure IV-14a, in the absence of insulin, nystatin induced a 38 % accumulation of RatGLUT4 at the cell surface whereas it had no effect on BtGLUT4. In the presence of insulin, nystatin had no effect on the endocytosis of either construct (Figure IV-14b).

In summary (Figure IV-14c), RatGLUT4 was internalized through cholesterol-dependent endocytosis solely in the absence of insulin and BtGLUT4 did not utilize this pathway.

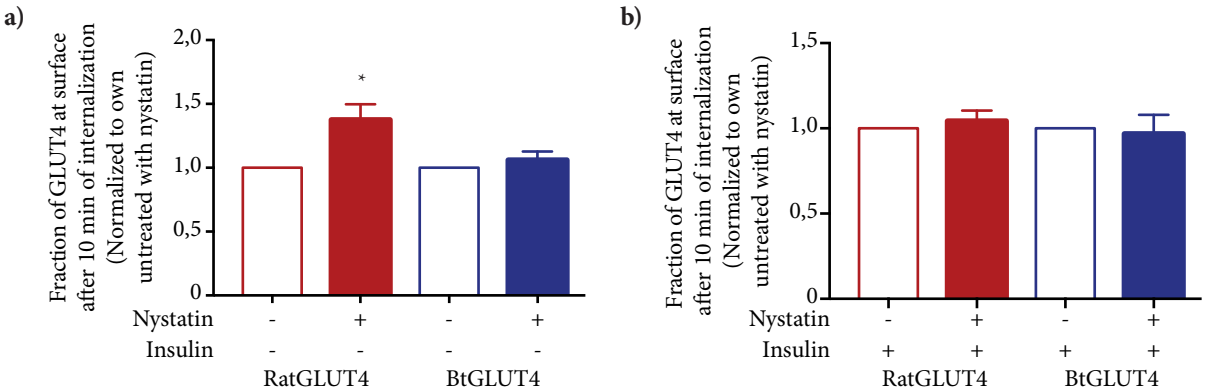

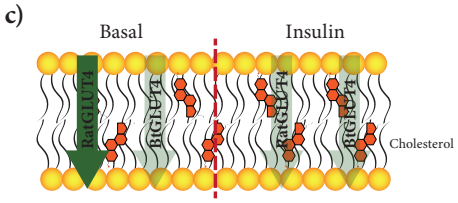

Figure IV-14. Inhibition of cholesterol-dependent endocytosis. Graphs represent the cell surface levels of RatGLUT4 and BtGLUT4 in 3T3-L1 adipocytes treated with or without nystatin, after 10 minutes of internalization, in the **a)** absence and **b)** presence of insulin. GLUT4 at the cell surface after 10 minutes of internalization was normalized to cell surface GLUT4 at the beginning of the internalization to determine the fraction of non-internalized GLUT4. The fraction of non-internalized GLUT4 was normalized to their own control (absence of nystatin) and data from **a)** seven or **b)** four independent experiments were plotted (mean ± SEM) and Student's t test was performed using GraphPad Prism software. Red represents RatGLUT4 and blue represents BtGLUT4. *, p<0,05 vs own control (absence of nystatin). **c)** Schematic representation of the obtained data. Green arrows represent internalization through cholesterol-dependent route; Dimmed arrow represents no change in internalization.

2.4. Caveolar endocytosis

2.4.1. Caveolae ablation by caveolin-1 knockdown.

The third endocytic pathway approached in this work is caveolar endocytosis. Caveolae are plasma membrane structures dependent on caveolin-1 (Cav-1). To inhibit this pathway we knocked down (KD) Cav-1, preventing caveolae formation. To do so, we produced lentiviruses carrying siRNA against Cav-1 or a scrambled siRNA sequence and infected our RatGLUT4- and BtGLUT4-expressing cell lines (Figure IV-15a).

As shown in Figure IV-15b, we were able to obtain a reduction of more than 90 % of Cav-1 protein expression in Cav-1 KD adipocytes expressing RatGLUT4 or BtGLUT4. Interestingly, Cav-1 KD induced a 50 % reduction on RatGLUT4 and BtGLUT4 protein levels as well.

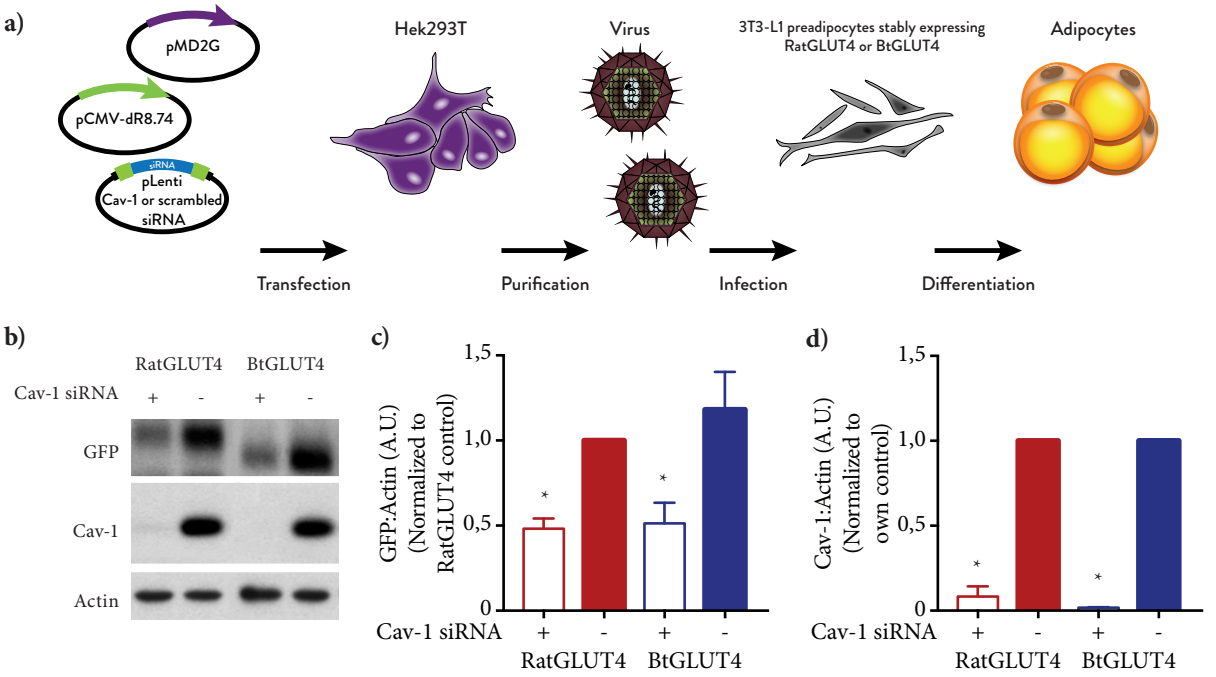

Figure IV-15. Caveolin-1 knockdown in 3T3-L1 adipocytes stably expressing RatGLUT4 or BtGLUT4. **a)** Schematic representation of the protocol used to knock down Cav-1 in 3T3-L1 adipocytes. Lentiviral vectors (pLVTHM)

encoding siRNA for caveolin-1 (Cav-1) or its scrambled sequence (control) were transfected into Hek293T cells along with plasmids encoding for viral packaging system and enveloped proteins (pCMV-dR8.74 and pMD2G, respectively). Hek293T growth media was collected twice, once a day, centrifuged and purified using a sucrose cushion. After purification, viruses were used to infect 3T3-L1 preadipocytes expressing GLUT4 constructs. Preadipocytes were induced to differentiate into adipocytes when needed. **b)** Figure shows GFP (RatGLUT4 and BtGLUT4), Cav-1 and actin protein expression levels in total lysates of Cav-1 KD and control RatGLUT4- and BtGLUT4-expressing 3T3-L1 adipocytes. Band intensities were quantified using Fiji processing software, and **c)** GFP and **d)** Cav-1 levels were normalized to Actin. GFP levels were normalized to RatGLUT4 Cav-1 control cells (**c**)); and Cav-1 levels were normalized to own Cav-1 control cells (**d**)). Data from three independent experiments were plotted (mean ± SEM) and Student's t test was performed using GraphPad Prism software. Red represents data from RatGLUT4-expressing adipocytes and blue represents data from BtGLUT4-expressing adipocytes. *, p<0,05 vs own Cav-1 control. A.U.: Arbitrary units.

2.4.2. RatGLUT4 and BtGLUT4 caveolar endocytosis.

To analyze the effect of caveolar ablation on RatGLUT4 and BtGLUT4 endocytosis, we probed exofacial myc on RatGLUT4- and BtGLUT4-expressing Cav-1 KD cells at low temperatures to halt GLUT4 trafficking, and then rewarmed cells to start the internalization stage (0 minutes and 10 minutes) in the absence and presence of insulin. After internalization, we measured the remaining GLUT4 at the plasma membrane.

As shown in Figure IV-16a, in the absence of insulin, Cav-1 KD increased RatGLUT4 internalization by 30 % while having no effect on BtGLUT4. In the presence of insulin (Figure IV-16b), internalization of RatGLUT4 and BtGLUT4 increased in Cav-1 KD cells by 13 % and 22 %, respectively.

In summary (Figure IV-16c), we observed that, in the absence of insulin, Cav-1 KD increased RatGLUT4 internalization alone while, in the presence of insulin, Cav-1 KD increased the endocytosis of transporters.

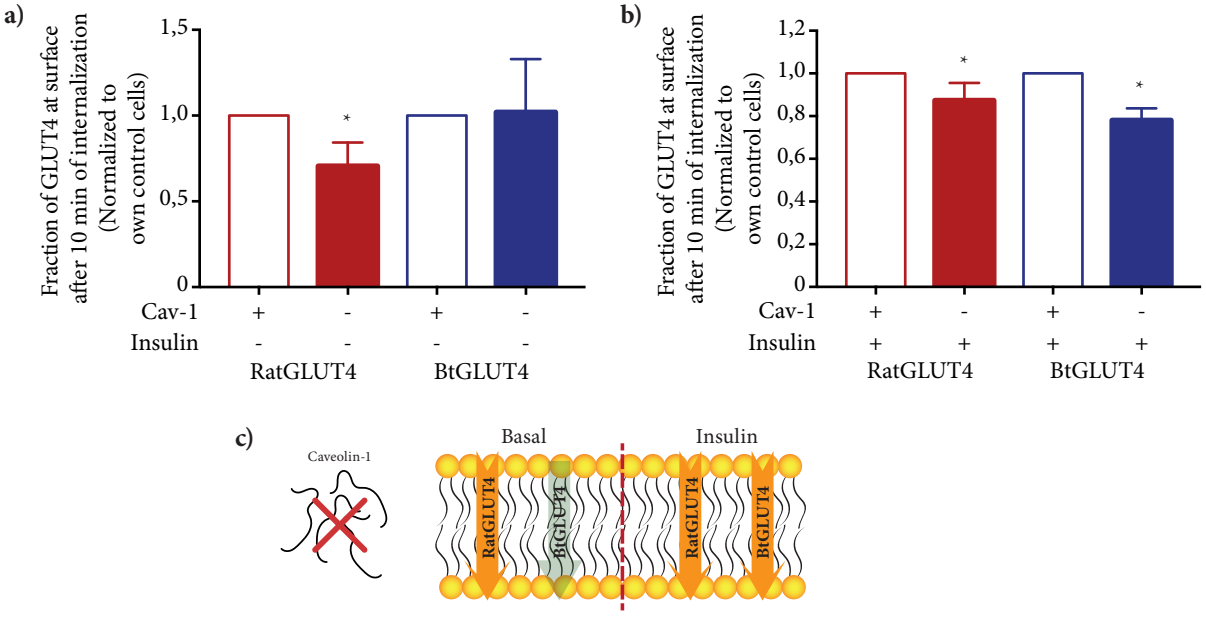

Figure IV-16. Inhibition of caveolar endocytosis. Graphs represent the cell surface levels of RatGLUT4 and BtGLUT4 in control or caveolin-1 (Cav-1)-depleted 3T3-L1 adipocytes, after 10 minutes of internalization, in the **a)** absence and **b)** presence of insulin. GLUT4 at the cell surface after 10 minutes of internalization was normalized to cell surface GLUT4 at the beginning of the internalization to determine the fraction of non-internalized GLUT4. The fraction of non-internalized GLUT4 was normalized to their own control (presence of Cav-1) and

data from **a)** six or **b)** five independent experiments were plotted (mean ± SEM) and Student's t test was performed using GraphPad Prism software. Red represents RatGLUT4 data and blue represents BtGLUT4 data. *, p<0,05 vs own control (presence of Cav-1). **c)** Schematic representation of the obtained data. Orange arrows represent increase in internalization; Dimmed arrow represents no change in internalization.

2.5. Clathrin-mediated and cholesterol-dependent endocytosis in Cav-1 KD adipocytes.

Cav-1 KD and, therefore, inhibition of caveolar endocytosis, induced an increase in RatGLUT4 and BtGLUT4 endocytosis. Because this was an unexpected result, we hypothesized that Cav-1 KD might have induced a change in the dependence pf RatGLUT4 and BtGLUT4 on clathrin-mediated and cholesterol-dependent endocytosis. We decided to inhibit these pathways in Cav-1 KD cells and analyze its impact on RatGLUT4 and BtGLUT4 internalization. To do so, we inhibited clathrin-mediated (Figure IV-17) and cholesterol-dependent endocytosis (Figure IV-18), in the absence and presence of insulin, and measured the remaining GLUT4 at plasma membrane after 0 minutes and 10 minutes of internalization (as described before).

Regarding inhibition of clathrin-mediated endocytosis in Cav-1 KD cells, we observed that RatGLUT4 internalization was only reduced in the presence of insulin (Figure IV-17b), whilst BtGLUT4 endocytosis was solely halted in the absence of insulin (Figure IV-17a). Therefore, when comparing these results with those obtained from cells expressing Cav-1, RatGLUT4 and BtGLUT4 endocytosis was less dependent on clathrin-mediated pathway in the absence of Cav-1 (Figure IV-13c and IV-17c).

Inhibition of cholesterol-dependent endocytosis in Cav-1 KD cells did not affect the internalization of either transporter in the absence or presence of insulin (Figure IV-18a and IV-18b, respectively). Again, comparing these data with those obtained from cells expressing Cav-1, RatGLUT4 no longer utilized a cholesterol-dependent pathway and BtGLUT4 remained independent of cholesterol in the absence of Cav-1 (Figure IV-15c and IV-18c).

In summary, knockdown of Cav-1 changed the routes of internalization utilized by RatGLUT4 and BtGLUT4. Cav-1 knockdown inhibited the internalization of RatGLUT4 through cholesterol-dependent endocytosis and also reduced the contribution of clathrin-mediated endocytosis for the internalization of both expressed constructs.

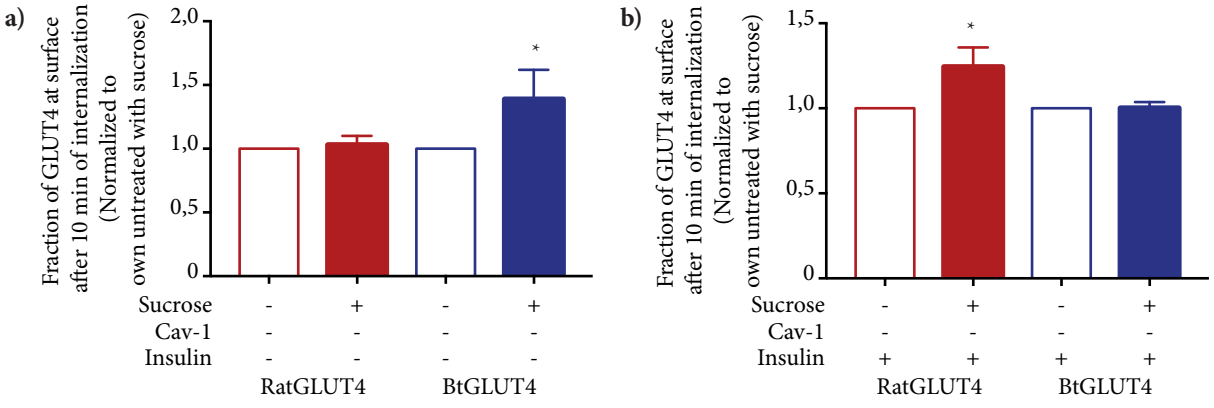

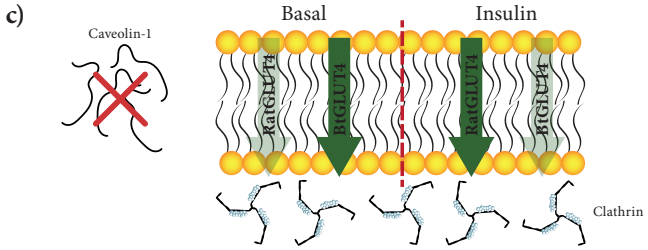

Figure IV-17. Inhibition of clathrin-mediated endocytosis in caveolin-1-depleted adipocytes. Graphs represent the cell surface levels of RatGLUT4 and BtGLUT4 in caveolin-1 (Cav-1)-depleted 3T3-L1 adipocytes treated with or without hypertonic sucrose, after 10 minutes of internalization, in the **a)** absence and **b)** presence of insulin. GLUT4 at the cell surface after 10 minutes of internalization was normalized to cell surface GLUT4 at the beginning of the internalization to determine the fraction of non-internalized GLUT4. The fraction of non-internalized GLUT4 was normalized to own control (absence of sucrose) and data from **a)** six or **b)** four independent experiments were plotted (mean ± SEM) and Student's t test was performed using GraphPad Prism software. Red represents RatGLUT4 and blue represents BtGLUT4. *, p<0,05 vs own control (absence of sucrose). **c)** Schematic representation of the obtained data. Green arrows represent internalization through clathrin-mediated route; Dimmed arrow represents no change in internalization.

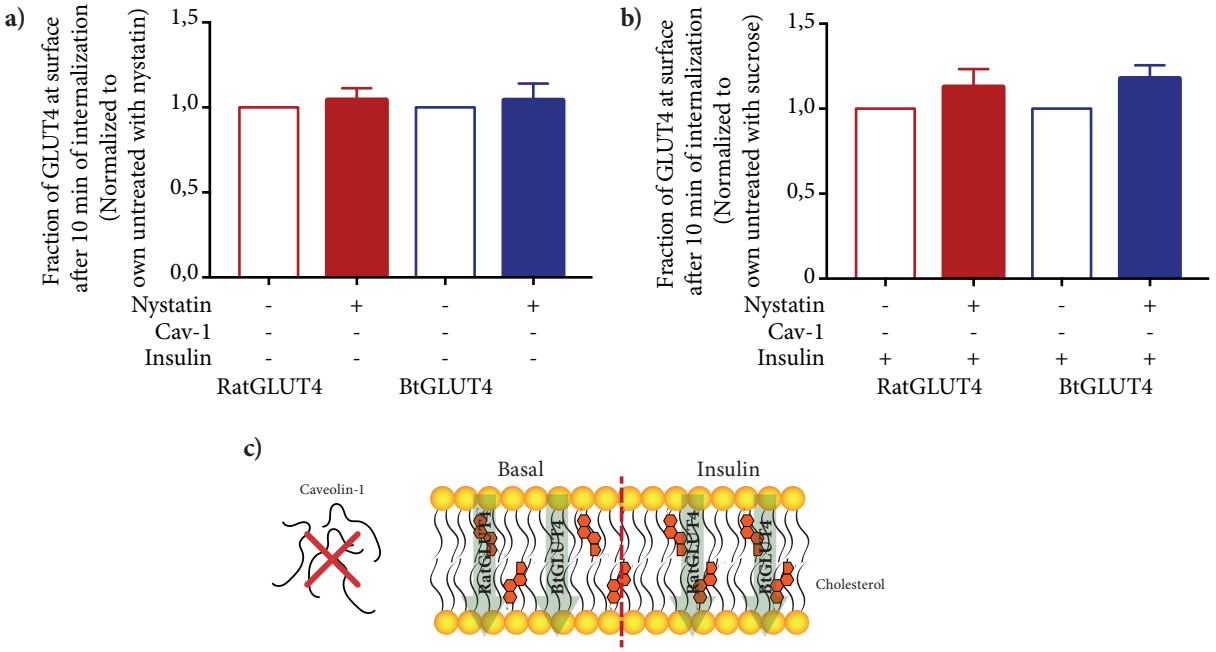

Figure IV-18. Inhibition of cholesterol-dependent endocytosis in caveolin-1-depleted adipocytes. Graphs represent the cell surface levels of RatGLUT4 and BtGLUT4 in caveolin-1 (Cav-1)-depleted 3T3-L1 adipocytes treated with or without nystatin, after 10 minutes of internalization, in the **a)** absence and **b)** presence of insulin. GLUT4 at the cell surface after 10 minutes of internalization was normalized to cell surface GLUT4 at the beginning of the internalization to determine the fraction of non-internalized GLUT4. The fraction of non-internalized GLUT4 was normalized to their own control (absence of nystatin) and data from **a)** six or **b)** three independent experiments were plotted (mean ± SEM) and Student's t test was performed using GraphPad Prism software. Red represents RatGLUT4 and blue represents BtGLUT4. *, p<0,05 vs own control (absence of nystatin). **c)** Schematic representation of the obtained data. Dimmed arrow represents no change in internalization.

3. DETERMINATION OF THE PRESENCE OF RATGLUT4 AND BTGLUT4 IN GSVs.

3.1. RATGLUT4 AND BTGLUT4 COLOCALIZATION WITH SYNTAXIN 6.

In the absence of insulin, the bulk of GLUT4 is kept inside the cell, mostly in specialized compartments called GLUT4 storage vesicles (GSVs). In the presence of insulin, GLUT4 in GSVs translocates to the plasma membrane and its exocytic rate constant increases to keep GLUT4 on the cell surface (Karylowski et al.2004, Martin et al. 2006, Blot and McGraw 2006). Because BtGLUT4 has a poor intracellular retention in the absence of insulin and because its exocytosis barely increases in the presence of insulin, we hypothesized that it does not reach GSVs. As a first approach to test this hypothesis, we analyzed the colocalization of RatGLUT4 and BtGLUT4 with Syntaxin 6 (STX6), a GSV-abundant protein. To do so, we electroporated 3T3-L1 adipocytes with RatGLUT4 or BtGLUT4, serum starved cells and probed STX6 with a α-STX6 antibody. We observed cells under confocal microscope and, as shown in Figure IV-19, we line scanned several perinuclear regions. We found regions of strong colocalization (line scan 1 of both constructs) and regions of weak colocalization (line scan 3 of both constructs). The differences in colocalization were not clear and difficult to evaluate since they varied considerably from cell to cell and it depended on the line scan area.

In summary, we were unable to assess the differences in colocalization, by confocal microscopy, of RatGLUT4 or BtGLUT4 with STX6 and therefore unable to determine if the presence of BtGLUT4 in GSVs was impaired.

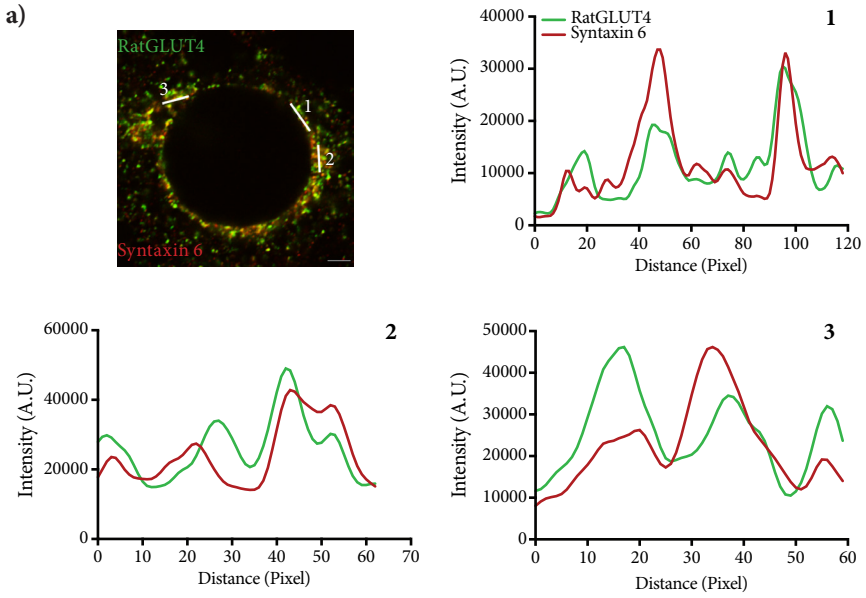

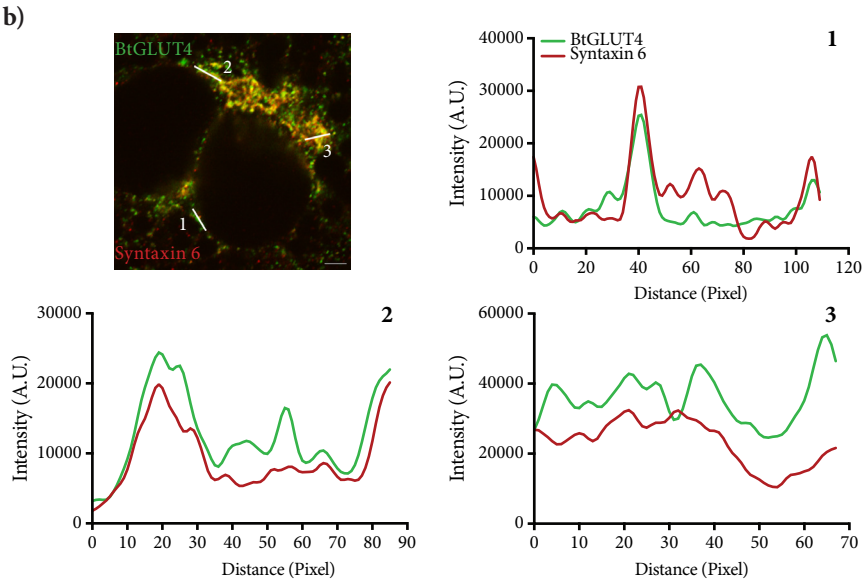

Figure IV-19. RatGLUT4 and BtGLUT4 colocalization with Syntaxin 6. Images of **a)** RatGLUT4- and **b)** BtGLUT4-expressing 3T3-L1 adipocytes under a a laser scanning microscope with airyscan using a 63x oil objective showing GFP (RatGLUT4 and BtGLUT4) and Alexa 555 (Syntaxin 6) signals of individual cells. Graphs show the colocalization of Syntaxin 6 with RatGLUT4 and BtGLUT4 in the areas indicated by the white lines. GFP and Alexa 555 signals were measured using Fiji processing software and plotted using GraphPad Prism software. Displayed cells and colocalization analysis are representative of obtained data. White lines indicate line scan areas; Green represents GFP (RatGLUT4 or BtGLUT4) and red represents Syntaxin 6. Scale bar, 5 µm. A.U.: Arbitrary units.

3.2. Immunoadsorption of GSVs in adipocytes expressing RatGLUT4 and BtGLUT4.

Since we were unable to determine if the presence of BtGLUT4 in GSVs was impaired using confocal microscopy, we decided to change our approach. Instead, we used serum-starved 3T3-L1 cells stably expressing our constructs and immunoadsorbed total RatGLUT4 and BtGLUT4 using a α-GFP antibody bound to magnetic beads and then the immunoadsorbed fractions were blotted for several proteins (Figure IV-20a). As shown in Figure IV-20b, the colocalization of BtGLUT4 with TUG, STX6 and AS160 (GSV-abundant proteins) was significantly weaker when compared to that of RatGLUT4, which indicates a stronger presence of RatGLUT4 in GSVs. On the other hand, BtGLUT4 showed a stronger colocalization with Cav-1, which, as stated above, is mainly present in caveolae at the plasma membrane. Insulin-Regulated Aminopeptidase (IRAP) is a protein that cotrafficks with GLUT4 and, although not significantly, its colocalization with BtGLUT4 was weaker than with RatGLUT4. Finally, transferrin receptor (TR) is a marker for recycling endosomes and, as shown in Figure IV-20b, we found no differences in its colocalization with either RatGLUT4 or BtGLUT4.

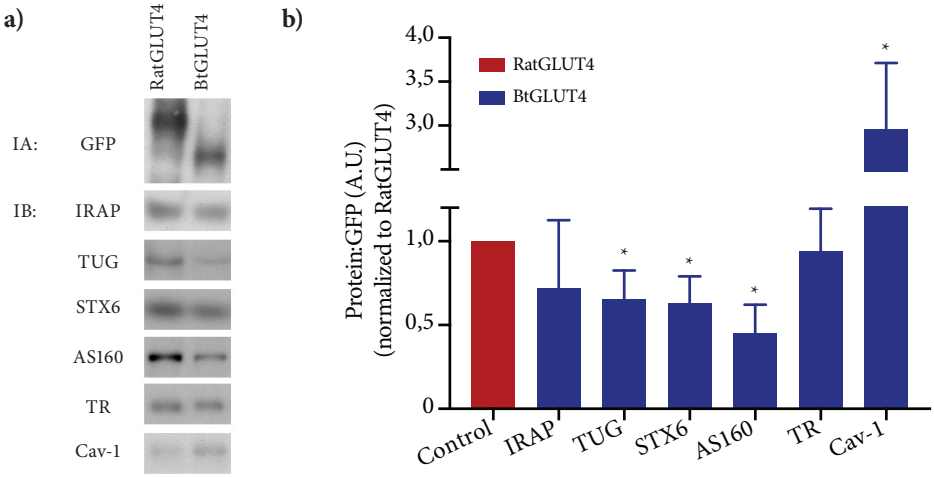

Figure IV-20. Immunoadsorption of rat and trout GLUT4 and colocalization for various proteins. **a)** Image shows the protein levels (IB: Immunoblotted) of IRAP, TUG, STX6, AS160, TR and Cav-1 in RatGLUT4- and BtGLUT4-immunoadsorbed (IA) lysates, obtained from 3T3-L1 adipocytes stably expressing these constructs (GFP). Band intensities of the various proteins were quantified using Fiji processing software and normalized to the amount of immunoadsorbed RatGLUT4 and BtGLUT4 (GFP). **b)** Graph shows the colocalization of BtGLUT4 with the different proteins, normalized to the corresponding RatGLUT4 colocalization value (control). Student's t test was performed using GraphPad Prism software. Red bar represents RatGLUT4 (control) and blue bars represent BtGLUT4. Figure represents the mean ± SEM of at least five independent experiments. *, $p<0,05$ vs RatGLUT4 (control). A.U.: Arbitrary units.

4. CHARACTERIZATION OF THE ROLES OF GLUT4 PROTEIN MOTIFS IN GLUT4 TRAFFICKING.

4.1. Trafficking of BtGLUT4 mutants.

4.1.1. Generation of BtGLUT4 mutants

After characterizing the traffic of RatGLUT4 and BtGLUT4 we were interested in defining the protein domains and regions in GLUT4 responsible for the observed differences.

We generated mutants of BtGLUT4 and analyzed how the mutations influenced its trafficking. As shown in Figure IV-21, we generated five mutants: two N-terminal end mutants (BtGLUT4-QL and BtGLUT4-QI), one C-terminal end mutant (BtGLUT4-CT), and two N-terminus and C-terminus mutants (BtGLUT4-QLCT; BtGLUT4-QICT). On the N-terminus we mutated the BtGLUT4 $FQHL^{8}$ domain into $FQQL^{8}$, which is the sequence found in coho salmon GLUT4, and into $FQQI^{8}$ which is the corresponding RatGLUT4 sequence. On the C-terminal end we mutated the $TELDY^{495}$ motif and two surrounding amino acids to the homologous RatGLUT4 sequence.

Using primers designed to introduce the desired mutation, we amplified the entire pcDNA3-BtGLUT4 to generate BtGLUT4-QL and BtGLUT4-QI. The resulting constructs were then used to generate BtGLUT4-QLCT and BtGLUT4-QICT, respectively.

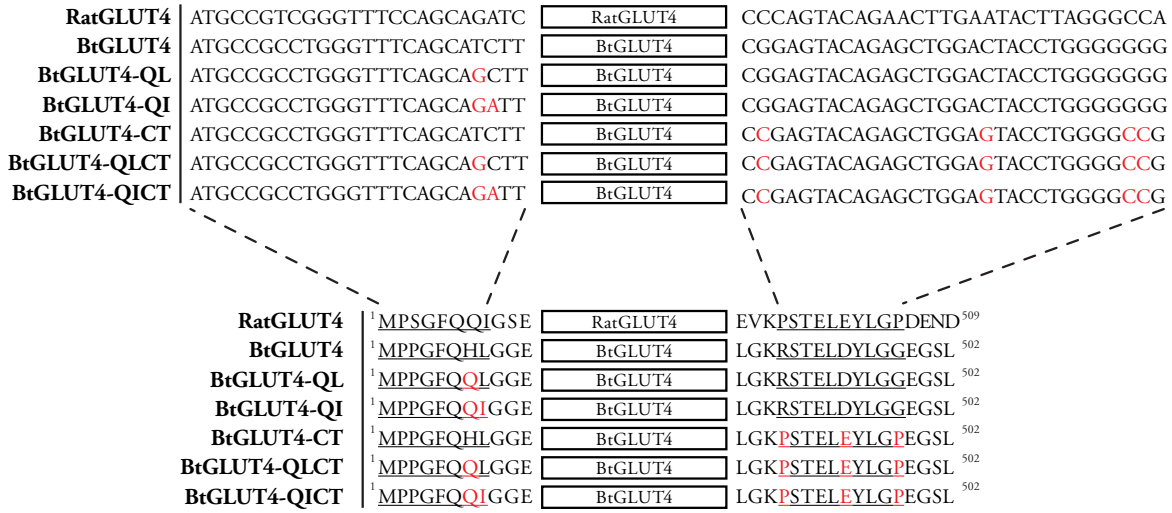

Figure IV-21. DNA and protein sequences of RatGLUT4, BtGLUT4 and BtGLUT4 mutants. Scheme shows the nucleic acid and amino acid sequences of RatGLUT4, BtGLUT4 and BtGLUT4 mutants, as well as the nucleotides and GLUT4 protein motifs mutated. Letters in red represent mutated nucleotides and amino acids. Underlined regions represent targeted protein motifs.

4.1.2. Plasma membrane levels of BtGLUT4 mutants.

Intracellular retention in the absence of insulin and translocation to the plasma membrane upon insulin action are essential GLUT4 mechanisms. To analyze how mutations in BtGLUT4 influenced its cell surface levels in the absence and presence of insulin, we electroporated 3T3-L1 adipocytes with BtGLUT4 or one of the generated mutants and probed the exofacial myc epitope with a α-myc antibody to detect surface GLUT4 in serum-starved and insulin-stimulated cells. We also used α-myc to detect total GLUT4 in permeabilized adipocytes (Figures IV-22a).

As observed in Figure IV-22b, mutations on the N-terminus (BtGLUT4-QL/QI/QLCT/QICT) improved BtGLUT4 intracellular retention in the absence of insulin, especially BtGLUT4-QL and Bt-GLUT4-QI. BtGLUT4-QL and Bt-GLUT4-QI basal surface levels were, respectively, 45 % and 28 % lower than those of BtGLUT4. On the other hand, the C-terminus mutant (BtGLUT4-CT) did not show any significant difference in its basal surface levels.

In the presence of insulin, all mutants except BtGLUT4-QI, showed lower surface levels than BtGLUT4. The BtGLUT4-CT mutation induced a 25 % reduction in surface levels whereas BtGLUT4-QL induced a 11 % reduction. The double mutants (BtGLUT4-QLCT/QICT) showed approximately a 17 % reduction of their surface levels when compared to BtGLUT4.

Taken all changes on cell surface levels into account (Figure IV-22c), BtGLUT4-QL had the strongest translocation to the plasma membrane as it increased its surface levels by 2,5-fold in response to insulin whilst BtGLUT4 increased by 1,5-fold. BtGLUT4-QI/QLCT/QICT also showed better translocation then BtGLUT4 (approximately 2-fold). Finally, BtGLUT4-CT had no improvement on its translocation.

In summary, mutations on BtGLUT4 FQHL[8] motif (N-terminal end) increased its translocation to the plasma membrane in response to insulin, mostly by improving its

intracellular retention in the absence of insulin. Mutations on TELDY[495] motif (C-terminal end) did not have a significant impact and double mutants behaved similarly to the corresponding N-terminus mutant.

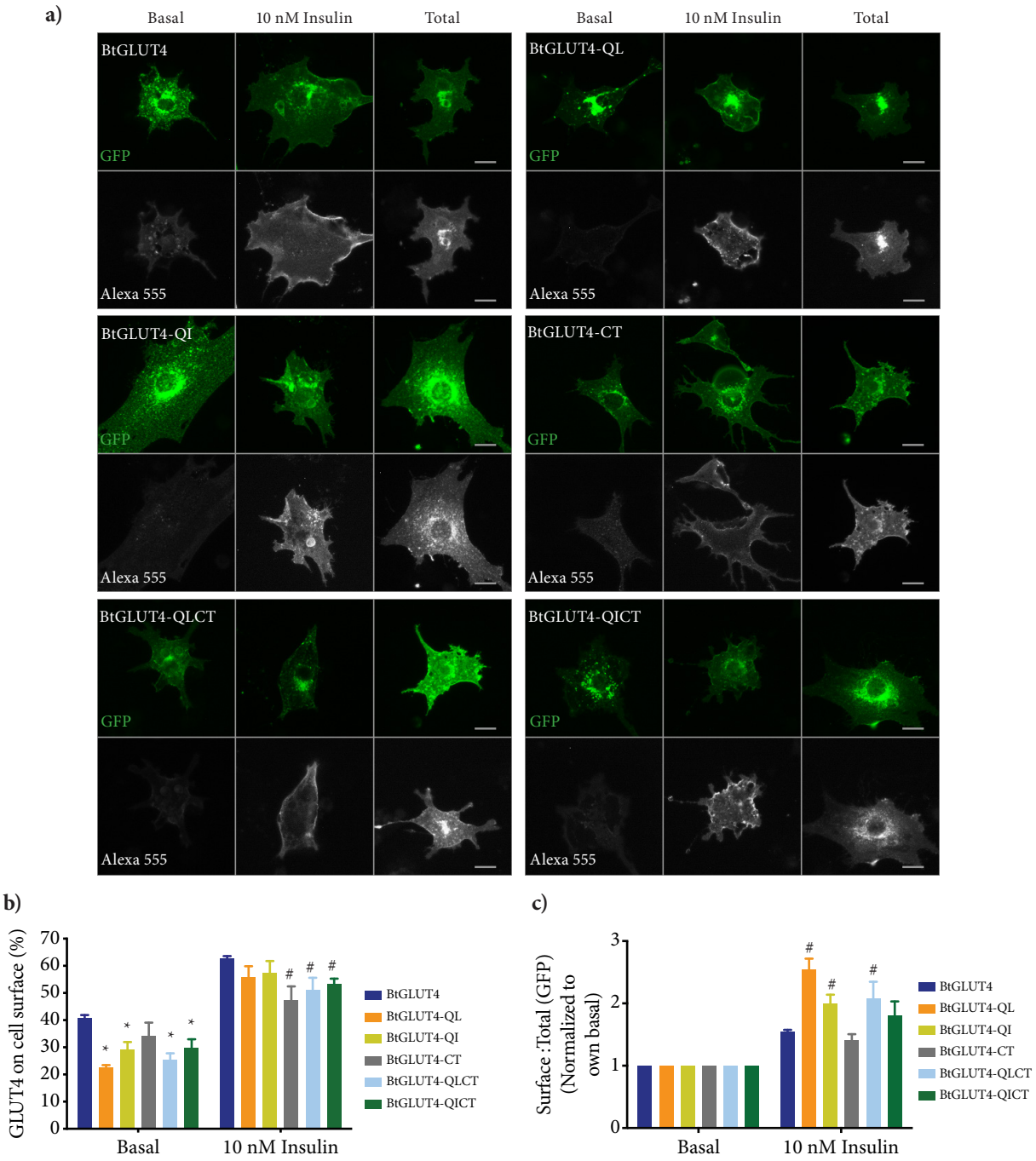

Figure IV-22. Plasma membrane levels of BtGLUT4 and BtGLUT4 in 3T3-L1 adipocytes. **a)** Images of RatGLUT4-, BtGLUT4- and BtGLUT4 mutants-expressing 3T3-L1 adipocytes under a DMIRB inverted Leica microscope using a 20 x air objective showing GFP (total GLUT4 expression) and Alexa 555 (surface GLUT4) signals of individual cells. Graphs show cell surface levels of expressed constructs in the absence and presence of 10 nM Insulin and data were expressed as **b)** cell surface levels normalized to total levels to determine GLUT4 percentage at cell surface and as **c)** cell surface levels in the presence of 10 nM Insulin normalized to the basal levels to determine GLUT4 translocation to the plasma membrane. Data were plotted and Student's t test was performed using GraphPad Prism software. Blue bars represent BtGLUT4; Orange bars represent BtGLUT4-QL; Yellow bars represents BtGLUT4-QI; Grey bars represent BtGLUT4-CT; Light blue bars represent BtGLUT4-QLCT; Green bars represent BtGLUT4-QICT. Figure represents the mean ± SEM of at least four independent experiments. *, $p<0,05$ vs BtGLUT4 Basal; #, $p<0,05$ vs BtGLUT4 10 nM Insulin. Scale bar, 20 µm.

4.1.3. Stable expression of BtGLUT4-QL in 3T3-L1 adipocytes.

Overall, the BtGLUT4-QL mutant showed the most interesting and promising results: its basal intracellular retention was improved over that of BtGLUT4 and its plasma membrane levels in the presence of insulin were comparable to those of BtGLUT4.

Next, we set out to determine if these changes were due to better retention inside GSVs but in order to do so required the establishment of a 3T3-L1 cell line stably expressing BtGLUT4-QL. Similarly to what was conducted for Rat and BtGLUT4, we infected 3T3-L1 pre-adipocytes with lentiviruses carrying BtGLUT4-QL in a lentiviral vector (Figure IV-23a). After cell differentiation, we analyzed RNA and protein expression levels (using the GFP construct tag). As shown in Figure IV-23b, we generated a BtGLUT4-QL-expressing cell line showing lower GFP mRNA levels than those of Rat and BtGLUT4-expressing cells, although the difference was not statistically different. Despite its apparent lower mRNA expression levels, BtGLUT4-QL protein levels were comparable to those of RatGLUT4 and BtGLUT4 (Figure IV-23c).

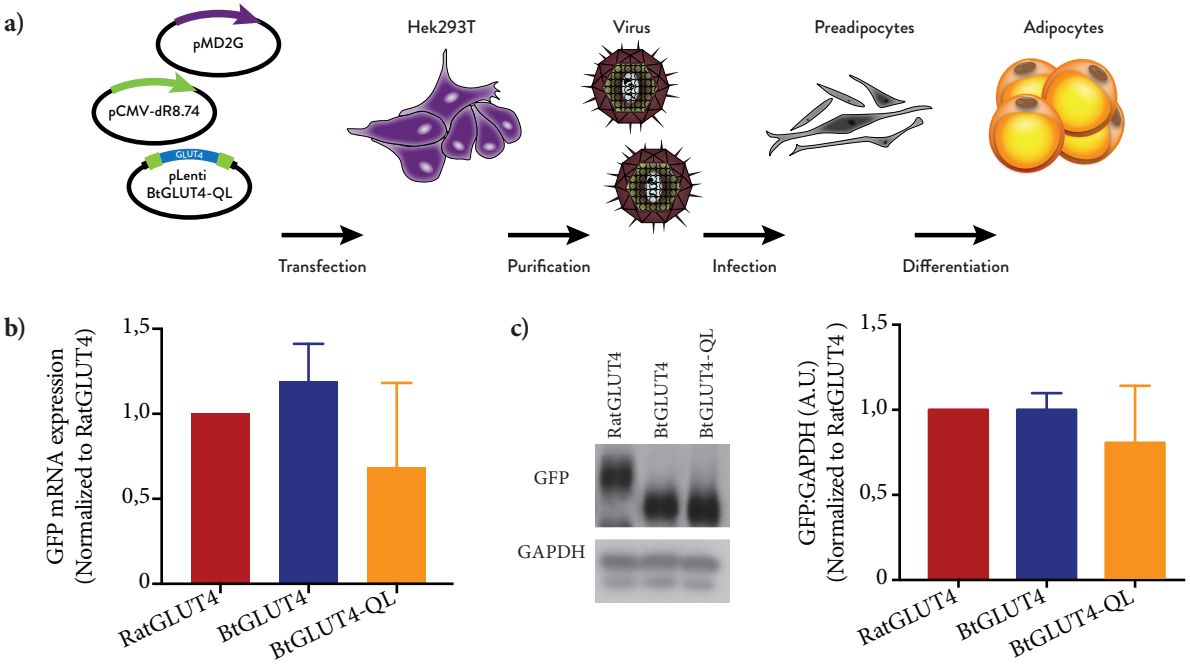

Figure IV-23. Generation of 3T3-L1 cell lines stably expressing RatGLUT4, BtGLUT4 and BtGLUT4-QL. **a)** Schematic representation of the protocol used to stably express GLUT4 constructs in 3T3-L1 adipocytes. Lentivirus production and 3T3-L1 cell infection workflow. Lentiviral vectors (pLenti CMV/TO Puro DEST) expressing RatGLUT4, BtGLUT4 or BtGLUT4-QL were transfected into Hek293T cells along with plasmids encoding for viral packaging system and enveloped proteins (pCMV-dR8.74 and pMD2G, respectively). Hek293T growth media was collected twice, once a day, centrifuged and purified using a sucrose cushion. After viral titration using flow cytometry, 3T3-L1 preadipocytes were infected at 75 MOI. Successfully infected cells were selected using puromycin (lentiviral vector selection antibiotic). Preadipocytes were induced to differentiate into adipocytes when needed. **b)** Graph shows GFP mRNA expression levels (RatGLUT4, BtGLUT4, and BtGLUT4-QL) relative to the mRNA expression levels of the ARP housekeeping gene. BtGLUT4 and BtGLUT4-QL mRNA expression levels were normalized to RatGLUT4 mRNA expression levels and data from three independent experiments were averaged and plotted (mean ± SEM) using GraphPad Prism software. **c)** Image on the left shows GFP (RatGLUT4, BtGLUT4 and BtGLUT4-QL) and GAPDH protein levels in total lysates of 3T3-L1 adipocytes expressing RatGLUT4, BtGLUT4 and BtGLUT4-QL. Graph shows the protein levels of the expressed constructs. Band intensities were quantified using Fiji processing software, and GFP level was normalized to GAPDH. BtGLUT4 and BtGLUT4-QL data were normalized to RatGLUT4 and data from six independent experiments

were plotted (mean ± SEM) using GraphPad Prism software. Red bars represent RatGLUT4, blue bars represent BtGLUT4 and orange bars represent BtGLUT4-QL. A.U.: Arbitrary units.

4.1.4. BtGLUT4-QL presence in GSVs.

To assess the effect of the FQQL mutation on the presence of BtGLUT4 inside GSVs we immunoadsorbed BtGLUT4 and BtGLUT4-QL (using a α-GFP antibody bound to magnetic beads) in serum-starved adipocytes stably expressing these constructs and blotted for STX6 and AS160, which are abundant proteins in GSVs. We also blotted for Cav-1 to evaluate the relative levels on the cell surface (Figure IV-24a). In Figure IV-24b we show that BtGLUT4 colocalization with Cav-1 was not stronger than that of BtGLUT4-QL, which is in contrast with the higher basal plasma membrane levels of BtGLUT4. Regarding AS160 and STX6, BtGLUT4-QL colocalization was stronger with the latter but not with the former, when compared to BtGLUT4. In summary, the mutation in BtGLUT4-QL enhanced its retention in a STX6-rich compartment. The fact that we did not observed differences in colocalization with AS160 suggests that BtGLUT4-QL may not be retained in GSVs.

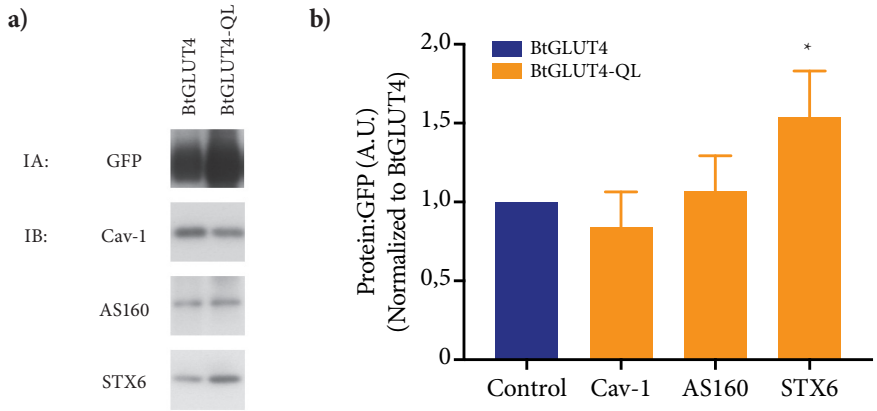

Figure IV-24. Immunoadsorption of BtGLUT4 and BtGLUT4-QL and colocalization for various proteins. **a)** Image shows the protein levels (IB: Immunoblotted) of Cav-1, AS160 and STX6 in BtGLUT4- and BtGLUT4-QL-immunoadsorbed (IA) lysates, obtained from 3T3-L1 adipocytes stably expressing these constructs (GFP). Band intensities of the various proteins were quantified using Fiji processing software and normalized to the amount of immunoadsorbed BtGLUT4 and BtGLUT4-QL (GFP). **b)** Graph shows the colocalization of BtGLUT4-QL with the different proteins, normalized to the corresponding BtGLUT4 colocalization value (control). Student's t test was performed using GraphPad Prism software. Blue bar represents BtGLUT4 (control) and orange bars represent BtGLUT4-QL. Figure represents the mean ± SEM of five independent experiments. *, $p<0,05$ vs BtGLUT4 (Control). A.U.: Arbitrary units.

4.2. Trafficking of RatGLUT4 and BtGLUT4 chimeras.

Previous studies showed that substituting the N-terminus and the large cytoplasmic loop of GLUT1 for those of GLUT4 is sufficient to confer to the chimeric GLUT1 protein the characteristics of GLUT4. Because of these observations, we decided to follow a similar approach. In this work, we used two RatGLUT4 and BtGLUT4 chimeras (Figure IV-25): N-GLUT4, consisting of the RatGLUT4 backbone with the N-terminus of BtGLUT4 (17 amino acids instead of 24 amino acids of RatGLUT4), and L-GLUT4, consisting of the RatGLUT4 backbone with

the large cytoplasmic loop of BtGLUT4 (65 amino acids). Like RatGLUT4 and BtGLUT4, both chimeras possess a myc epitope in the first exofacial loop and a GFP tag in the C-terminal end. These chimeras were kindly provided by Dr. Encarnación Capilla.

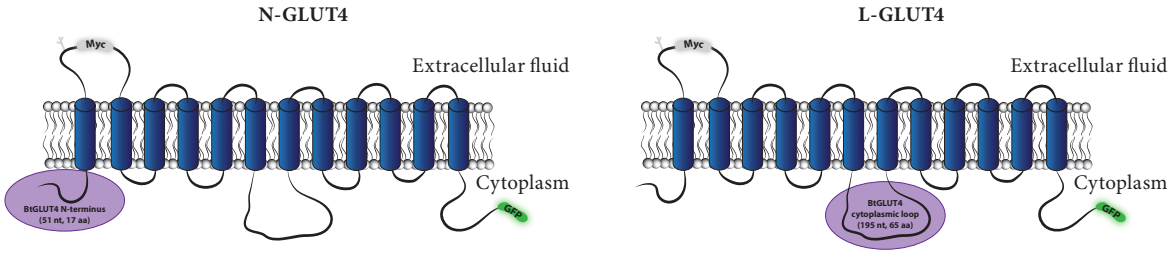

Figure IV-25. RatGLUT4 and BtGLUT4 chimeras: N-GLUT4 and L-GLUT4. Schematic representation of N-GLUT4 and L-GLUT4 constructs. Purple circles represent areas of RatGLUT4 and BtGLUT4 sequence exchange. Similarly to RatGLUT4 and BtGLUT4, both chimeras possess a myc tag in the first extracellular loop and GFP on the C-terminal end.

4.2.1. Cellular distribution of N-GLUT4.

To study the trafficking of the chimeras we electroporated them in 3T3-L1 adipocytes. However, as shown in Figure IV-26, very often N-GLUT4 presented a chamber-like distribution typical of endoplasmic reticulum (ER) localization. This distribution suggested that N-GLUT4 release from ER was impaired and as such we could not use this construct for trafficking studies.

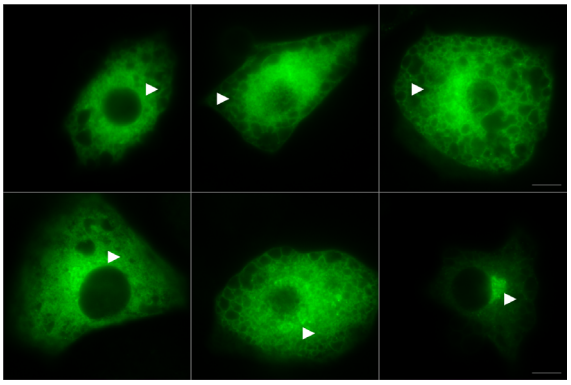

Figure IV-26. N-GLUT4 expression in 3T3-L1 adipocytes. Images of N-GLUT4-expressing 3T3-L1 adipocytes under a DMIRB inverted Leica microscope using a 100 x air objective. White arrowheads indicate endoplasmic reticulum localization. Scale bar, 10 μm.

4.2.2. Plasma membrane levels of L-GLUT4.

To analyse L-GLUT4 trafficking , and similarly to what we previously did for every construct, we first measured its plasma membrane levels in the absence and presence of insulin. To do so, we electroporated RatGLUT4 and L-GLUT4 into 3T3-L1 adipocytes and probed surface GLUT4 using a α-myc antibody in serum-starved and insulin-challenged cells. We also labelled total GLUT4 on permeabilized adipocytes. In Figure IV-27a, we observe that, unlike N-GLUT4, which localized to the ER, L-GLUT4 displayed a similar cellular distribution to RatGLUT4.

Nonetheless, in Figure IV-27b we show that in the absence of insulin, L-GLUT4 levels at the plasma membrane were almost 2-fold higher (77 %) than those of RatGLUT4. In the presence of insulin, L-GLUT4 surface levels were slightly higher than those of RatGLUT4 but the difference was not statistically significant. However, by analysing the insulin-driven translocation of these constructs we observed that the translocation of L-GLUT4 was 40 % weaker than that of RatGLUT4 in response to insulin (Figure IV-27c).

In summary, we observed that substitution of RatGLUT4 cytoplasmic loop by BtGLUT4 sequence reduces its intracellular retention in the absence of insulin.

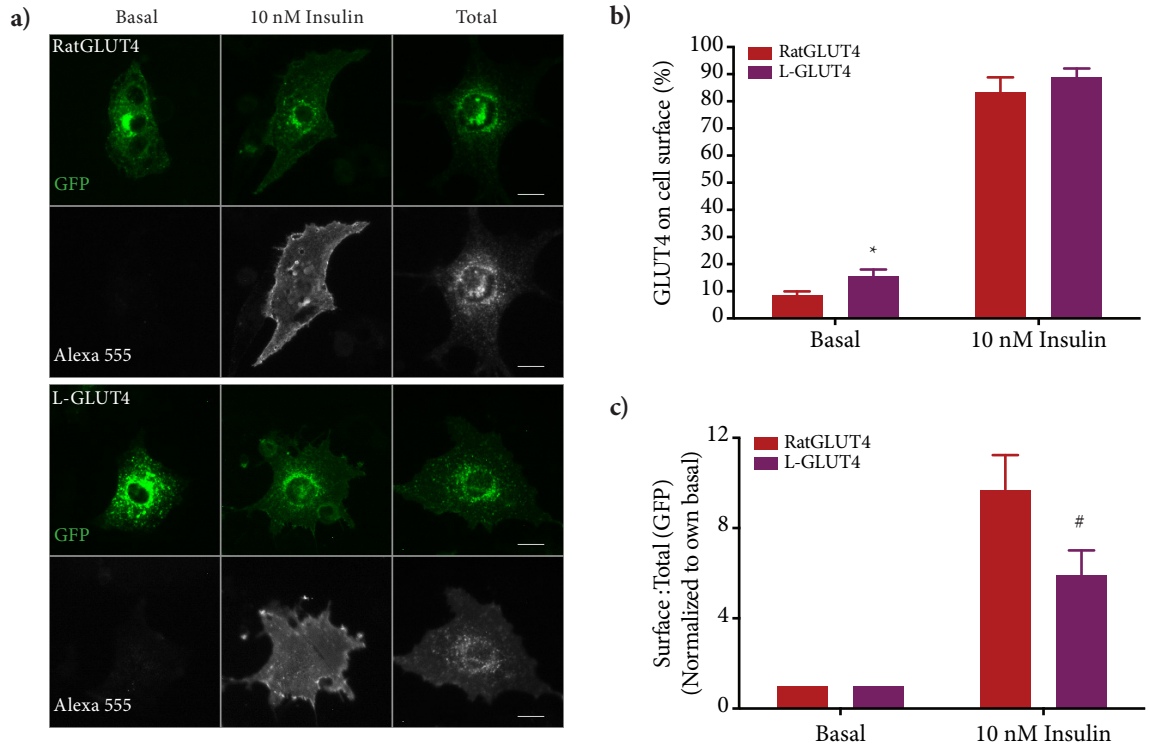

Figure IV-27. RatGLUT4 and L-GLUT4 plasma membrane levels in 3T3-L1 adipocytes. **a)** Images of RatGLUT4- and L-GLUT4-expressing 3T3-L1 adipocytes under a DMIRB inverted Leica microscope using a 20 x air objective showing GFP (total GLUT4 expression) and Alexa 555 (surface GLUT4) signals of individual cells. Graphs show cell surface levels of RatGLUT4 and BtGLUT4 in the absence and presence of 10 nM Insulin and data were expressed as **b)** cell surface levels normalized to total levels to determine GLUT4 percentage at the cell surface and as **c)** cell surface levels in the presence of 10 nM Insulin normalized to the basal levels to determine GLUT4 translocation to the plasma membrane. Data were plotted and Student's t test was performed using GraphPad Prism software. Red bars represent RatGLUT4 and purple bars represent L-GLUT4. Figure represents the mean ± SEM of four independent experiments. *, p<0,05 vs RatGLUT4 Basal; #, p<0,05 vs RatGLUT4 10 nM Insulin. Scale bar, 20 µm.

4.2.3. Endocytosis of L-GLUT4.

In the absence of insulin, GLUT4 exocytosis is very slow and its contribution to the increase in GLUT4 surface levels is small. Because GLUT4 levels at the cell surface depend on the balance between its exocytosis and endocytosis, we hypothesized that a slow L-GLUT4 internalization might be the cause for its increased plasma membrane levels in the absence of insulin, when

compared to RatGLUT4.

To analyze the endocytosis of RatGLUT4, BtGLUT4 and L-GLUT4 we electroporated these constructs into 3T3-L1 adipocytes, we serum starved cells and incubated them with a α-myc antibody for different times. We then detected cell surface GLUT4 and measured the fraction of it that was internalized (Figure IV-28a). As indicated above, it is important to use short incubation times to avoid recycling of myc-bound GLUT4 back to the surface.

In Figure IV-28b and IV-28c we show that the endocytic rate of L-GLUT4 was 23 % slower than that of RatGLUT4; however, it was 36 % faster than that of BtGLUT4.

In summary, we observed that the substitution of the cytoplasmic loop of RatGLUT4 slows down its basal internalization which contributes to increase the presence of L-GLUT4 at plasma membrane in the absence of insulin.

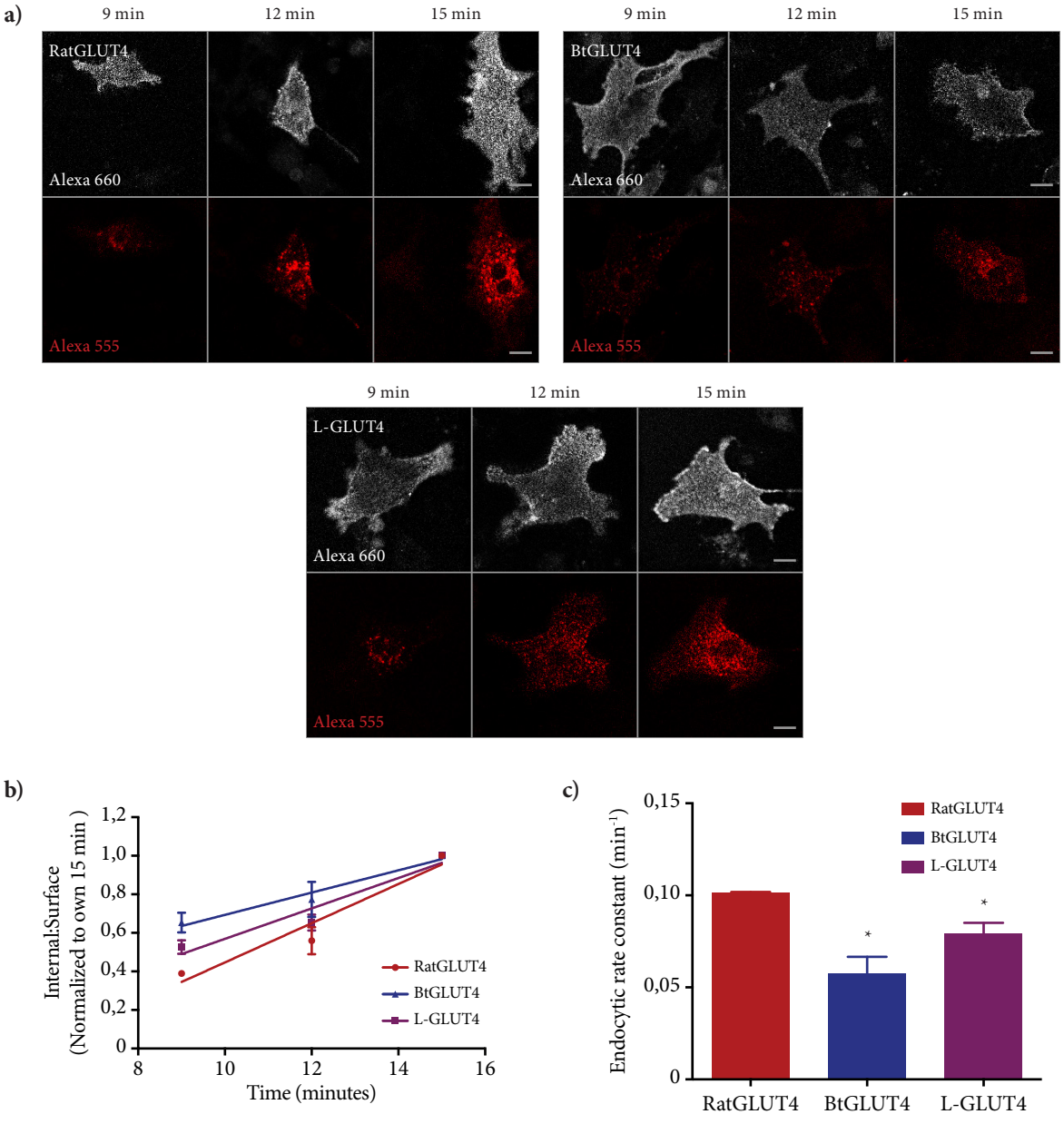

Figure IV-28. RatGLUT4 and L-GLUT4 endocytosis in the absence of insulin. **a)** Images of RatGLUT4- and L-GLUT4-expressing 3T3-L1 adipocytes under a Leica TCS SP2 microscope using a 20 x air objective showing

Alexa 660 (surface GLUT4) and Alexa 555 (internalized GLUT4) signals of individual cells. **b)** Graph shows internalization of RatGLUT4 and L-GLUT4 over time in the absence of insulin, expressed as internalized GLUT4 normalized to cell surface GLUT4. Data were also normalized to their own 15 minute time point. Data were plotted and linear regression curves were fit to data using GraphPad Prism software. Figure represents the mean ± SEM of three independent experiments. **c)** Graph shows endocytic rate constants of RatGLUT4 and L-GLUT4 and were determined by measuring and averaging the individual slopes of the curves of three independent experiments (mean ± SEM). Red represents RatGLUT4, blue represents BtGLUT4 and purple represents L-GLUT4. Student's t test was performed using GraphPad Prism software; *, p<0,05 vs RatGLUT4. Scale bar, 20 µm.

4.2.4. L-GLUT4 routes of internalization.

Changing the cytoplasmic loop of RatGLUT4 by that of BtGLUT4 reduces its endocytosis in the absence of insulin. For this reason, we wanted to observe if this substitution also changed the routes of internalization used by RatGLUT4. To do so we first needed to stably express L-GLUT4 in 3T3-L1 adipocytes. We accomplished this by producing viruses carrying L-GLUT4 cloned in a lentiviral vector and infecting 3T3-L1 pre-adipocytes (Figure IV-29a). In Figure IV-29b and IV-29c we show that we were able to obtain a stable 3T3-L1 cell line with L-GLUT4 RNA and protein levels comparable to those of RatGLUT4 and BtGLUT4.

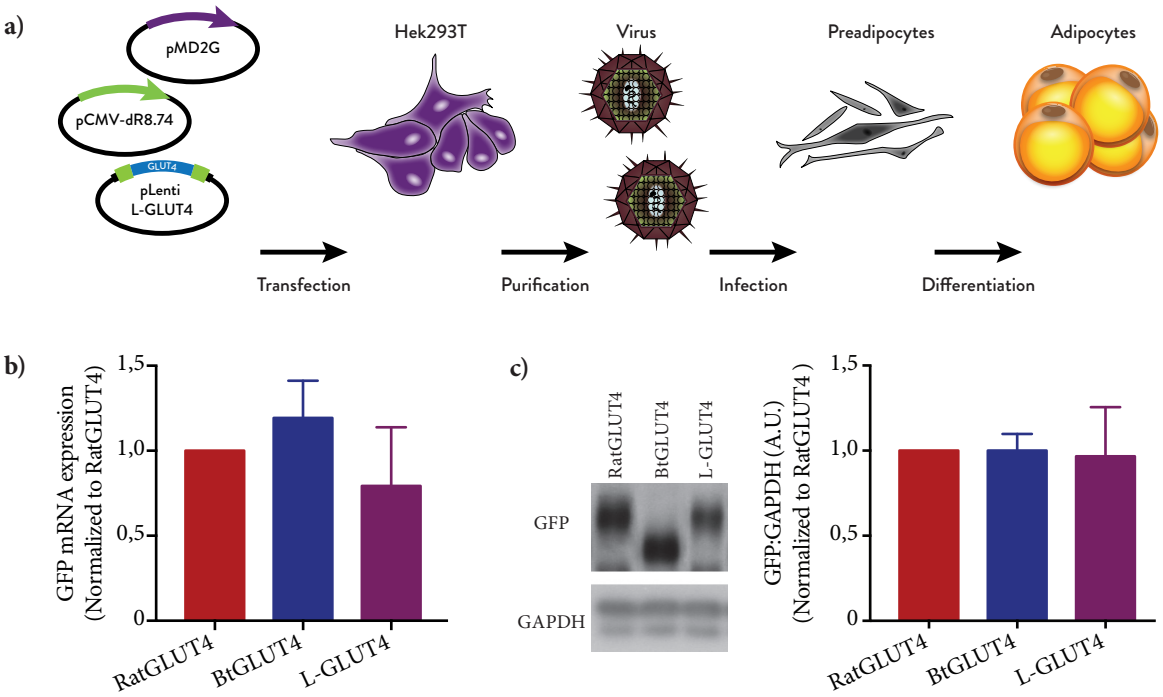

Figure IV-29. Generation of 3T3-L1 cell line stably expressing RatGLUT4, BtGLUT4 and L-GLUT4. **a)** Schematic representation of the protocol used to stably express GLUT4 constructs in 3T3-L1 adipocytes. Lentivirus production and 3T3-L1 cell infection workflow. Lentiviral vectors (pLenti CMV/TO Puro DEST) expressing RatGLUT4, BtGLUT4 or L-GLUT4 were transfected into Hek293T cells along with plasmids encoding for viral packaging system and enveloped proteins (pCMV-dR8.74 and pMD2G, respectively). Hek293T growth media was collected twice, once a day, centrifuged and purified using a sucrose cushion. After viral titration using flow cytometry, 3T3-L1 preadipocytes were infected at 75 MOI. Successfully infected cells were selected using puromycin (lentiviral vector selection antibiotic). Preadipocytes were induced to differentiate into adipocytes when needed. **b)** Graph shows GFP mRNA expression levels (RatGLUT4, BtGLUT4, and L-GLUT4) relative to the mRNA expression levels of the ARP housekeeping gene. BtGLUT4 and L-GLUT4 mRNA expression levels were normalized to RatGLUT4 mRNA expression levels and data from three independent experiments were averaged and plotted (mean ± SEM) using GraphPad Prism software. **c)** Image on the left shows GFP (RatGLUT4, BtGLUT4 and L-GLUT4) and GAPDH protein levels in total lysates of 3T3-L1 adipocytes expressing RatGLUT4, BtGLUT4 and L-GLUT4. Graph shows the protein levels of the expressed constructs. Band intensities were quantified using

Fiji processing software, and GFP level was normalized to GAPDH. BtGLUT4and L-GLUT4 data were normalized to RatGLUT4 and data from six independent experiments were plotted (mean ± SEM) using GraphPad Prism software. Red bars represent RatGLUT4, blue bars represent BtGLUT4 and purple bars represent L-GLUT4. A.U.: Arbitrary units.

4.2.4.1. L-GLUT4 clathrin-mediated endocytosis.

After generating a 3T3-L1 cell line stably expressing L-GLUT4 we first analysed its clathrin-mediated endocytosis in the absence of insulin. To do so, we treated cells with or without sucrose and then cooled them down to label the exofacial myc epitope of cell surface GLUT4. Next, we rewarmed cells and incubated them for 0 or 10 minutes (internalization stage). After the internalization, we detected the remaining α-myc antibody at the cell surface. As shown in Figure IV-30a, the substitution of the cytoplasmic loop in RatGLUT4 (L-GLUT4) did not affect its clathrin-mediated endocytosis.

In summary, in the absence of insulin, RatGLUT4, BtGLUT4 and L-GLUT4 utilize clathrin-mediated endocytosis (Figure IV-30b).

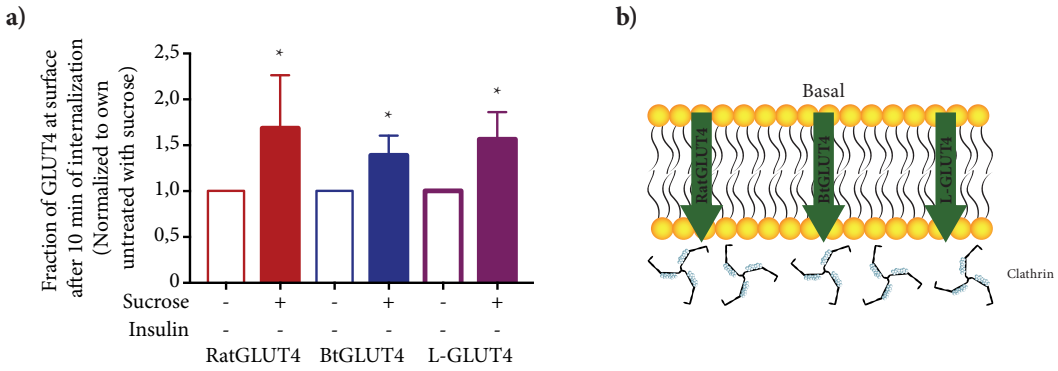

Figure IV-30. Inhibition of clathrin-mediated endocytosis in 3T3-L1 adipocytes stably expressing RatGLUT4, BtGLUT4 and L-GLUT4. **a)** Graph represents the cell surface levels of RatGLUT4, BtGLUT4 and L-GLUT4 in 3T3-L1 adipocytes treated with or without hypertonic sucrose, after 10 minutes of internalization and in the absence of insulin. GLUT4 at the cell surface after 10 minutes of internalization was normalized to cell surface GLUT4 at the beginning of the internalization to determine the fraction of non-internalized GLUT4. The fraction of non-internalized GLUT4 was normalized to own control (absence of sucrose) and data from six independent experiments were plotted (mean ± SEM) and Student's t test was performed using GraphPad Prism software. Red bars represent RatGLUT4, blue bars represent BtGLUT4 and purple bars represent L-GLUT4. *, $p<0,05$ vs own control (absence of sucrose). **b)** Schematic representation of the obtained data. Green arrows represent internalization through clathrin-mediated route.

4.2.4.2. L-GLUT4 cholesterol-mediated endocytosis.

After analysing L-GLUT4 clathrin-mediated internalization, we studied its cholesterol-dependent endocytosis (Figure IV-31a). We inhibited this pathway using nystatin and measured L-GLUT4 internalization by myc detection of surface GLUT4 before and after 10 minutes of internalization. In Figure IV-31a we observe that nystatin induced only 10 % accumulation of L-GLUT4 at plasma membrane, while inducing 38 % accumulation of RatGLUT4, which represents a 3,8-fold difference.

In summary (Figure IV-31b), we observe that loop substitution reduced RatGLUT4 (L-GLUT4) cholesterol-dependent endocytosis.

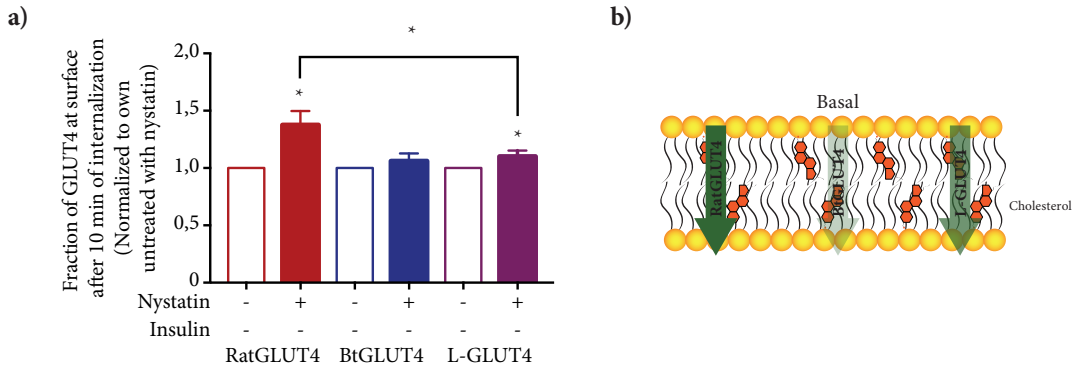

Figure IV-31. Inhibition of cholesterol-dependent endocytosis in 3T3-L1 adipocytes stably expressing RatGLUT4, BtGLUT4 and L-GLUT4. **a)** Graphs represent the cell surface levels of RatGLUT4, BtGLUT4 and L-GLUT4 in 3T3-L1 adipocytes treated with or without nystatin, after 10 minutes of internalization, in the absence of insulin. GLUT4 at the cell surface after 10 minutes of internalization was normalized to cell surface GLUT4 at the beginning of the internalization to determine the fraction of non-internalized GLUT4. The fraction of non-internalized GLUT4 was normalized to their own control (absence of nystatin) and data from seven independent experiments were plotted (mean ± SEM) and Student's t test was performed using GraphPad Prism software. Red bars represent RatGLUT4, blue bars represent BtGLUT4 and purple bars represent L-GLUT4. *, $p<0,05$ vs own control (absence of nystatin). **b)** Schematic representation of the obtained data. Green arrows represent internalization through cholesterol-dependent route; Dimmed arrow represents no change in internalization.

4.2.4.3. L-GLUT4 caveolar endocytosis.

To observe how the substitution of the cytoplasmic loop affects RatGLUT4 caveolar endocytosis, we knocked down Cav-1 in L-GLUT4-expressing cells.

Infecting L-GLUT4-expressing preadipocytes with lentiviruses carrying siRNA for Cav-1 (Figure IV-32a) we were able to knockdown Cav-1 in a cell line stably expressing L-GLUT4. As observed in Figure IV-32b, we obtained a 90 % reduction of Cav-1 protein levels. Concomitant with Cav-1 KD we obtained a 50 % reduction of L-GLUT4 expression levels, similarly to what was observed when generating RatGLUT4 and BtGLUT4 Cav-1 KD cell lines.

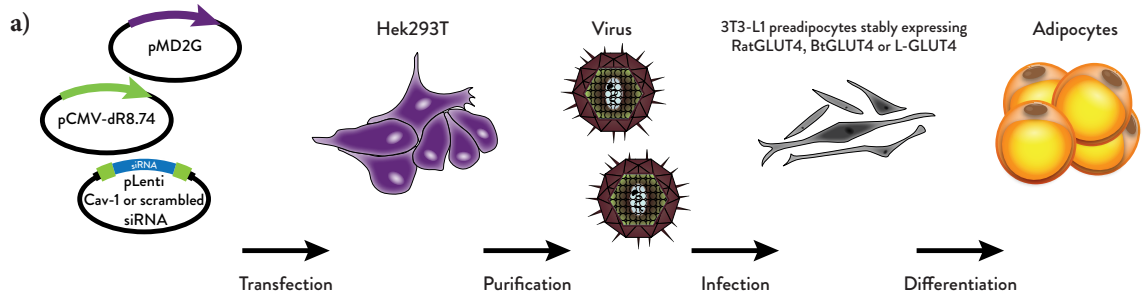

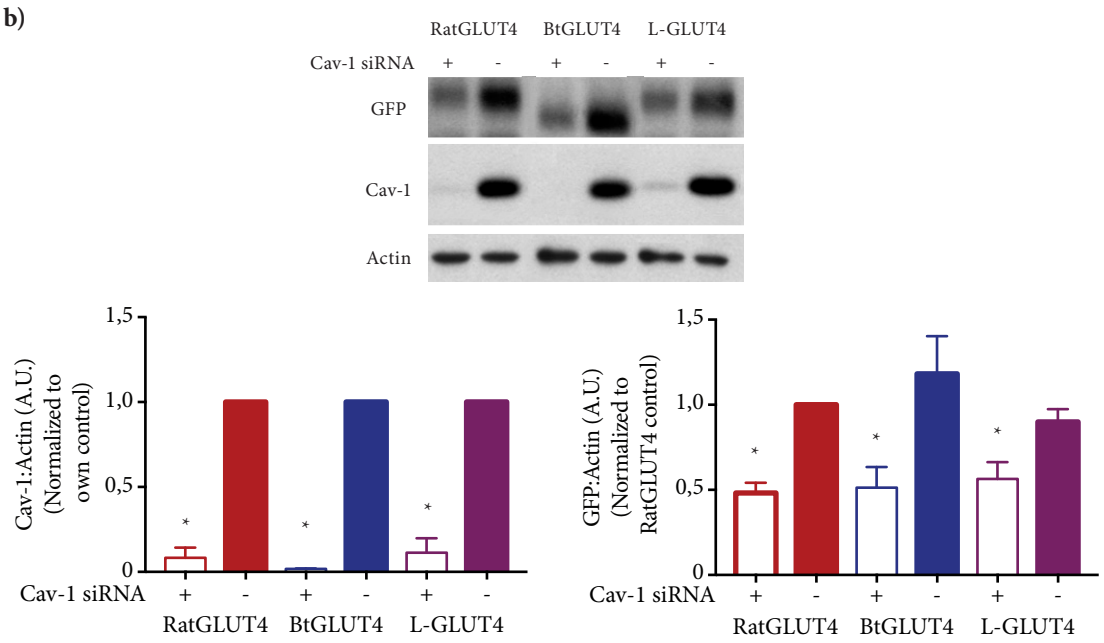

Figure IV-32. Caveolin-1 knockdown in 3T3-L1 adipocytes stably expressing RatGLUT4, BtGLUT4 or L-GLUT4. **a)** Schematic representation of the protocol used to knock down Cav-1 in 3T3-L1 adipocytes. Lentiviral vectors (pLVTHM) encoding siRNA for caveolin-1 (Cav-1) or its scrambled sequence (control) were transfected into Hek293T cells along with plasmids encoding for viral packaging system and enveloped proteins (pCMV-dR8.74 and pMD2G, respectively). Hek293T growth media was collected twice, once a day, centrifuged and purified using a sucrose cushion. After purification, viruses were used to infect 3T3-L1 preadipocytes expressing GLUT4 constructs. Preadipocytes were induced to differentiate into adipocytes when needed. **b)** Figure shows GFP (RatGLUT4, BtGLUT4 and L-GLUT4), Cav-1 and actin protein expression levels in total lysates of Cav-1-depleted and control RatGLUT4-, BtGLUT4-and L-GLUT4-expressing 3T3-L1 adipocytes. Band intensities were quantified using Fiji processing software, and GFP and Cav-1 levels were normalized to Actin. GFP levels were normalized to RatGLUT4 Cav-1 control cells; and Cav-1 levels were normalized to their own Cav-1 control cells. Data from three independent experiments were plotted (mean ± SEM) and Student's t test was performed using GraphPad Prism software. Red represents data from RatGLUT4-expressing adipocytes, blue represents data from BtGLUT4-expressing adipocytes and purple represents data form L-GLUT4-expressing adipocytes. *, $p<0,05$ vs own Cav-1 control. A.U.: Arbitrary units.

After measuring the L-GLUT4 clathrin-mediated and cholesterol-dependent endocytosis of L-GLUT4 we analysed its caveolar endocytosis. To measure L-GLUT4 endocytosis in the absence of insulin we probed exofacial L-GLUT4 myc, using a α-myc antibody, in serum-starved adipocytes and detected surface L-GLUT4 before and after 10 minutes of internalization. We previously observed that Cav-1 KD, and therefore caveolae ablation, increased RatGLUT4 internalization. In Figure IV-33a we show that Cav-1 KD also induced an increase in L-GLUT4 internalization; however, the difference was not statistically significant.

In summary (Figure IV-33b), we observed that cytoplasmic loop substitution of RatGLUT4 reduced its internalization in Cav-1-depleted adipocytes.

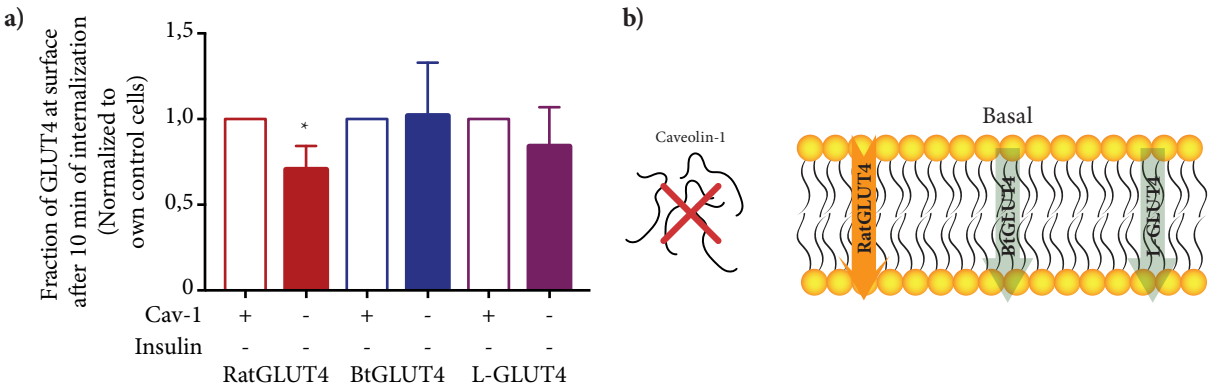

Figure IV-33. Inhibition of caveolar endocytosis in 3T3-L1 adipocytes stably expressing RatGLUT4, BtGLUT4 and L-GLUT4. **a)** Graphs represent the cell surface levels of RatGLUT4, BtGLUT4 and L-GLUT4 in control or Cav-1-depleted 3T3-L1 adipocytes, after 10 minutes of internalization, in the absence insulin. GLUT4 at the cell surface after 10 minutes of internalization was normalized to cell surface GLUT4 at the beginning of the internalization to determine the fraction of non-internalized GLUT4. The fraction of non-internalized GLUT4 was normalized to their own control (presence of Cav-1) and data from six independent experiments were plotted (mean ± SEM) and Student's t test was performed using GraphPad Prism software. Red bars represent RatGLUT4, blue bars represent BtGLUT4 and purple bars represent L-GLUT4. *, $p<0,05$ vs own control (presence of Cav-1). **b)** Schematic representation of the obtained data. Orange arrows represent increase in internalization; Dimmed arrow represents no change in internalization.

4.2.4.4. L-GLUT4 clathrin-mediated and cholesterol-dependent endocytosis in Cav-1 KD adipocytes.

Similarly to what we did for RatGLUT4 and BtGLUT4, we set out to measure L-GLUT4 clathrin-mediated and cholesterol-dependent internalization in the absence of caveolin-1.

In order to block clathrin-mediated endocytosis, we induced hypertonic sucrose shock (to halt this pathway) and measured the internalization of L-GLUT4 in cells subjected to Cav-1 KD. In Figure IV-34a, we show that in the absence of insulin and Cav-1, inhibition of the clathrin-mediated endocytic pathway induced a 35 % accumulation of L-GLUT4 at the cell surface, similarly to BtGLUT4 (38 %). On the other hand, RatGLUT4 was not affected by inhibition of this route.

In summary (Figure IV-34b), the substitution of the cytoplasmic loop of RatGLUT4 induced its internalization through clathrin-mediated endocytosis in Cav-1-depleted adipocytes in the absence of insulin.

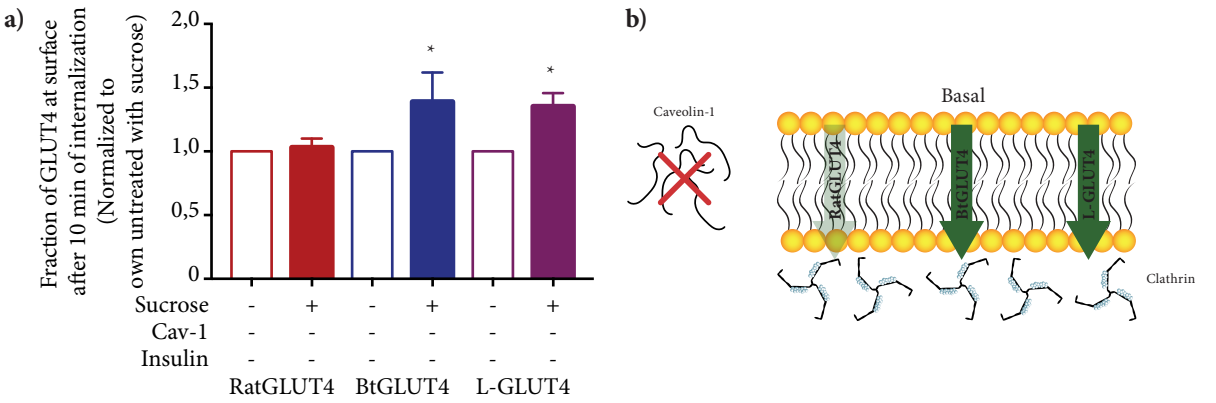

Figure IV-34. Inhibition of clathrin-mediated endocytosis in caveolin-1-depleted 3T3-L1 adipocytes stably expressing RatGLUT4, BtGLUT4 and L-GLUT4. **a)** Graphs represent the cell surface levels of RatGLUT4,

BtGLUT4 and L-GLUT4 in Cav-1-depleted 3T3-L1 adipocytes treated with or without hypertonic sucrose, after 10 minutes of internalization, in the absence of insulin. GLUT4 at the cell surface after 10 minutes of internalization was normalized to cell surface GLUT4 at the beginning of the internalization to determine the fraction of non-internalized GLUT4. The fraction of non-internalized GLUT4 was normalized to their own control (absence of sucrose) and data from six independent experiments were plotted (mean ± SEM) and Student's t test was performed using GraphPad Prism software. Red bars represent RatGLUT4, blue bars represent BtGLUT4 and purple bars represent L-GLUT4. *, p<0,05 vs own control (absence of sucrose). **b)** Schematic representation of the obtained data. Green arrows represent internalization through clathrin-mediated route; Dimmed arrow represents no change in internalization.

Nystatin inhibition of cholesterol-dependent internalization, in the absence of insulin and Cav-1, induced a 35 % accumulation of L-GLUT4 at plasma membrane whereas it had no effect on RatGLUT4 and BtGLUT4 surface levels (Figure IV-35a).

In summary (Figure IV-35b), the substitution of the cytoplasmic loop of RatGLUT4 induced its internalization through cholesterol-dependent endocytosis in Cav-1-depleted adipocytes, in the absence of insulin.

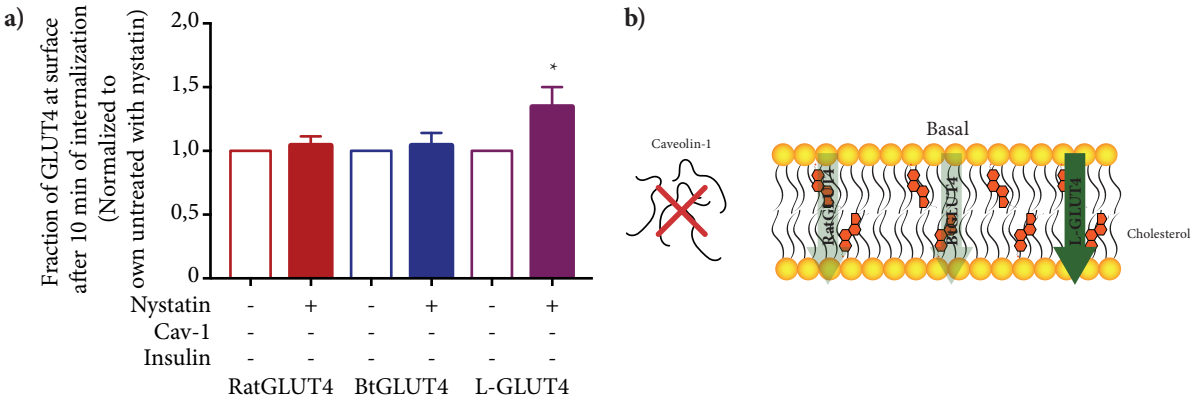

Figure IV-35. Inhibition of cholesterol-dependent endocytosis in caveolin-1-depleted 3T3-L1 adipocytes stably expressing RatGLUT4, BtGLUT4 and L-GLUT4. **a)** Graphs represent the cell surface levels of RatGLUT4 and BtGLUT4 in Cav-1-depleted 3T3-L1 adipocytes treated with or without nystatin, after 10 minutes of internalization, in the absence of insulin. GLUT4 at the cell surface after 10 minutes of internalization was normalized to cell surface GLUT4 at the beginning of the internalization to determine the fraction of non-internalized GLUT4. The fraction of non-internalized GLUT4 was normalized to their own control (absence of nystatin) and data from six independent experiments were plotted (mean ± SEM) and Student's t test was performed using GraphPad Prism software. Red bars represent RatGLUT4, blue bars represent BtGLUT4 and purple bars represent L-GLUT4. *, p<0,05 vs own control (absence of nystatin). **b)** Schematic representation of the obtained data. Dimmed arrow represents no change in internalization.

V. DISCUSSION

Glucose uptake by muscle and adipose tissue is essential for the maintenance of whole-body glucose homeostasis and, in these tissues, GLUT4 is the main glucose transporter. The functioning of GLUT4 is tightly regulated by accessory proteins that interact with GLUT4 motifs and move the transporter between several intracellular compartments and the plasma membrane. Therefore, understanding the mechanism involved in GLUT4 trafficking is fundamental to comprehend glucose homeostasis. In fish, GLUT4 variants have been cloned (Planas et al. 2000, Capilla et al. 2004) and, despite being highly similar in sequence to mammalian GLUT4, fish GLUT4 possesses differences in protein motifs known to be important for GLUT4 trafficking. In this work we aimed to compare rat and brown trout GLUT4 trafficking in 3T3-L1 adipocytes and by doing so help to define the protein motifs involved in this process.

1. CHARACTERIZATION OF THE GENERAL TRAFFICKING OF RatGLUT4 AND BtGLUT4.

To study the trafficking of RatGLUT4 and BtGLUT4 we expressed constructs of these GLUT4 variants (possessing myc epitopes in the first exofacial loop and GFP in the C-terminal end, (Figure IV-1a) in 3T3-L1 adipocytes using transient and stable expression techniques. In both cases we quantified total protein levels (Figures IV-1c and IV-9c) to ensure, first, that we were not oversaturating the cellular machinery, which would be indicated by the existence of blobs or other abnormal accumulation of GFP, and, second, that differences in trafficking between RatGLUT4 and BtGLUT4 would not be attributed to differences in expression levels. Moreover, we waited 24 hours before using cells electroporated with our constructs, as it has been determined that expressed GLUT4 requires 9 hours for synthesis and targeting to GSVs (Khan et al. 2004, Watson et al. 2004). Although we did not analyze the insulin-responsiveness timeframe of these constructs in the present study, previous studies have shown that BtGLUT4 undergoes insulin-stimulated translocation before RatGLUT4, as early as 3 hours after transfection (Capilla et al. 2010). We also measured glucose transport in 3T3-L1 preadipocytes expressing RatGLUT4 and BtGLUT4 to avoid expression of endogenous GLUT4 and verified that they were capable of increasing glucose (2-deoxyglucose) uptake in these cells by 30 % and 10 %, respectively. Undifferentiated 3T3-L1 cells have been shown to be able to translocate GLUT4 to the PM (Kanai et al. 1993, Lampson et al. 2000); however, these are not ideal for glucose uptake assays since they still lack expression of the GLUT4 trafficking machinery which might be the cause for the shy increase of glucose transport in preadipocytes expressing our GLUT4 constructs, especially BtGLUT4.

Despite the complex trafficking of GLUT4, glucose uptake is ultimately dependent on the presence of GLUT4 at the PM. By expressing RatGLUT4 in 3T3-L1 adipocytes, we observed that in unstimulated cells approximately 8 % of total RatGLUT4 was targeted to the PM and that after insulin stimulation this fraction increased to 80 %, which corresponds to a 10-fold increase (Figure IV-2). The observed fractions of RatGLUT4 at the PM under basal and insulin-

stimulated conditions differ from previously published data that described that GLUT4 PM levels in 3T3-L1 adipocytes were 5 % and 50 %, respectively, but the fold change in response to insulin was equal (Blot and McGraw 2008). Although the general method used for determining the fraction of GLUT4 at the PM was the same, the discrepancy in the values might be due to differences in the utilized 3T3-L1 clones and their differentiation, as well as to the fact that the previously described values were obtained using human HA-GLUT4 in contrast to our rat myc-GLUT4. On the other hand, our values are similar to those obtained by Capilla and colleagues that observed that RatGLUT4 (myc) basal and insulin-stimulated surface levels were approximately 10 % and 80 %, respectively (Capilla et al. 2010).

The most interesting information obtained from these experiments was that BtGLUT4 basal surface levels were more than 4-fold higher than those of RatGLUT4. This is in accordance with previous studies that showed that BtGLUT4 basal surface levels were higher than those of RatGLUT4 in adipocytes and muscle cells (Díaz et al. 2007a, Capilla et al. 2010). Moreover, we observed that, mainly as a consequence of its poor basal intracellular retention, BtGLUT4 translocation in response to insulin was weaker than that of RatGLUT4 (1,5-fold vs 10-fold) (Figure IV-2c). This was also observed by Capilla et al. (2010) in adipocytes and by Díaz et al. (2007a) in muscle cells. In addition to the poor basal intracellular retention, we also observed that the cell surface levels of BtGLUT4 in the presence of insulin were lower than those of RatGLUT4 (which also contributes to the weaker translocation of BtGLUT4) (Figure IV-2b). This was unexpected since previous studies reported higher BtGLUT4 PM levels in unstimulated conditions, as indicated above, but not lower surface levels in the presence of insulin (Díaz et al. 2007a, Capilla et al. 2010). The differences might be a consequence of the different methodologies used in the various studies: in Capilla et al. (2010) the surface levels were determined by full-rimed cell counts; Díaz et al. (2007a), on the other hand, determined the global BtGLUT4 surface levels of an entire cell population. In our case, we analyzed cells individually and normalized surface myc to total expression (GFP) levels. Because it is important to use values determined by the same fluorescent molecules (i.e. surface myc-Alexa555/total myc-Alexa555 as opposed to surface myc-Alexa555/total GFP) to calculate the percentage of cell surface over total, we permeabilized cells and labelled total GLUT4 with α-myc to calculate cell surface myc over total myc. Notwithstanding, we suggest that the lower BtGLUT4 PM levels in the presence of insulin were caused by its slower exocytic rate (Figure IV-6) (this will be further discussed below).

Interestingly, we also observed that BtGLUT4 translocation was more resistant to low temperatures than that of RatGLUT4 (Figure IV-3). Whilst BtGLUT4 translocation did not change by lowering the temperature from 37 ºC to 25 ºC, RatGLUT4 reduced its translocation by 26 %. Usually, the body temperature of adult brown trout ranges from 0 ºC to 26 ºC, but because we were using mammalian adipocytes as expression system we could not lower the incubation temperature below 25 ºC without risking inhibition of the cellular machinery. Thus, it would be interesting to perform this analysis using fish primary adipocytes that grow at 18 ºC. Nonetheless, our data are interesting and could mean that throughout evolution, fish maintained

a less temperature-sensitive GLUT4 traffic than mammals in order to better withstand the variations of body temperature that they experience throughout the year.

After insulin action, GLUT4 must be removed from the PM and return to its intracellular compartments. We analyzed the ability of RatGLUT4 and BtGLUT4 to return to their basal surface levels after insulin washout (Figure IV-4) and observed that the mechanism of RatGLUT4 to return to basal was more efficient than that of BtGLUT4. Upon insulin action, RatGLUT4 surface levels increased by 85 % and, 30 minutes after insulin removal by extensive washing, they were reduced them by 72 % (85 % recovery). On the other hand, BtGLUT4 surface levels increased by 45 % in response to insulin and were reduced by 26 % after insulin removal (57 % recovery). These data are in accordance with a previous study that showed that human GLUT4 recovers 72 % of its basal PM levels by 30 minutes after insulin washout (Blot and McGraw 2006). In the study by Blot and McGraw work (2006) it was also suggested that the N-terminus $FQQI^{8}$ and the C-terminus LL^{490} motifs are involved in the return-to-basal mechanism; and Capilla et al. (2007) also implicated both motifs in the endocytosis of GLUT4. Therefore, we suggest that the lower return-to-basal mechanism of BtGLUT4 was, at least in part, due to the lack of the LL^{490} motif and possibly to alterations in its $FQHL^{8}$ motif. Regarding differences between rat and trout in the N-terminal end ($FQQI^{8}$ vs $FQHL^{8}$), we could argue that while an isoleucine (I)-leucine (L) change might not have major effects since these are both non-polar amino acids, glutamine (Q)-histidine (H) are, respectively, uncharged and positively charged amino acids and such change might affect interactions with accessory proteins and/or with other GLUT4 motifs.

GLUT4 surface levels are intimately related to the rates of exocytosis and endocytosis and it is the balance between these two rates that determines the amount of GLUT4 at the PM. Therefore, we measured RatGLUT4 and BtGLUT4 exocytic rates in the absence and presence of insulin. We observed that in response to the hormone, RatGLUT4 exocytic rate increased 6-fold (from 0,005 min-1 to 0,031 min-1) (Figures IV-5c and IV-6c). This increase was much lower than the 26-fold increase reported in a previous study in which the exocytic rate of human HA-GLUT4 was measured using a similar method in 3T3-L1 adipocytes (Karylowski et al. 2004). However, when measuring basal exocytosis, they followed α-HA labelling for a longer time period (240 min vs 1400 min). This is important because it allowed them to completely label the entire pool of human GLUT4 (at 600 min) and, therefore, to better fit a curve to the data whose slope was the exocytic rate constant. In other words, by extending the time points of their experiment they obtained a more reliable basal exocytic rate constant. Nonetheless, our rate constant values and the ones obtained in the referred study are within the same order of magnitude. As future work, it would be recommended to repeat these experiments using the parameters from Karylowski et al. (2004) to accurately determine basal exocytic rates. However, in this work we focused on the comparison between RatGLUT4 and BtGLUT4 and regarding the latter, we observed a 1,3-fold increase of the exocytic rate constant in response to insulin (0,004 min-1 vs 0,005 min-1) (Figures IV-5c and IV-6c) but it was not statistically significant. It is possible that we need to repeat the

measurement of the basal exocytic rate using longer time points in order to accurately determine this parameter and detect significant differences. Notwithstanding, the data on the exocytic rate constant correlates with the translocation observations: in response to insulin, RatGLUT4 increased its surface distribution by 10-fold and its exocytosis by 6-fold; BtGLUT4, on the other hand, increased its surface levels by 1,5-fold and its exocytosis by 1,3-fold. Comparing the two transporters, the increase in surface levels and exocytosis of RatGLUT4 was, respectively, 6,7-fold and 7,8-fold stronger than BtGLUT4. Díaz and colleagues also analyzed the exocytosis of RatGLUT4 and BtGLUT4 in L6 muscle cells; however, their observations differ from ours since they observed that BtGLUT4 basal exocytosis was faster than that of RatGLUT4 (Díaz et al. 2007a). Apart from differences in the methodology, it is also important to note that adipocytes and muscle cells differ in terms of GLUT4 translocation and trafficking. For example, insulin-stimulated GLUT4 translocation is weaker in muscle cells than in adipocytes (Antonescu et al. 2009) and was earlier corroborated by Díaz et al. (2007a) (2-fold and 1,4-fold translocation of RatGLUT4 and BtGLUT4, respectively). Moreover, internalization pathways and accessory proteins are also partially cell-type specific (Ishikura et al. 2007, Antonescu et al. 2009, Sadacca et al. 2013).

As indicated above, endocytosis is important to define GLUT4 availability at the PM. Contrary to exocytosis, endocytosis has been described to deaccelerate upon insulin action and Blot and McGraw (2006) observed a reduction of approximately 60 % in the endocytic rate of human GLUT4 when expressed in 3T3-L1 adipocytes. In this study, we failed to observe a statistically significant decrease in endocytosis of RatGLUT4 and BtGLUT4 in response to insulin (10% and 7 % reduction, respectively) (Figures IV-7c and IV-8c). The difference between this and the study of Blot and McGraw is probably due because in the latter study, basal endocytosis was determined using longer time points which could help reveal and accentuate differences that would otherwise be not clear at shorter times. Nonetheless, regarding our own data we observed that in the absence of insulin, RatGLUT4 endocytosis was 1,75-fold faster than that of BtGLUT4 (0,102 min-1 vs 0,058 min-1) (Figure IV-7) and in the presence of insulin, RatGLUT4 internalization was 1,72-fold faster than that of BtGLUT4 (0,093 min-1 vs 0,054 min-1) (Figure IV-8). As indicated above, BtGLUT4 lacks the LL^{490} motif and its corresponding $FQQI^{8}$ motif is $FQHL^{8}$ that, combined with the fact that BtGLUT4 had a slower endocytosis, supports the notion that the $FQQI^{8}$ and LL^{490} motifs are important for endocytosis and that mutations in these motifs reduce GLUT4 endocytosis without completely inhibiting it, as previously suggested (Corvera et al. 1994, Al-Hasani et al. 2002, Blot and McGraw 2006, Capilla et al. 2007).

Because in our methodology we used different fluorophores to label surface and internalized GLUT4, we obtained an apparent endocytic rate; however, this rate is proportional to the (real) rate constant. Therefore, we cannot directly compare the apparent endocytic rate constant to our exocytic rate constant but we can compare the ratios between the RatGLUT4 and BtGLUT4 rates. In the absence of insulin, RatGLUT4 exocytosis was 1,6-fold faster and its endocytosis was also 1,75-fold faster than those of BtGLUT4. Thus, in the absence of insulin, the balance

between RatGLUT4 exocytosis and endocytosis favored lower PM levels when compared to BtGLUT4, supporting our observations on the cell surface levels (Figure IV-2). In the presence of insulin, we observed that RatGLUT4 exocytosis was 7,8-fold faster and its endocytosis was 1,72-fold faster than those of BtGLUT4. In this case, it is clearer that the exocytosis/endocytosis balance favored higher RatGLUT4 PM levels in the presence of insulin, which also correlates with our data on cell surface levels (Figure IV-2). Previous studies also analyzed RatGLUT4 and BtGLUT4 internalization: Díaz et al. (2007a) observed that both GLUT4 variants had similar basal endocytosis when expressed in muscle cells; Capilla et al. (2010) also analyzed RatGLUT4 and BtGLUT4 internalization after insulin removal and observed no differences between the constructs. It is hard to compare data from both studies with our observations since the methods, experimental conditions and cellular models differ. In the case of the study by Díaz et al. (2007a), internalization experiments were performed in muscle cells and, as indicated above, GLUT4 trafficking in adipocytes and in muscle cells is not identical. On the other hand, Capilla et al. (2010) followed internalization in 3T3-L1 adipocytes for 3 hours, a period of time that we believe that allows each GLUT4 molecule enough time to undergo internalization and recycle back to the surface. Therefore, it is possible that Capilla et al. (2010) measured the cell surface levels of GLUT4 molecules that suffered several cycles of endocytosis and exocytosis during the 3-hour experiment and, consequently, measured both events and not solely the endocytosis.

2. DETERMINATION OF THE ROUTES OF INTERNALIZATION OF RatGLUT4 AND BtGLUT4.

Blot and McGraw (2006) postulated that insulin reduces endocytosis by inhibiting a cholesterol-dependent pathway. In our work we analyzed the contribution of different endocytic pathways for the internalization of RatGLUT4 and BtGLUT4. We observed that, in the absence of insulin, RatGLUT4 internalization was sensible to hypertonic sucrose and to cholesterol depletion with nystatin, suggesting a role for CME and cholesterol-dependent endocytosis, respectively (Figures IV-12a and IV-14a). Moreover, in the presence of insulin, RatGLUT4 endocytosis was still affected by hypertonic sucrose but not by cholesterol depletion (Figures IV-12b and IV-14b). Our data are in accordance with Blot and McGraw's observations in the sense that in unstimulated conditions, RatGLUT4 internalized through clathrin-mediated and cholesterol-dependent pathways but, upon insulin action, the cholesterol-dependent route was inhibited. Blot and McGraw (2006) also suggested that when active (absence of insulin), the cholesterol-dependent pathway was responsible for the majority of GLUT4 internalization (80 %). In our study we observed that ablation of CME resulted in a 69 % accumulation of RatGLUT4 at PM while inhibition of the cholesterol-dependent pathway reduced internalization by 38 %, suggesting a larger contribution of CME (Figures IV-12a and IV-14a). The analysis of routes of internalization is a delicate task since treatments that inhibit one pathway might also affect or be compensated by another, let alone because there would be more GLUT4 available

at the surface (Doherty and McMahon 2009). Therefore, the facts that Blot and McGraw (2006) used electroporated cells whilst we used stable-expressing cells and that they inhibited CME by knocking down AP-2 while we used hypertonic sucrose, might contribute to the differences between both studies. In fact, in some studies, more than one drug/treatment is used to study the same internalization pathway. Regarding BtGLUT4 internalization, we found that it was affected by hypertonic sucrose but immune to nystatin-induced cholesterol depletion (in the absence and presence of insulin) (Figures IV-12 and IV-14). Thus, BtGLUT4 seemed to utilize solely a clathrin-mediated pathway. Our observations differ from data obtained in L6 muscle cells: in this cell line, BtGLUT4 was shown to solely utilize a cholesterol-dependent pathway, which was suggested to be the IL-2 receptor route (Antonescu et al. 2008). However, it is important to note that in muscle cells, the IL-2 receptor pathway is suggested to be the default GLUT4 cholesterol-dependent route whereas caveolar endocytosis fulfills that role in adipocytes (Ros-Baro et al. 2001, Shigematsu et al. 2003, Antonescu et al. 2008, 2009, Doherty and McMahon 2009). Furthermore, caveolae in muscle cells are different from caveolae in adipocytes since they do not possess Cav-1 and Cav-2 but Cav-3 instead. In addition, their content in cavins is also different (Bastiani et al. 2009, Briand et al. 2011). Therefore, it is plausible to assume that BtGLUT4 internalization pathways differ between these cell types.

Our experiments also suggested that, in comparison to RatGLUT4, BtGLUT4 internalization through CME is slower since hypertonic sucrose resulted in less accumulation of BtGLUT4 at the PM (approximately, 39 % for RatGLUT4 vs 65 % for BtGLUT4) in both the absence and presence of insulin (Figure IV-12). These results correlate with our observations on the slower endocytic rate of BtGLUT4 than RatGLUT4 and it might be due to the particular $FQHL^{8}$ motif in BtGLUT4 and to the absence of the LL^{490} motif, both suggested to be important for GLUT4 internalization (Corvera et al. 1994, Al-Hasani et al. 2002, Blot and McGraw 2006, Capilla et al. 2007).

In adipocytes, caveolar endocytosis is suggested to be the main cholesterol-dependent pathway involved in GLUT4 internalization (Ros-Baro et al. 2001, Shigematsu et al. 2003, Antonescu et al. 2008, 2009, Doherty and McMahon 2009). In our work, we knocked down Cav-1 (required for caveolae formation) to disrupt caveolar endocytosis and analyzed the effects on RatGLUT4 and BtGLUT4 internalization. Knockdown of Cav-1 resulted in a reduction of about 50 % in the protein levels of our expressed constructs (Figure IV-15); however, this was expected since it has been previously shown by our group that Cav-1 KD increases GLUT4 degradation (González-Muñoz et al. 2009). The observed reduction in GLUT4 protein levels did not compromise our objective to study caveolar internalization of RatGLUT4 and BtGLUT4 because we analyzed the effect of Cav-1 KD on GLUT4 PM levels in control and KD cells, separately. Contrary to our initial expectation, we observed that Cav-1 KD resulted in an increase of RatGLUT4 endocytosis in the absence and presence of insulin (30 % and 13 %, respectively) (Figure IV-16). In a previous study, caveolae ablation by expression of a Cav-1 mutant (Cav1/S80E) resulted in a decrease in GLUT4 endocytosis (Shigematsu et al. 2003). This mutant blocks

caveolae formation because Cav-1 is targeted to the endoplasmic reticulum instead of the PM (Schlegel et al. 2001). On the other hand, other studies observed that the expression of Cav-1, Cav-3 and cavins (also abundant in caveolae and essential for its formation) inhibited the CLIC/GEEC internalization pathway, possibly by impeding early formation of CLIC/GEEC carriers in a process independent of caveolar formation (Kirkham et al. 2005, Cheng et al. 2010, Chaudhary et al. 2014). Furthermore, the CLIC/GEEC internalization pathway is upregulated in cells lacking Cav-1 and cavin-1 (Chaudhary et al. 2014). The fact that Cav-1 (as well as cavin-1) expression interferes with other internalization pathways suggests that inhibition of caveolar endocytosis by expression of a Cav-1 mutant or Cav-1 KD might produce different effects. Taking this information into account we suggest that by knocking down Cav-1 we unlocked other internalization pathways and as a result we increased RatGLUT4 endocytosis. Alternatively, caveolae ablation might have accelerated internalization of existing pathways by disturbing PM fluidity, as it has been shown that caveolae disruption by Cav-1 KD increases PM fluidity (González-Muñoz et al. 2009). Nonetheless, the fact that RatGLUT4 internalization was strongly affected by Cav-1 KD suggested that RatGLUT4 internalized through the caveolar pathway in the absence of insulin. In the presence of insulin, this did not seem to be the case because in the presence of Cav-1 KD, RatGLUT4 internalization was cholesterol-independent (caveolar endocytosis is cholesterol-dependent). Thus, it is more plausible that, in the presence of insulin, the increase in internalization of RatGLUT4 was due to the possible unlocking of "new" endocytic pathways. While RatGLUT4 was sensitive to Cav-1 KD in the absence and presence of insulin, BtGLUT4 was only affected in the presence of insulin (Figure IV-16). Since BtGLUT4 was cholesterol-independent in the presence of Cav-1 KD, it is possible that upon Cav-1 removal BtGLUT4 started to internalize through previously inhibited routes. Interestingly, we also found that in the absence of Cav-1, insulin reduced RatGLUT4 internalization by more than 50 %, which is more than what we observed when determining the basal and insulin-stimulated endocytic rates and when inhibiting the clathrin-mediated and cholesterol-dependent pathways. This observation supports the hypothesis that in the absence of Cav-1, RatGLUT4 utilized different internalization pathways, with higher sensitivity to inhibition by insulin.

To analyze the effects of Cav-1 KD on the contribution of the CME and cholesterol-dependent endocytosis pathways to the RatGLUT4 and BtGLUT4 internalization, we inhibited these pathways in Cav-1 KD cells (Figure IV-17 and IV-18). We observed that, in the absence of insulin, RatGLUT4 seemed to internalize through a clathrin- and cholesterol- independent pathway since it was unaffected by hypertonic sucrose or nystatin treatments (Figures IV-17a and IV-18a), suggesting that the CLIC/GEEC (cholesterol-dependent) pathway was not being utilized. Currently, we do not know which pathway could be involved in RatGLUT4 endocytosis in the absence of Cav-1. However, since not all cholesterol-dependent pathways are affected in the same way by different cholesterol-depleting drugs and concentrations, it is possible that by using 50 mg/mL of nystatin we were not inhibiting the main cholesterol-dependent pathway (Doherty and McMahon 2009) and, thus, failed to observe differences in internalization. In fact, in various

studies examining the CLIC/GEEC pathway, methyl-β-cyclodextrin or 7-ketocholesterol but not nystatin are used as cholesterol-depleting agents (Kirkham et al. 2005, Chadda et al. 2007, Chaudhary et al. 2014). It would be interesting to use different cholesterol-depleting drugs and to follow CD44 internalization to verify if CLIC/GEEC was indeed "unlocked" and if it was affected by nystatin. It would also be interesting to determine the dynamin-dependence of the endocytic pathway involved. In the presence of insulin, RatGLUT4 internalized through CME as shown by its sensitivity to hypertonic sucrose (Figure IV-17b). However, it is possible that RatGLUT4 was utilizing additional endocytic pathways because we observed an increase in its total internalization although sucrose treatment in Cav-1 KD cells halted GLUT4 endocytosis to a lesser extent than in Cav-1-expressing cells (24 % and 60 % reduction, respectively) (Figures IV-17b and IV-12b). BtGLUT4, on the other hand, internalized through CME in the absence of insulin and through a clathrin- and cholesterol- independent route in the presence of insulin (Figures IV-17 and IV-18). Cav-1 KD did not affect BtGLUT4 internalization in the absence of insulin since neither its total internalization nor its internalization through CME changed (Figures IV-12a, IV-16a and IV-17a). It is intriguing that we were unable to detect any dependence of cholesterol-mediated traffic at all in cells lacking Cav-1. These results suggest that either our expressed constructs follow a cholesterol (and clathrin)- independent pathway or, as discussed above, we missed the detection of a cholesterol-dependent route due to the particular concentration and type of cholesterol-depleting agent used in these experiments. What appears to be clear is that both RatGLUT4 and BtGLUT4 likely internalize through some undefined route since we detected an increase of RatGLUT4 and BtGLUT4 endocytosis in cells lacking Cav-1.

3. DETERMINATION OF THE PRESENCE OF RatGLUT4 AND BtGLUT4 IN GSVs.

A strong translocation to the PM in response to insulin is dependent on an effective intracellular retention of GLUT4 in GSVs. We observed that BtGLUT4 has neither an efficient intracellular retention nor a potent insulin-stimulated translocation. Thus, we expected to observe a poor sorting of BtGLUT4 into GSVs. To assess the presence of our expressed constructs in GSVs we started by labelling Syntaxin 6 and analyzed its colocalization with our expressed constructs (expressing GFP) using fluorescence microscopy (Airyscan) (Figure IV-19). However, because the various intracellular compartments were visually indistinguishable it was impossible to restrict our analysis to GSVs. Moreover, colocalization between Syntaxin 6 and our expressed constructs varied considerably depending on the selected area and cell analyzed. Therefore, to better assess their presence in GSVs, we immunoadsorbed RatGLUT4 or BtGLUT4 and blotted for GSVs proteins (Figure IV-20). Immunoadsorption consists in an immunoprecipitation in which the lysis is done in the absence of detergents that allows to pull down compartment's membranes which can be identified by blotting for protein markers of these compartments.

We observed that in the absence of insulin, the fraction of BtGLUT4 in GSVs was 40 %-50 % lower than that of RatGLUT4, as indicated by their colocalization with TUG, STX6 and especially AS160 (Figure IV-20). This observation is in accordance with previous data showing that RatGLUT4 and BtGLUT4 intracellular colocalization was not perfect (Díaz et al. 2007a, Capilla et al. 2010). TUG and STX6 are also present in the TGN; therefore, it is possible that part of the immunoadsorbed GLUT4 colocalizing with these proteins was actually present in the TGN. This could be especially true for BtGLUT4 since its colocalization with AS160, which is only present in GSVs, was much weaker than that of RatGLUT4. Additionally, BtGLUT4 lacks the LL^{490} motif which has been suggested to be involved in the sorting of newly synthetized GLUT4 from TGN to GSVs (Hou et al. 2006). The C-terminal $TELEY^{502}$ motif and, more specifically, the Y^{502} residue, have also been implicated in GLUT4 sorting into GSVs (Martinez-Arca et al. 2000, Blot and McGraw 2008). BtGLUT4 possesses a variant of the motif $TELEY^{502}$ ($TELDY^{495}$) that contains the Y^{502} (Y^{495}) and the substitution of glutamic acid (E) for aspartic acid (D) that is a very mild amino acid change since both have negatively charged side chains. Therefore, the poor retention of BtGLUT4 in GSVs might be due to the absence of the LL^{490} motif but not to the $TELDY^{495}$ variation. AS160 is specifically localized to the GSVs and its colocalization with BtGLUT4 was 55 % weaker than with RatGLUT4, strongly suggesting that the former is poorly sorted into GSVs. Nonetheless, some fraction of BtGLUT4 appears to reach these compartments because we observed some degree of colocalization with AS160 (and with TUG and STX6, as well) and also, although weak, an insulin-stimulated translocation to the PM. In accordance with our data, Capilla et al. (2010) observed that in 3T3-L1 adipocytes BtGLUT4 trafficking was not dependent on AS160 but argued that a fraction of BtGLUT4 might reach GSVs since it was able to significantly translocate to the PM in response to insulin. It would be interesting to use the non-phosphorylable mutant AS160-4P, which inhibits GSV translocation, to assess if the translocable BtGLUT4 corresponds to a GSV-localized pool.

Several previous studies also reported that impairment in GLUT4 retention in GSVs results in an increase of GLUT4 at the PM (Govers et al. 2004, Capilla et al. 2007, Blot and McGraw 2008). These observations correlate with our data on BtGLUT4 surface levels in the absence of insulin (Figure IV-2a). In addition, we observed that colocalization of Cav-1, a major component of caveolae (PM domains), with BtGLUT4 was 3-fold stronger than with RatGLUT4 (Figure IV-20).

It has been reported that the inability to access the GSVs redistributes GLUT4 to transferrin receptor (TR)-containing vesicles which undergo fast recycling with the PM (Xiong et al. 2010). In addition, it has been shown that TR increases its PM levels by 2-fold in response to insulin (Blot and McGraw 2008). Since we observed (1) that BtGLUT4 basal PM levels were higher than those of RatGLUT4, (2) that BtGLUT4 translocation in response to insulin was approximately 2-fold and (3) that it showed a reduced presence of BtGLUT4 in GSVs, we suspected that BtGLUT4 was mainly distributed to the TR recycling pathway (cycle 1 in Figure I-6). To analyze if this was the case, we compared TR colocalization with our expressed constructs (Figure IV-20) but found

a similar colocalization between TR and RatGLUT4 or BtGLUT4 which does not support our hypothesis. Instead, it is possible that BtGLUT4 is highly static at the PM which is in accordance with its slow endocytic and exocytic rates, with its high basal surface levels and weaker presence in GSVs. Finally, we analyzed the colocalization with IRAP. IRAP co-traffics with GLUT4, and it is not a specific compartment marker but a general marker of GLUT4 trafficking. In addition, it has been shown that GLUT4 sorting into GSVs depends on IRAP (Yeh et al. 2007, Jordens et al. 2010). We observed that IRAP colocalization with our expressed constructs was highly variable and, despite a tendency towards a poor colocalization with BtGLUT4 when compared to RatGLUT4 that would indicate alterations in intracellular distribution, the difference was not statistically significant (Figure IV-20). At first glance this would appear to contradict part of our data and suggest that RatGLUT4 and BtGLUT4 trafficking is similar. Nonetheless, what we observed was that BtGLUT4 seemed to be present in regular GLUT4 trafficking compartments, however its fraction within the cell differed from that of RatGLUT4. Thus, a similar colocalization with IRAP was expected.

4. CHARACTERIZATION OF THE ROLES OF GLUT4 MOTIFS IN GLUT4 TRAFFICKING.

In this work we were also interested in defining the trafficking roles of GLUT4 motifs and to do so we mutated two GLUT4 trafficking motifs in BtGLUT4: FQHL (N-terminal) and TELDY (C-terminal) (Figure IV-21). None of the mutations induced visually evident changes in GLUT4 intracellular distribution (Figure IV-22a). This was not unexpected since the various intracellular compartments are visually indistinguishable and other studies also failed to detect visual differences when using GLUT4 mutants (Blot and McGraw 2008, Govers 2014). The TELEY^{502} motif has been postulated to regulate movement of GLUT4 from ERC to GSV (Figure I-13) and in addition it has been suggested that the surrounding amino acids are also important (Xiao et al. 2008, Blot and McGraw 2008). Thus, in addition to mutating TELDY to TELEY in BtGLUT4 we also mutated two surrounding amino acids (Figure IV-21). Mutation of this motif (BtGLUT4-CT) had little impact on BtGLUT4 surface levels under basal conditions but blunted BtGLUT4 translocation by reducing its PM levels in the presence of insulin (Figure IV-22). Altogether, this suggests that, in the context of BtGLUT4, the incorporation of the TELEY motif did not ameliorate BtGLUT4 sorting into GSVs. Blot and McGraw (2008) observed that a TALAY human GLUT4 mutant displayed higher PM levels, weaker translocation and impaired sorting into GSVs when compared to wild type human GLUT4. The trafficking of the TALAY human GLUT4 mutant is similar to that of BtGLUT4; however, in our work, mutating the BtGLUT4 TELDY^{495} motif to TELEY (mammalian sequence) did not produce major changes in BtGLUT4 trafficking. Nonetheless, it is important to take into account that the glutamic acid (E)-alanine (A) (TELEY-TALAY) mutation is more deleterious than a glutamic acid (E)-aspartic acid (D) (TELEY-TELDY) change since both glutamic and aspartic acids have negatively charged

side groups. Other studies suggest that it is the tyrosine Y^{502} within the $TELEY^{502}$ motif that is required for correct sorting into GSVs (Martinez-Arca et al. 2000). In this case, both rat and trout GLUT4 are identical and as such it is expected that a TELDY to TELEY mutation does not produce a change in trafficking. Therefore, one could assume that there should be no difference in GSV content between RatGLUT4 and BtGLUT4; however, this was not true as shown by our immunoadsorption data. Thus, it is more plausible that in the context of BtGLUT4, mutation of TELDY motif alone does not improve BtGLUT4 sorting into GSVs, as previously indicated, and that other motifs might play a more relevant role in this process.

Regarding the N-terminal end, we mutated the $FQHL^{8}$ motif in BtGLUT4 to produce two sequence variants: $FQQI^{8}$, present in mammalian GLUT4 (BtGLUT4-QI) and $FQQL^{8}$, present in coho salmon (OkGLUT4) (BtGLUT4-QL) (Figure IV-21). OkGLUT4 is a very interesting variant of GLUT4 because it is practically identical to BtGLUT4 (95 % protein identity) but it has been shown to have PM levels and trafficking (GGA- and AS160-dependent) more similar to RatGLUT4 than to BtGLUT4 (Capilla et al. 2010). Both N-terminal mutations induced a decrease in basal surface levels: BtGLUT4-QI and BtGLUT4-QL basal PM levels were, respectively, 28 % and 45 % lower than those of BtGLUT4 (Figure IV-22). As a result of better basal intracellular retention, the translocation of BtGLUT4-QL/QI improved, especially BtGLUT4-QL (65 % higher insulin-stimulated translocation in comparison to BtGLUT4). The improvement in basal surface levels was not sufficient to recapitulate RatGLUT4 retention but it was in accordance with the study by Capilla et al. (2010) which showed that OkGLUT4 had basal PM levels approximately 2-fold lower than those of BtGLUT4 and 2-fold higher than those of RatGLUT4. N- and C-terminal double mutants behaved like the corresponding single N-terminal mutant (Figure IV-22) which suggested that in the context of BtGLUT4, the C-terminal end TELEY/TELDY motif is not defining BtGLUT4 trafficking.

Among all mutants, BtGLUT4-QL exhibited the most evident changes in surface levels and translocation. The substitution of a positively charge amino acid (histidine-H) by a non-charged one (glutamine-Q) might have influenced protein folding and/or interaction with accessory proteins or other structural motifs. In comparison to BtGLUT4, BtGLUT4-QL showed much better intracellular retention that resulted in a stronger BtGLUT4-QL translocation to the PM in response to insulin (Figure IV-22b). To identify the compartments where BtGLUT4-QL was being retained, we immunoadsorbed BtGLUT4 and BtGLUT4-QL and compared their colocalization with Cav-1, AS160 and STX6 (Figure IV-24). We observed no differences in AS160 colocalization with BtGLUT4 and with BtGLUT4-QL which suggested that the increase in intracellular retention of BtGLUT4-QL did not correspond to an increase in sorting into GSVs. On the other hand, the data suggested that BtGLUT4-QL had increased distribution to the TGN as shown by its colocalization with STX6. This hypothesis is further supported by Blot and McGraw (2008) which proposed that the $FQQI^{8}$ motif is involved in ERC-to-TGN trafficking. Therefore, we hypothesize that BtGLUT4-QL improved its transport from the ERC to the subdomain of TGN rich in STX6, which in turn ameliorated its basal intracellular

retention. Furthermore, the lack of other trafficking motifs hampered its entry into the GSVs and, consequently, its insulin-stimulated translocation. One possible involved motif is the LL^{490} which has been implicated in the sorting of newly synthetized IRAP from the TGN to GSVs (Hou et al. 2006); however, this was challenged by the observation that OkGLUT4, which like BtGLUT4 lacks LL^{490}, was able to translocate to the membrane in response to insulin to the same extent as RatGLUT4 (Capilla et al. 2010). Our data also suggested that the TELEY motif, which has also been implicated in the ERC to GSV transport, was not favoring sorting of BtGLUT4 into GSVs, neither introduced alone (BtGLUT4-CT) nor together with the FQQL or FQQI mutations (BtGLUT4-QLCT; BtGLUT4-QICT) (Figure IV-22). The not so studied large cytoplasmic loop in GLUT4 might have also been involved as it has been shown to be necessary to recapitulate GLUT4 trafficking (Khan et al. 2004, Capilla et al. 2007). However, it is likely that more than one motif is necessary to fully recreate "normal" (as in mammalian) GLUT4 trafficking. In fact, studies suggest that to fully recapitulate GLUT4 trafficking in a GLUT1 backbone it was necessary to introduce the N-terminal $FQQI^{8}$ motif and cytoplasmic loop of GLUT4 simultaneously as the independent substitution of these domains had no effect (Khan et al. 2004, Capilla et al. 2007). This implies that motifs do not function independently and that the presence of various motifs and the context in which they exist are fundamental for GLUT4 trafficking. Regarding Cav-1, we were surprised to observe that its colocalization with BtGLUT4-QL was only slightly weaker (and not statistically relevant) than with BtGLUT4, since both constructs have very different PM levels in the absence of insulin (Figure IV-24). Currently we cannot explain this result.

In this work, we also studied the trafficking behavior of RatGLUT4/BtGLUT4 chimeras. We used two chimeras consisting of: 1) RatGLUT4 backbone with BtGLUT4 N-terminus (N-GLUT4) and 2) RatGLUT4 backbone with BtGLUT4 large cytoplasmic loop (L-GLUT4) (Figure IV-25). When electroporated into 3T3-L1 adipocytes, we observed that N-GLUT4 presented a typical endoplasmic reticulum distribution and, therefore, we considered it to be unfit for trafficking studies (Figure IV-26). In this chimera the entire N-terminus of BtGLUT4 (17 amino acids) substituted the entire RatGLUT4 N-terminus (24 amino acids). It is possible that the substitution of the entire N-terminus by a smaller sequence led to miss-folding issues.

L-GLUT4, on the other hand, displayed similar intracellular distribution to RatGLUT4 when observed under the microscope (Figure IV-27a). We quantified L-GLUT4 surface levels and observed that in the absence of insulin, its PM levels were 77 % higher than those of RatGLUT4 and that its surface levels in the presence of insulin were roughly unchanged (Figure IV-27b). As a result, L-GLUT4 translocation was approximately 40 % lower than that of RatGLUT4 (Figure IV-27c). Our observations are in accordance with previous studies that also observed that substitution of the large cytoplasmic loop of GLUT4 by the corresponding GLUT1 sequence reduced basal intracellular retention while not affecting cell surface levels in the insulin-stimulated state (Khan et al. 2004, Capilla et al. 2007). Our data suggested that the large cytoplasmic loop played a role in basal endocytosis or exocytosis, but because the exocytosis

in the absence of insulin is very slow, the loop substitution effect was probably stronger on endocytosis. We determined the L-GLUT4 endocytic rate (apparent) in the absence of insulin and observed that L-GLUT4 internalization was 23 % slower than that of RatGLUT4 but 36 % faster than that of BtGLUT4 (Figure IV-28c). Interestingly, the endocytic rates correlated with the basal PM levels: RatGLUT4 had the lowest PM levels and the fastest endocytosis, BtGLUT4 had the highest surface levels and the slowest endocytosis and L-GLUT4 possessed intermediate PM levels and endocytic rate. In summary, we suggest that substitution of the large cytoplasmic loop induced an increase of RatGLUT4 basal PM levels, at least in part, by slowing its endocytosis. The dileucine (LL^{490}) and $FQQI^{8}$ motifs have been implicated in endocytosis and our data further suggested that the large cytoplasmic loop also plays a role in this mechanism. In contrast to BtGLUT4, the presence of the $FQQI^{8}$ and LL^{490} motifs in L-GLUT4 might explain why its endocytic rate was not as slow as that of BtGLUT4. Our proposal that the substitution of more than one domain is necessary to recapitulate a trafficking behavior is in accordance with previous studies on GLUT1/GLUT4 chimeras (Khan et al. 2004, Capilla et al. 2007). Despite the effects on endocytosis, cytoplasmic loop substitution might have also affected exocytosis, especially because L-GLUT4 surface levels were 77 % higher than those of RatGLUT4 but its endocytic rate was only 23 % slower. Moreover, the large cytoplasmic loop has been suggested to be the target of TUG during basal intracellular retention of GSVs (Yu et al. 2007). We have not investigated L-GLUT4 exocytosis or TUG association, but it could be of value in order to better understand the trafficking role of the large cytoplasmic loop.

To further investigate L-GLUT4 basal endocytosis we analyzed its routes of internalization. We observed that loop substitution had little effect on L-GLUT4 internalization through CME (Figure IV-30), which correlates with the knowledge that $FQQI^{8}$ (present in RatGLUT4 and L-GLUT4) is required for CME (Al-Hasani et al. 2002, Owen et al. 2004, Blot and McGraw 2006), but it greatly affected internalization through the cholesterol-dependent pathway (Figure IV-31). Whilst statistical analysis resulted in a significant internalization of L-GLUT4 through a cholesterol-dependent pathway, it represented a reduction of 73 % when compared to RatGLUT4 internalization through this pathway. Altogether, our data on L-GLUT4 endocytosis suggest that substitution of the large cytoplasmic loop reduced RatGLUT4 internalization by diminishing its internalization through the cholesterol-dependent pathway while having no effect on CME. Cytoplasmic loop substitution in RatGLUT4 also prevented the increase in basal endocytosis after Cav-1 KD but not to the extent of BtGLUT4 (Figure IV-33). Moreover, in the absence of Cav-1 and insulin, L-GLUT4 internalized through CME, similarly to BtGLUT4 (Figure IV-34). Thus, insertion of BtGLUT4 cytoplasmic loop in RatGLUT4 recapitulated BtGLUT4 CME in the absence of Cav-1. We also analyzed L-GLUT4 cholesterol-dependent internalization in cells lacking Cav-1 and observed that, unlike rat and trout GLUT4, the L-GLUT4 chimera internalized through this pathway while barely doing so in the presence of Cav-1, as indicated above (Figure IV-35). Assuming that RatGLUT4 cholesterol-dependent internalization occurred through caveolae (because it was greatly affected by Cav-1 KD) and based on the fact that loop

substitution reduced cholesterol-dependent endocytosis (in cells expressing Cav-1), we suggest that the loop of BtGLUT4 reduced RatGLUT4 internalization through caveolae. Moreover, since L-GLUT4 but not RatGLUT4 or BtGLUT4 internalization in the absence of Cav-1 was cholesterol-dependent, we hypothesize that the BtGLUT4 loop in the context of RatGLUT4 facilitated entry through a non-caveolar cholesterol-dependent pathway, possibly CLIC/GEEC. Nonetheless, to confirm this theory we would need to analyze L-GLUT4 endocytosis through CLIC/GEEC using, for example, CD44 as cargo control. In summary, it seems clear that the large cytoplasmic loop intervenes in basal GLUT4 endocytosis.

There is still scare information regarding fish GLUT4 trafficking and, as such, there is still a lot to learn. In this study we have contributed to increase the knowledge on BtGLUT4 trafficking in 3T3-L1 adipocytes and on the roles of the N-terminal FQQI[8] motif and the large cytoplasmic loop of GLUT4. In Figures V-1 and V-2 we summarize the most important observations of this work. We have shown that BtGLUT4 retention inside GSVs was impaired and that it was greatly targeted to the PM in the absence of insulin. Nonetheless, BtGLUT4 was able to translocate to the PM in response to insulin although to a lesser extent than RatGLUT4. Notwithstanding, BtGLUT4 translocation was more resistant to a decrease in temperature. BtGLUT4 was also more static than RatGLUT4 since its exocytosis and endocytosis were slower. In accordance, its return-to-basal was also slower. We analyzed BtGLUT4 internalization pathways and showed that BtGLUT4 entered the cell mainly through clathrin-mediated endocytosis. We also observed that Cav-1 KD accelerated overall BtGLUT4 internalization but blocked its internalization through CME, in the presence of insulin. We have mutated the N- and C-terminal ends of BtGLUT4 and concluded that while mutations on TELDY[495] C-terminal motif had little effect on BtGLUT4 trafficking, mutations on FQHL[8] improved its basal intracellular retention by increasing its targeting to the STX6-rich subdomain of the TGN. Moreover, we observed that substitution of the large cytoplasmic loop of RatGLUT4 by the corresponding BtGLUT4 sequence increased its basal surface levels. This increase was, at least in part, due to a reduction in the endocytic rate, suggesting a role for this domain in GLUT4 endocytosis. Our data suggested that loop substitution reduced RatGLUT4 basal internalization by inhibiting internalization through caveolae. Moreover, it facilitated internalization through CME and cholesterol-dependent endocytosis (not caveolar pathway) in the absence of Cav-1.

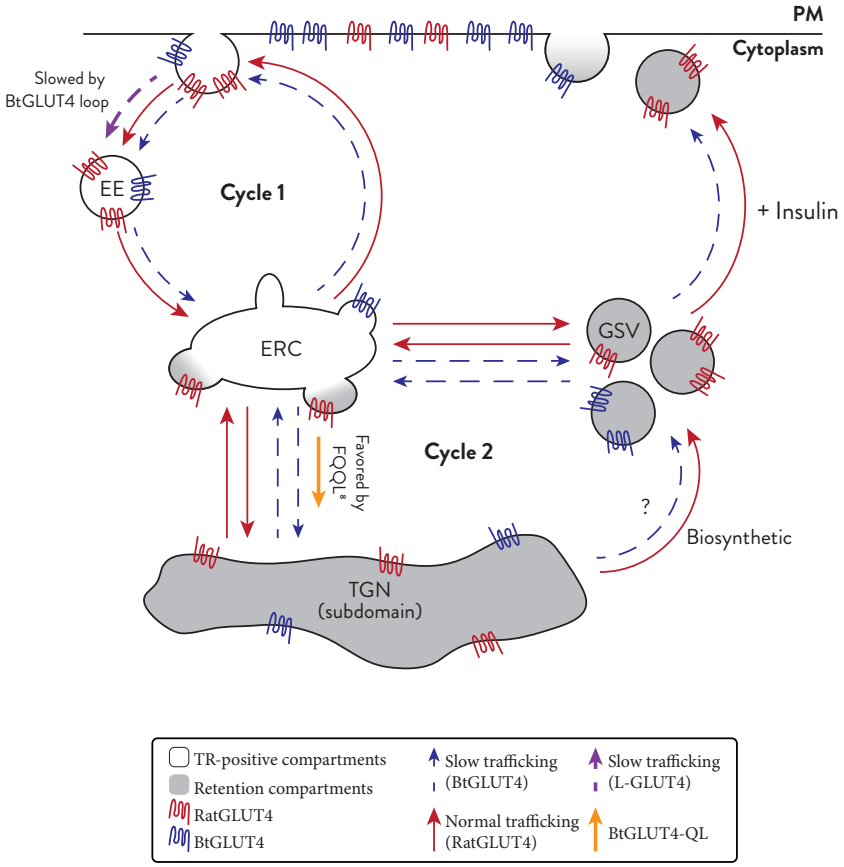

Figure V-1. Schematic representation of RatGLUT4 and BtGLUT4 trafficking in 3T3-L1 adipocytes. Roles of the FQQL[8] motif and large cytoplasmic loop roles in GLUT4 trafficking.

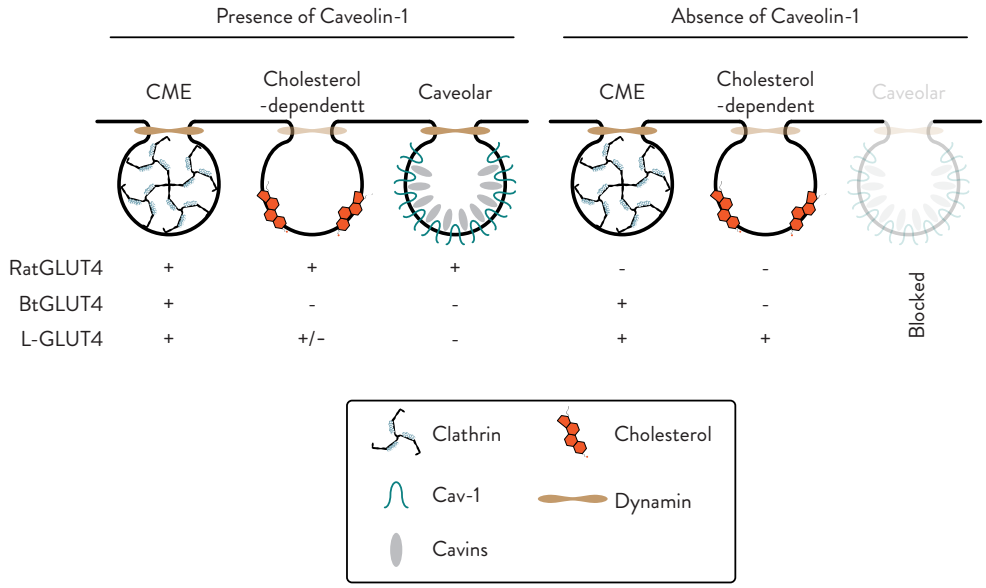

Figure V-2. Schematic representation of endocytic pathways utilized by RatGLUT4, BtGLUT4 and L-GLUT4 in unstimulated 3T3-L1 adipocytes in the presence and absence of Caveolin-1. Dimmed dynamin represents dynamin-independent pathway. Dimmed caveolar vesicle indicates ablation of caveolar endocytosis. + and – represent internalization through the indicated pathway. +/- represents almost no internalization through the indicated pathway.

VI. CONCLUSIONS

1. The cellular trafficking of BtGLUT4 is slower than that of RatGLUT4, as shown by the slower exocytosis, endocytosis and return-to-basal of BtGLUT4.

2. The translocation of BtGLUT4 to the plasma membrane in response to insulin is weaker in comparison to that of RatGLUT4. This is likely due to an impaired retention of BtGLUT4 inside the GSVs and increased release of BtGLUT4 to the plasma membrane in the absence of insulin.

3. BtGLUT4 internalizes solely through the clathrin-mediated pathway while RatGLUT4 internalizes through the clathrin-mediated and cholesterol-dependent pathways.

4. Caveolin-1 knockdown increases RatGLUT4 internalization but inhibits its internalization though clathrin-mediated endocytosis in the absence of insulin and through the cholesterol-dependent pathway in the presence of insulin. On the other hand, caveolin-1 knockdown increases BtGLUT4 internalization solely in the presence of insulin but blocks its internalization through clathrin-mediated endocytosis in the same condition. Therefore, we suggest that BtGLUT4 internalization is less dependent on caveolin-1.

5. The presence of the TELEY motif in the context of BtGLUT4 does not affect BtGLUT4 trafficking. The presence of the FQQI and FQQL motifs in the N-terminal end of BtGLUT4 improves its basal intracellular retention and, consequently, improves BtGLUT4 translocation to the plasma membrane in response to insulin. Moreover, the FQQL motif improves BtGLUT4 intracellular retention by targeting it to a Syntaxin 6-rich compartment, possibly the TGN. Therefore, we suggest that the FQQL motif promotes BtGLUT4 sorting into the Syntaxin 6-rich subdomain of the TGN.

6. Substitution of the large cytoplasmic loop of RatGLUT4 by that of BtGLUT4 increases the plasma membrane levels of RatGLUT4 in the absence of insulin, at least in part, by slowing its basal endocytosis. Moreover, the substitution of the large cytoplasmic loop reduces RatGLUT4 internalization through the cholesterol-dependent pathway in the absence of insulin and also prevents the increase of RatGLUT4 basal endocytosis in the absence of caveolin-1 and insulin. Therefore, we suggest that the large cytoplasmic loop of RatGLUT4 is necessary for the caveolae- (and cholesterol) dependent pathway.

7. Substitution of the large cytoplasmic loop of RatGLUT4 by that of BtGLUT4 improves RatGLUT4 internalization through clathrin-mediated endocytosis and cholesterol-dependent endocytosis (not caveolar pathway) in the absence of caveolin-1. Moreover, since loop substitution increases RatGLUT4 internalization through cholesterol-dependent endocytosis in the absence of caveolin-1 but not in its presence, suggests that caveolin-1 expression blocks alternative cholesterol-dependent endocytic routes.

8. BtGLUT4 can be used as a tool to study GLUT4 trafficking, especially to further investigate the roles of the FQQI and large cytoplasmic loop in this process, since alterations in these

motifs induced changes in trafficking.

9. BtGLUT4 trafficking is less regulated than mammalian GLUT4 due to differences in GLUT4 protein motifs suggesting an improvement in the mechanims regulating GLUT4 traffic during evolution from fish to mammals that paralleled their increase reliance on dietary carbohydrates.

VII. REFERENCES

Al-Hasani, H., R. K. Kunamneni, K. Dawson, C. S. Hinck, D. Müller-Wieland, and S. W. Cushman. 2002. Roles of the N- and C-termini of GLUT4 in endocytosis. Journal of Cell Science 115:131–40.

Albiston, A. L., S. G. McDowall, D. Matsacos, P. Sim, E. Clune, T. Mustafa, J. Lee, F. A. O. Mendelsohn, R. J. Simpson, L. M. Connolly, and S. Y. Chai. 2001. Evidence That the Angiotensin IV (AT4) Receptor Is the Enzyme Insulin-regulated Aminopeptidase. Journal of Biological Chemistry 276:48623–48626.

Alessi, D. R., and C. P. Downes. 1998. The role of PI 3-kinase in insulin action. Biochimica et Biophysica Acta - Lipids and Lipid Metabolism 1436:151-164.

Amir Shaghaghi, M., B. Murphy, and P. Eck. 2016. The SLC2A14 gene: genomic locus, tissue expression, splice variants, and subcellular localization of the protein. Biochemistry and Cell Biology 94:331–5.

Antonescu, C. N., M. Díaz, G. Femia, J. V. Planas, and A. Klip. 2008. Clathrin-Dependent and independent endocytosis of glucose transporter 4 (GLUT4) in myoblasts: Regulation by mitochondrial uncoupling. Traffic 9:1173–1190.

Antonescu, C. N., M. Foti, N. Sauvonnet, and A. Klip. 2009. Ready, set, internalize: mechanisms and regulation of GLUT4 endocytosis. Bioscience Reports 29:1.

Augustin, R. 2010. The protein family of glucose transport facilitators: It's not only about glucose after all. International Union of Biochemistry and Molecular Biology Life 62:315–33.

Augustin, R., M. O. Carayannopoulos, L. O. Dowd, J. E. Phay, J. F. Moley, and K. H. Moley. 2004. Identification and Characterization of Human Glucose Transporter-like Protein-9 (GLUT9). Journal of Biological Chemistry 279:16229–16236.

Bae, S. S., H. Cho, J. Mu, and M. J. Birnbaum. 2003. Isoform-specific regulation of insulin-dependent glucose uptake by Akt/protein kinase B. Journal of Biological Chemistry 278:49530–49536.

Bai, L., Y. Wang, J. Fan, Y. Chen, W. Ji, A. Qu, P. Xu, D. E. James, and T. Xu. 2007. Dissecting Multiple Steps of GLUT4 Trafficking and Identifying the Sites of Insulin Action. Cell Metabolism 5:47–57.

Bandyopadhyay, G., M. P. Sajan, Y. Kanoh, M. L. Standaert, M. J. Quon, R. Lea-Currie, A. Sen, and R. V. Farese. 2002. PKC-ζ Mediates Insulin Effects on Glucose Transport in Cultured Preadipocyte-Derived Human Adipocytes. Journal of Clinical Endocrinology & Metabolism 87:716–723.

Barron, C. C., P. J. Bilan, T. Tsakiridis, and E. Tsiani. 2016. Facilitative glucose transporters: Implications for cancer detection, prognosis and treatment. Metabolism 65:124–139.

Basquin, C., V. Malarde, P. Mellor, D. H. Anderson, V. Meas-Yedid, J.-C. Olivo-Marin, A. Dautry-Varsat, and N. Sauvonnet. 2013. The signalling factor PI3K is a specific regulator of the clathrin-independent dynamin-dependent endocytosis of IL-2 receptors. Journal of Cell Science 126:1099–1108.

Basquin, C., and N. Sauvonnet. 2013. Phosphoinositide 3-kinase at the crossroad between

endocytosis and signaling of cytokine receptors. Communicative & Integrative Biology 6:e24243.

Bastiani, M., L. Liu, M. M. Hill, M. P. Jedrychowski, S. J. Nixon, H. P. Lo, D. Abankwa, R. Luetterforst, M. Fernandez-Rojo, M. R. Breen, S. P. Gygi, J. Vinten, P. J. Walser, K. N. North, J. F. Hancock, P. Pilch, and R. G. Parton. 2009. MURC/Cavin-4 and cavin family members form tissue-specific caveolar complexes. Journal of Cell Biology 185:1259–1273.

Baumann, C. A., V. Ribon, M. Kanzaki, D. C. Thurmond, S. Mora, S. Shigematsu, P. E. Bickel, J. E. Pessin, and A. R. Saltiel. 2000. CAP defines a second signalling pathway required for insulin-stimulated glucose transport. Nature 407:202–207.

Belman, J. P., E. N. Habtemichael, and J. S. Bogan. 2014. A proteolytic pathway that controls glucose uptake in fat and muscle. Reviews in Endocrine and Metabolic Disorders 15:55–66.

Bibert, S., S. K. Hess, D. Firsov, B. Thorens, K. Geering, J. D. Horisberger, and O. Bonny. 2009. Mouse GLUT9: evidences for a urate uniporter. American Journal of Physiology-Renal Physiology 297:F612–F619.

Bickel, P. E. 2002. Lipid rafts and insulin signaling. American Journal of Physiology-Endocrinology and Metabolism 282:E1–E10.

Birnbaum, M. J. 1989. Identification of a novel gene encoding an insulin-responsive glucose transporter protein. Cell 57:305–315.

Blot, V., and T. E. McGraw. 2006. GLUT4 is internalized by a cholesterol-dependent nystatin-sensitive mechanism inhibited by insulin. The EMBO journal 25:5648–58.

Blot, V., and T. E. McGraw. 2008. Molecular Mechanisms Controlling GLUT4 Intracellular Retention. Molecular Biology of the Cell 19:3477–3487.

Bogan, J. S., N. Hendon, A. E. McKee, T. S. Tsao, and H. F. Lodish. 2003. Functional cloning of TUG as a regulator of GLUT4 glucose transporter trafficking. Nature 425:727–733.

Bogan, J. S., and K. V. Kandror. 2010. Biogenesis and regulation of insulin-responsive vesicles containing GLUT4. Current Opinion in Cell Biology 22:506-512.

Bogan, J. S., B. R. Rubin, C. Yu, M. G. Löffler, C. M. Orme, J. P. Belman, L. J. McNally, M. Hao, and J. A. Cresswell. 2012. Endoproteolytic Cleavage of TUG Protein Regulates GLUT4 Glucose Transporter Translocation. Journal of Biological Chemistry 287:23932–23947.

Bonifacino, J. S., and E. C. Dell'Angelica. 1999. Molecular bases for the recognition of tyrosine-based sorting signals. Journal of Cell Biology 5:923-926.

Bonifacino, J. S., and L. M. Traub. 2003. Signals for Sorting of Transmembrane Proteins to Endosomes and Lysosomes. Annual Review of Biochemistry 72:395–447.

Breen, M. R., M. Camps, F. Carvalho-Simoes, A. Zorzano, and P. Pilch. 2012. Cholesterol depletion in adipocytes causes caveolae collapse concomitant with proteosomal degradation of cavin-2 in a switch-like fashion. PLoS ONE 7:2–9.

Briand, N., I. Dugail, and S. Le Lay. 2011. Cavin proteins: New players in the caveolae field. Biochimie 93:71–77.

Bryant, N. J., and G. W. Gould. 2011. SNARE Proteins Underpin Insulin-Regulated GLUT4

Traffic. Traffic 12:657–664.

Bryant, N. J., R. Govers, and D. E. James. 2002. Regulated transport of the glucose transporter GLUT4. Nature Reviews Molecular Cell Biology 3:267–277.

Burant, C. F., and G. I. Bell. 1992. Mammalian Facilitative Glucose Transporters: Evidence for Similar Substrate Recognition Sites in Functionally Monomeric Proteins. Biochemistry 31:10414–10420.

Canuel, M., S. Lefrancois, J. Zeng, and C. R. Morales. 2008. AP-1 and retromer play opposite roles in the trafficking of sortilin between the Golgi apparatus and the lysosomes. Biochemical and Biophysical Research Communications 366:724–730.

Capilla, E., M. Díaz, A. Albalat, I. Navarro, J. E. Pessin, K. Keller, and J. V. Planas. 2004. Functional characterization of an insulin-responsive glucose transporter (GLUT4) from fish adipose tissue. American Journal of Physiology-Endocrinology and Metabolism 287:E348–E357.

Capilla, E., M. Díaz, J. Gutiérrez, and J. V. Planas. 2002. Physiological regulation of the expression of a GLUT4 homolog in fish skeletal muscle. American Journal of Physiology-Endocrinology and Metabolism 283:E44-9.

Capilla, E., M. Díaz, J. C. Hou, J. V. Planas, and J. E. Pessin. 2010. High basal cell surface levels of fish GLUT4 are related to reduced sensitivity of insulin-induced translocation toward GGA and AS160 inhibition in adipocytes. American Journal of Physiology-Endocrinology and Metabolism 298:E329–E336.

Capilla, E., N. Suzuki, J. E. Pessin, and J. C. Hou. 2007. The Glucose Transporter 4 FQQI Motif Is Necessary for Akt Substrate of 160-Kilodalton-Dependent Plasma Membrane Translocation But Not Golgi-Localized γ-Ear-Containing Arf-Binding Protein-Dependent Entry into the Insulin-Responsive Storage Compartment. Molecular Endocrinology 21:3087–3099.

Carruthers, A., J. DeZutter, A. Ganguly, and S. U. Devaskar. 2009. Will the original glucose transporter isoform please stand up! American Journal of Physiology-Endocrinology and Metabolism 297:E836–E848.

Carvalho, E., S. E. Schellhorn, J. M. Zabolotny, S. Martin, E. Tozzo, O. D. Peroni, K. L. Houseknecht, A. Mundt, D. E. James, and B. B. Kahn. 2004. GLUT4 overexpression or deficiency in adipocytes of transgenic mice alters the composition of GLUT4 vesicles and the subcellular localization of GLUT4 and insulin-responsive aminopeptidase. Journal of Biological Chemistry 279:21598–605.

Castillo, J., D. Crespo, E. Capilla, M. Díaz, F. Chauvigné, J. Cerdà, and J. V. Planas. 2009. Evolutionary structural and functional conservation of an ortholog of the GLUT2 glucose transporter gene (SLC2A2) in zebrafish. American Journal of Physiology-Regulatory, Integrative and Comparative Physiology 297:R1570–R1581.

Chadda, R., M. T. Howes, S. J. Plowman, J. F. Hancock, R. G. Parton, and S. Mayor. 2007. Cholesterol-sensitive Cdc42 activation regulates actin polymerization for endocytosis via the GEEC pathway. Traffic 8:702–717.

Charron, M. J., F. C. Brosius 3rd, S. L. Alper, and H. F. Lodish. 1989. A glucose transport

protein expressed predominately in insulin-responsive tissues. Proceedings of the National Academy of Sciences USA USA 86:2535–2539.

Chaudhary, N., G. A. Gomez, M. T. Howes, H. P. Lo, K. A. McMahon, J. A. Rae, N. L. Schieber, M. M. Hill, K. Gaus, A. S. Yap, and R. G. Parton. 2014. Endocytic Crosstalk: Cavins, Caveolins, and Caveolae Regulate Clathrin-Independent Endocytosis. PLoS Biology 12(4):e1001832.

Cheeseman, C. I. 2008. GLUT7: a new intestinal facilitated hexose transporter. American Journal of Physiology-Endocrinology and Metabolism 295:E238–E241.

Cheng, Z. J., R. D. Singh, E. L. Holicky, C. L. Wheatley, D. L. Marks, and R. E. Pagano. 2010. Co-regulation of caveolar and Cdc42-dependent fluid phase endocytosis by phosphocaveolin-1. Journal of Biological Chemistry 285:15119–15125.

Chiang, S.-H., C. A. Baumann, M. Kanzaki, D. C. Thurmond, R. T. Watson, C. L. Neudauer, I. G. Macara, J. E. Pessin, and A. R. Saltiel. 2001. Insulin-stimulated GLUT4 translocation requires the CAP-dependent activation of TC10. Nature 410:944–948.

Choi, K., and Y.-B. Kim. 2010. Molecular Mechanism of Insulin Resistance in Obesity and Type 2 Diabetes. The Korean Journal of Internal Medicine 25:119.

Clarke, J. F., P. W. Young, K. Yonezawa, M. Kasuga, and G. D. Holman. 1994. Inhibition of the translocation of GLUT1 and GLUT4 in 3T3-L1 cells by the phosphatidylinositol 3-kinase inhibitor, wortmannin. The Biochemical Journal 300(3):631–5.

Colville, C. A., M. J. Seatter, T. J. Jess, G. W. Gould, and H. M. Thomas. 1993. Kinetic analysis of the liver-type (GLUT2) and brain-type (GLUT3) glucose transporters in Xenopus oocytes: substrate specificities and effects of transport inhibitors. Biochemical Journal 290(3):701–6.

Corvera, S., A. Chawla, R. Chakrabarti, M. Joly, J. Buxton, and M. P. Czech. 1994. A double leucine within the GLUT4 glucose transporter COOH-terminal domain functions as an endocytosis signal. Journal of Cell Biology 126:979–989.

Corvera, S., and M. P. Czech. 1998. Direct targets of phosphoinositide 3-kinase products in membrane traffic and signal transduction. Trends in Cell Biology 8(11): 442-446.

Coucke, P. J., A. Willaert, M. W. Wessels, B. Callewaert, N. Zoppi, J. De Backer, J. E. Fox, G. M. S. Mancini, M. Kambouris, R. Gardella, F. Facchetti, P. J. Willems, R. Forsyth, H. C. Dietz, S. Barlati, M. Colombi, B. Loeys, and A. De Paepe. 2006. Mutations in the facilitative glucose transporter GLUT10 alter angiogenesis and cause arterial tortuosity syndrome. Nature Genetics 38:452–457.

Cura, A. J., A. Carruthers, A. J. Cura, and A. Carruthers. 2012. Role of Monosaccharide Transport Proteins in Carbohydrate Assimilation, Distribution, Metabolism, and Homeostasis. Comprehensive Physiology. John Wiley & Sons, Inc., Hoboken, NJ, USA. ISBN: 978-047-065-0714. pp. 863-914.

Cushman, S. W., and L. J. Wardzala. 1980. Potential Mechanism of Insulin Action on Glucose Transport in the Isolated Rat Adipose Cell. The Journal of Biological Chemistry 255:4758–4762.

Dawson, P. A., J. C. Mychaleckyj, S. C. Fossey, S. J. Mihic, A. L. Craddock, and D. W. Bowden.

2001. Sequence and functional analysis of GLUT10: A glucose transporter in the type 2 diabetes-linked region of chromosome 20q12-13.1. Molecular Genetics and Metabolism 74:186:199.

Díaz, M., C. N. Antonescu, E. Capilla, A. Klip, and J. V. Planas. 2007a. Fish Glucose Transporter (GLUT)-4 Differs from Rat GLUT4 in Its Traffic Characteristics but Can Translocate to the Cell Surface in Response to Insulin in Skeletal Muscle Cells. Endocrinology 148:5248–5257.

Díaz, M., E. Capilla, and J. V. Planas. 2007b. Physiological regulation of glucose transporter (GLUT4) protein content in brown trout (Salmo trutta) skeletal muscle. The Journal of Experimental Biology 210:2346–51.

Doege, H., A. Bocianski, H.-G. Joost, and A. Schürmann. 2000. Activity and genomic organization of human glucose transporter 9 (GLUT9), a novel member of the family of sugar-transport facilitators predominantly expressed in brain and leucocytes. The Biochemical Journal 350(3):771–6.

Doherty, G. J., and H. T. McMahon. 2009. Mechanisms of Endocytosis. Annual Review of Biochemistry 78:857–902.

Dohm, G. L. 2002. Invited Review: Regulation of skeletal muscle GLUT-4 expression by exercise. Journal of Applied Physiology 93:782–787.

Douard, V., and R. P. Ferraris. 2008. Regulation of the fructose transporter GLUT5 in health and disease. American Journal of Physiology-Endocrinology and Metabolism 295:E227–E237.

Dugani, C. B., and A. Klip. 2005. Glucose transporter 4: Cycling, compartments and controversies. EMBO Reports 12:1137-1142.

Eguez, L., A. Lee, J. A. Chavez, C. P. Miinea, S. Kane, G. E. Lienhard, and T. E. McGraw. 2005. Full intracellular retention of GLUT4 requires AS160 Rab GTPase activating protein. Cell Metabolism 2:263–72.

Eyster, C. A., J. D. Higginson, R. Huebner, N. Porat-Shliom, R. Weigert, W. Wu, R.-F. Shen, and J. G. Donaldson. 2009. Discovery of New Cargo Proteins that Enter Cells through Clathrin-Independent Endocytosis. Traffic 10:590–599.

Fan, J., J. L. Carpentier, E. van Obberghen, C. Grunfeld, P. Gorden, and L. Orci. 1983. Morphological changes of the 3T3-L1 fibroblast plasma membrane upon differentiation to the adipocyte form. Journal of Cell Science 61:219–30.

Farese, R. V., M. P. Sajan, and M. L. Standaert. 2005. Insulin-sensitive protein kinases (atypical protein kinase C and protein kinase B/Akt): actions and defects in obesity and type II diabetes. Experimental Biology and Medicine 230:593–605.

Farese, R. V., M. P. Sajan, H. Yang, P. Li, S. Mastorides, W. R. Gower, S. Nimal, C. S. Choi, S. Kim, G. I. Shulman, C. R. Kahn, U. Braun, and M. Leitges. 2007. Muscle-specific knockout of PKC-lambda impairs glucose transport and induces metabolic and diabetic syndromes. The Journal of Clinical Investigation 117:2289–301.

Felip, O., A. Ibarz, J. Fernández-Borràs, M. Beltrán, M. Martín-Pérez, J. V. Planas, and J. Blasco. 2012. Tracing metabolic routes of dietary carbohydrate and protein in rainbow trout

(Oncorhynchus mykiss) using stable isotopes ([13C]starch and [15N]protein): effects of gelatinisation of starches and sustained swimming. British Journal of Nutrition 107:834–844.

Foley, K., S. Boguslavsky, and A. Klip. 2011. Endocytosis, Recycling, and Regulated Exocytosis of Glucose Transporter 4. Biochemistry 50:3048–3061.

Fukumoto, H., S. Seino, H. Imura, Y. Seino, R. L. Eddy, Y. Fukushima, M. G. Byers, T. B. Shows, and G. I. Bell. 1988. Sequence, tissue distribution, and chromosomal localization of mRNA encoding a human glucose transporter-like protein. Proceedings of the National Academy of Sciences USA USA 85:5434–5438.

Gammeltoft, S., and E. Van Obberghen. 1986. Protein kinase activity of the insulin receptor. The Biochemical Journal 235:1–11.

Ganapathy, V., M. Thangaraju, and P. D. Prasad. 2009. Nutrient transporters in cancer: Relevance to Warburg hypothesis and beyond. Pharmacology and Therapeutics 121:29-40.

Gastaldelli, A., E. Toschi, M. Pettiti, S. Frascerra, A. Quiñones-Galvan, A. M. Sironi, A. Natali, and E. Ferrannini. 2001. Effect of physiological hyperinsulinemia on gluconeogenesis in nondiabetic subjects and in type 2 diabetic patients. Diabetes 50:1807–12.

Gauthier, N. C., P. Monzo, V. Kaddai, A. Doye, V. Ricci, and P. Boquet. 2005. Helicobacter pylori VacA Cytotoxin: A Probe for a Clathrin-independent and Cdc42-dependent Pinocytic Pathway Routed to Late Endosomes. Molecular Biology of the Cell 16:4852–4866.

Gesbert, F., N. Sauvonnet, and A. Dautry-Varsat. 2004. Clathrin-lndependent endocytosis and signalling of interleukin 2 receptors IL-2R endocytosis and signalling. Current Topics in Microbiology and Immunology 286:119–48.

Giorgino, F., O. De Robertis, L. Laviola, C. Montrone, S. Perrini, K. C. McCowen, and R. J. Smith. 2000. The Sentrin-Conjugating Enzyme mUbc9 Interacts with GLUT4 and GLUT1 Glucose Transporters and Regulates Transporter Levels in Skeletal Muscle Cells. Proceedings of the National Academy of Sciences USA of the USA 97:1125–1130.

González-Muñoz, E., C. López-Iglesias, M. Calvo, M. Palacín, A. Zorzano, and M. Camps. 2009. Caveolin-1 loss of function accelerates glucose transporter 4 and insulin receptor degradation in 3T3-L1 adipocytes. Endocrinology 150:3493–3502.

Gonzalez, E., and T. E. McGraw. 2006. Insulin signaling diverges into Akt-dependent and -independent signals to regulate the recruitment/docking and the fusion of GLUT4 vesicles to the plasma membrane. Molecular biology of the Cell 17:4484–93.

Gonzalez, E., and T. E. McGraw. 2009. Insulin-modulated Akt subcellular localization determines Akt isoform-specific signaling. Proceedings of the National Academy of Sciences USA of the USA 106:7004–9.

Le Good, J. A., W. H. Ziegler, D. B. Parekh, D. R. Alessi, P. Cohen, and P. J. Parker. 1998. Protein kinase C isotypes controlled by phosphoinositide 3-kinase through the protein kinase PDK1. Science 281:2042–5.

Govers, R. 2014. Cellular regulation of glucose uptake by glucose transporter GLUT4. Advances

in Clinical Chemistry 66:173–240.

Govers, R., A. C. F. Coster, and D. E. James. 2004. Insulin Increases Cell Surface GLUT4 Levels by Dose Dependently Discharging GLUT4 into a Cell Surface Recycling Pathway. Molecular and Cellular Biology 24:6456–6466.

Grant, B. D., and J. G. Donaldson. 2009. Pathways and mechanisms of endocytic recycling. Nature Reviews Molecular Cell Biology 10:597–608.

Grassart, A., A. Dujeancourt, P. B. Lazarow, A. Dautry-Varsat, and N. Sauvonnet. 2008. Clathrin-independent endocytosis used by the IL-2 receptor is regulated by Rac1, Pak1 and Pak2. EMBO Reports 9:356–62.

Grassart, A., V. Meas-Yedid, A. Dufour, J.-C. Olivo-Marin, A. Dautry-Varsat, and N. Sauvonnet. 2010. Pak1 Phosphorylation Enhances Cortactin-N-WASP Interaction in Clathrin-Caveolin-Independent Endocytosis. Traffic 11:1079–1091.

Hall, J. R., T. J. MacCormack, C. A. Barry, and W. R. Driedzic. 2004. Sequence and expression of a constitutive, facilitated glucose transporter (GLUT1) in Atlantic cod Gadus morhua. The Journal of Experimental Biology 207:4697–706.

Hall, J. R., R. C. Richards, T. J. MacCormack, K. V. Ewart, and W. R. Driedzic. 2005. Cloning of GLUT3 cDNA from Atlantic cod (Gadus morhua) and expression of GLUT1 and GLUT3 in response to hypoxia. Biochimica et Biophysica Acta - Gene Structure and Expression 1730:245–252.

Hall, J. R., C. E. Short, and W. R. Driedzic. 2006. Sequence of Atlantic cod (Gadus morhua) GLUT4, GLUT2 and GPDH: Developmental stage expression, tissue expression and relationship to starvation-induced changes in blood glucose. The Journal of Experimental Biology 209:4490–502.

Hansen, C. G., and B. J. Nichols. 2010. Exploring the caves: cavins, caveolins and caveolae. Trends in Cell Biology 20:177–186.

Hayer, A., M. Stoeber, D. Ritz, S. Engel, H. H. Meyer, and A. Helenius. 2010. Caveolin-1 is ubiquitinated and targeted to intralumenal vesicles in endolysosomes for degradation. Journal of Cell Biology 191:615–29.

Henley, J. R., E. W. Krueger, B. J. Oswald, and M. A. McNiven. 1998. Dynamin-mediated internalization of caveolae. Journal of Cell Biology 141:85–99.

Henne, W. M., E. Boucrot, M. Meinecke, E. Evergren, Y. Vallis, R. Mittal, and H. T. McMahon. 2010. FCHo proteins are nucleators of Clathrin-Mediated endocytosis. Science 328:1281–1284.

Heuser, J. E., and R. G. Anderson. 1989. Hypertonic media inhibit receptor-mediated endocytosis by blocking clathrin-coated pit formation. Journal of Cell Biology 108:389–400.

Hinrichsen, L., J. Harborth, L. Andrees, K. Weber, and E. Ungewickell. 2003. Effect of Clathrin Heavy Chain- and α-Adaptin-specific Small Inhibitory RNAs on Endocytic Accessory Proteins and Receptor Trafficking in HeLa Cells. Journal of Biological Chemistry 278:45160–45170.

Hou, J. C., and J. E. Pessin. 2007. Ins (endocytosis) and outs (exocytosis) of GLUT4 trafficking. Current Opinion in Cell Biology 19:466–473.

Hou, J. C., N. Suzuki, J. E. Pessin, and R. T. Watson. 2006. A specific dileucine motif is required for the GGA-dependent entry of newly synthesized insulin-responsive aminopeptidase into the insulin-responsive compartment. Journal of Biological Chemistry 281:33457–66.

Howes, M. T., M. Kirkham, J. Riches, K. Cortese, P. J. Walser, F. Simpson, M. M. Hill, A. Jones, R. Lundmark, M. R. Lindsay, D. J. Hernandez-Deviez, G. Hadzic, A. McCluskey, R. Bashir, L. Liu, P. Pilch, H. T. McMahon, P. J. Robinson, J. F. Hancock, S. Mayor, and R. G. Parton. 2010. Clathrin-independent carriers form a high capacity endocytic sorting system at the leading edge of migrating cells. Journal of Cell Biology 190:675–691.

Hresko, R. C., and M. Mueckler. 2005. mTOR.RICTOR is the Ser473 kinase for Akt/protein kinase B in 3T3-L1 adipocytes. Journal of Biological Chemistry 280:40406–16.

Hu, J., J. Liu, R. Ghirlando, A. R. Saltiel, and S. R. Hubbard. 2003. Structural basis for recruitment of the adaptor protein APS to the activated insulin receptor. Molecular Cell 12:1379–89.

Huang, J., T. Imamura, and J. M. Olefsky. 2001. Insulin can regulate GLUT4 internalization by signaling to Rab5 and the motor protein dynein. Proceedings of the National Academy of Sciences USA of the USA 98:13084–9.

Huang, S., and M. P. Czech. 2007. The GLUT4 Glucose Transporter. Cell Metabolism 5:237–252.

Huang, S., L. M. Lifshitz, C. Jones, K. D. Bellve, C. Standley, S. Fonseca, S. Corvera, K. E. Fogarty, and M. P. Czech. 2007. Insulin Stimulates Membrane Fusion and GLUT4 Accumulation in Clathrin Coats on Adipocyte Plasma Membranes. Molecular and Cellular Biology 27:3456–3469.

Hudson, A. W., M. Ruiz, and M. J. Birnbaum. 1992. Isoform-specific subcellular targeting of glucose transporters in mouse fibroblasts. Journal of Cell Biology 116:785–797.

Ibberson, M., B. M. Riederer, M. Uldry, B. Guhl, J. Roth, and B. Thorens. 2002. Immunolocalization of GLUTX1 in the testis and to specific brain areas and vasopressin-containing neurons. Endocrinology 143:276–284.

Ibberson, M., M. Uldry, and B. Thorens. 2000. GLUTX1, a novel mammalian glucose transporter expressed in the central nervous system and insulin-sensitive tissues. Journal of Biological Chemistry 275:4607–12.

Illsley, N. P. 2000. Glucose transporters in the human placenta. Placenta 21:14–22.

Infante, J., C. Prieto, M. Sierra, P. Sánchez-Juan, I. González-Aramburu, C. Sánchez-Quintana, J. Berciano, O. Combarros, and J. Sainz. 2015. Identification of candidate genes for Parkinson's disease through blood transcriptome analysis in LRRK2-G2019S carriers, idiopathic cases, and controls. Neurobiology of Aging 36:1105–1109.

Inoue, M., L. Chang, J. Hwang, S.-H. Chiang, and A. R. Saltiel. 2003. The exocyst complex is required for targeting of Glut4 to the plasma membrane by insulin. Nature 422:629–633.

Ishiki, M., and A. Klip. 2005. Minireview: Recent developments in the regulation of glucose transporter-4 traffic: New signals, locations, and partners. Endocrinology 146:5071-5078.

Ishikura, S., P. J. Bilan, and A. Klip. 2007. Rabs 8A and 14 are targets of the insulin-regulated Rab-GAP AS160 regulating GLUT4 traffic in muscle cells. Biochemical and Biophysical Research Communications 353:1074–1079.

Ishikura, S., and A. Klip. 2008. Muscle cells engage Rab8A and myosin Vb in insulin-dependent GLUT4 translocation. American Journal of Physiology-Cell Physiology 295:C1016–C1025.

James, D. E., R. Brown, J. Navarro, and P. Pilch. 1988. Insulin-regulatable tissues express a unique insulin-sensitive glucose transport protein. Nature 333:183–185.

James, D. E., M. Strube, and M. Mueckler. 1989. Molecular cloning and characterization of an insulin-regulatable glucose transporter. Nature 338:83–7.

Januchowski, R., P. Zawierucha, M. Andrzejewska, M. Ruciński, and M. Zabel. 2013. Microarray-based detection and expression analysis of ABC and SLC transporters in drug-resistant ovarian cancer cell lines. Biomedicine and Pharmacotherapy 67:240-245.

JeBailey, L., A. Rudich, X. Huang, C. Di Ciano-Oliveira, A. Kapus, and A. Klip. 2004. Skeletal muscle cells and adipocytes differ in their reliance on TC10 and Rac for insulin-induced actin remodeling. Molecular Endocrinology 18:359–72.

Jedrychowski, M. P., C. A. Gartner, S. P. Gygi, L. Zhou, J. Herz, K. V. Kandror, and P. Pilch. 2010. Proteomic analysis of GLUT4 storage vesicles reveals LRP1 to be an important vesicle component and target of insulin signaling. Journal of Biological Chemistry 285:104–114.

Jiang, T., G. Sweeney, M. T. Rudolf, A. Klip, A. Traynor-Kaplan, and R. Y. Tsien. 1998. Membrane-permeant esters of phosphatidylinositol 3,4,5-trisphosphate. Journal of Biological Chemistry 273:11017–11024.

Jimenez-Amilburu, V., S. Jong-Raadsen, J. Bakkers, H. P. Spaink, and R. Marin-Juez. 2015. GLUT12 deficiency during early development results in heart failure and a diabetic phenotype in zebrafish. Journal of Endocrinology 224:1–15.

Joost, H.-G., and B. Thorens. 2001. The extended GLUT-family of sugar/polyol transport facilitators: nomenclature, sequence characteristics, and potential function of its novel members (review). Molecular Membrane Biology 18:247–56.

Jordens, I., D. Molle, W. Xiong, S. R. Keller, and T. E. McGraw. 2010. Insulin-regulated aminopeptidase is a key regulator of GLUT4 trafficking by controlling the sorting of GLUT4 from endosomes to specialized insulin-regulated vesicles. Molecular Biology of the Cell 21:2034–44.

Jost, M., F. Simpson, M. Kavran, M. A. Lemmon, and S. L. Schmid. 1998. Phosphatidylinositol-4,5-bisphosphate is required for endocytic coated vesicle formation. Current Biology 8:1399–402.

Kalia, M., S. Kumari, R. Chadda, M. M. Hill, R. G. Parton, and S. Mayor. 2006. Arf6-independent GPI-anchored protein-enriched early endosomal compartments fuse with sorting endosomes via a Rab5/phosphatidylinositol-3'-kinase-dependent machinery. Molecular Biology of the Cell 17:3689–704.

Kanai, F., Y. Nishioka, H. Hayashi, S. Kamohara, M. Todaka, and Y. Ebina. 1993. Direct

demonstration of insulin-induced GLUT4 translocation to the surface of intact cells by insertion of a c-myc epitope into an exofacial GLUT4 domain. Journal of Biological Chemistry 268:14523–6.

Kandror, K. V. 2017. The role of sortilin in the "Glut4 Pathway". Communicative & Integrative Biology:e1393592.

Kane, S., H. Sano, S. C. H. Liu, J. M. Asara, W. S. Lane, C. C. Garner, and G. E. Lienhard. 2002. A Method to Identify Serine Kinase Substrates. Journal of Biological Chemistry 277:22115–22118.

Karylowski, O., A. Zeigerer, A. Cohen, and T. E. Mcgraw. 2004. GLUT4 Is Retained by an Intracellular Cycle of Vesicle Formation and Fusion with Endosomes. Molecular Biology of the Cell 15:870–882.

Keembiyehetty, C., R. Augustin, M. O. Carayannopoulos, S. Steer, A. Manolescu, C. I. Cheeseman, and K. H. Moley. 2006. Mouse Glucose Transporter 9 Splice Variants Are Expressed in Adult Liver and Kidney and Are Up-Regulated in Diabetes. Molecular Endocrinology 20:686–697.

Khan, A. H., E. Capilla, J. C. Hou, R. T. Watson, J. E. Smith, and J. E. Pessin. 2004. Entry of newly synthesized GLUT4 into the insulin-responsive storage compartment is dependent upon both the amino terminus and the large cytoplasmic loop. Journal of Biological Chemistry 279:37505–37511.

Khayat, Z., T. Tsakiridis, A. Ueyama, R. Somwar, Y. Ebina, and A. Klip. 1998. Rapid stimulation of glucose transport by mitochondrial uncoupling depends in part on cytosolic Ca2+ and cPKC. American Journal of Physiology 275:C1487–C1497.

Kim, S., M. Nahm, N. Kim, Y. Kwon, J. Kim, S. Choi, E. Y. Choi, J. Shim, C. Lee, and S. Lee. 2017. Graf regulates hematopoiesis through GEEC endocytosis of EGFR. Development (Cambridge, England) 144:4159–4172.

Kimura, A., C. A. Baumann, S.-H. Chiang, and A. R. Saltiel. 2001. The sorbin homology domain: A motif for the targeting of proteins to lipid rafts. Proceedings of the National Academy of Sciences USA of the USA 98:9098–9103.

Kioumourtzoglou, D., P. R. Pryor, G. W. Gould, and N. J. Bryant. 2015. Alternative routes to the cell surface underpin insulin-regulated membrane trafficking of GLUT4. Journal of Cell Science 128:2423–2429.

Kirchhausen, T. 2009. Imaging endocytic clathrin structures in living cells. Trends in Cell Biology 19:596–605.

Kirkham, M., A. Fujita, R. Chadda, S. J. Nixon, T. V. Kurzchalia, D. K. Sharma, R. E. Pagano, J. F. Hancock, S. Mayor, and R. G. Parton. 2005. Ultrastructural identification of uncoated caveolin-independent early endocytic vehicles. Journal of Cell Biology 168:465–476.

Kirkham, M., and R. G. Parton. 2005. Clathrin-independent endocytosis: New insights into caveolae and non-caveolar lipid raft carriers. Biochimica et Biophysica Acta - Molecular Cell Research 1745:273–286.

Klip, A. 2009. The many ways to regulate glucose transporter 4. Applied Physiology, Nutrition, and Metabolism 34:481–487.

Kovtun, O., V. A. Tillu, N. Ariotti, R. G. Parton, and B. M. Collins. 2015. Cavin family proteins and the assembly of caveolae. Journal of Cell Science 128:1269–78.

Krasnov, A., H. Teerijoki, and H. Mölsä. 2001. Rainbow trout (Onchorhynchus mykiss) hepatic glucose transporter. Biochimica et Biophysica Acta 1520:174–8.

Kumari, S., and S. Mayor. 2008. ARF1 is directly involved in dynamin-independent endocytosis. Nature Cell Biology 10:30–41.

Kumari, S., S. MG, and S. Mayor. 2010. Endocytosis unplugged: multiple ways to enter the cell. Cell Research 20:256–275.

Kurzchalia, T. V., P. Dupree, R. G. Parton, R. Kellner, H. Virta, M. Lehnert, and K. Simons. 1992. VIP21, a 21-kD membrane protein is an integral component of trans-Golgi-network-derived transport vesicles. Journal of Cell Biology 118:1003–14.

Kurzchalia, T. V., and R. G. Parton. 1999. Membrane microdomains and caveolae. Current Opinion in Cell Biology 11:424–31.

Lamaze, C., A. Dujeancourt, T. Baba, C. G. Lo, A. Benmerah, and A. Dautry-Varsat. 2001. Interleukin 2 receptors and detergent-resistant membrane domains define a clathrin-independent endocytic pathway. Molecular Cell 7:661–71.

Lamb, C. A., R. K. McCann, J. Stöckli, D. E. James, and N. J. Bryant. 2010. Insulin-regulated trafficking of GLUT4 requires ubiquitination. Traffic 11:1445–1454.

Lampson, M. A., A. Racz, S. W. Cushman, and T. E. McGraw. 2000. Demonstration of insulin-responsive trafficking of GLUT4 and vpTR in fibroblasts. Journal of Cell Science 113:4065–4076.

Larance, M., G. Ramm, J. Stöckli, E. M. van Dam, S. Winata, V. Wasinger, F. Simpson, M. Graham, J. R. Junutula, M. Guilhaus, and D. E. James. 2005. Characterization of the role of the Rab GTPase-activating protein AS160 in insulin-regulated GLUT4 trafficking. Journal of Biological Chemistry 280:37803–13.

Lee, J., and P. F. Pilch. 1994. The insulin receptor: structure, function, and signaling. The American Journal of Physiology 266:C319–C334.

Leto, D., and A. R. Saltiel. 2012. Regulation of glucose transport by insulin: traffic control of GLUT4. Nature Reviews Molecular Cell Biology 13:383–396.

Li, D., V. K. Randhawa, N. Patel, M. Hayashi, and A. Klip. 2001. Hyperosmolarity Reduces GLUT4 Endocytosis and Increases Its Exocytosis from a VAMP2-independent Pool in L6 Muscle Cells. Journal of Biological Chemistry 276:22883–22891.

Li, J., A. W. Malaby, M. Famulok, H. Sabe, D. G. Lambright, and V. W. Hsu. 2012. Grp1 Plays a Key Role in Linking Insulin Signaling to Glut4 Recycling. Developmental Cell 22:1286–1298.

Li, L. V, and K. V. Kandror. 2005. Golgi-localized, gamma-ear-containing, Arf-binding protein adaptors mediate insulin-responsive trafficking of glucose transporter 4 in 3T3-L1

adipocytes. Molecular Endocrinology 19:2145–2153.

Li, Q., X. Zhu, S. Ishikura, D. Zhang, J. Gao, Y. Sun, A. Contreras-Ferrat, K. Foley, S. Lavandero, Z. Yao, P. J. Bilan, A. Klip, and W. Niu. 2014. Ca 2+ signals promote GLUT4 exocytosis and reduce its endocytosis in muscle cells. American Journal of Physiology-Endocrinology and Metabolism 307:E209–E224.

Lin, B. Z., P. Pilch, and K. V. Kandror. 1997. Sortilin is a major protein component of Glut4-containing vesicles. Journal of Biological Chemistry 272:24145–24147.

Lisinski, I., A. Schürmann, H.-G. Joost, S. W. Cushman, and H. Al-Hasani. 2001. Targeting of GLUT6 (formerly GLUT9) and GLUT8 in rat adipose cells. Biochemical Journal 358:517–22.

Liu, J., A. Kimura, C. A. Baumann, and A. R. Saltiel. 2002. APS facilitates c-Cbl tyrosine phosphorylation and GLUT4 translocation in response to insulin in 3T3-L1 adipocytes. Molecular and Cellular Biology 22:3599–609.

Liu, L., W. Omata, I. Kojima, and H. Shibata. 2007. The SUMO conjugating enzyme Ubc9 is a regulator of GLUT4 turnover and targeting to the insulin-responsive storage compartment in 3T3-L1 adipocytes. Diabetes 56:1977–1985.

Liu, L., and P. Pilch. 2008. A Critical Role of Cavin (Polymerase I and Transcript Release Factor) in Caveolae Formation and Organization. Journal of Biological Chemistry 283:4314–4322.

Livingstone, C., D. E. James, J. E. Rice, D. Hanpeter, and G. W. Gould. 1996. Compartment ablation analysis of the insulin-responsive glucose transporter (GLUT4) in 3T3-L1 adipocytes. The Biochemical Journal 315(2):487–95.

Lizunov, V. A., J. P. Lee, M. C. Skarulis, J. Zimmerberg, S. W. Cushman, and K. G. Stenkula. 2013. Impaired tethering and fusion of GLUT4 vesicles in insulin-resistant human adipose cells. Diabetes 62(9):3114-9.

Lizunov, V. A., H. Matsumoto, J. Zimmerberg, S. W. Cushman, and V. A. Frolov. 2005. Insulin stimulates the halting, tethering, and fusion of mobile GLUT4 vesicles in rat adipose cells. Journal of Cell Biology 169:481–489.

Lodhi, I. J., D. Bridges, S.-H. Chiang, Y. Zhang, A. Cheng, L. M. Geletka, L. S. Weisman, and A. R. Saltiel. 2008. Insulin Stimulates Phosphatidylinositol 3-Phosphate Production via the Activation of Rab5. Molecular Biology of the Cell 19:2718–2728.

Lodhi, I. J., S.-H. Chiang, L. Chang, D. Vollenweider, R. T. Watson, M. Inoue, J. E. Pessin, and A. R. Saltiel. 2007. Gapex-5, a Rab31 Guanine Nucleotide Exchange Factor that Regulates Glut4 Trafficking in Adipocytes. Cell Metabolism 5:59–72.

Lundmark, R., G. J. Doherty, M. T. Howes, K. Cortese, Y. Vallis, R. G. Parton, and H. T. McMahon. 2008. The GTPase-Activating Protein GRAF1 Regulates the CLIC/GEEC Endocytic Pathway. Current Biology 18:1802–1808.

Mallard, F., B. L. Tang, T. Galli, D. Tenza, A. Saint-Pol, X. Yue, C. Antony, W. Hong, B. Goud, and L. Johannes. 2002. Early/recycling endosomes-to-TGN transport involves two SNARE complexes and a Rab6 isoform. Journal of Cell Biology 156:653–64.

Marín-Juez, R., Capilla, E., Simoes, F., Camps, M., Planas, J.V. 2014. Structural and Functional Evolution of Glucose Transporter 4 (GLUT4): a Look at GLUT4 in Fish. In: "Glucose Homeostasis", Szablewski, L., ed. InTech Open Access Publisher, Rijeka, Croatia. ISBN: 980-953-307-1140-0. pp. 37-67.

Marsh, B. J., R. A. Alm, S. R. McIntosh, and D. E. James. 1995. Molecular regulation of GLUT-4 targeting in 3T3-L1 adipocytes. Journal of Cell Biology 130:1081–1091.

Martin, O. J., A. Lee, and T. E. McGraw. 2006. GLUT4 distribution between the plasma membrane and the intracellular compartments is maintained by an insulin-modulated bipartite dynamic mechanism. Journal of Biological Chemistry 281:484–490.

Martin, S., B. Reaves, G. Banting, and G. W. Gould. 1994. Analysis of the co-localization of the insulin-responsive glucose transporter (GLUT4) and the trans Golgi network marker TGN38 within 3T3-L1 adipocytes. Biochemical Journal 300(3):743–749.

Martin, S. S., T. Haruta, A. J. Morris, A. Klippel, L. T. Williams, and J. M. Olefsk. 1996. Activated phosphatidylinositol 3-kinase is sufficient to mediate actin rearrangement and GLUT4 translocation in 3T3-L1 adipocytes. Journal of Biological Chemistry 271:17605–17608.

Martinez-Arca, S., V. Lalioti, and I. V Sandoval. 2000. Intracellular targeting and retention of the glucose transporter GLUT4 by the perinuclear storage compartment involves distinct carboxyl-tail motifs. Journal of Cell Science 113(1):1705–15.

Mayor, S., and R. E. Pagano. 2007. Pathways of clathrin-independent endocytosis. Nature Reviews Molecular Cell Biology 8(8): 603-612.

Mayor, S., R. G. Parton, and J. G. Donaldson. 2014. Clathrin-independent pathways of endocytosis. Cold Spring Harbor Perspectives in Biology 6(6): a016758.

McMahon, H. T., and E. Boucrot. 2011. Molecular mechanism and physiological functions of clathrin-mediated endocytosis. Nature Reviews Molecular Cell Biology 12:517–533.

McVie-Wylie, A. J., D. R. Lamson, and Y. T. Chen. 2001. Molecular cloning of a novel member of the GLUT family of transporters, SLC2A10 (GLUT10), localized on chromosome 20q13.1: A candidate gene for NIDDM susceptibility. Genomics 72:113–117.

Mîinea, C. P., H. Sano, S. Kane, E. Sano, M. Fukuda, J. Peränen, W. S. Lane, and G. E. Lienhard. 2005. AS160, the Akt substrate regulating GLUT4 translocation, has a functional Rab GTPase-activating protein domain. Biochemical Journal 391:87–93.

Min, J., S. Okada, M. Kanzaki, J. S. Elmendorf, K. J. Coker, B. P. Ceresa, L. J. Syu, Y. Noda, A. R. Saltiel, and J. E. Pessin. 1999. Synip: a novel insulin-regulated syntaxin 4-binding protein mediating GLUT4 translocation in adipocytes. Molecular Cell 3:751–60.

Moren, B., C. Shah, M. T. Howes, N. L. Schieber, H. T. McMahon, R. G. Parton, O. Daumke, and R. Lundmark. 2012. EHD2 regulates caveolar dynamics via ATP-driven targeting and oligomerization. Molecular Biology of the Cell 23:1316–1329.

Mousavi, S. A., L. Malerød, T. Berg, and R. Kjeken. 2004. Clathrin-dependent endocytosis. Biochemical Journal 377:1–16.

Mueckler, M. 1995. Glucose Transport and Glucose Homeostasis: New Insights From Transgenic

Mice. Physiology 10:22–29.

Mueckler, M., C. Caruso, S. A. Baldwin, M. Panico, I. Blench, H. R. Morris, W. J. Allard, G. E. Lienhard, and H. F. Lodish. 1985. Sequence and structure of a human glucose transporter. Science 229:941–945.

Mueckler, M., and B. Thorens. 2013. The SLC2 (GLUT) family of membrane transporters. Molecular Aspects of Medicine 34 (2-3) 121:38.

Munson, M., and P. Novick. 2006. The exocyst defrocked, a framework of rods revealed. Nature Structural & Molecular Biology 13:577–581.

Nagase, T., K.-I. Ishikawa, N. Miyajima, A. Tanaka, H. Kotani, N. Nomura, and O. Ohara. 1998. Prediction of the Coding Sequences of Unidentified Human Genes. IX. The Complete Sequences of 100 New cDNA Clones from Brain Which Can Code for Large Proteins in vitro. DNA Research 5:31–39.

Naslavsky, N., R. Weigert, and J. G. Donaldson. 2004. Characterization of a Nonclathrin Endocytic Pathway: Membrane Cargo and Lipid Requirements. Molecular Biology of the Cell 15:3542–3552.

Oh, P., D. P. McIntosh, and J. E. Schnitzer. 1998. Dynamin at the neck of caveolae mediates their budding to form transport vesicles by GTP-driven fission from the plasma membrane of endothelium. Journal of Cell Biology 141:101–14.

Okada, T., Y. Kawano, T. Sakakibara, O. Hazeki, and M. Ui. 1994. Essential role of phosphatidylinositol 3-kinase in insulin-induced glucose transport and antilipolysis in rat adipocytes. Studies with a selective inhibitor wortmannin. Journal of Biological Chemistry 269:3568–73.

Owen, D. J., B. M. Collins, and P. R. Evans. 2004. Adaptors for Clathrin coats: Structure and Function. Annual Review of Cell and Developmental Biology 20:153–191.

Palacios, S., V. Lalioti, S. Martinez-Arca, S. Chattopadhyay, and I. V. Sandoval. 2001. Recycling of the Insulin-sensitive Glucose Transporter GLUT4. Journal of Biological Chemistry 276:3371–3383.

Pan, X., N. Zaarur, M. Singh, P. Morin, and K. V. Kandror. 2017. Sortilin and retromer mediate retrograde transport of Glut4 in 3T3-L1 adipocytes. Molecular Biology of the Cell 28:1667–1675.

Parton, R. G., and M. A. Del Pozo. 2013. Caveolae as plasma membrane sensors, protectors and organizers. Nature Reviews Molecular Cell Biology 14:98–112.

Parton, R. G., and K. Simons. 2007. The multiple faces of caveolae. Nature Reviews Molecular Cell Biology 8:185–194.

Peck, G. R., S. Ye, V. Pham, R. N. Fernando, S. L. Macaulay, S. Y. Chai, and A. L. Albiston. 2006. Interaction of the Akt Substrate, AS160, with the Glucose Transporter 4 Vesicle Marker Protein, Insulin-Regulated Aminopeptidase. Molecular Endocrinology 20:2576–2583.

Perera, H. K., M. Clarke, N. J. Morris, W. Hong, L. H. Chamberlain, and G. W. Gould. 2003. Syntaxin 6 regulates Glut4 trafficking in 3T3-L1 adipocytes. Molecular Biology of the Cell

14:2946–2958.

Phay, J. E., H. B. Hussain, and J. F. Moley. 2000. Cloning and expression analysis of a novel member of the facilitative glucose transporter family, SLC2A9 (GLUT9). Genomics 66:217–20.

Piper, R. C., C. Tai, P. Kulesza, S. Pang, D. Warnock, J. Baenziger, J. W. Slot, H. J. Geuze, C. Puri, and D. E. James. 1993. GLUT-4 NH2terminus contains a phenylalanine-based targeting motif that regulates intracellular sequestration. Journal of Cell Biology 121:1221–1232.

Planas, J. V., E. Capilla, and J. Gutiérrez. 2000. Molecular identication of a glucose transporter from fish muscle. FEBS Letters. 481:266–270.

Ploug, T., B. Van Deurs, H. Ai, S. W. Cushman, and E. Ralston. 1998. Analysis of GLUT4 distribution in whole skeletal muscle fibers: Identification of distinct storage compartments that are recruited by insulin and muscle contractions. Journal of Cell Biology 142:1429–1446.

Proctor, K. M., S. C. M. Miller, N. J. Bryant, and G. W. Gould. 2006. Syntaxin 16 controls the intracellular sequestration of GLUT4 in 3T3-L1 adipocytes. Biochemical and Biophysical Research Communications 347:433–438.

Ramm, G., M. Larance, M. Guilhaus, and D. E. James. 2006. A Role for 14-3-3 in Insulin-stimulated GLUT4 Translocation through Its Interaction with the RabGAP AS160. Journal of Biological Chemistry 281:29174–29180.

Rand, E. B., A. M. Depaoli, N. O. Davidson, G. I. Bell, and C. F. Burant. 1993. Sequence, tissue distribution, and functional characterization of the rat fructose transporter GLUT5. American Journal of Physiology 264:G1169-1176.

Randhawa, V. K., S. Ishikura, I. Talior-Volodarsky, A. W. P. Cheng, N. Patel, J. H. Hartwig, and A. Klip. 2008. GLUT4 vesicle recruitment and fusion are differentially regulated by Rac, AS160, and Rab8A in muscle cells. Journal of Biological Chemistry 283:27208–27219.

Rapoport, I., Y. Chen, P. Cupers, S. E. Shoelson, and T. Kirchhausen. 1998. Dileucine-based sorting signals bind to the β chain of AP-1 at a site distinct and regulated differently from the tyrosine-based motif-binding site. EMBO Journal 17:2148–2155.

Ribon, V., S. Hubbell, R. Herrera, and A. R. Saltiel. 1996. The product of the cbl oncogene forms stable complexes in vivo with endogenous Crk in a tyrosine phosphorylation-dependent manner. Molecular and Cellular Biology 16:45–52.

Ribon, V., R. Herrera, B. K. Kay, and A. R. Saltiel. 1998a. A role for CAP, a novel, multifunctional Src homology 3 domain-containing protein in formation of actin stress fibers and focal adhesions. Journal of Biological Chemistry 273:4073–80.

Ribon, V., J. A. Printen, N. G. Hoffman, B. K. Kay, and A. R. Saltiel. 1998b. A novel, multifuntional c-Cbl binding protein in insulin receptor signaling in 3T3-L1 adipocytes. Molecular and Cellular Biology 18:872–9.

Robinson, L. J., S. Pang, D. S. Harris, J. E. Heuser, and D. E. James. 1992. Translocation of the glucose transporter (GLUT4) to the cell surface in permeabilized 3T3-L1 adipocytes: effects

of ATP insulin, and GTP gamma S and localization of GLUT4 to clathrin lattices. Journal of Cell Biology 117:1181–96.

Rogers, S., M. L. Macheda, S. E. Docherty, M. D. Carty, M. A. Henderson, W. C. Soeller, E. M. Gibbs, D. E. James, and J. D. Best. 2002. Identification of a novel glucose transporter-like protein-GLUT-12. American Journal of Physiology-Endocrinology and Metabolism 282:E733-8.

Ros-Baro, A., C. Lopez-Iglesias, S. Peiro, D. Bellido, M. Palacín, A. Zorzano, and M. Camps. 2001. Lipid rafts are required for GLUT4 internalization in adipose cells. Proceedings of the National Academy of Sciences USA of the USA 98:12050–12055.

Ross, S. A., H. M. Scott, N. J. Morris, W. Y. Leung, F. Mao, G. E. Lienhard, and S. R. Keller. 1996. Characterization of the insulin-regulated membrane aminopeptidase in 3T3-L1 adipocytes. Journal of Biological Chemistry 271:3328–32.

Rothberg, K. G., J. E. Heuser, W. C. Donzell, Y. S. Ying, J. R. Glenney, and R. G. Anderson. 1992. Caveolin, a protein component of caveolae membrane coats. Cell 68:673–82.

Rothman, D. L., I. Magnusson, G. Cline, D. Gerard, C. R. Kahn, R. G. Shulman, and G. I. Shulman. 1995. Decreased muscle glucose transport/phosphorylation is an early defect in the pathogenesis of non-insulin-dependent diabetes mellitus. Proceedings of the National Academy of Sciences USA of the USA 92:983–7.

Rowland, A. F., D. J. Fazakerley, and D. E. James. 2011. Mapping Insulin/GLUT4 Circuitry. Traffic 12:672–681.

Rubin, B. R., and J. S. Bogan. 2009. Intracellular Retention and Insulin-Stimulated Mobilization of GLUT4 Glucose Transporters. Vitamins and Hormones 80:155-92.

Sabharanjak, S., P. Sharma, R. G. Parton, and S. Mayor. 2002. GPI-anchored proteins are delivered to recycling endosomes via a distinct cdc42-regulated, clathrin-independent pinocytic pathway. Developmental Cell 2:411–23.

Sadacca, L. A., J. Bruno, J. Wen, W. Xiong, and T. E. McGraw. 2013. Specialized sorting of GLUT4 and its recruitment to the cell surface are independently regulated by distinct Rabs. Molecular Biology of the Cell 24:2544–57.

Sadler, J., N. J. Bryant, and G. W. Gould. 2015. Characterization of VAMP isoforms in 3T3-L1 adipocytes: implications for GLUT4 trafficking. Molecular Biology of the Cell 26:530–536.

Saltiel, A. R., and C. R. Kahn. 2001. Insulin signalling and the regulation of glucose and lipid metabolism. Nature 414:799–806.

Sano, H., L. Eguez, M. N. Teruel, M. Fukuda, T. D. Chuang, J. A. Chavez, G. E. Lienhard, and T. E. McGraw. 2007. Rab10, a target of the AS160 Rab GAP, is required for insulin-stimulated translocation of GLUT4 to the adipocyte plasma membrane. Cell Metabolism 5:293–303.

Sano, H., S. Kane, E. Sano, C. P. Mîinea, J. M. Asara, W. S. Lane, C. W. Garner, and G. E. Lienhard. 2003. Insulin-stimulated Phosphorylation of a Rab GTPase-activating Protein Regulates GLUT4 Translocation. Journal of Biological Chemistry 278:14599–14602.

Sano, H., W. G. Roach, G. R. Peck, M. Fukuda, and G. E. Lienhard. 2008. Rab10 in insulin-

stimulated GLUT4 translocation. Biochemical Journal 411:89–95.

Sarbassov, D. D., D. A. Guertin, S. M. Ali, and D. M. Sabatini. 2005. Phosphorylation and Regulation of Akt/PKB by the Rictor-mTOR Complex. Science 307:1098–1101.

Sargeant, R. J., and M. R. Pâquet. 1993. Effect of insulin on the rates of synthesis and degradation of GLUT1 and GLUT4 glucose transporters in 3T3-L1 adipocytes. Biochemical Journal 290 (3):913–9.

Sasaki, T., S. Minoshima, A. Shiohama, A. Shintani, A. Shimizu, S. Asakawa, K. Kawasaki, and N. Shimizu. 2001. Molecular cloning of a member of the facilitative glucose transporter gene family GLUT11 (SLC2A11) and identification of transcription variants. Biochemical and Biophysical Research Communications 289:1218–1224.

Satoh, T. 2014. Molecular mechanisms for the regulation of insulin-stimulated glucose uptake by small guanosine triphosphatases in skeletal muscle and adipocytes. International Journal of Molecular Sciences 15:18677-18692.

Scheepers, A., H.-G. Joost, and A. Schürmann. 2004. The glucose transporter families SGLT and GLUT: molecular basis of normal and aberrant function. Journal of Parenteral and Enteral Nutrition 28:364–371.

Scheepers, A., S. Schmidt, A. Manolescu, C. I. Cheeseman, A. Bell, C. Zahn, H.-G. Joost, and A. Schürmann. 2005. Characterization of the human SLC2A11 (GLUT11) gene: alternative promoter usage, function, expression, and subcellular distribution of three isoforms, and lack of mouse orthologue. Molecular Membrane Biology 22:339–351.

Scherer, P. E., M. P. Lisanti, G. Baldini, M. Sargiacomo, C. C. Mastick, and H. F. Lodish. 1994. Induction of caveolin during adipogenesis and association of GLUT4 with caveolin-rich vesicles. Journal of Cell Biology 127:1233–1243.

Schlegel, A., P. Arvan, and M. P. Lisanti. 2001. Caveolin-1 binding to endoplasmic reticulum membranes and entry into the regulated secretory pathway are regulated by serine phosphorylation. Protein sorting at the level of the endoplasmic reticulum. Journal of Biological Chemistry 276:4398–4408.

Schlossman, D. M., S. L. Schmid, W. A. Braell, and J. E. Rothman. 1984. An enzyme that removes clathrin coats: Purification of an uncoating ATPase. Journal of Cell Biology 99:723–733.

Schultz, M. L., L. Tecedor, C. S. Stein, M. A. Stamnes, and B. L. Davidson. 2014. CLN3 deficient cells display defects in the ARF1-Cdc42 pathway and actin-dependent events. PloS ONE 9 (5):e96647.

Shewan, A. M., E. M. van Dam, S. Martin, T. B. Luen, W. Hong, N. J. Bryant, and D. E. James. 2003. GLUT4 Recycles via a trans-Golgi Network (TGN) Subdomain Enriched in Syntaxins 6 and 16 But Not TGN38: Involvement of an Acidic Targeting Motif. Molecular Biology of the Cell 14:973–986.

Shewan, A. M., B. J. Marsh, D. R. Melvin, S. Martin, G. W. Gould, and D. E. James. 2000. The cytosolic C-terminus of the glucose transporter GLUT4 contains an acidic cluster endosomal targeting motif distal to the dileucine signal. Biochemical Journal 350(1):99–107.

Shi, J., and K. V. Kandror. 2005. Sortilin is essential and sufficient for the formation of glut4 storage vesicles in 3T3-L1 adipocytes. Developmental Cell 9:99–108.

Shigematsu, S., R. T. Watson, A. H. Khan, and J. E. Pessin. 2003. The Adipocyte Plasma Membrane Caveolin Functional/Structural Organization Is Necessary for the Efficient Endocytosis of GLUT4. Journal of Biological Chemistry 278:10683–10690.

Shin, B. C., K. Fujikura, T. Suzuki, S. Tanaka, and K. Takata. 1997. Glucose transporter GLUT3 in the rat placental barrier: A possible machinery for the transplacental transfer of glucose. Endocrinology 138:3997–4004.

Simons, K., and E. Ikonen. 1997. Functional rafts in cell membranes. Nature 387:569–572.

Simpson, I. A., A. Carruthers, and S. J. Vannucci. 2007. Supply and Demand in Cerebral Energy Metabolism :The Role of Nutrient Transporters. Journal of Cerebral Blood Flow & Metabolism 27:1766–1791.

Simpson, I. A., D. Dwyer, D. Malide, K. H. Moley, A. Travis, and S. J. Vannucci. 2008. The facilitative glucose transporter GLUT3: 20 years of distinction. American Journal of Physiology-Endocrinology and Metabolism 295:E242–E253.

Song, X. M., C. F. Lichti, R. R. Townsend, and M. Mueckler. 2013. Single Point Mutations Result in the Miss-Sorting of Glut4 to a Novel Membrane Compartment Associated with Stress Granule Proteins. PLoS ONE 8(7):e68516.

Standaert, M. L., G. Bandyopadhyay, L. Perez, D. Price, L. Galloway, A. Poklepovic, M. P. Sajan, V. Cenni, A. Sirri, J. Moscat, A. Toker, and R. V. Farese. 1999. Insulin activates protein kinases C-zeta and C-lambda by an autophosphorylation-dependent mechanism and stimulates their translocation to GLUT4 vesicles and other membrane fractions in rat adipocytes. Journal of Biological Chemistry 274:25308–16.

Stenkula, K. G., V. A. Lizunov, S. W. Cushman, and J. Zimmerberg. 2010. Insulin Controls the Spatial Distribution of GLUT4 on the Cell Surface through Regulation of Its Postfusion Dispersal. Cell Metabolism 12:250–259.

Stöckli, J., D. J. Fazakerley, and D. E. James. 2011. GLUT4 exocytosis. Journal of Cell Science 124:4147–4159.

Stuart, C. A., M. E. A. Howell, Y. Zhang, and D. Yin. 2009. Insulin-stimulated translocation of glucose transporter (GLUT) 12 parallels that of GLUT4 in normal muscle. Journal of Clinical Endocrinology and Metabolism 94:3535–3542.

Sun, Y., P. J. Bilan, Z. Liu, and A. Klip. 2010. Rab8A and Rab13 are activated by insulin and regulate GLUT4 translocation in muscle cells. Proceedings of the National Academy of Sciences USA of the USA 107:19909–19914.

Suzuki, K., and T. Kono. 1980. Evidence that insulin causes translocation of glucose transport activity to the plasma membrane from an intracellular storage site. Proceedings of the National Academy of Sciences USA USA 77:2542–2545.

Takei, K., and V. Haucke. 2001. Clathrin-mediated endocytosis: membrane factors pull the trigger. Trends in Cell Biology 11:385–91.

Tan, S.-X., Y. Ng, J. G. Burchfield, G. Ramm, D. G. Lambright, J. Stöckli, and D. E. James. 2012. The Rab GTPase-activating protein TBC1D4/AS160 contains an atypical phosphotyrosine-binding domain that interacts with plasma membrane phospholipids to facilitate GLUT4 trafficking in adipocytes. Molecular and Cellular Biology 32:4946–59.

Taniguchi, C. M., B. Emanuelli, and C. R. Kahn. 2006. Critical nodes in signalling pathways: insights into insulin action. Nature Reviews Molecular Cell Biology 7:85–96.

Taylor, K. H., K. E. Pena-Hernandez, J. W. Davis, G. L. Arthur, D. J. Duff, H. Shi, F. B. Rahmatpanah, O. Sjahputera, and C. W. Caldwell. 2007. Large-scale CpG methylation analysis identifies novel candidate genes and reveals methylation hotspots in acute lymphoblastic leukemia. Cancer Research 67:2617–2625.

Teerijoki, H., A. Krasnov, T. I. Pitkänen, and H. Mölsä. 2000. Cloning and characterization of glucose transorter in teleost fish rainbow trout (Oncorhynchus mykiss). Biochimica et Biophysica Acta 1494:290–4.

Teerijoki, H., A. Krasnov, T. I. Pitkänen, and H. Mölsä. 2001a. Monosaccharide uptake in common carp (Cyprinus carpio) EPC cells is mediated by a facilitative glucose carrier. Comparative Biochemistry and Physiology. Part B, Biochemistry & Molecular Biology 128:483–91.

Teerijoki, H., a Krasnov, Y. Gorodilov, S. Krishna, and H. Mölsä. 2001b. Rainbow trout glucose transporter (OnmyGLUT1): functional assessment in Xenopus laevis oocytes and expression in fish embryos. Journal of Experimental Biology 204:2667–2673.

Thorens, B. 2014. GLUT2, glucose sensing and glucose homeostasis. Diabetologia 58:221-232.

Thorens, B., and M. Mueckler. 2010. Glucose transporters in the 21st Century. American Journal of Physiology-Endocrinology and Metabolism 298: E141-5

Uhlig, M., W. Passlack, and J. Eckel. 2005. Functional role of Rab11 in GLUT4 trafficking in cardiomyocytes. Molecular and Cellular Endocrinology 235:1–9.

Uldry, M., M. Ibberson, J. D. Horisberger, J. Y. Chatton, B. M. Riederer, and B. Thorens. 2001. Identification of a mammalian H+-myo-inositol symporter expressed predominantly in the brain. EMBO Journal 20:4467–4477.

Uldry, M., M. Ibberson, M. Hosokawa, and B. Thorens. 2002. GLUT2 is a high affinity glucosamine transporter. FEBS Letters 524:199–203.

Uldry, M., P. Steiner, M.-G. Zurich, P. Béguin, H. Hirling, W. Dolci, and B. Thorens. 2004. Regulated exocytosis of an H+/myo-inositol symporter at synapses and growth cones. EMBO Journal 23:531–40.

Ungewickell, E., H. Ungewickell, S. E. H. Holstein, R. Lindner, K. Prasad, W. Barouch, B. Martini, L. E. Greene, and E. Eisenberg. 1995. Role of auxilin in uncoating clathrin-coated vesicles. Nature 378:632–635.

Urner, F., and D. Sakkas. 1999. A possible role for the pentose phosphate pathway of spermatozoa in gamete fusion in the mouse. Biology of Reproduction 60:733–739.

Vannucci, S. J., F. Maher, and I. A. Simpson. 1997. Glucose transporter proteins in brain: Delivery

of glucose to neurons and glia. Glia 21:2–21.

Venkataraman, A., D. J. Nevrivy, T. M. Filtz, and M. Leid. 2012. Grp1-associated scaffold protein (GRASP) is a regulator of the ADP ribosylation factor 6 (Arf6)-dependent membrane trafficking pathway. Cell Biology International 36:1115–1128.

Volchuk, A., R. J. Sargeant, S. Sumitani, Z. Liu, L. He, and A. Klip. 1995. Cellubrevin is a resident protein of insulin-sensitive GLUT4 glucose transporter vesicles in 3T3-L1 adipocytes. Journal of Biological Chemistry 270:8233–40.

Waller, A. P., M. George, A. Kalyanasundaram, C. Kang, M. Periasamy, K. Hu, and V. A. Lacombe. 2013. GLUT12 functions as a basal and insulin-independent glucose transporter in the heart. Biochimica et Biophysica Acta - Molecular Basis of Disease 1832:121–127.

Walmsley, A. R., M. P. Barrett, F. Bringaud, and G. W. Gould. 1998. Sugar transporters from bacteria, parasites and mammals: Structure-activity relationships. Trends in Biochemical Sciences 23:476-481.

Watson, R. T., J. C. Hou, and J. E. Pessin. 2008. Recycling of IRAP from the plasma membrane back to the insulin-responsive compartment requires the Q-SNARE syntaxin 6 but not the GGA clathrin adaptors. Journal of Cell Science 121:1243–51.

Watson, R. T., M. Kanzaki, and J. E. Pessin. 2004a. Regulated membrane trafficking of the insulin-responsive glucose transporter 4 in adipocytes. Endocrine Reviews 25:177-204.

Watson, R. T., A. H. Khan, M. Furukawa, J. C. Hou, L. Li, M. Kanzaki, S. Okada, K. V. Kandror, and J. E. Pessin. 2004b. Entry of newly synthesized GLUT4 into the insulin-responsive storage compartment is GGA dependent. EMBO Journal 23:2059–2070.

Watson, R. T., S. Shigematsu, S.-H. Chiang, S. Mora, M. Kanzaki, I. G. Macara, A. R. Saltiel, and J. E. Pessin. 2001. Lipid raft microdomain compartmentalization of TC10 is required for insulin signaling and GLUT4 translocation. Journal of Cell Biology 154:829–840.

Wijesekara, N., A. Tung, F. Thong, and A. Klip. 2006. Muscle cell depolarization induces a gain in surface GLUT4 via reduced endocytosis independently of AMPK. American Journal of Physiology-Endocrinology and Metabolism 290:E1276–E1286.

Williams, D., S. W. Hicks, C. E. Machamer, and J. E. Pessin. 2006. Golgin-160 is required for the Golgi membrane sorting of the insulin-responsive glucose transporter GLUT4 in adipocytes. Molecular Biology of the Cell 17:5346–55.

Williams, T. M., and M. P. Lisanti. 2004. The caveolin proteins. Genome Biology 5(3):214.

Wu, X., and H. H. Freeze. 2002. GLUT14, a duplicon of GLUT3, is specifically expressed in testis as alternative splice forms. Genomics 80:553–557.

Xiao, M. S., R. C. Hresko, and M. Mueckler. 2008. Identification of amino acid residues within the C terminus of the Glut4 glucose transporter that are essential for insulin-stimulated redistribution to the plasma membrane. Journal of Biological Chemistry 283:12571–12585.

Xie, X., Z. Gong, V. Mansuy-Aubert, Q. L. Zhou, S. A. Tatulian, D. Sehrt, F. Gnad, L. M. Brill, K. Motamedchaboki, Y. Chen, M. P. Czech, M. Mann, M. Krüger, and Z. Y. Jiang. 2011. C2 domain-containing phosphoprotein CDP138 regulates GLUT4 insertion into the plasma

membrane. Cell Metabolism 14:378–89.

Xiong, W., I. Jordens, E. Gonzalez, and T. E. McGraw. 2010. GLUT4 is sorted to vesicles whose accumulation beneath and insertion into the plasma membrane are differentially regulated by insulin and selectively affected by insulin resistance. Molecular Biology of the Cell 21:1375–86.

Xu, Z., and K. V. Kandror. 2002. Translocation of small preformed vesicles is responsible for the insulin activation of glucose transport in adipose cells. Evidence from the in vitro reconstitution assay. Journal of Biological Chemistry 277:47972–47975.

Yamada, E., S. Okada, T. Saito, K. Ohshima, M. Sato, T. Tsuchiya, Y. Uehara, H. Shimizu, and M. Mori. 2005. Akt2 phosphorylates Synip to regulate docking and fusion of GLUT4-containing vesicles. Journal of Cell Biology 168:921–8.

Yan, N. 2017. A Glimpse of Membrane Transport through Structures—Advances in the Structural Biology of the GLUT Glucose Transporters. Journal of Molecular Biology 429:2710–2725.

Yang, J., and G. D. Holman. 2005. Insulin and contraction stimulate exocytosis, but increased AMP-activated protein kinase activity resulting from oxidative metabolism stress slows endocytosis of GLUT4 in cardiomyocytes. Journal of Biological Chemistry 280:4070–4078.

Yeh, J. I., K. J. Verhey, and M. J. Birnbaum. 1995. Kinetic analysis of glucose transporter trafficking in fibroblasts and adipocytes. Biochemistry 34:15523–31.

Yeh, T., J. I. Sbodio, Z.-Y. Tsun, B. Luo, and N.-W. Chi. 2007. Insulin-stimulated exocytosis of GLUT4 is enhanced by IRAP and its partner tankyrase. Biochemical Journal 402:279–90.

Yeh, W., C. Lin, and W. Fu. 2008. Enhancement of glucose transporter expression of brain endothelial cells by vascular endothelial growth factor derived from glioma exposed to hypoxia. Molecular Pharmacology 73:170–7.

Yki-Järvinen, H., K. Sahlin, J. M. Ren, and V. A. Koivisto. 1990. Localization of rate-limiting defect for glucose disposal in skeletal muscle of insulin-resistant type I diabetic patients. Diabetes 39:157–167.

Yu, C., J. A. Cresswell, M. G. Löffler, and J. S. Bogan. 2007. The Glucose transporter 4-regulating protein TUG is essential for highly insulin-responsive glucose uptake in 3T3-L1 adipocytes. Journal of Biological Chemistry 282:7710–7722.

Zaid, H., C. N. Antonescu, V. K. Randhawa, and A. Klip. 2008. Insulin action on glucose transporters through molecular switches, tracks and tethers. Biochemical Journal 413:201–215.

Zeigerer, A., M. A. Lampson, O. Karylowski, D. D. Sabatini, M. Adesnik, M. Ren, and T. E. McGraw. 2002. GLUT4 Retention in Adipocytes Requires Two Intracellular Insulin-regulated Transport Steps. Molecular Biology of the Cell 13:2421–2435.

Zeigerer, A., M. K. McBrayer, and T. E. McGraw. 2004. Insulin Stimulation of GLUT4 Exocytosis, but Not Its Inhibition of Endocytosis, Is Dependent on RabGAP AS160. Molecular Biology of the Cell 15:4406–4415.

Zerial, M., and H. McBride. 2001. Rab proteins as membrane organizers. Nature Reviews

Molecular Cell Biology 2:107–117.

Zhang, Z., R. S. S. Wu, H. O. L. Mok, Y. Wang, W. W. L. Poon, S. H. Cheng, and R. Y. C. Kong. 2003. Isolation, characterization and expression analysis of a hypoxia-responsive glucose transporter gene from the grass carp, Ctenopharyngodon idellus. European Journal of Biochemistry 270:3010–7.

VIII.PUBLICATIONS AND CONFERENCE PRESENTATIONS

PUBLICATIONS

- **Authors:** Rubén Marín-Juez, Encarnación Capilla, Francisco Carvalho-Simoes, Marta Camps and Josep V. Planas.
- **Book title:** Glucose Homeostasis.
- **Chapter title:** Structural and Functional Evolution of Glucose Transporter 4 (GLUT4): A Look at GLUT4 in Fish (pp.37-67).
- **Editorial:** Intech, USA.
- **Year:** 2014.
- **DOI:** 10.5772/58094.

CONFERENCE PRESENTATIONS

Poster presentation

- **Authors:** Francisco Carvalho-Simoes, Marta Camps, Josep V.Planas.
- **Poster title:** Fish-mammalian GLUT4 chimera proteins as tools for studying GLUT4 trafficking and endocytosis.
- **Event:** The EMBO Meeting 2013.
- **Place:** Amsterdam, Netherlands.
- **Date:** September, 2013.

- **Authors:** Francisco Carvalho-Simoes, Marta Camps, Josep V.Planas.
- **Poster title:** Fish-mammalian GLUT4 chimera proteins as tools for studying GLUT4 trafficking and endocytosis.
- **Event:** 40th FEBS Congress.
- **Place:** Berlin, Germany.
- **Date:** July, 2015.

- **Authors:** Francisco Carvalho-Simoes, Marta Camps, Josep V.Planas.
- **Poster title:** Fish GLUT4 as a tool for studying GLUT4 trafficking.
- **Event:** The 1st FEBS3+ Joint Meeting of the French-Portuguese-Spanish Biochemical and Molecular Biology Societies.
- **Place:** Barcelona, Spain.
- **Date:** October, 2017.

Oral presentation

- **Title:** Fish-mammalian GLUT4 chimera proteins as tools for studying GLUT4 trafficking and endocytosis.
- **Event:** 40th FEBS Congress.
- **Place:** Berlin, Germany.
- **Date:** July, 2015.